

ADA023055

**ARPA/NRL X-Ray Laser Program
Semiannual Technical Report to
Defense Advanced Research Projects Agency
1 July 1975 to 31 December 1975**

*Interaction Physics Branch
Optical Sciences Division* ✓

March 1976

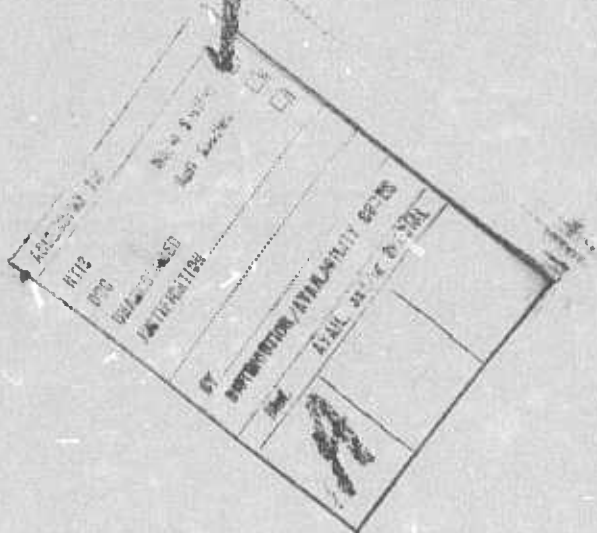
DDC
APR 15 1976
JEC



**NAVAL RESEARCH LABORATORY
Washington, D.C.**

Approved for public release; distribution unlimited.

The Interaction Physics Branch of the Optical Sciences Division, Naval Research Laboratory, Washington, D.C., prepared this semiannual report on work sponsored jointly by the Defense Advanced Research Projects Agency, DARPA Order 2694, and the Naval Research Laboratory. Co-authors of the report were R.C. Elton, J. Reintjes, R.C. Eckardt, R.H. Dixon, R. Waynant, T.N. Lee, and L.J. Palumbo.



SECURITY CLASSIFICATION OF THIS PAGE (When Data Entered)

REPORT DOCUMENTATION PAGE		READ INSTRUCTIONS BEFORE COMPLETING FORM
1. REPORT NUMBER NRL Memorandum Report, 3241	2. GOVT ACCESSION NO. 14 NRL-MR-3241	3. RESIDENT'S CATALOG NUMBER
4. TITLE (and Subtitle) ARPA/NRL X-RAY LASER PROGRAM - SEMIANNUAL TECHNICAL REPORT TO DEFENSE ADVANCED RE- SEARCH PROJECTS AGENCY, July 1975 to 31 December 1975	5. TYPE OF REPORT & PERIOD COVERED Interim semiannual technical report; 1 July 1975 - 31 December 1975	6. PERFORMING ORG. REPORT NUMBER
7. AUTHOR(s) Interaction Physics Branch Optical Sciences Division	8. CONTRACT OR GRANT NUMBER(s) 15 ✓ ARPA Order - 2694	
9. PERFORMING ORGANIZATION NAME AND ADDRESS Naval Research Laboratory Washington, D.C. 20375	10. PROGRAM ELEMENT, PROJECT, TASK AREA & WORK UNIT NUMBERS NRL Problems N01-43 & N01-33 ARPA Order 2694, Program Code 4D10	
11. CONTROLLING OFFICE NAME AND ADDRESS Defense Advanced Research Projects Agency Arlington, Va. 22209	12. REPORT DATE 11 Mar 1975	
13. MONITORING AGENCY NAME & ADDRESS (if different from Controlling Office) 16 NRL-N01-43, NRL-N01-33	14. NUMBER OF PAGES 286 p.	15. SECURITY CLASS. (of this report) 12 UNCLASSIFIED
15a. DECLASSIFICATION/DOWNGRADING SCHEDULE		
16. DISTRIBUTION STATEMENT (of this Report) Approved for public release; distribution unlimited.		
17. DISTRIBUTION STATEMENT (of the abstract entered in Block 20, if different from Report)		
18. SUPPLEMENTARY NOTES		
19. KEY WORDS (Continue on reverse side if necessary and identify by block number) X-ray lasers Lasers Ultraviolet lasers Laser-plasma interactions		
20. ABSTRACT (Continue on reverse side if necessary and identify by block number) The ARPA/NRL x-ray laser program is concerned with demonstrating gain in the soft x-ray region. The program is jointly supported by ARPA and NRL. The approaches include electron-collisional pumping of ions, resonant charge transfer pumping, optical parametric mixing to short wavelengths, traveling wave e-beam and discharge pumping, and analysis and numerical modeling. This report covers the progress made during the first half of FY-76.		

DD FORM 1 JAN 73 1473

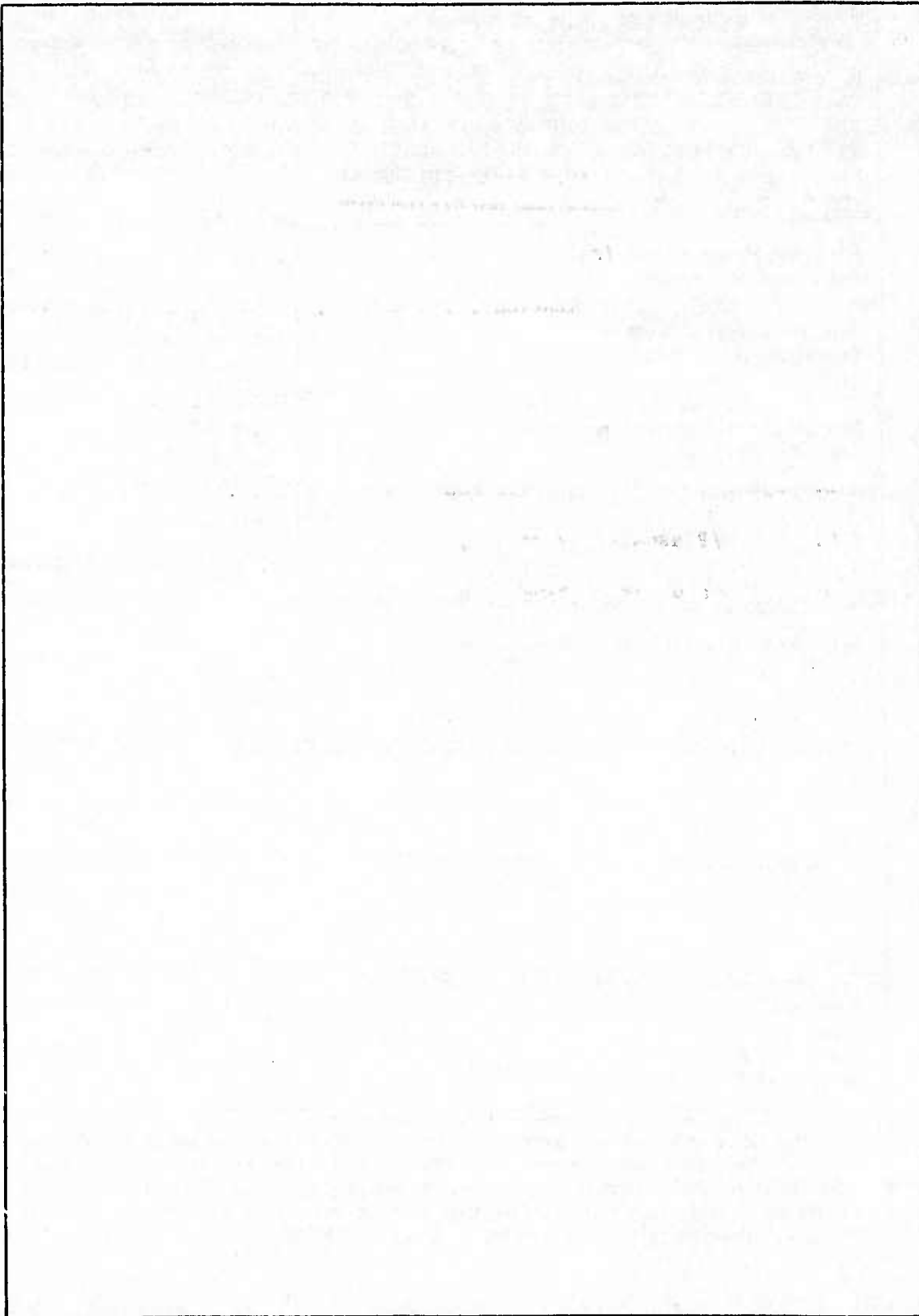
EDITION OF 1 NOV 65 IS OBSOLETE
S/N 0102-014-6601

SECURITY CLASSIFICATION OF THIS PAGE (When Data Entered)

257950

13

SECURITY CLASSIFICATION OF THIS PAGE(When Data Entered)



CONTENTS

I.	INTRODUCTION	2
II.	COHERENT VACUUM-UV/SOFT X-RAY PULSES BY NONLINEAR MIXING AND AMPLIFICATION	6
	A. Nonlinear Mixing	5
	B. Vacuum-UV Amplification :	11
III.	ELECTRON-COLLISIONAL PUMPING VIA PICOSECOND LASER PUMPING OF PLASMAS	19
	A. Numerical Modeling	19
	B. Synchronized Dual Laser Facility	25
	C. Laser/Plasma Experiments	28
	D. Plans and Alternatives	42
IV.	RESONANT CHARGE TRANSFER PUMPING	43
	A. Soft X-ray Spectra	45
	B. Visible Helium Spectra	45
	C. Plasma Diagnostics	48
	D. Techniques	48
	E. Analysis	49
V.	SUMMARY	50
VI.	APPENDIX (Separate Contents)	52

SEMIANNUAL TECHNICAL REPORT

Reporting Period

1 July 1975 - 31 December 1975

1. DARPA Order	2694
2. Program Code No.	4D10
3. Name of Contractor	Naval Research Laboratory Optical Sciences Division
4. Effective Date of Contract	1 January 1974
5. Contract Expiration Date	Continuing
6. Amount of Contract	\$250K (FY 76)
7. Contract No.	N/A
8. Principal Investigator	Dr. R. C. Elton (Acting)
9. Telephone No.	202-767-3528
10. Scientific Officer	Dr. C. M. Stickley, ARPA
11. Title of Work	X-Ray Lasers

Sponsored by

Defense Advance Research Projects Agency

ARPA ORDER 2694

ARPA/NRL X-RAY LASER PROGRAM
Semiannual Technical Report to Defense Advanced Research Projects Agency
1 July 1975 - 31 December 1975

I. INTRODUCTION

This is the fourth semiannual technical progress report for the ARPA/NRL X-Ray Laser Program. There is no intention to duplicate background material from previous reports*, since the format is similar and copies are available upon request. Rather, the intent here is to provide an update on program progress during this reporting period with brief statements of motivation and goals.

The basic individual activities in the program have remained essentially same, i.e.,

Nonlinear optical mixing for producing coherent radiation in the vacuum-UV region,

Amplification of such coherent radiation as necessary, beginning in the 1600 Å region, in preparation for further frequency up-conversion,

Electron collisional pumping of ions in schemes amenable to isoelectronic extrapolation to short vacuum-uv wavelengths,

Investigation of resonant charge transfer pumping at a high rate into preferential levels as an advanced soft x-ray amplifier, and

Theory, analysis and numerical modeling in support of these approaches and continual investigation of new concepts.

The overall theme in this program is to generate a coherent, collimated laser beam at as short a wavelength as possible for materials diagnostic applications. The general approach is to transfer a high degree of coherence from long wavelengths, with amplification through molecular and ionic devices in an eventual chain system as illustrated in Fig. 1. The areas of current NRL activity are bounded

*Previous semiannual reports on this project are referred to liberally in the present report. These are published as NRL Memorandum Reports No. 2910 (October 1974), No. 3057 (March 1975), and No. 3130 (September 1975). Copies are available on request.

NOTE: Manuscript submitted March 3, 1976.

SOFT X-RAY LASERS —NONLINEAR MIXING/AMPLIFIER CHAIN—

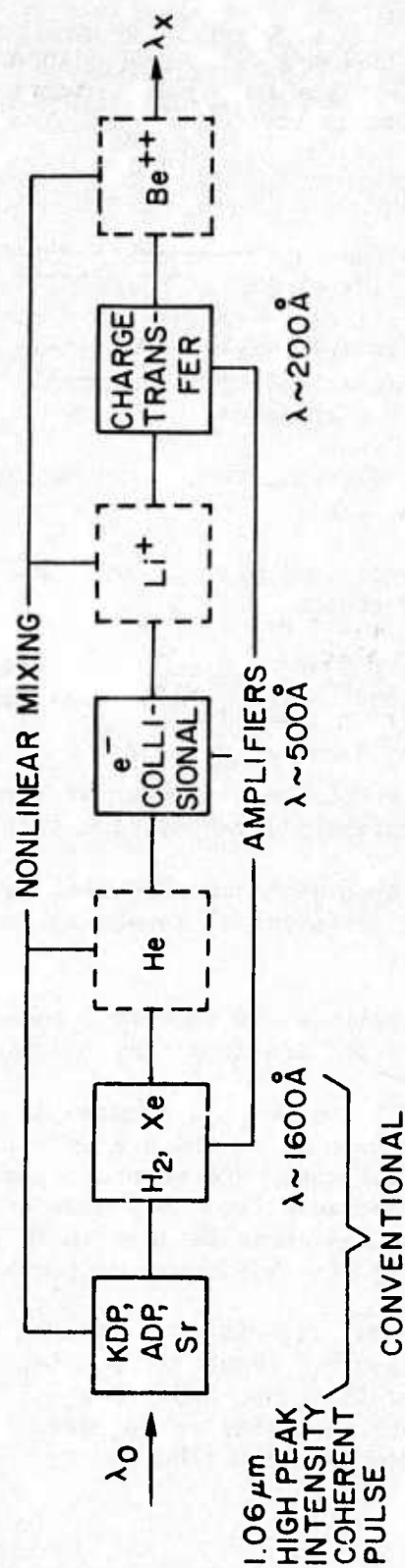


Fig. 1 — Block diagram of coherent amplification scheme

by solid lines; those of conceivable future activity by dashed lines. A high peak intensity pulse from a coherent laser at $1\ \mu\text{m}$ is frequency upconverted by "conventional" means into the vacuum ultraviolet (vuv) region near $1600\ \text{\AA}$, possibly with accurate tuning capability. This step is described in Section II. A. Amplification of the beam at this point may be required to achieve sufficient power for further upconversion, using either a H_2 or Xe "molecular" laser and existing technology. The details here are described in Section II.B. Electron collisional population inversion at shorter vuv wavelengths appears promising in either laser-heated plasmas (Section III.B) or with transverse discharges such as originally developed for N_2 and H_2 and later extended¹ to ions such as C^{3+} (Section III.D.). At shorter soft x-ray wavelengths, the rapid resonance charge transfer process remains most interesting for achieving significant inversion, and progress on the current definitive experiments is described in Section IV.

Each component of this chain is in a somewhat different phase of development. The non-linear mixing has approached the vacuum-uv region and optimization is beginning. A delay was encountered in obtaining the xenon diode for amplification, so that we are preparing for H_2 amplification as required. In the laser heated plasma experiments for electron collisional pumping, both careful numerical analysis and sophisticated interferometric diagnostics have illuminated the difficulties in absorbing a significant amount of laser radiation in the very thin layer of a specific density appropriate for inversion and gain. Quantitative measurements are continuing; however the indications are that electron pumping in either a transverse discharge or beam may be more appropriate a pump mechanism, so that additional emphasis is being placed now on the traveling wave device that has been a unique workhorse at NRL. The direct and definitive resonance charge transfer experiment has progressed to the point where space-resolved spectra from both the ions and the background helium gas are achieved, and detailed measurements at various densities are possible.

A major accomplishment of this reporting period has been the completion of a comprehensive review article² on the subject of short wavelength lasers. A preprint is reproduced in the Appendix. Of the 268 references gathered there (as of October 1975), the ones directly related to short-wavelength lasing are compiled chronologically in Fig. 2, which is an indication of the growth of interest in this field.

The following sections of this report describe the details of progress made in each of these areas during the last six months. A summary of the important points is included in the last section. In some instances the work has been prepared for publication or has been published. In these cases the reprint has been included as an appendix and only brief mention of the work is made in the main body of the report. Each section also contains a few sentences about where the work is headed and plans for the next reporting period.

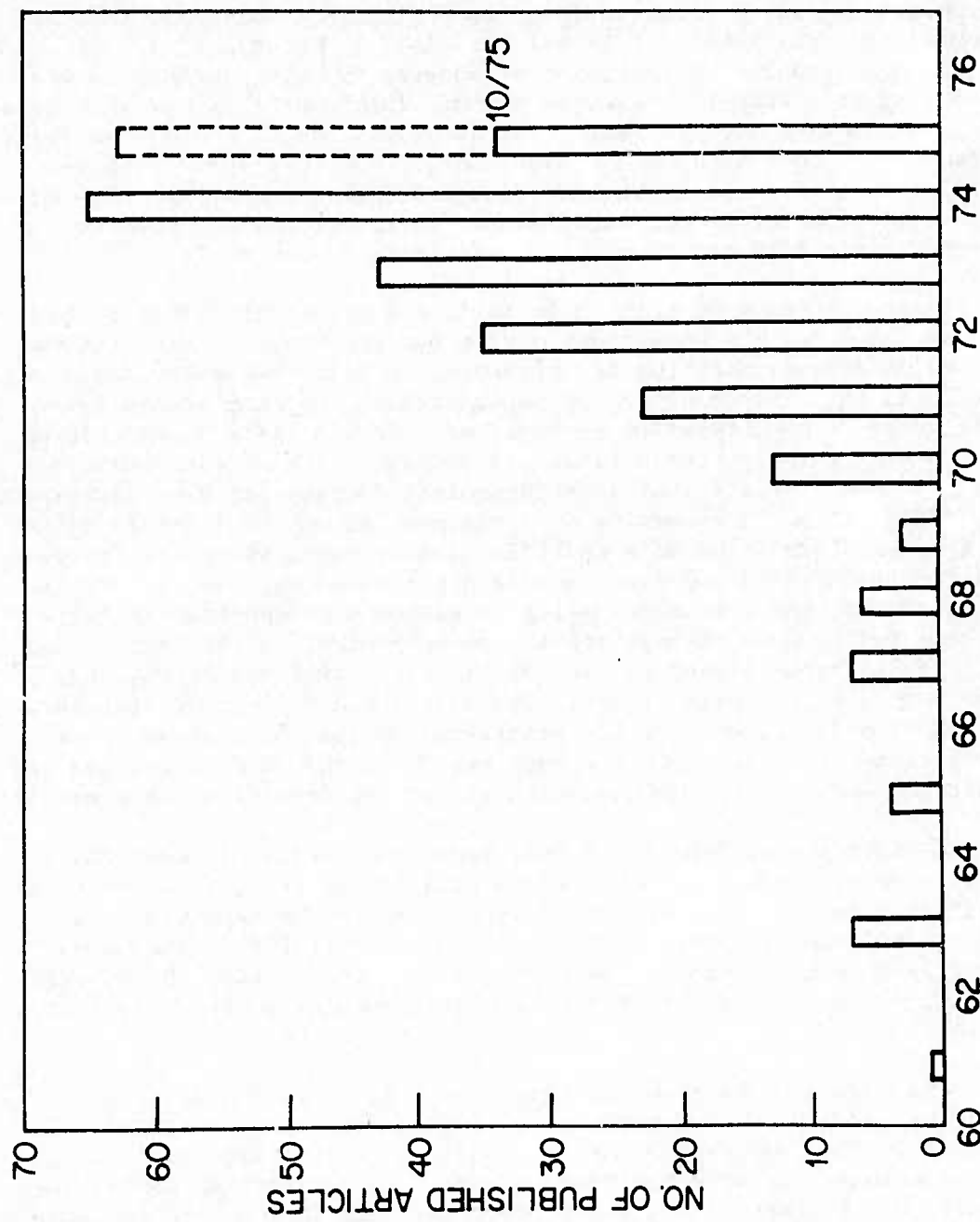


Fig. 2 — Record of activity in short wavelength laser research as compiled from the references on this topic in a recent review. The data for 1975 are as of October and still incomplete, particularly for those articles not yet translated.

SOFT X-RAY LASERS — TUNABLE NON-LINEAR MIXING —

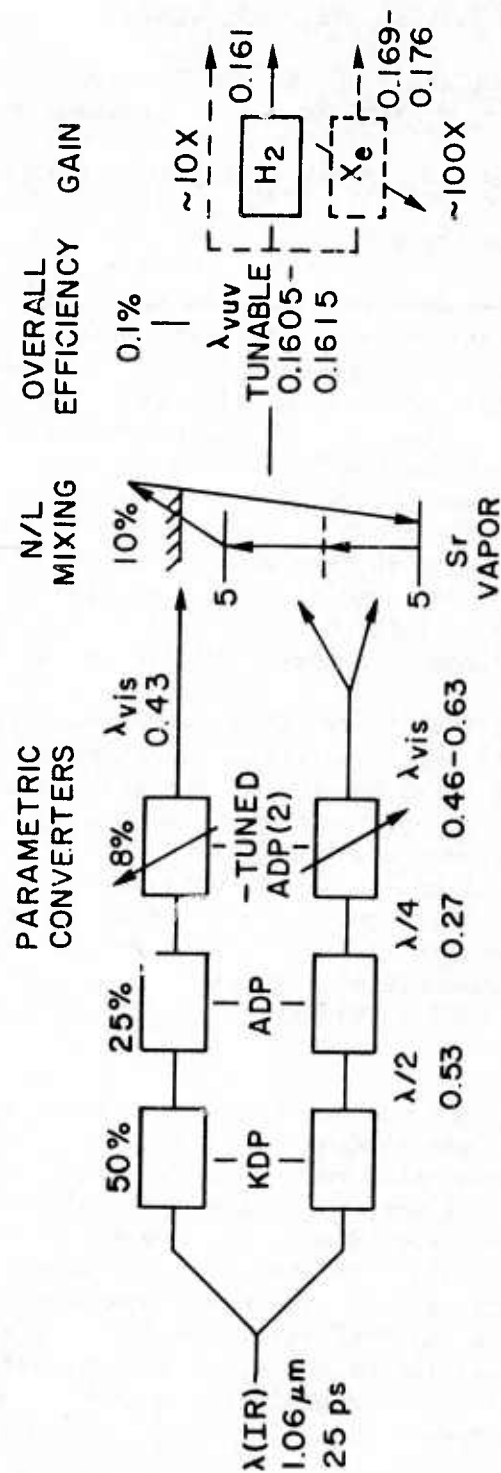


Fig. 3 — Schematic of proposed scheme for generating amplified pulses in the VUV

REFERENCES

1. R. W. Waynant, "Vacuum Ultraviolet Laser Emission from C IV", Appl. Phys. Letters, 22, 419, (1973).
2. R. W. Waynant and R. C. Elton, "Review of Short Wavelength Laser Research", Proc. IEEE (submitted); see Appendix for preprint.

II. COHERENT VUV/SOFT X-RAY PULSES BY NONLINEAR MIXING AND AMPLIFICATION

II.A. NONLINEAR MIXING

This section describes our approach and recent progress towards the generation of coherent soft-x-radiation through nonlinear mixing processes. The motivation and general technique was described in detail in previous reports in this series and is outlined briefly in Fig. 3. The output of a Nd:YAG mode locked laser is converted to tunable visible radiation by successive frequency doubling and parametric frequency conversion in each of two arms. The tunable visible light in each arm is combined and converted to the vacuum-UV (VUV) region through resonantly enhanced frequency mixing in a suitable metal vapor, and is then amplified in a VUV amplifier (as is discussed below). A further stage of resonantly enhanced nonlinear mixing is then used to convert the VUV to the soft x-ray range.

As was outlined in previous semiannual reports, the technique of parametric generation was chosen to convert the 1.06 μm YAG output into tunable visible light because of its potential for generating higher powers and shorter pulse durations with the available laser system. During the previous reporting period, one arm of the visible radiation generator was set up and preliminary investigation of its operating characteristics was begun. Measurements of conversion efficiency in the first two stages of harmonic generation were made. The parametric (frequency) down-conversion system was assembled and radiation was generated from 4600 to 6300 \AA by tuning the crystal temperature from 52 to 70°C.

During the present reporting period the performance of the second harmonic stages was studied in more detail, with attempts to optimize their performance being made. In the first stage, conversion from 1.064 μm to 5320 \AA was obtained with an efficiency between 50 and 60%, which is considered adequate for our purposes. Conversion efficiency from 5320 \AA to 2660 \AA in the second stage was measured in the range of 25%, a value which was unexpectedly low although comparable with performance reported elsewhere. Since the efficiency of the parametric generation in the subsequent stages depends critically on the strength of the UV signal, the fourth harmonic generation stage was studied in some detail.

The conversion from 5320 \AA to 2660 \AA was studied in a 1" long

ADP crystal by measuring the depletion of the transmitted pump signal at 5320 Å simultaneously with the generated signal at 2660 Å as the crystal temperature was adjusted on and off the 90° phase matching value (Fig. 4.) These measurements were made as the intensity of the pump radiation was varied by introducing a 2:1 reducing telescope into the beam. The results are summarized in Table 1, where the various signals are shown referenced to the pump pulse. Comparison of the UV signal with and without the telescope with the crystal temperature set at 53.7°C shows that addition of the telescope results in an increase of relative UV signal by 4.8 times, in good agreement with the nominal expected increase of 4 times. A similar comparison with the crystal temperature set at the 90° phase matching value of 51.7°C shows an increase in UV signal of 1.4 times. Simultaneous measurements of pump transmission show a depletion of 23% for the untelescoped beam and 55% for the telescoped beam.

TABLE 1
RELATIVE CONVERSION 5320 to 2660 Å

	Relative UV Signal I_{uv}/I_{pump_0}	Relative Transmitted Pump Signal I_{pump}/I_{pump_0}
T = 53.7°C Pump Untelescoped	1.0	1.0
T = 53.7°C Pump Telescoped	4.38	1.0
T = 51.7°C Pump Untelescoped	36.5	0.77
T = 51.7°C Pump Untelescoped	50.9	0.45

These results can be interpreted with the aid of Fig. 5 in which are shown curves for pump and second harmonic (SH) signals for an ideal plane wave as a function of the parameter LE_p . The results for the untelescoped beam are indicated by points A and A' (Linear attenuation due to absorption and surface reflection is not considered at this point in the discussion.) An increase in pump depletion to 55% upon addition of the telescope is indicated by point B, with the corresponding predicted UV signal as B'. The ideal increase in signal relative to the untelescoped case is 2.2 times rather than the observed 1.4 times (point B''). The discrepancy of a factor-of-1.7 appears to arise from nonlinear losses at 2660 Å, since the increase in signal off the phase match temperature is in agreement with the theoretical value.

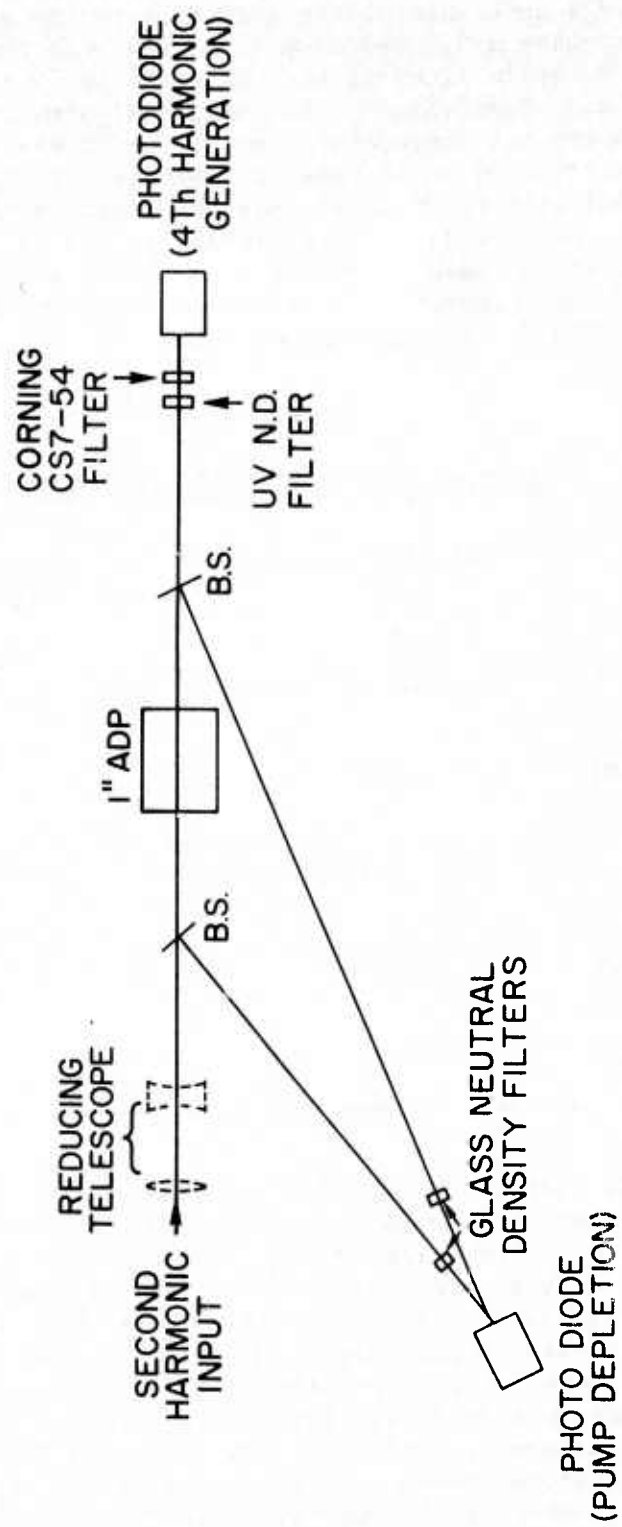


Fig. 4 — Schematic diagram of experiment used to measure fourth harmonic generation in ADP

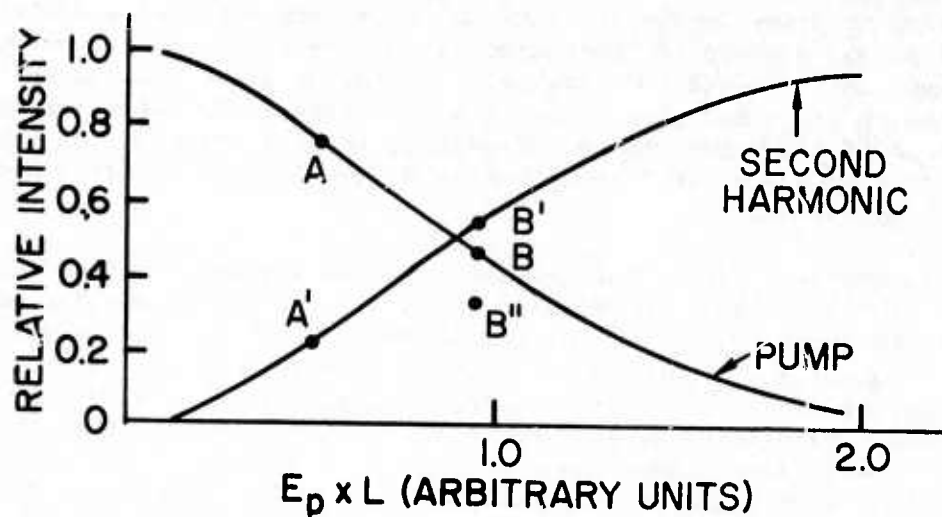


Fig. 5 — Intensities of the pump and SH fields as a function of the product of the crystal length L and the input pump electric field E_0 for an ideal plane wave

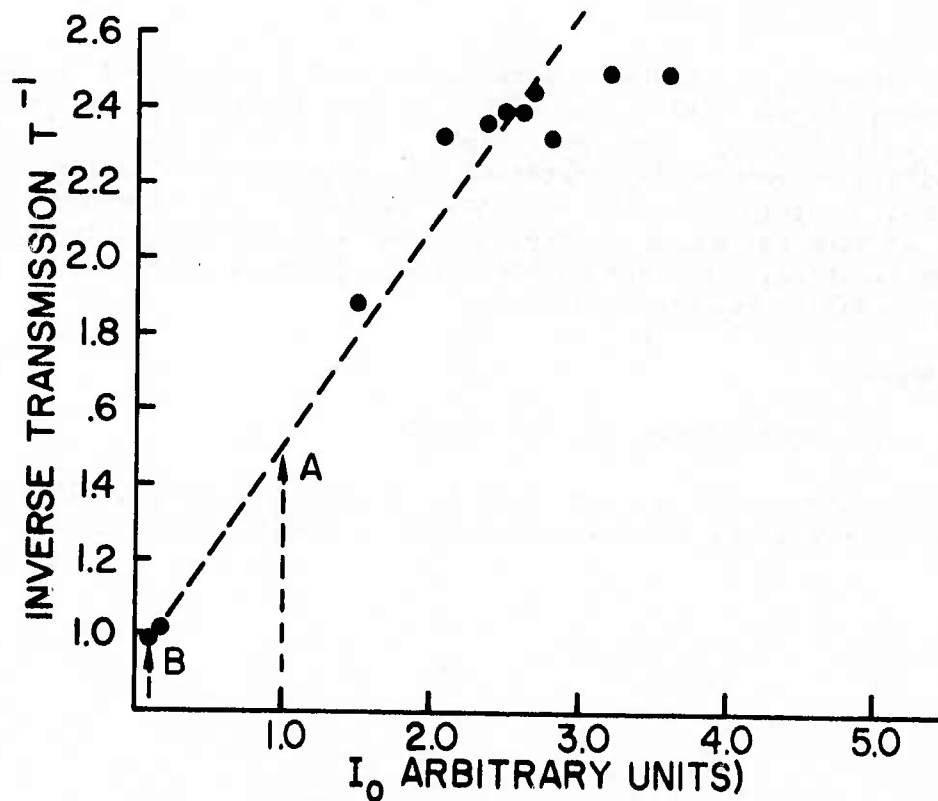


Fig. 6 — Inverse transmission of a 2-in.-long ADP crystal at 2660\AA as a function of incident pulse intensity I_0

Observation of reduced harmonic generation due to two-photon absorption at power levels of 35 MW/cm^2 have been reported elsewhere. In addition, reports of limitation of SH generation in semiconductor systems due to two photon absorption of the SH light and sum frequency absorption of SH and pump light have been made.² To determine the importance of these effects in our system, we also measured the transmission of a 2" long ADP crystal at 2660 \AA as a function of intensity both at 2660 \AA and 5320 \AA .

Intensity variation of the 2660 \AA light was again accomplished with a reducing telescope, the time of value 5:1. The transmission measurements are shown in Fig. 6. At the highest UV intensities used (around 800 MW/cm^2) nonlinear absorption is seen to have reduced the transmission by a factor-of-2. The corresponding intensity in the telescoped harmonic generation experiment is also shown (A) (taking into account surface reflections, filter transmission and crystal lengths), indicating a reduction in UV signal by a factor of 1.55. Thus, the discrepancy between the observed and predicted increase of the SH UV-signal in the harmonic generation experiment is almost entirely accounted for by the observed level of two-photon absorption. The intensity of the untelescoped beam in the harmonic generation experiment is also indicated (B), and at this level the two photon absorption should be negligible. No effect on the transmission at 2660 \AA was observed when the pump intensity was varied.

In summary, two photon absorption at 2660 \AA appears to be important in limiting SH conversion from 5320 \AA at pump intensities around 2.5 GW/cm^2 . Although large pump depletions can be obtained at higher intensities, corresponding increases in generated SH radiation are not realized. At pump intensities around 600 MW/cm^2 , the attenuation of the UV signal from two photon absorption appears to be negligible. At these pump intensities, a conversion efficiency of 23% is observed, in agreement with values reported elsewhere.

REFERENCES

1. K. Kato, Optics Comm. 13, 361 (1975).
2. C. A. Schwartz, J. L. Oudur and E. N. Batifol, JQE 11, 616 (1975); J. L. Ouddar, C. A. Schwartz, and E. M. Batifol JQE 11, 623 (1975).

II. B. VACUUM-UV AMPLIFICATION

As described above, the generation of tunable picosecond vacuum ultraviolet (vuv) laser pulses using nonlinear optical upconversion techniques¹ largely preserves the coherence of the fundamental driving laser beam. However, because of a rather low (frequency) upconversion efficiency, large amounts of driving power are necessary both for practical applications² and for reaching the threshold level for further upconversion steps. Driving power cannot be increased without bound because other processes such as multiphoton absorption limit the power which can be transmitted through the non-linear medium. It is thus desirable to have amplifiers between some of the up-conversion stages to restore the pulse power level. Several amplifier approaches have been under study at the Naval Research Laboratory and are described specifically below following some more general considerations.

II. B.1. INJECTION

The general problem of injecting a short vuv pulse into an amplifier deserves careful study. Below 1000 Å all amplifiers will most likely be mirror-less gain configurations constrained by the pumping geometry and probably pumped in a traveling-wave manner (termed the swept-gain method by Bonifacio, et al.³). All of these mirrorless systems, called amplified spontaneous emission (ASE) devices, normally operate by amplifying and building a pulse from their own spontaneous emission. Bonifacio, et al.³ have shown that the width of the steady-state pulse developed by these systems depends inversely upon the gain achieved. For high peak power applications, the most desirable pulse output is obtained for the case of high gain.

The injection of a pulse into ASE systems has been considered theoretically by Allen and Peters⁴. While their results do not apply specifically to traveling-wave excitation, it is useful to consider their results of output intensity as a function of input intensity. Figure 7 shows that for the injected signal, I_b , to exceed in amplitude the forward going ASE pulse, I_a , the input ($x = 0$) intensity must exceed a threshold value which they give as

$$I_b(0)_{\text{thresh}} = \frac{K (L - L_c)}{L L_c} , \quad (1)$$

where K is a constant, L_c is the critical length for threshold "unity" gain, and L is the total amplifier length. Also, a greater input signal results in a greater ratio of amplified pulse intensity to ASE pulse intensity. It also seems reasonable to expect an even greater increase in pulse intensity and a lowering in the threshold when traveling-wave excitation is used.

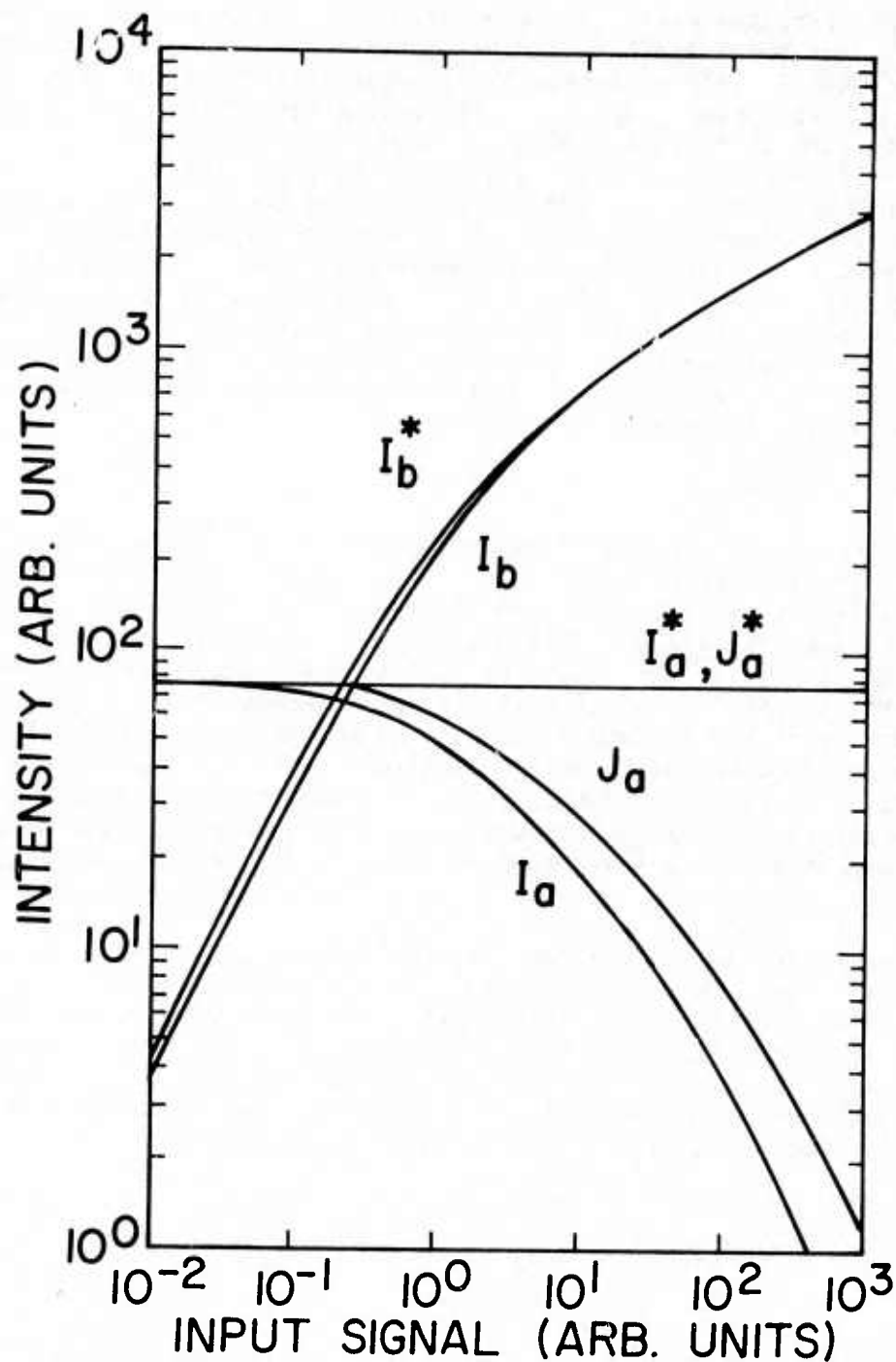


Fig. 7 — Intensity of ASE pulse, I_a , and the amplified input pulse, I_b , as a function of the input pulse intensity for a fixed length and inversion density. J_a is the intensity of the wave traveling in the opposite direction, and the starred values are intensities in the absence of an input signal (I_a^* , J_a^*) or in the absence of spontaneous emission (I_b^*). Note that this study does not consider traveling-wave pumping. [After Allen and Peters, Ref. 4.]

II. B.2. TRAVELING-WAVE (SWEPT-GAIN) AMPLIFIER THEORY

Bonifacio, et al.³ have considered traveling-wave pumped amplifiers (without injection) in considerable detail showing that steady state pulses with rather wide pulse width arise for the case of limited gain; but that for very high gain the steady state pulse becomes a π pulse with characteristics similar to those predicted for super-radiance. Fig. 8 shows examples of pulse shapes for three gain (g)/loss(k) ratios. In the case of high gain it is shown that no limit exists for the power because no cooperation length limit exists, and that the pulse width decreases as $1/\rho_0$ where ρ_0 is the inversion density. These results apply directly to the traveling-wave pumped N_2 and H_2 lasers at NRL and the behavior described (gain narrowing) has been seen experimentally; but the effects of injecting pulses into the system can so far be judged only by the theory of Allen and Peters described above.

II. B.3. EXPERIMENTAL CONSIDERATIONS

The theoretical treatments presented above are not sufficiently complete to model the behavior expected when a 30 picosecond up-converted laser pulse is injected into a vacuum ultraviolet amplifier. Such questions remain as to whether an injected pulse would be significantly amplified and narrowed in a traveling-wave excited medium and whether the input signal intensity threshold can be met. If a non traveling-wave amplifier is used, a further question is whether the injected signal will need to be greater than in the traveling-wave case to compete with the internally generated signal. Experiments to determine these points are very important. It appears from the theory that high gains and long lengths are desirable from the standpoint of raising the amplified input signal intensity well above any amplified spontaneous signal intensity. From the viewpoint of easing the acceptance of the frequency of the input signal, it would be desirable to have a reasonably broad amplifier bandwidth. These considerations cause the consideration of two different types of amplifier: (a) the electron-beam pumped, rare gas (xenon) amplifier; and (b) the traveling-wave (swept gain) hydrogen amplifier. (Recent work at NRL by Burnham and Djeu⁵ on chemical lasers such as XeF spur the hope that broad bandwidth and higher energy might be obtained with a long traveling-wave amplifier using vacuum ultraviolet gain from such molecules as NeF.) Progress on both types of amplifier will be discussed.

II. B.3.A. XENON AMPLIFIER

A proven 6,7 coaxially pumped xenon amplifier of approximately 10 cm length and 4 mm diameter has been ordered from D. J. Bradley of Imperial College. This diode will be mated with an existing Fexitron high voltage pulse generator which produces approximately 10 J of 600 keV electrons. From an unmodified Febetron pulse generator

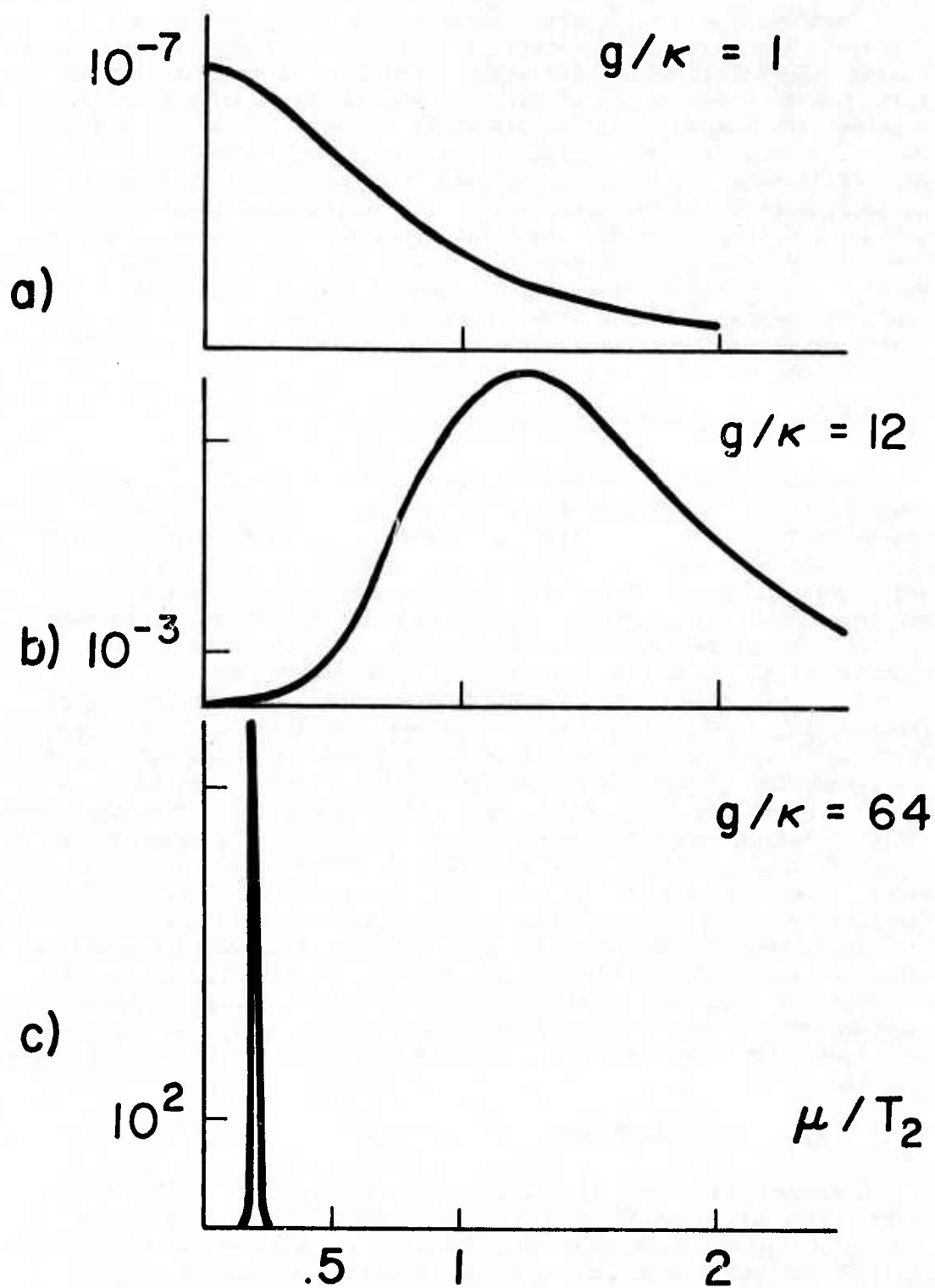


Fig. 8 — Theoretical pulse shapes for a traveling-wave excited (swept-gain) amplifier for several gain (g)/loss(κ) ratios where μ/T_2 is a reduced (dimensionless) time

(similar to NRL's), Bradley achieved 3 mJ pulses at 1690 - 1760 Å having 3 ns width when operated in a resonant cavity. Bradley obtained 9 mJ by lengthening the amplifier and modifying the Febetron to pump for 5 ns at a 500 keV energy level.

From these oscillator measurements it would, of course, be desirable to make quantitative statements about the performance of this device as an amplifier for the 30 picosecond up-converted pulses mentioned above. It is difficult to predict whether a 5 Å wide 30 picosecond pulse will be able to stimulate and remove all the energy stored. In the oscillator measurements of Bradley, et al. the emission was spread over a 70 Å bandwidth. When prism tuning was introduced the power fell by a factor of four, but the output bandwidth was reduced to 1.3 Å. In this case the xenon pulse had the entire 5 ns pumping time as well as several passes through the gain medium to attain the output measured.

Mies⁸ has calculated the vibrational wave functions for bound-continuum transitions and has predicted the emission lineshapes. It would appear difficult for an incoming pulse to stimulate all of the vibrational levels of xenon, but no data are available to allow a quantitative estimate of how much energy can be extracted from a xenon amplifier. Experimental efforts to answer this question are being initiated.

Since the gain coefficient reported by Bradley, et al. is 0.25 cm^{-1} , an ASE pulse will clearly build-up in addition to the amplified pulse. Because the ASE pulse will have the entire frequency band to feed upon, it may contain more total energy than the narrow band amplified pulse, but would have a longer pulse length (proportional to $1/\rho_0$). In summary, experiments must be performed to ascertain the input signal required to overcome the ASE signal which will be generated in this amplifier. Other techniques, such as reducing the length below that sufficient for ASE build-up, may also be investigated experimentally.

II. B.3.B. HYDROGEN AMPLIFIER

Several traveling-wave pumped hydrogen lasers have been built. The largest and most sophisticated is at NRL and produces 1 - 2 mJ of energy over a number of lines in the 1600 Å region.* When divided proportionally to their intensities, each of the strongest lines of hydrogen would have on the order of 0.1 to 0.2 mJ of energy. This hydrogen laser operates with more than 0.1 cm^2 cross section at a pressure of 30 Torr. (Suggestions* that the Soviet hydrogen laser energy can be scaled upward by increasing their cross section--

*In one proposal to ARPA (CMR-P-74-1) the output of a Soviet hydrogen laser was incorrectly stated as 5 mJ rather than 0.5 mJ.

presently at 0.005 cm^{-2} --may not hold true. The Soviet ability to operate at high ($\sim 1 \text{ atm}$) pressure likely comes from surface discharges due at such close electrode spacing.)

Increased power may also be produced by increasing the length of the traveling-wave discharge. As Bonifacio, et al.³ point out, the intensity will grow proportionally to the square of the inversion density, and the pulse width will decrease inversely proportionally to the inversion density. Pulse shapes corresponding to Bonifacio's high gain case have been observed emerging from the forward direction of the NRL traveling-wave system (Fig. 9), while pulse shapes corresponding to much lower gain (greater pulse widths) have been seen from the reverse direction. These experimental results confirm the theoretical trend predicted by Bonifacio, while also emphasizing that a lower gain reverse direction pulse does build up in a swept-gain system.

II. B.3.C COMPARISON OF AMPLIFIERS

To summarize and compare these two vuv amplifiers, Table I lists some of the pertinent characteristics. Xenon appears to store more energy, but its wide bandwidth may greatly reduce the energy which can be swept out by line radiation. Also it is difficult to estimate the effect of repumping on the energy obtained from xenon in oscillator experiments. On a narrow equal bandwidth basis the intense lines of hydrogen may provide more energy; it is certain that the H_2 numbers shown have not been increased by repumping since the transition is self-terminating. Both systems will amplify their own noise, and this may present problems in obtaining a maximum gain for low injection powers. Some power increase may be obtained by the pulse narrowing in the traveling-wave pumped system.

As shown in Table 2 the gain coefficients, gain lifetimes, and cross sectional areas are comparable. Presently 100 cm and 160 cm long hydrogen lasers exist at NRL and the length of these traveling-wave systems can be increased, in principal, without limit. Extension of the active length of the coaxial xenon amplifier is possible with higher energy electron beam systems, but the finite cooperation length would limit the length to about 150 cm.

While not elaborated upon here, both systems present about equal problems in synchronization with the picosecond injection pulse. The longer lifetime of xenon may assist somewhat, but this cannot be assessed without a knowledge of when and with what precision the external picosecond pulse must be injected to enable it to dominate the spontaneous noise that will be amplified.

Some consideration should be given to new traveling-wave pumped discharge systems such as NeF which would amplify at shorter wavelengths ($\sim 1070 \text{ \AA}$) and which may store even greater energy than with xenon

PULSE NARROWING IN GAIN-SWEPT* AMPLIFIERS

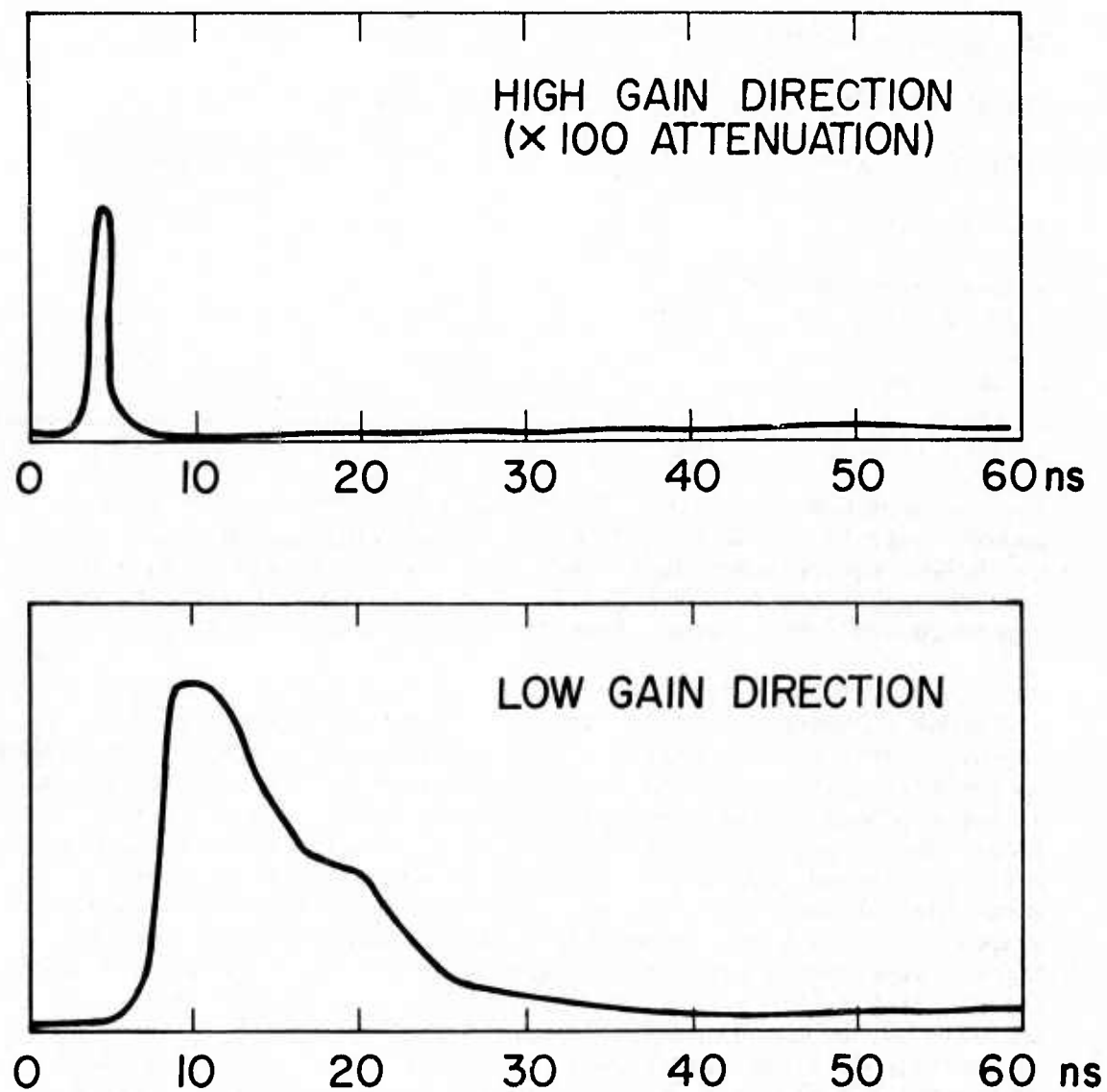


Fig. 9 — Measured output pulse shape for the forward high-gain direction of a traveling-wave excited laser, and the shape of the pulse traveling in the reverse direction where the gain is much less

TABLE 2

COMPARISON OF XENON VS. HYDROGEN AMPLIFIERS

	<u>H₂</u>	<u>Xe₂[*]</u>
Wavelength	1610 Å	1690-1760 Å (Peak at 1730 Å)
Energy Stored (Total)	1 - 2 mJ	3 - 9 mJ
Energy Available (0.1 Å bandwidth)	0.1 - 0.2 mJ	?
Gain Coefficient	0.18 cm ⁻¹	0.25 cm ⁻¹
Gain Lifetime	1 - 3 ns	5 - 10 ns
Active Length Available For Amplification	100 cm	10 cm
Active Area	0.1 cm ²	0.125 cm ²

for the same configuration. These chemical lasers may generate enough power in an ASE mode to allow higher harmonic up-conversion to follow, giving wavelengths near 200 Å or lower (e.g. 3rd, 5th, and 7th harmonics of 1070 Å = 357, 214, and 154 Å, etc.). The coherence would be limited, however, as with any ASE system.

It is difficult to decide at this time which of these very different approaches will be best suited for amplification of an injected short pulse coherent beam. Considerable practical experience in the swept-gain amplifier has been acquired at NRL and the concept of swept gain has vital general importance to short wavelength laser generation, particularly since it operates without a resonant cavity. (Indeed, considerable effort is presently being spent in extending the device to shorter wavelengths with electron collisional pumped ion transitions as described in Section III.D.) For the initial experiments and for an input pulse of several Angstroms width, instead of 0.1 Å in Table 2 xenon may provide comparable energy and also may be easier to synchronize with the injection laser initially. Both amplifiers need much experimental investigation to characterize their performance. This is to be expected, of course, for an advanced concept of this nature, and attempts to increase the input power may pay great dividends in increased amplifier performance.

REFERENCES

1. S. E. Harris, J. F. Young, A. H. Kung, D. M. Bloom, and G. C. Bjorklund, "Generation of Ultraviolet and Vacuum Ultraviolet Radiation" in Physics of Quantum Electronics, S. F. Jacobs, M. O. Scully, and M. Sargent III, eds, vol. 2, Reading, Mass: Addison Wesley, 1975, pp. 181-197.
2. G. C. Bjorklund, S. E. Harris, and J. F. Young, Appl. Phys. Ltrs., 25, 451 (1974).
3. R. Bonifacio, F. A. Hopf, P. Meystre, and M. G. Scully, "Steady State Pulses and Superradiance in Short Wavelength, Sept-Gain Amplifiers", (to be published).
4. L. Allen and G. I. Peters, "Amplified Spontaneous Emission and External Signal Amplification in an Inverted Medium", Phys. Rev. A., 8, pp. 2031-2047, October 1973.
5. R. Burnham and N. Djeu (to be published).
6. D. J. Bradley, D. R. Hull, M. H. R. Hutchinson, and M. W. McGeoch, "Megawatt VUV Xenon Laser Employing Coaxial Electron-Beam Excitation", Opt. Commun., 11, pp. 335-338, August 1974.
7. D. J. Bradley, D. R. Hull, M. H. R. Hutchinson, and M. W. McGeoch, "Co-axially Pumped, Narrow Band, Continuously Tunable High Power VUV Xenon Laser", Opt. Commun., 14, 1, May 1975.
8. F. H. Mies, "Stimulated Emission and Population Inversion in Diatomic Band-Continuum Transitions", Mol. Phys., 26, pp. 1233-1246, November 1973.
9. I. N. Kynazev, (private communication).

III. ELECTRON COLLISIONAL PUMPING

Pumping of population inversions in ions by inelastic collisions of free electrons in high temperature plasmas is attractive, since proven laser transitions can at least in principle be then extrapolated to shorter wavelengths along isoelectronic sequences.

III.A. NUMERICAL MODELING

The overall x-ray laser numerical modeling effort during this reporting period is included in this section rather than separately as in previous reports, since the current results are most appropriate for guidance of the electron-collisional pumping experiments. The numerical

program under continual development is, however, of sufficient general applicability for extension to other schemes, as will be described in Section III.A.3 below.

III.A.1. 3p→3s LASING WITH CARBON-LIKE IONS

Development of the analysis and modeling for electron-collisional pumping of ions along a particular isoelectronic sequence is detailed in the three previous reports in this series and in publications¹⁻⁵, and will not be extensively reviewed here. The advantages of quasi-cw operation as well as an extrapolation from proven near-ultra violet laser transitions in light elements remain.

The initial analysis as well as the initial numerical modeling² were performed for lasing on 3p→3s transitions pumped from a $1s^2 2s^2 2p$ ground configuration in a 6-electron carbon-like ion (such as O^{2+}) as shown in Fig. 10. Encouragingly large gains were predicted for rather moderate densities (such as typically produced in the H_2 discharge laser device). With the major intent to pump such ions experimentally in a laser-produced plasma with a second synchronized short pulse laser (Fig. 11), it became clear that a higher density plasma would be required, since inverse bremsstrahlung absorption in relative short lengths occurs only for densities approaching the critical value ($\sim 10^{21} \text{ cm}^{-3}$ for $1 \mu\text{m}$ radiation). For this reason an extension of the analysis and modeling to higher densities was undertaken. During this reporting period, we have concentrated on "critical" level densities of 10^{21} and 10^{22} cm^{-3} corresponding to the neodymium, ruby, or frequency-doubled pump-laser ranges. This decision followed from the experimental results described in Section III.C. below on interferometric diagnostics of the expanding laser evaporated plasma, as well as from space-resolved diagnostics from the charge transfer experiment (Section IV), which indicated the presence of a very thin (few micrometers) near-critical-density layer in which absorption would dominate (possibly from a normal incidence second pumping pulse).

The modeling to date includes electron-collisional as well as radiative-decay processes between all nearby levels for carbon-like ions for $Z=20-45$, and indicates peak gain coefficients for $Z=25-30$ (700-300 Å laser wavelength range) in the range of $50-300 \text{ cm}^{-1}$ for kinetic temperatures of $KT \approx 500 \text{ eV}$ to 5 keV (considered reasonable for present and near-future laser heated plasmas). In this high density modeling, electron and ion temperatures are assumed equal due to extremely short energy-equipartition times in the plasma. Other processes such as ionization and recombination as well as resonance-radiation absorption are yet to be included, with some expected effect on the results. The resonance-radiation trapping is expected to increase the lower laser state accumulation density and could possibly lead to restrictions on the maximum diameter of the linear plasma, i.e., to be maintained nearly optically-thin in the transverse direction. These effects are currently being added to the model and the final results presented in the next report in this series.

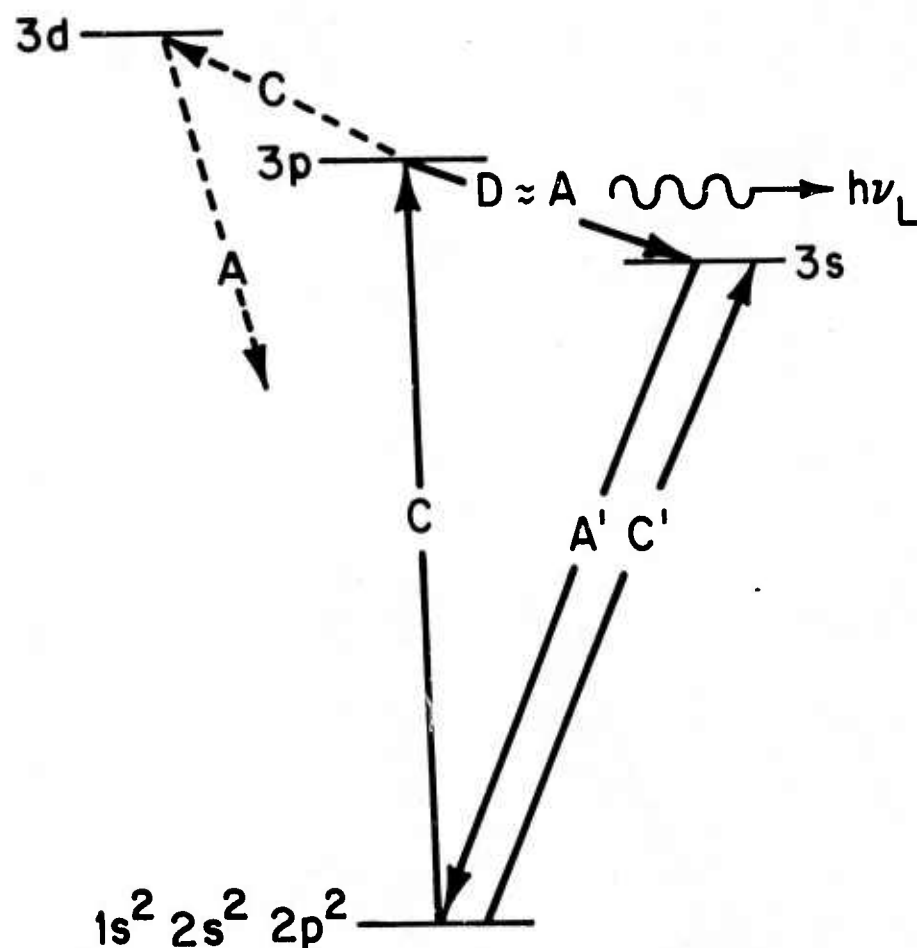


Fig. 10 — Simplified energy level diagram for $3p \rightarrow 3s$ lasing in 6-electron carbon-like ions showing the most relevant interaction channels so far included within a specific ion. C , D , and A represent collisional excitation, collisional deexcitation, and radiative decay, respectively. The dashed lines represent alternate upper-level depopulation channels.

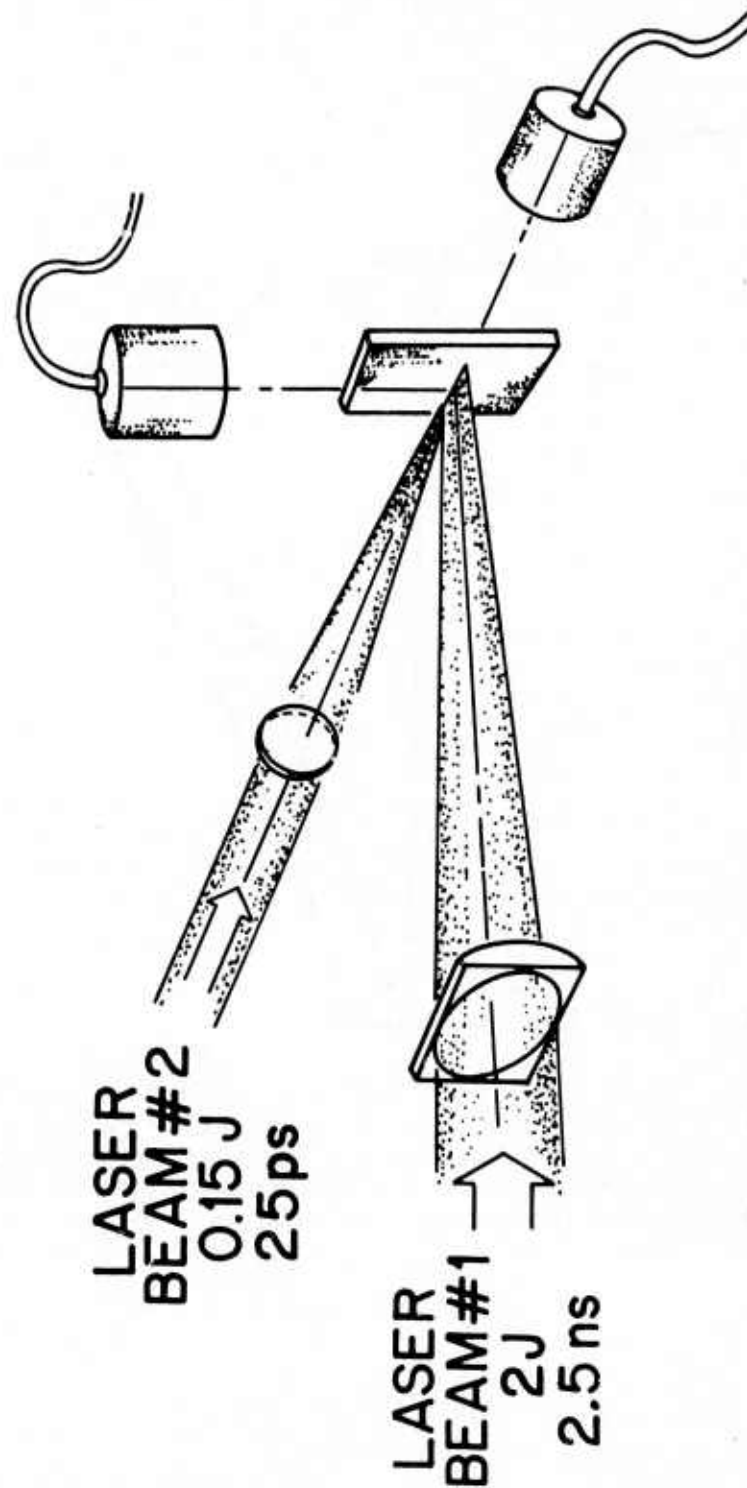


Fig. 11 — Schematic of synchronized dual laser experiment designed to generate population inversions in plasma ions produced by laser beam No. 1 and further heated by beam No. 2

III.A.2. $3s \rightarrow 2p$ LASING WITH HELIUM-LIKE IONS

The $3p \rightarrow 3s$ scheme described above is most promising in the hundreds-of-Angstrom range. For shorter wavelengths, there is a similarly promising $3s \rightarrow 2p$ singlet transition in 2-electron helium-like ions, pumped by electron collisions from the $1s^2$ ground configuration as shown in Fig. 12. For ions in the $Z=12-25$ range, lasing with wavelengths between 12 and 70 Å could be expected. Preliminary modeling as described above has also been extended to such ions and indicates maximum gain coefficients in the $3-15 \text{ cm}^{-1}$ range for temperatures between 2 and 10 keV. Again, the additional processes described above are being included in the modeling for this transitions, and the results will be detailed in the next report. It is worth noting that helium-like ions have already been observed in laser-produced plasmas for Z as high as 22 and in vacuum spark plasmas for Z as high as 29.

A preliminary analysis indicates that the required pumping power densities are not considered to be a problem for these schemes, once the ions are created. A portion of the continuing modeling will be devoted to predicting the feasibility of direct measurement of inverted-level population densities prior to the demonstration of significant net amplification.

III.A.3. EXTENSION OF MODELING TO OTHER SCHEMES

The present modeling has more general application than these two particular schemes. With the inclusion of additional radiative transfer effects it will be convenient to adapt the present numerical program to model a resonance radiation absorption pumping scheme recently proposed^{6,7}. In this scheme, intense resonance line radiation emitted from an ion in a plasma is to be absorbed by a second ion, exciting an electron to a higher lying level from which lasing can take place to a vacant lower level, with subsequent rapid decay to the ground state. This scheme has the attraction of preferential excitation of a particular level and relies on the coincidence of matching transition energies in two ions, several of which have been identified already. Problems such as maximum collection efficiency of the pump radiation and additional effects of collisions have not yet been fully addressed and will be included in the numerical modeling codes.

In the following three sections will be described the current results and status of the dual-laser plasma-heating experiment, as well as plans for investigating the $3p \rightarrow 3s$ and eventually $3s \rightarrow 2p$ laser transitions described above in both the laser plasma and transverse electric discharge devices.

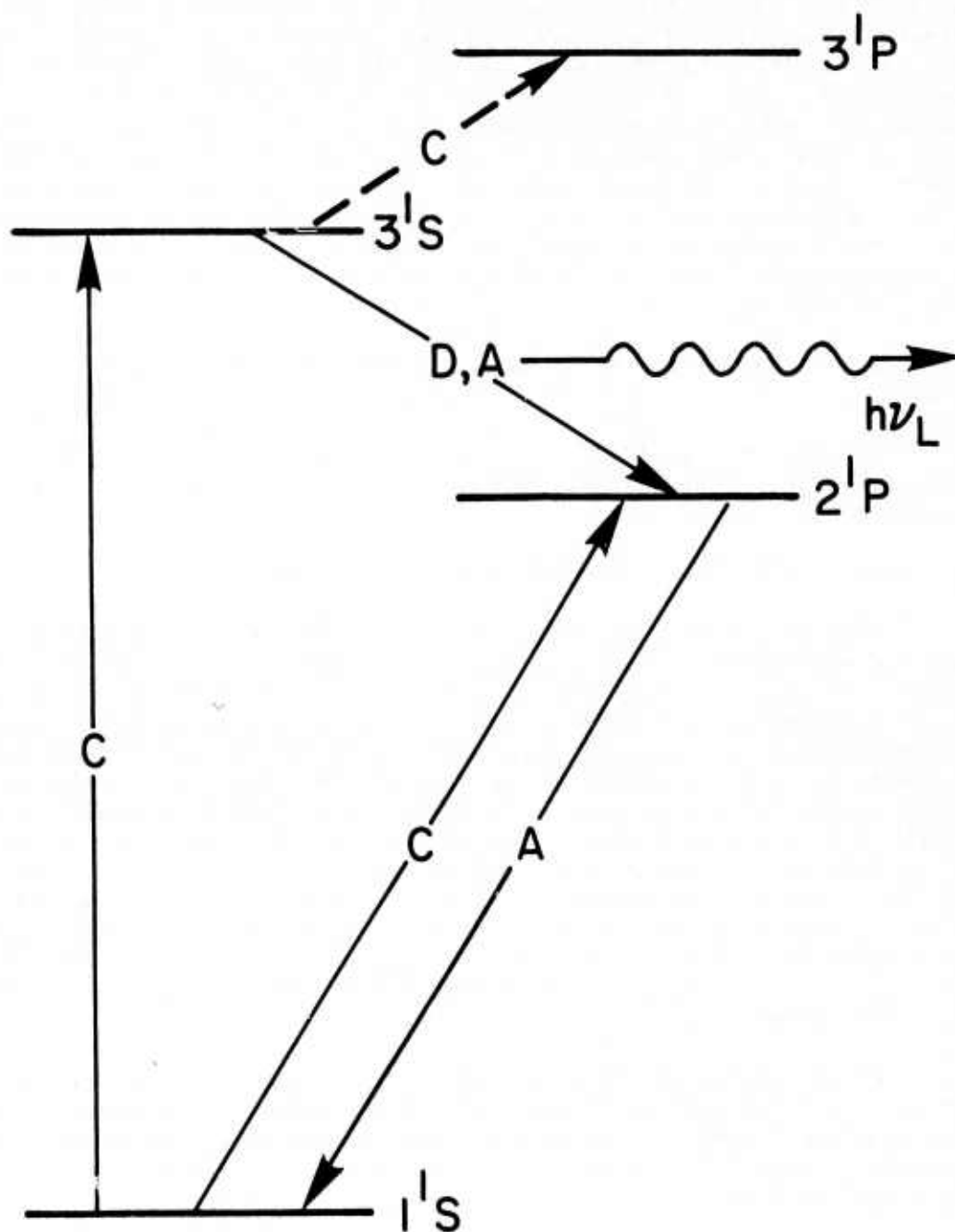


Fig. 12 — Simplified energy level diagram for $3s \rightarrow 2p$ lasing in 2-electron helium-like ions showing the most relevant interaction channels so far included within a specific ion. C, D, and A represent collisional excitation, collisional deexcitation, and radiative decay, respectively. The dashed lines represent alternate upper-level depopulation channels.

REFERENCES

1. R. C. Elton, *Applied Optics* 14, 97 (1975); also NRL Memorandum Rpt. No. 2799 (May 1974).
2. R. C. Elton, in "Progress in Lasers and Laser Fusion," B. Kursunoglu, A. Perlmutter, and S. M. Widmayer, eds., Plenum Publ. Co., New York, 1975.
3. R. C. Elton, in "Proceedings IV International Conference on Vacuum Ultraviolet Radiation Physics" and "Vacuum Ultraviolet Physics," R. Haensch, E. E. Koch, and C. Kunz, eds., Pergamon Press, 1975.
4. R. C. Elton, T. N. Lee, J. Davis, J. F. Reintjes, R. H. Dixon, R. C. Eckardt, K. Whitney, J. L. DeRosa, L. J. Plaumbo, and R. A. Andrews, *Physica Fennica* 9, 397 (1974).
5. R. C. Elton and R. H. Dixon, *Annals New York Academy of Sciences*, 1976.
6. A. V. Vinogradov, I. I. Sobel'man, and E. A. Yukov, *Sov. J. Quant. Electron.* 5, 59 (1975).
7. B. A. Norton and N. J. Peacock, *J. Phys. B.* 8, 989 (1975).

III.B. SYNCHRONIZED DUAL LASER SYSTEM

Before proceeding to a description of recent experiments with the dual laser/plasma experiment shown in Fig. 11, a description of recent progress in development of the laser system is presented.

The laser facility is now operational, and most of the effort in this area has been directed toward application of the system to experiments described in other sections of this report. Construction and characterization has been described in the three earlier semiannual technical reports. To summarize briefly: two Nd:YAG laser oscillators, one mode-locked, the other Q-switched, are synchronized. A single 25-psec pulse from the mode-locked oscillator is produced with variable delays and with a jitter of ± 0.1 nsec with respect to the appearance of a rectangular segment of the Q-switched pulse of duration from 1 to 10 nsec. Both laser outputs are at the $1.064 \mu\text{m}$ Nd:YAG wavelength. The 25-psec pulse is amplified and divided in a Nd:YAG amplifier chain to produce 200 mJ pulses separated by a variable delay. A segment of the Q-switched pulse is amplified in a Nd:glass amplifier chain to an output power level of 10 W. The two lasers are used either synchronized or individually as the experiments require. Laser development performed during this reporting period included the final characterization of the single-mode Q-switched oscillator and the addition of an isolating Pockels cell at the output of the Q-switched amplifier chain.

It was necessary to add the Pockels cell for the plasma experiments. Without the isolation provided, reflections of the laser pulse returned through the amplifiers and damaged the polarizing prism and the Pockels cell in the shutter that selected the segment of the Q-switched pulse (Fig. 13). Damage to optical components ceased with the addition of the isolator. Also, secondary pulses on target and anomalously deep holes drilled in the target by the laser beam were prevented with the isolation installed. Voltage is switched to the isolating Pockels cell when a laser triggered spark gap is fired by a portion of the beam from the Q-switched oscillator (Fig. 13). The isolator shutter stays open for 14 nsec, long enough to allow complete transmission of the Q-switched pulse segment. Light requires 29 nsec to travel the 4.4-m distance from shutter to target and back to the shutter. In that time voltage is again removed from the Pockels cell, and reflections are prevented from entering the amplifier chain.

Single-mode operation of the Q-switched oscillator is desired to provide well-defined pulses for laser plasma studies and to allow maximum amplification, while avoiding damage due to excessive instantaneous intensities. Such single-mode operation was achieved with a short build-up time of 125 nsec, which allows synchronization with the pulse train of the mode-locked oscillator. Frequency selection was obtained with a two-element resonant reflector and a birefringent filter of calcite. The cavity Q was not completely spoiled to allow buildup of quasimonochromatic radiation before the cavity was switched to high Q. The birefringent filter discriminates against widely spaced cavity modes, and it is tunable to the peak of the Nd:YAG fluorescence by rotation of the calcite crystal. The resonant reflector consisted of a flat 45% mirror and a 5 cm thick fused silica flat, with ends parallel to within 3 seconds of arc. The resonant reflector provides discrimination against oscillation on adjacent modes, and its peak reflectivity is tuned to the transmission of the filter by fine adjustment of the spacing of the two elements. This adjustment is provided by a translation stage driven by a differential screw micrometer with resolution of 1/8 wavelength. With proper adjustment, single mode operation was obtained and would last for typically 10 shots before readjustment was required.

It is necessary that the resonant cavity be held stable to interferometric tolerances to maintain frequency selection characteristics. The oscillator is affected by changes in temperature and air pressure. Thermal expansion coefficients for common alloys are typically $20 \times 10^{-6} (^{\circ}\text{C})^{-1}$. To hold the length of a 1-m bench constant to $1/4 \mu\text{m}$ requires a temperature stability of 0.0013°C . A stability of $1/4 \mu\text{m}$ in cavity optical length requires that air pressure be constant to 0.7 Torr and air temperature be constant to 0.3°C . A sealed, temperature controlled enclosure with constant gas density would be required to obtain longer-term stability of single-mode performance. If the Q-switched laser is operated independently, a short build-up time will not be required for synchronization. In the case of independent operation it would be simpler to use a saturable absorber Q-switch. The long

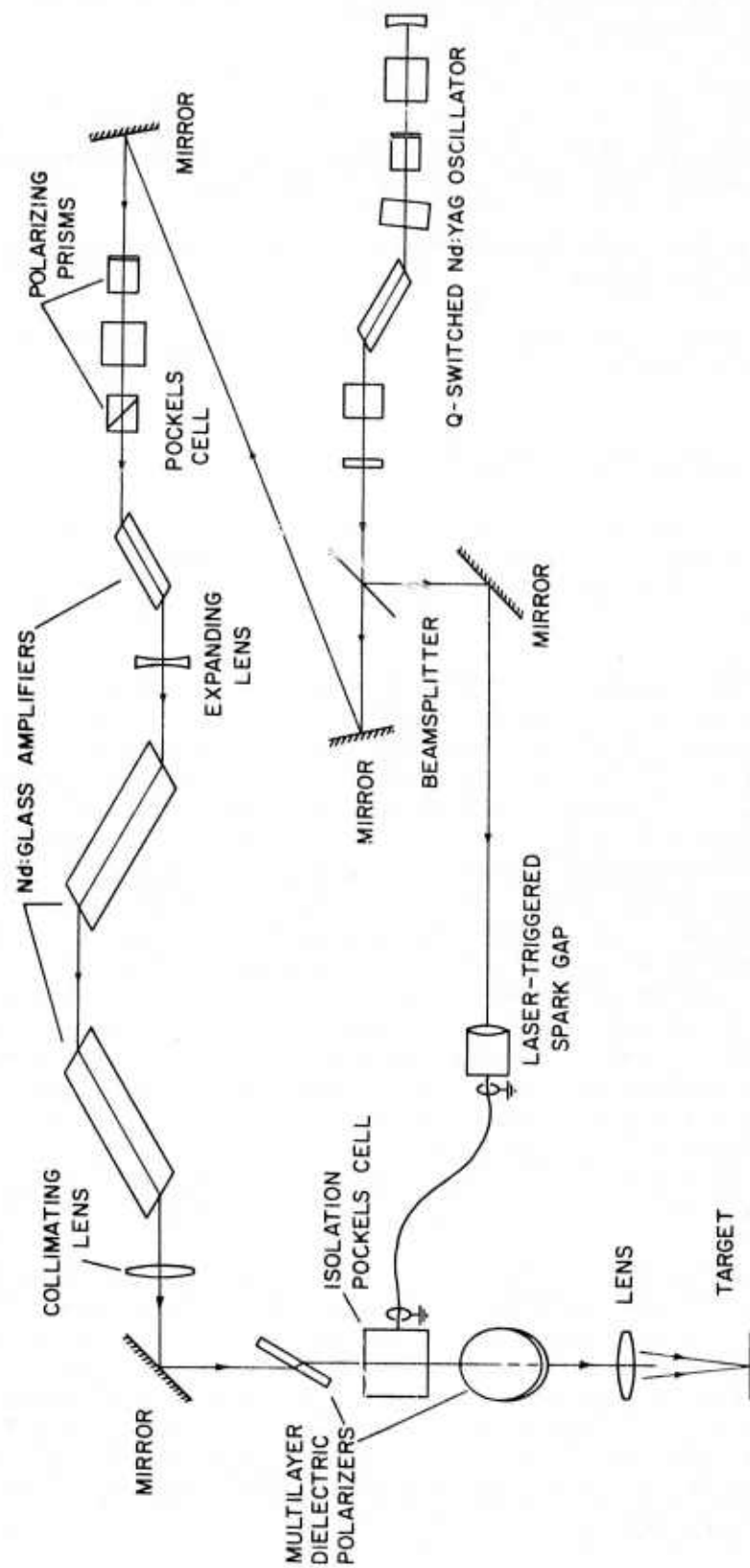


Fig. 13 — Schematic diagram of Q-switched laser used to produce plasmas. Optical components of pulse segment shutter damaged before addition of isolating Pockels cell.

build-up times of these Q switches greatly reduces the problems of frequency selection^{2,3}.

REFERENCES

1. American Institute of Physics Handbook (2nd Edition), New York, McGraw-Hill Book Co., Inc., pp. 6-96, 1963.
2. M. Hercher, "Single-Mode Operation of a Q-Switched Ruby Laser," Appl. Phys. Lett., 7, pp. 39-41, 1965.
3. W. R. Sooy, "The Natural Selection of Modes in a Passively Q-Switched Laser," Appl. Phys. Lett. 7, pp. 36-37, 1965.

III.C. LASER/PLASMA EXPERIMENTS

During this reporting period, the dual-laser system just described was used mainly for plasma measurements (the mode-locked laser alone was also used for analysis of losses in up-conversion as described in Section II.A.).

One of the proposed methods of achieving short wavelength lasing via electron collisional pumping is to make an elongated plasma by focusing a pulse from a Q-switched Nd:glass laser with a relatively long pulse length onto a slab target; and to subsequently inject a second, shorter pulse from a mode-locked laser into the expanding plasma as shown in Fig. 11. The role of the second laser pulse is to heat the expanding plasma rapidly enough to create a high-temperature plasma state which will result in an inverted population in the $n=3$ level (Section III.A.). The Q-switched glass laser pulse should be powerful enough to produce a sufficient number of the desired ionic species of multiply ionized atoms. Several experiments were performed to characterize the expansion of laser-produced plasmas. Pulses of 5-nsec duration and 4J energy from the Q-switched laser were used to produce Mg plasmas which were investigated with VUV spectroscopy. As described in the last semiannual report, spectroscopic data were obtained showing line radiation arising from such ionic species as Mg X and Mg XI in the x-ray region between 7.5 \AA and 9.5 \AA , from Mg III, Mg IV, and possibly a Mg VII $2p^3s \text{ } ^1P - 2p^3p \text{ } ^1D$ transition near 1625 \AA .

This lasing scheme also requires a rather careful selection of the time-when, and the location-in the expanding plasma where the second laser pulse is injected. This restriction results from a combination of a maximum electron density (depending on the element) above which the level coupling becomes collision dominated and, perhaps more importantly, on a sufficiently high density to absorb the pump radiation from the short-pulse laser in a finite plasma length. The last condition implies densities approaching the "critical" value as described in Section III.A. above.

It is therefore essential to have detailed information on the characteristics of the expanding plasma, including the electron density profile as a function of time. Unfortunately, no previous work in this direction has been made, particularly for the case of the line focus. The purpose of the present study is to obtain such experimental data with high spatial ($\sim 10 \mu\text{m}$) and temporal ($\sim 5 \times 10^{-10}$ sec) resolution. One way of achieving such a goal is to use a micro-interferometric technique¹ which allows one to probe the plasma with spatial resolution much smaller than the focal spot size ($50 \mu\text{m}$ for the point focus). Because of the high streaming velocity ($v \sim 3-4 \times 10^7$ cm/sec) of the expanding plasma, the spatial resolution of the required magnitude can only be obtained with probing pulses lasting less than 100 psec.

The experimental arrangement² is shown schematically in Fig. 14 where the focusing optics for the Q-switched laser beam, the probing laser beam, and the interferometer are indicated. A simple Jamin-type interferometer is placed inside the target vacuum chamber, with the probing laser beam passing parallel to the target surface and transverse to the Q-switch glass laser beam. The 30 ps, mode-locked Nd:YAG laser which is frequency doubled ($\lambda = 0.53 \mu\text{m}$) through a KDP second harmonic generating (SHG) crystal is utilized as a probing beam, and the interferometric image is photographed through a 10 X telescope on ASA-3000 speed polaroid film. With the present arrangement, the spatial resolution of the interferogram is limited at about $10 \mu\text{m}$ by both the length of the probing pulse and the imaging optics. The arrangement (see Fig. 15) for the synchronization of the Q-switched laser and the mode-locked laser is described in the previous semiannual reports. The plasma is generated from either a point ($\approx 50 \mu\text{m}$) or a line focus of the Q-switched glass laser at three different pulse lengths of 1.5 ns, 2.5 ns, and 5.5 ns and at power levels of about 1 GW. The targets used in the experiment are slab targets of aluminum (1 mm, 0.25 mm, and 0.025 mm thick), magnesium, and polyethylene.

Figs. 16 (a and b -- enlarged for detail) show interferograms from a 0.25 mm Al target irradiated with a point focus and a 2.5 ns pulse duration. The time evolution of the plasma expansion is obtained with separate shots by varying the delay time between the main laser pulse and the probing laser pulse. The delay times shown in the figures are measured from the 10% point on the rise of the Q-switched laser pulse. As can be seen, during the early phase of the expansion (≤ 0.3 ns) the plasma is a well-defined hemispherical shell with a diameter roughly the same as the focal spot size. It expands rapidly outward until the cessation of the Q-switched laser pulse. The boundary of the opaque region corresponds to the region of high electron density gradient, where the probing laser beam is deflected out of the telescope due to a large refraction in the plasma. After the cessation of the laser pulse, the expanding plasma front becomes increasingly diffused and the shell (opaque region) flattens and expands parallel to the target surface. Figs. 17 (a, b, and c) show similar interferograms obtained with a line focus on a Mg target, where the axial as well as side view of the

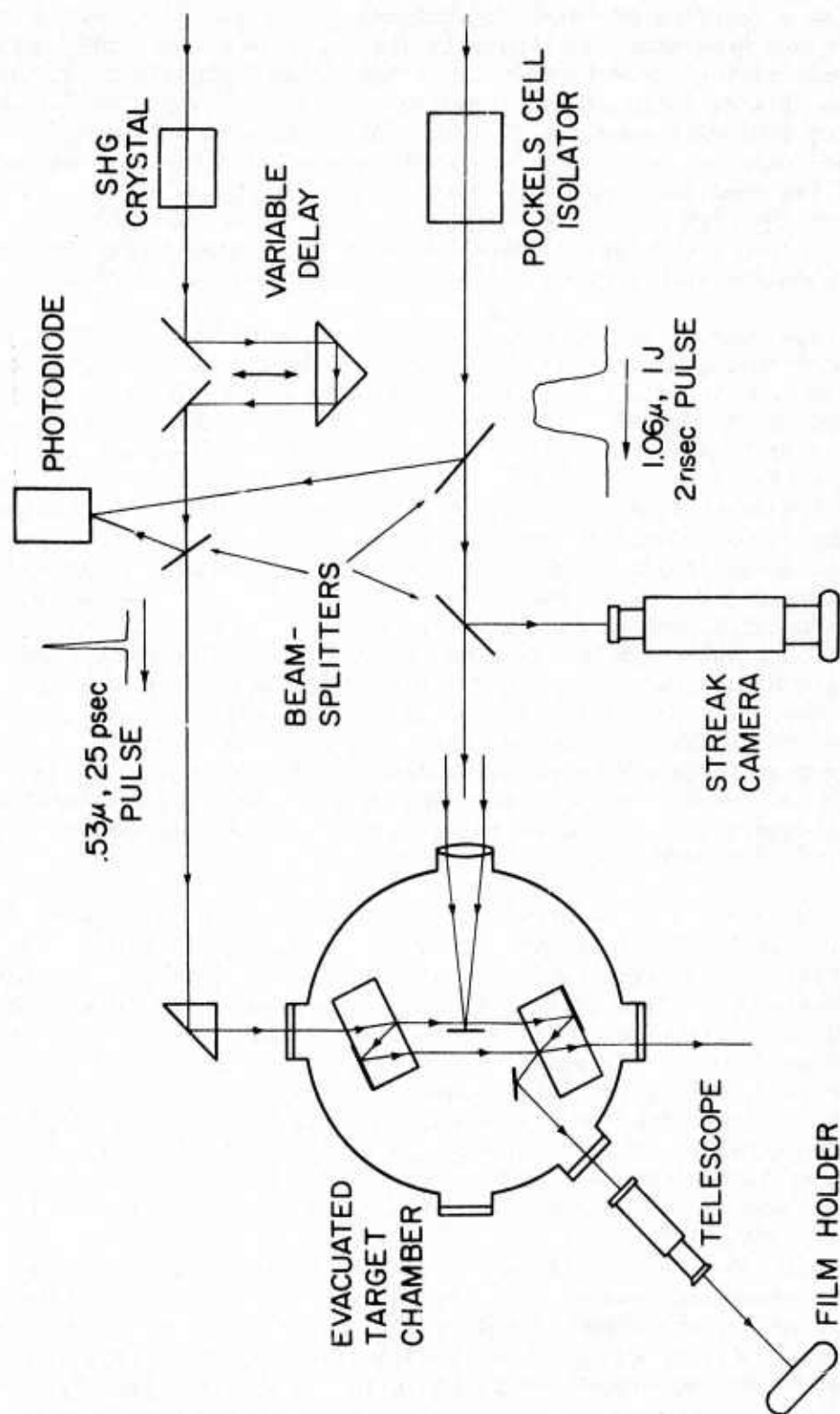


Fig. 14 — Schematic diagram showing laser focusing optics, frequency doubled ($\lambda = 0.53 \mu\text{m}$) probing laser beam, Jamin-type interferometer, and recording system

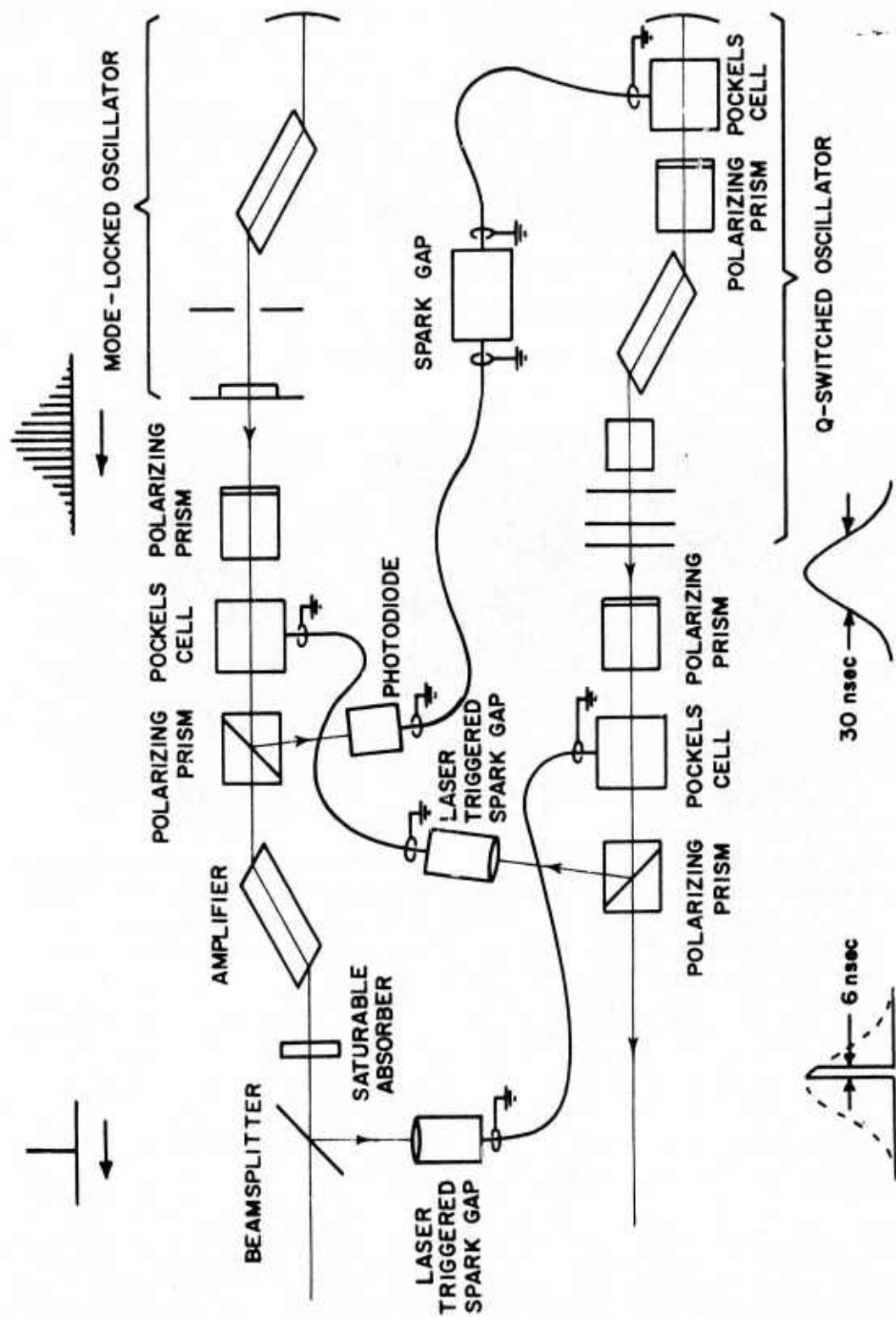


Fig. 15 — Synchronization scheme between Q-switched Nd:glass laser and 30 ps, mode locked Nd:YAG pulse (probing laser)

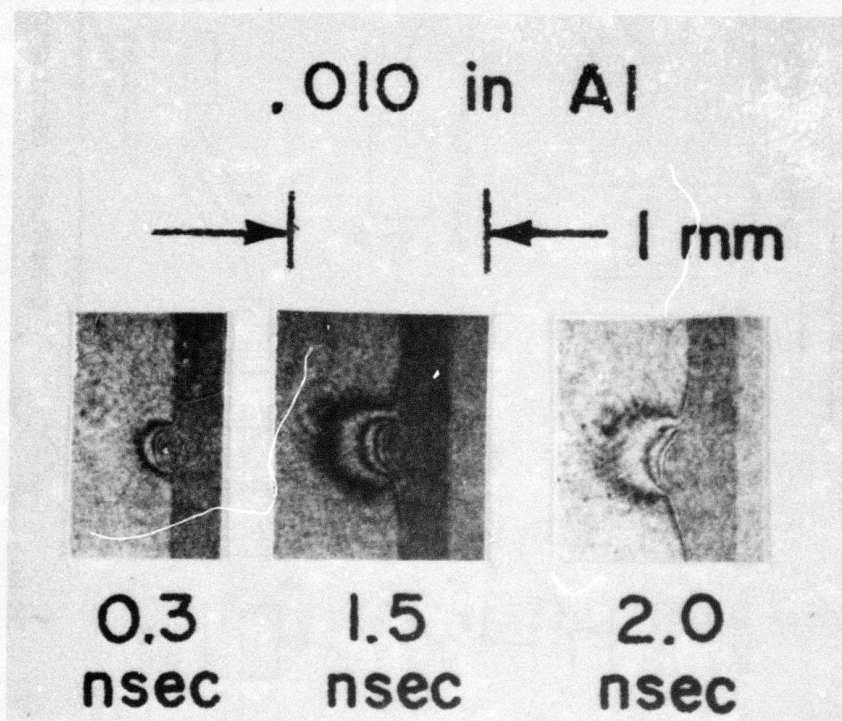


Fig. 16(a) — Interferograms (with no background fringes) showing time evolution of expanding plasma. The plasma is produced by irradiating a 0.25 mm Al-target with a point focus and with a 2.5 ns laser pulse duration. The time sequence is obtained with separate shots by varying the delay time between the main laser pulse and the probing laser pulse.

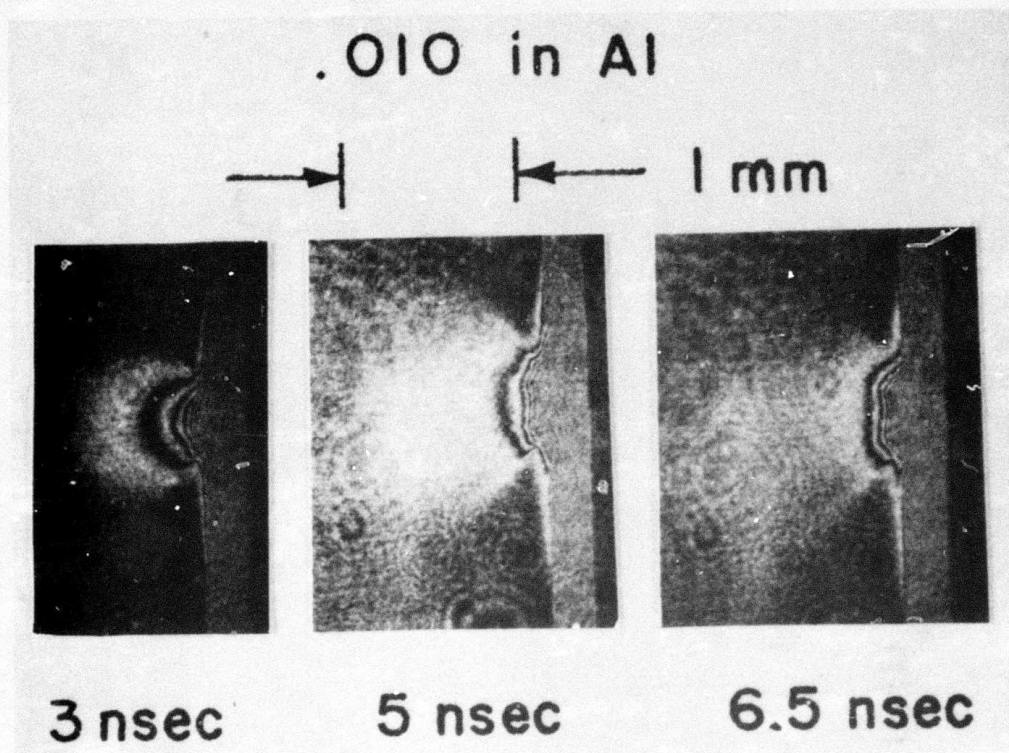
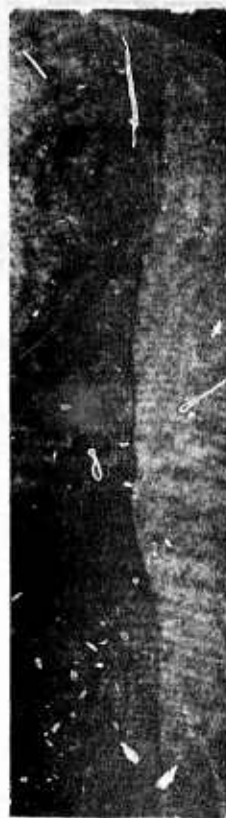


Fig. 16(b) — Interferograms (with no background fringes) showing time evolution of expanding plasma. The plasma is produced by irradiating a 0.25 mm Al-target with a point focus and with a 2.5 ns laser pulse duration. The time sequence is obtained with separate shots by varying the delay time between the main laser pulse and the probing laser pulse.

1 mm Mg



0.3 nsec

0.8 nsec



1.5 nsec



Fig. 17(a) — Interferograms obtained with a line focus on a Mg target, where axial as well as side view of the elongated plasma are recorded. The interferograms taken along the axial view have background fringes.

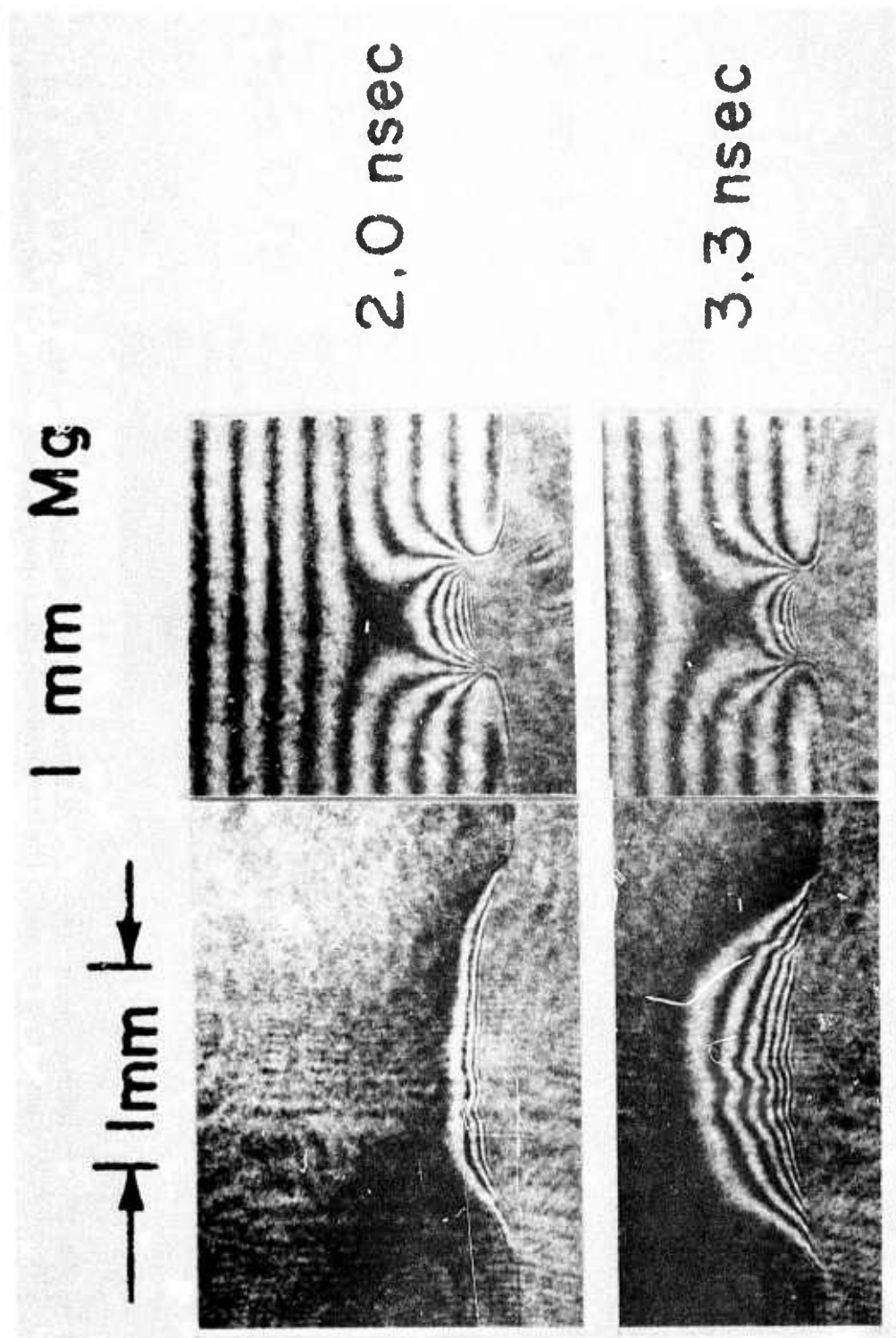


Fig. 17(b) — Interferograms obtained with a line focus on a Mg-target, where axial as well as side view of the elongated plasma are recorded. The interferograms taken along the axial view have background fringes.

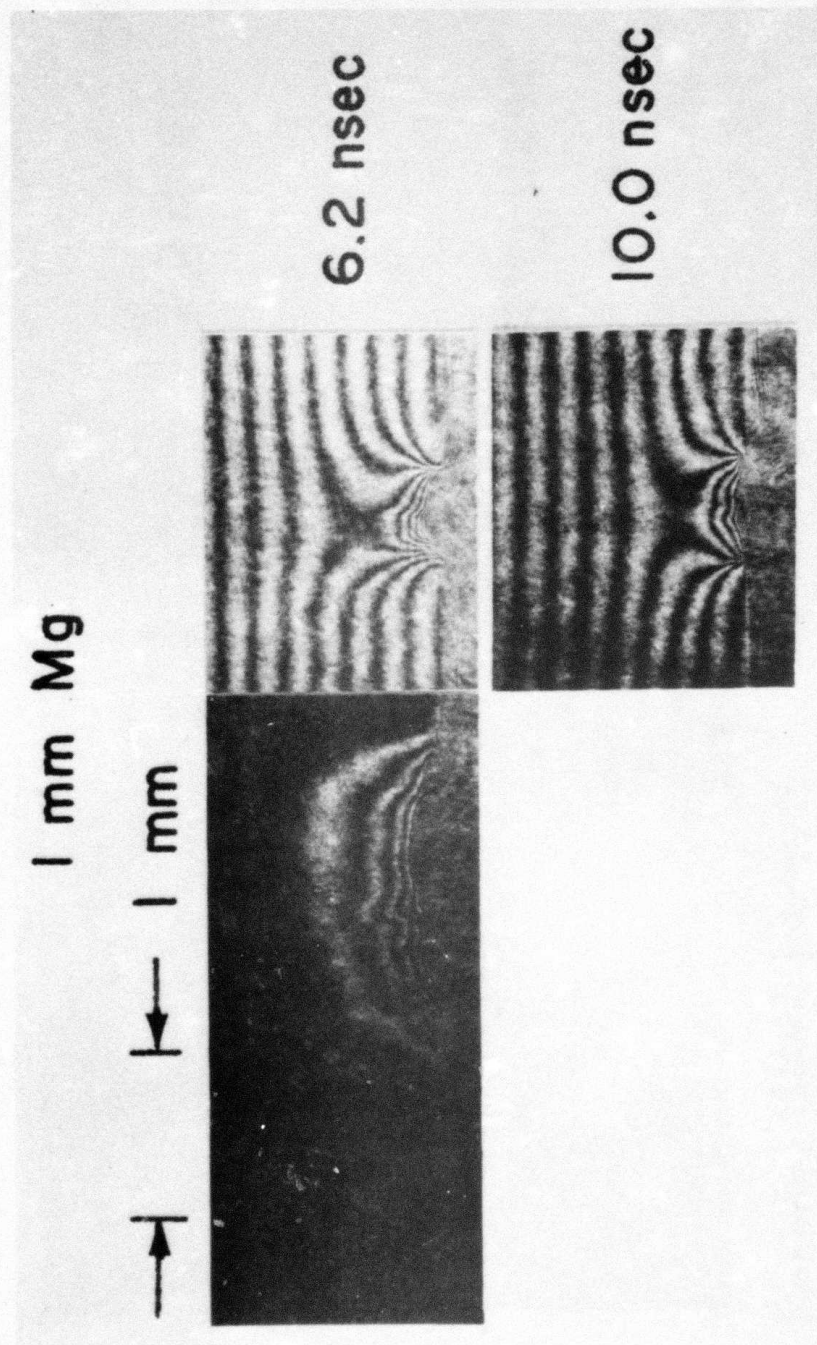


Fig. 17(c) -- Interferograms obtained with a line focus on a Mg-target, where axial as well as side view of the elongated plasma are recorded. The interferograms taken along the axial view have background fringes.

elongated plasma are recorded. The interferograms taken along the axial view have background fringes, allowing time- and space-resolved electron density measurements to be made. The electron density of the expanding cylindrical plasma is plotted as a function of distance away from the target surface at various time delays in Fig. 18. Since the plasma is considerably elongated along the line of sight compared with its width, a vigorous Abel inversion of the experimental points is not required for the present study. As can be seen, the electron density gradient of the plasma front is fairly steep at the early stage of the expansion, but the front becomes quickly diffused as time elapses, particularly after the end of the laser pulse. As mentioned earlier, the maximum electron density measurable is limited to value of about 2.5×10^{19} electrons/cm³ due to the steep electron density gradient at a distance about 100 μ m from the target. Note that there is nearly a two orders-of-magnitude difference in electron density at this location and the critical ($\sim 10^{21}$ cm⁻³) surface. The lower limit of the measurable electron density ($\sim 10^{18}$ cm⁻³) on the other hand is determined by the minimum detectable fringe shift ($\sim 1/4$ fringe). In Figs. 19 through 21, the location of extreme detectable edge of the plasma is plotted as a function of time for three different Q-switched pulse lengths. The electron density at this position is roughly constant ($\sim 10^{18}$ cm⁻³). The following conclusions can be derived from such experimental data:

- 1) The acceleration of the plasma takes place at very early times (< 200 psec) and within a very short distance from the target (≤ 50 μ m).
- 2) The velocity of the iso-density front remains nearly constant during the duration of the laser pulse (except in the case of the longest pulse duration) and the measured velocity [$(3.5 - 4) \times 10^7$ cm/sec] is apparently independent of the laser power density ($10^{11} - 10^{13}$ watts/cm²), the laser pulse length (1.5 - 5.5 ns), and the target material.
- 3) In the case of a very thin target (Al: 250 μ m and 25 μ m thick) the iso-density front contracts rapidly towards the target as soon as the laser pulse ceases.
- 4) In the case of the polyethylene target (~ 2.5 mm thick) the velocity seems to remain constant ($\sim 3.5 \times 10^7$ cm/sec) until well after the laser pulse.
- 5) The plasma produced by the line focus remains relatively stable and free of macroscopic plasma instabilities during and well after the duration of the laser pulse.

REFERENCES

1. D. T. Attwood and L. W. Coleman, Appl. Phys. Lett. 24, p. 408, 1974;
D. T. Attwood, L. W. Coleman, and D. W. Sweeney, Appl. Phys. Lett. 26, p. 616, 1975.

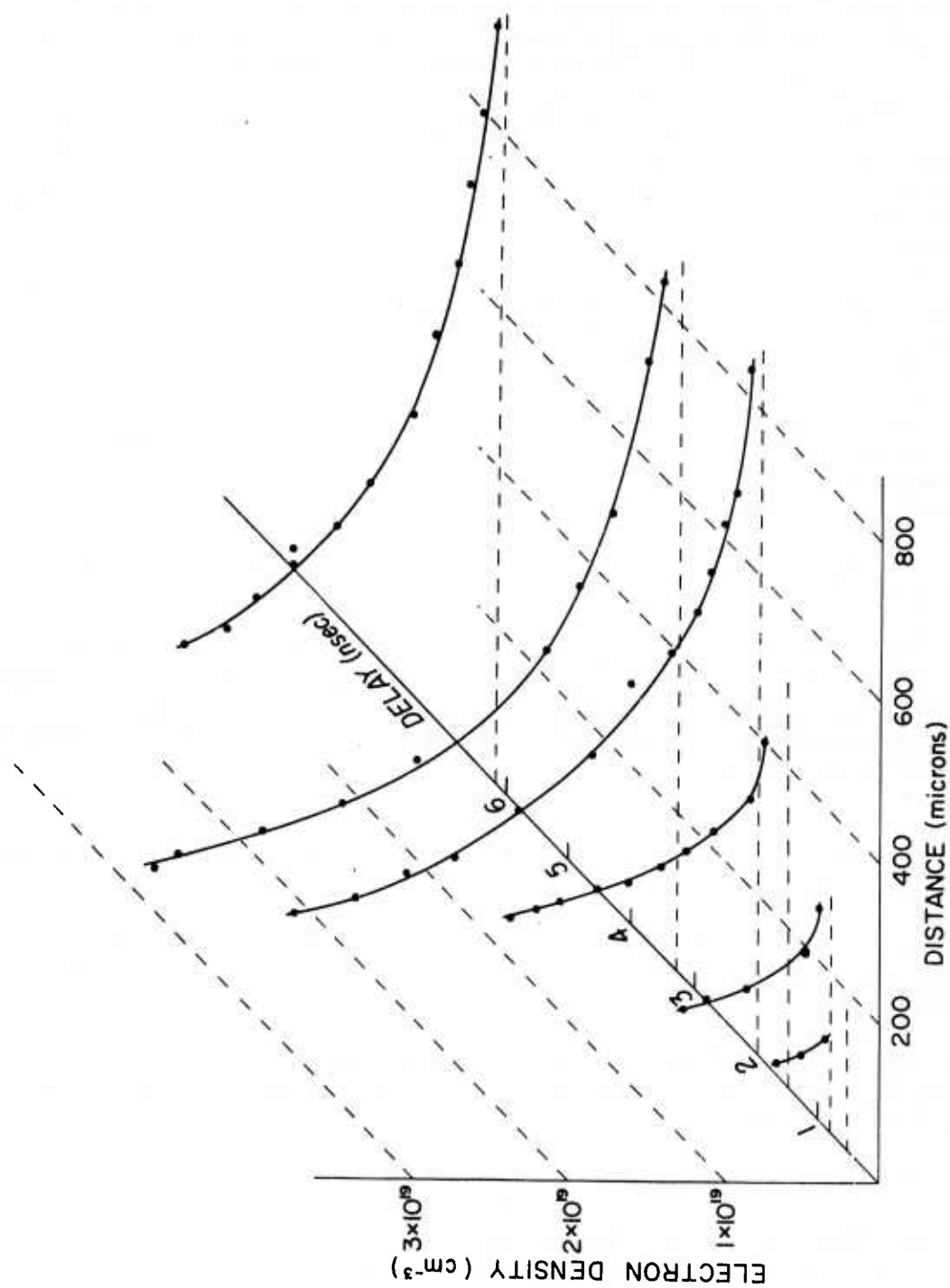


Fig. 18 — Electron density distribution of the expanding cylindrical plasma as a function of distance at various time delays

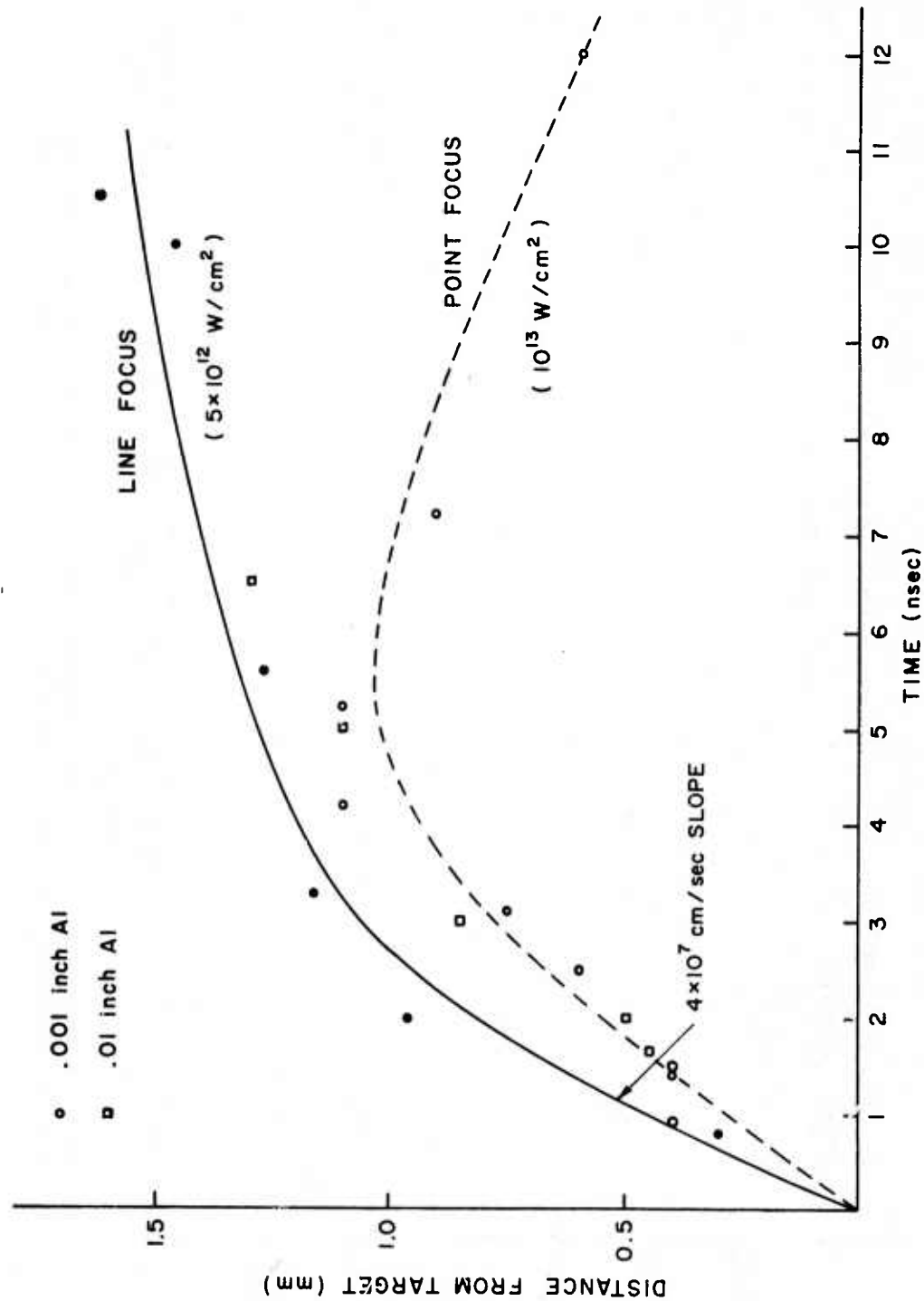


Fig. 19 — Location of iso-electron density front ($\sim 10^{18}/\text{cm}^3$) as a function of time. The duration of the main laser pulse is 2.5 ns and plasmas are produced by line focus onto a 0.25 mm Al-target and by a point focus onto a 0.25 mm Al-target, respectively.

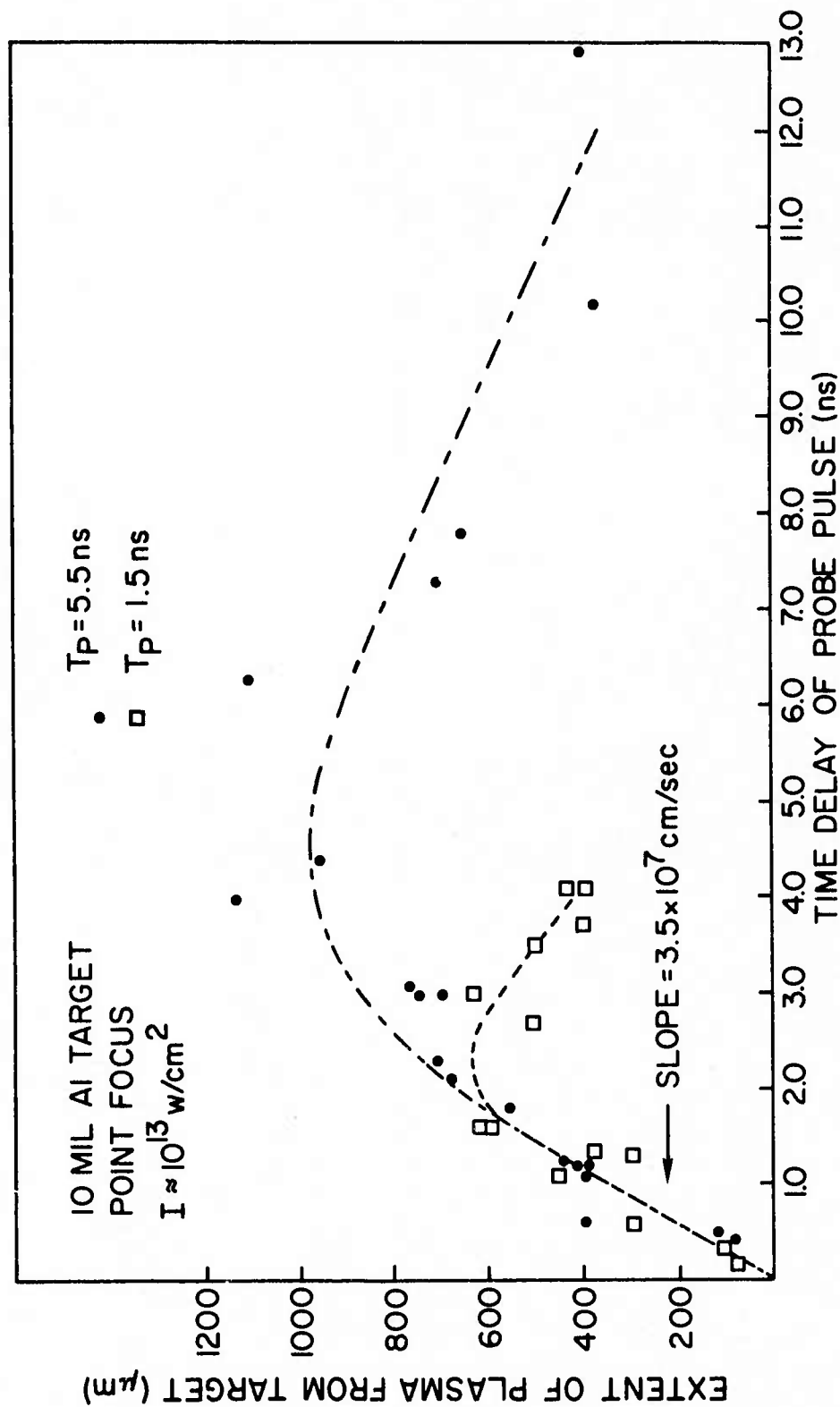


Fig. 20 — Iso-electron density front of expanding plasma as a function of time. A 0.25 mm Al target is irradiated by a point focus of 5.5 ns and 1.5 ns main laser pulse, respectively.

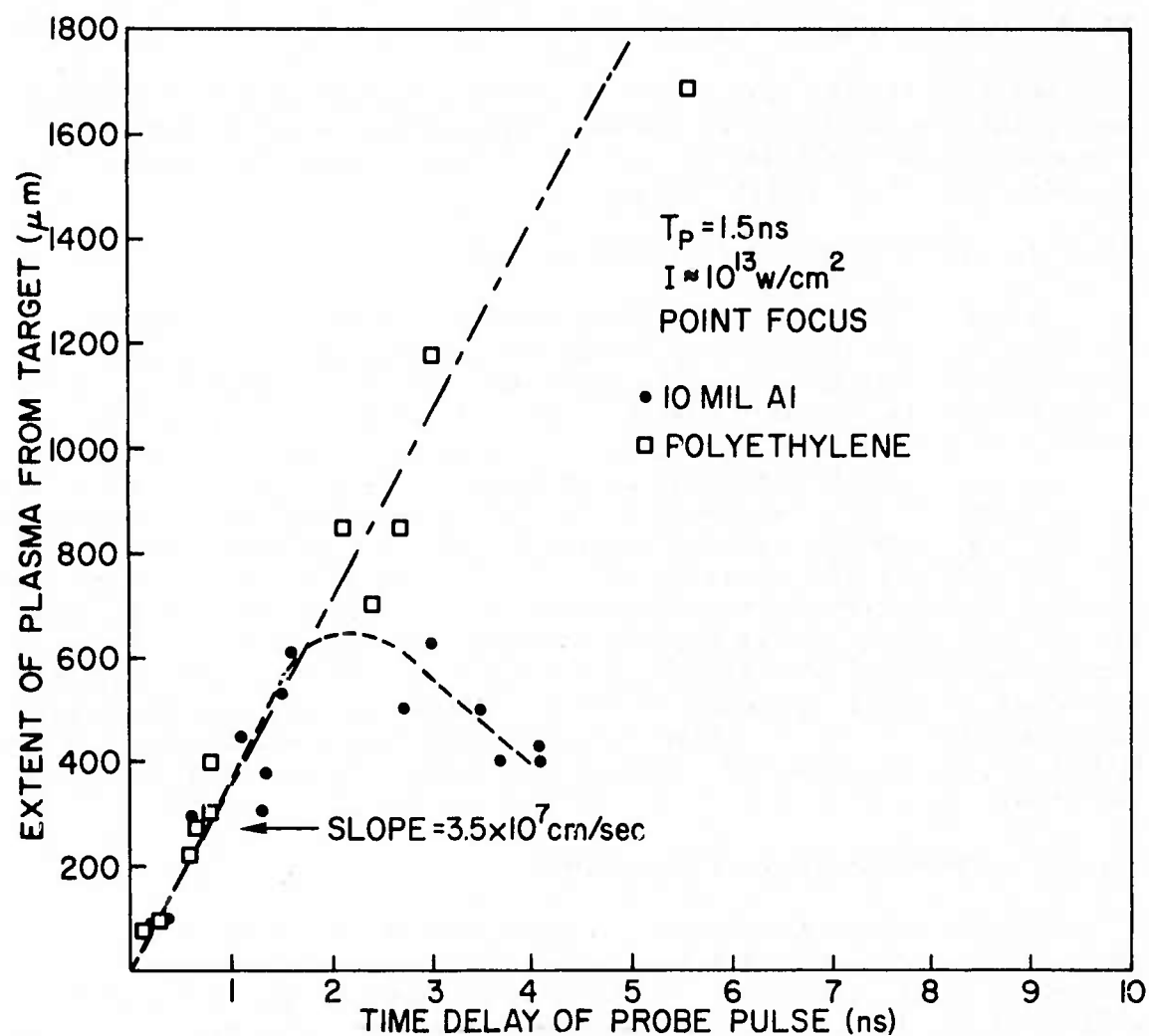


Fig. 21 — Iso-electron density front of expanding plasma as a function of time. The 0.25 mm Al and polyethylene targets are irradiated by the 1.5 ns main laser pulse.

2. J. F. Reintjes, T. N. Lee, R. C. Eckardt, R. C. Elton, and R. A. Andrews, Bull. Am. Phys. Soc. 20, p. 1336, 1975; also Bull. Am. Phys. Soc. 21, 1976 (Proc. APS Topical Conf. Plasma Diagnostics).

III.D. PLANS AND ALTERNATIVES

While it is still premature to attempt to pinpoint either a single most promising transition or the best experimental approach and conditions for electron collisional pumping, a brief summary of current thinking is perhaps in order at this point.

III.D.1. TRANSITIONS AND OPERATING REGIMES

The two schemes currently being modeled as described in Section III.A. above, namely $3p \rightarrow 3s$ and $3s \rightarrow 2p$, are representative of typical vacuum-UV and soft x-ray possibilities and possess the additional attraction of potential quasi-cw operation and extrapolation from existing near-UV lasers. They appear to be appropriate test cases for modeling "conventional" electron-collisional pumping at least. The results derived to date are probably most reliable for the $3p \rightarrow 3s$ transition in the vacuum-UV region at "moderate" plasma densities ($\sim 10^{17} \text{ cm}^{-3}$), where resonance trapping and collisional mixing effects can be minimized and, perhaps, an enhanced electron temperature (compared to ion temperature) can be maintained for a useful lasing period, yielding even high gain. At higher densities, the analysis becomes more complex as such additional effects are added and the full impact is not yet known. The most recent modeling described above is at very high "critical absorption" densities ($\sim 10^{21} \text{ cm}^{-3}$), and it is possible that some intermediate value will prove to be most promising.

III.D.2. LASER/TARGET PRODUCED PLASMAS

From the extensive diagnostic experiments described in Section III.C. above, it appears clear that small, cylindrical plasmas created by vaporization of target material by a focused high-power laser beam are best defined at density greater than 10^{19} cm^{-3} , a regime where further modeling will be necessary to fully access the potential in a freely expanding plasma of this sort. It is also clear now that further impulse heating would have to be performed near a normal to the target surface plane rather than transverse (axially) as indicated in Fig. 11, since significant absorption only occurs in the 10^{20} - 10^{21} cm^{-3} density range very close to the target surface in a high gradient region. It would be extremely difficult to align and synchronize a narrow beam with a uniform layer in such an orthogonal configuration. It is with these thoughts in mind that the analysis described in Section III.A. above are underway at a density of 10^{21} cm^{-3} .

III.D.3. TRANSVERSE DISCHARGE DEVICE

Electrons have a much shorter absorption length than photons and are more attractive for plasma heating at moderate densities ($\sim 10^{17} \text{ cm}^{-3}$). A transverse excited traveling wave discharge device such as developed at NRL for H_2 lasing operates in this density region over lengths of 1 meter or more, and should be considered further for electron-pumped ion laser development. An encouraging factor here is a past observation of CIV emission at low pressures, probably initiated by surface discharge vaporization. There was also evidence of net gain on the $2p \rightarrow 2s$ resonance lines (near 1500 \AA) of this C^{3+} species. It is therefore planned for the next reporting period to further study ion production in this device, with one goal being the achievement of $3p \rightarrow 3s$ lasing. Initial studies will concentrate on reproducing the C IV results with increased supporting diagnostics, on ascertaining the axial distribution of emission, and on comparing with other carbon-line emission. An understanding of the mechanism for amplification on the C IV lines observed would be of immense importance, both for the possibility of isoelectronic extrapolation of lasing to shorter wavelengths and for the very fundamental process of inverting a resonance transition involving a lower ground state of an ion.

III.D.4. SUMMARY

In summary, current high density modeling will determine the future direction of laser/target plasma experiments for electron-collisional pumping. Reactivation of the transverse discharge device at low pressure operation with improved diagnostics will ascertain the desirability of proceeding with and expanding future efforts in direct discharge heating for this basic pumping scheme.

REFERENCE

1. R. W. Waynant, Appl. Phys. Letters 22, 410 (1973).

IV. RESONANT CHARGE TRANSFER PUMPING

Ion-atom collisions in which the resonant charge transfer process predominates have been discussed in previous reports for this program and elsewhere^{1,2,3} and particularly promising ion-atom combinations have been cited. The initial experiment to determine enhanced level populations of specific spectral lines is diagrammed in Fig. 22. The 6 Joule, 20 nsec laser pulse is point focused onto the carbon target to obtain the maximum laser beam energy density. Analysis of the laser plasma emission as it expands into a background gas is primarily done using spatially-resolved grazing-incidence spectra.

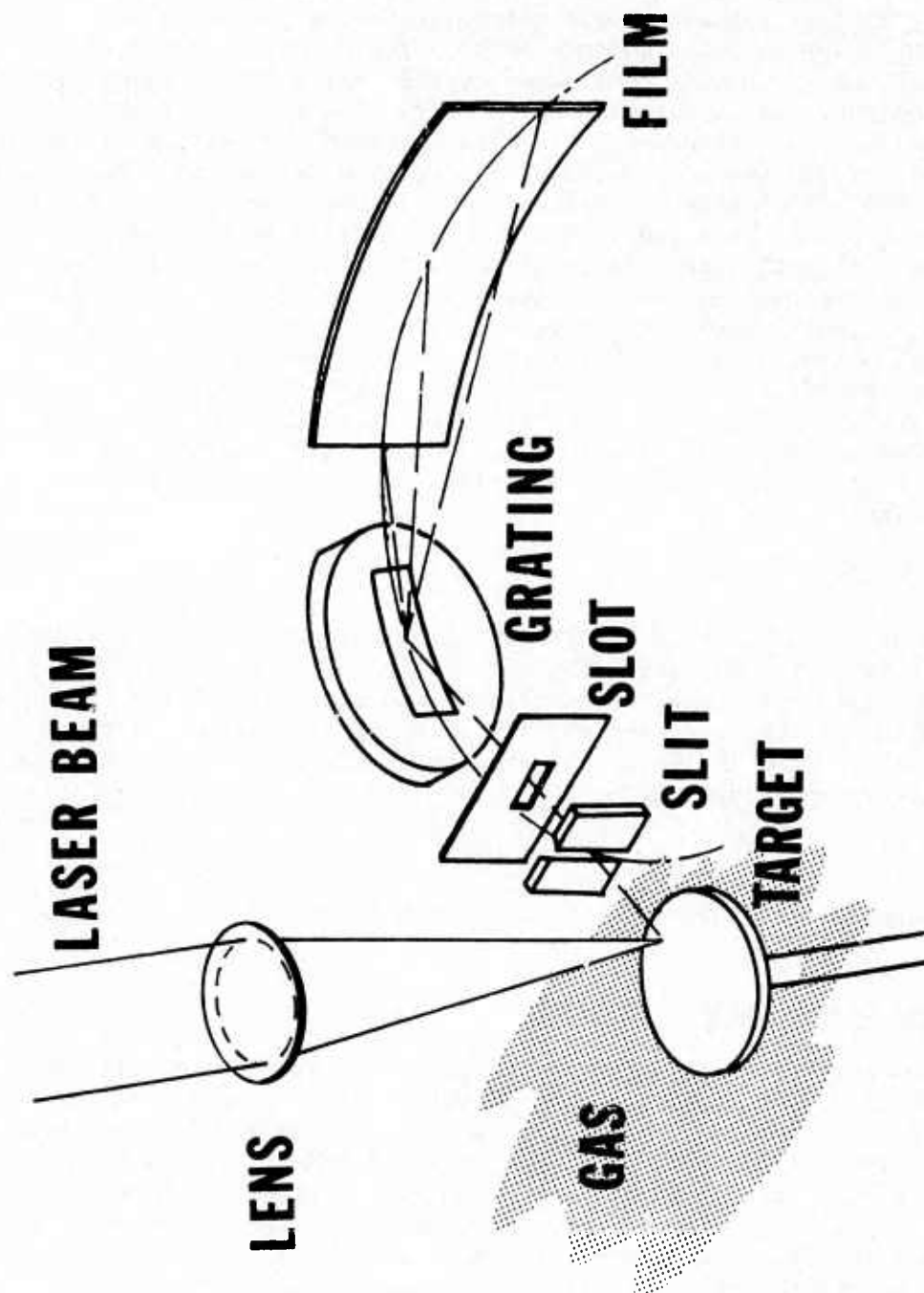


Fig. 22 — Schematic diagram of the point focus NRL resonance charge transfer experiment, including the main features of the grazing incidence vacuum spectrograph. The horizontal slot provides spatial resolution perpendicular to the target surface. The prism and normal incidence grating spectrographs observed the plasma from a position diametrically opposite the grazing incidence spectrograph slit.

IV.A. SOFT X-RAY SPECTRA

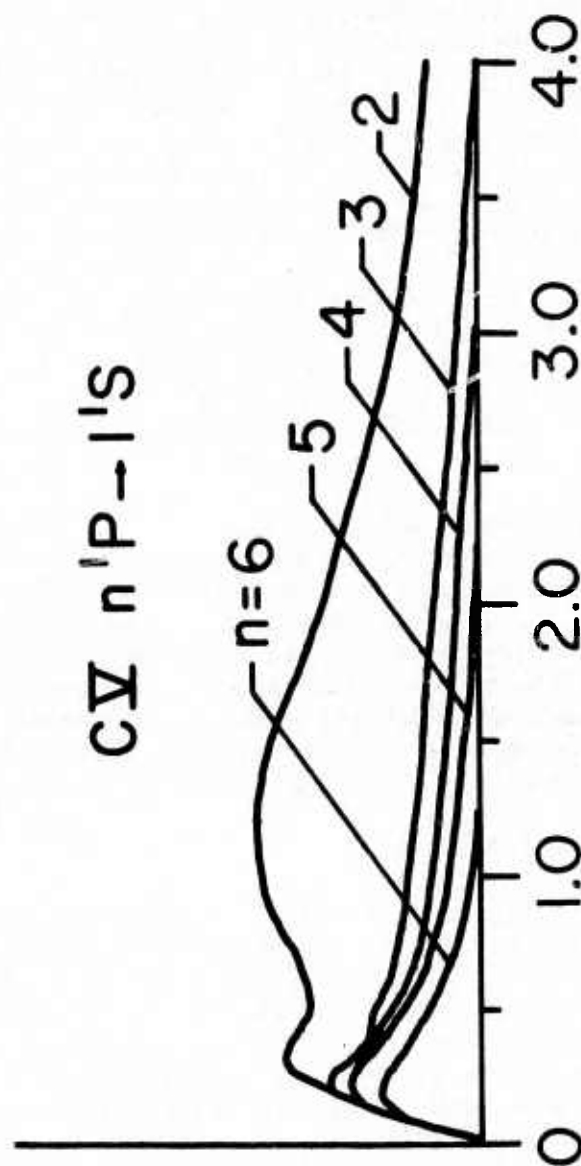
Enhanced level populations will be determined by comparing line ratios obtained with a background gas to line ratios obtained in a vacuum. In order to facilitate this determination, and as a check on the reproducibility of the experiment, a plot of photographic density vs. distance from target was generated for the CV $n^1P \rightarrow 1^1S$ series in vacuum. These plots are shown in Fig. 23 (and can be converted to exposure vs. distance). The curves will be adjusted as additional vacuum data become available; however, their basic features are expected to remain intact. At distances greater than 0.8 mm, the total line intensity ratios scale approximately as expected, particularly for those lines associated with transitions originating on levels with principal quantum number $n \geq 3$. The $2^1P \rightarrow 1^1S$ first resonance line appears to have an enhanced emission which may be associated with a correspondingly higher oscillator strength compared to the other lines of the series. In the region below 0.8 mm a deviation from the normal intensity probably results from reabsorption caused by opacity effects. These curves are used to establish the vacuum line-intensity ratios for comparison with the background-gas line-ratios.

Grazing incidence spectra of the laser plasma formed at the surface of a carbon target have now been obtained³ with and without helium background gas. The analysis remains inconclusive at this point because the CV $n^1P \rightarrow 1^1S$ ($n=3,4,5$) lines are very weak in the region of interest (see IV.B. below) and are below the linear range of the emulsion density-exposure characteristic curve. Plans are now underway to move the target closer to the entrance slit for better x-ray collection. Also, laser reproducibility is being checked in anticipation of having to take more shots per plate exposure.

IV.B. VISIBLE HELIUM SPECTRA

In addition to the grazing incidence spectrograph, both prism and grating spectrographs were set up to observe the visible region of the laser-plasma emission. These were stigmatic instruments whose main purpose was to determine the ratio of neutral helium to He^+ ion concentration, especially around the plasma density region ($\leq 10^{19} \text{ cm}^{-3}$) where charge transfer is expected to be observed.⁴ Extrapolation of data from a similar experiment⁴ indicates this density region occurs around 2 mm from the target surface. An excess of He^+ ions in this region would indicate a depletion of carbon ion-neutral helium charge transfer reactions. In Fig. 24 portions of the visible spectra obtained using a carbon target are shown with tentative line identifications. The top spectrum was taken with a stigmatic prism spectrograph. Because of the limited resolution of the prism instrument at longer wavelengths, a portion of the spectrum was observed with a 0.75 m grating spectrograph. This spectrograph produced the middle spectrum of the figure. In order to isolate the HeII 686 Å line from nearby carbon emission, the bottom spectrum was taken through the grating instrument using a boron-nitride

PHOTOGRAPHIC DENSITY



DISTANCE FROM TARGET [mm]

Fig. 23 — Photographic density versus distance from target taken from a space-resolved grazing incidence spectrum for the CV resonance series. This spectrum was taken with no background gas.

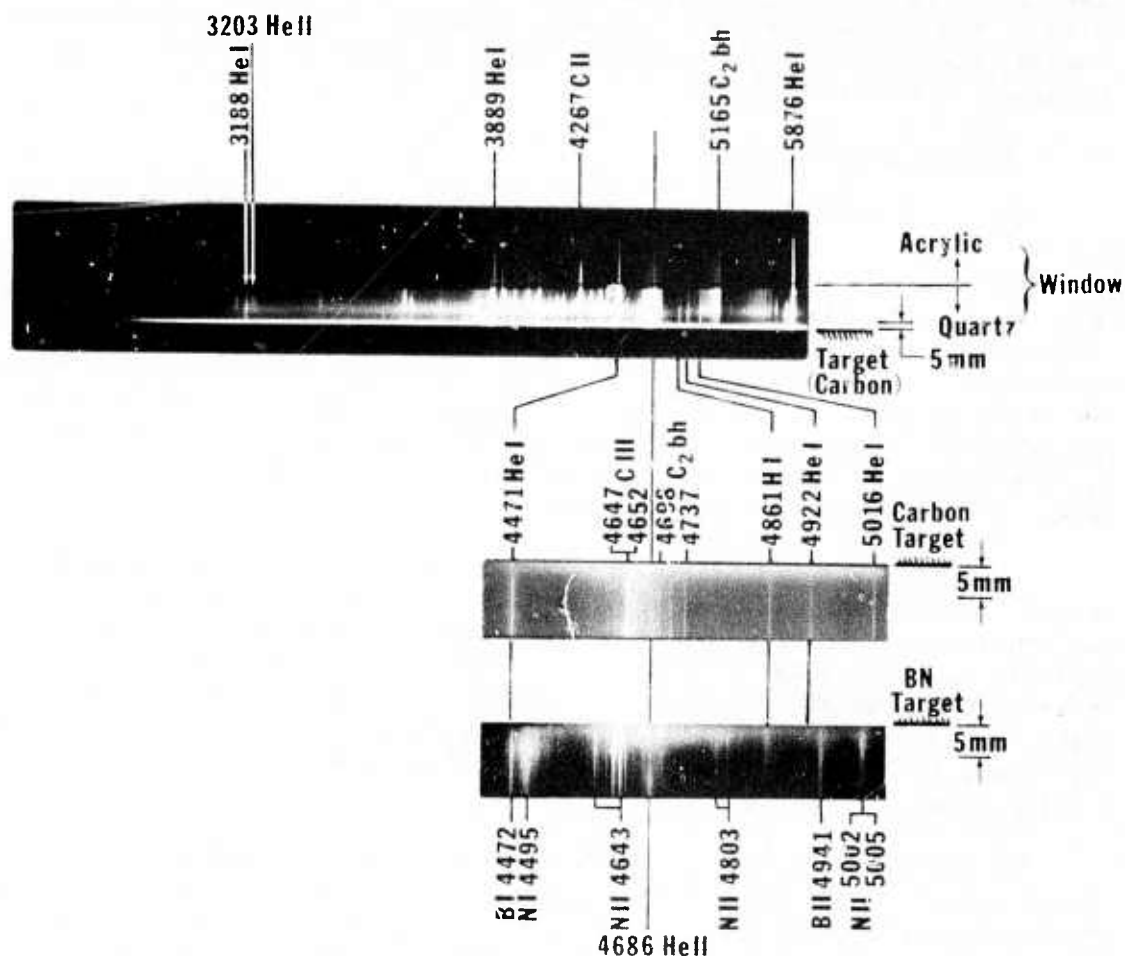


Fig. 24 — Spectra of the visible/near-UV emission from a laser-target plasma immersed in a 20 Torr He background gas. The top spectrum was taken with a quartz prism spectrograph which observes 59 mms of the plasma, both through the acrylic plexiglass chamber wall and also through a quartz window. The second and third spectra were taken using a normal incidence grating spectrograph with a linear plate factor of 11 Å/min. In the bottom spectrum a boron nitride target was used; the top two spectra were taken with carbon targets. Emphasized here is the presence of two He⁺ ion lines (He II) at distances greater than 4 mm from the target surface.

target. Although preliminary observations indicate a weak He^+ (and strong neutral helium) concentration beginning several millimeters away from the target, and a minimum amount of He^+ within 5 mm of the target, a conclusive determination of the location of He^+ ions will be obtained when the HeII lines are completely identified and analyzed. This identification process is now in progress. Note also in Fig. 24 that many of the neutral helium lines (at 4471 Å, for instance) continue into the continuum surrounding the target, indicating the strong presence of neutral helium throughout the plasma region.

IV.C. PLASMA DIAGNOSTICS

Line identification of the carbon target spectrum, especially the impurity line emission, is helpful in obtaining the plasma temperature in spatially resolved regions. This line analysis is continuing, and determination of several persistent impurity lines in the grazing incidence spectrum (which have been observed but not identified in other experiments) have been made. These lines have now been identified with 3→2 transitions in a lithium-like Na^{8+} impurity ion. They occur in the region of the plasma near the target and indicate a plasma temperature in that region of around 100 eV, consistent with the appearance of strong C^{5+} ion lines in the same area.

A knowledge of the plasma density in the very dense, near-target region would be extremely helpful in several respects. Information on the density in this area can be extrapolated to greater distances by relative line broadening measurements. Also, the space-resolved soft x-ray spectra can yield valuable information on the critical density layer for the electron-collisional pumping research described in Section III above, and possibly for the resonance-line absorption scheme to be modeled soon.

Two surprising features of the soft x-ray carbon spectra, besides the relatively weak $2^1\text{P} \rightarrow 1^1\text{S}$ CV resonance line in the high density region, are the strong satellite lines for C_1IV and the presence of an intense line at the wavelength for the $2^3\text{P} \rightarrow 1^1\text{S}$ intercombination line, which is not expected to be present at such high densities. A preliminary association of this latter line with, instead, a plasma satellite line yields a density very close to the critical plasma density expected for laser absorption. This is a matter deserving further study, particularly if the high-density collisional pumping modeling continues to prove optimistic.

IV.D. TECHNIQUES

In the previous semiannual technical report a problem with target debris clogging the spectrograph entrance slit, especially with background gas present, was outlined. At that time an apparatus to back flush the slit after each shot was being designed. This unit is now installed and has successfully eliminated the slit debris problem.

Because of some inherited surface damage to the laser rod, the maximum power of 500 MW could never be realized without further damaging the ruby rod. In order to increase the power and simplify the laser damage situation, the ruby rod has been replaced with a neodymium glass rod (which requires no antireflectance coatings). The Pockels cell crystal suffered from similar surface damage and is presently being replaced.

IV.E. ANALYSIS

Stimulated by a recent discussion with Professor Isler from the University of Florida following a conference presentation,⁶ the charge exchange cross section analysis was reexamined. After a recheck of the Zwally-Koopman formulation presently used for calculating Landau-Zener cross-sections and further communications with Professor Isler, calculations were also completed using the Landau-Zener type approach preferred by Professor Isler. Both methods yield similar results and predict a high cross section for the $\text{He} + \text{C}^{+5} \rightarrow \text{He}^{+} + \text{C}^{+4}$ resonance charge exchange reaction currently under study. Again, it should be emphasized that the Landau-Zener theory, when applied to our situation, is at best inexact because of the approximations made in the derivation. The theory should be used only as an indicator of the transition most likely to experience the resonance charge transfer effect. In this respect, the relatively simple experiment serves as a check on the applicability of the theory.

REFERENCES

1. R. C. Elton, "Three Quasi-CW Approaches to Short Wavelength Lasers," in "Progress in Lasers and Laser Fusion," edited by E. Kursunoglu, A. Perlmutter, and S. M. Widmayer, Plenum Press, New York, 1975.
2. R. C. Elton and R. H. Dixon, "X-Ray Laser Research: Guidelines and Progress at NRL, Annals, New York Academy of Sciences (in press).
3. R. C. Elton and R. H. Dixon, "Spectroscopy of Plasmas for Short Wavelength Lasers," Proceedings 4th International Conference on Beam Foil Spectroscopy (in press).
4. A. M. Malvezzi, E. Jannitti, and G. Tondello (to be published).
5. H. R. Griem, private communication.
6. R. H. Dixon, J. L. DeRosa, R. A. Andrews, and R. C. Elton, Bull. Am. Phys. Soc. 20, 1283 (1975).

V. SUMMARY

As planned, we have concentrated during this reporting period on definitive measurements, at some cost in pump-source development, for an interim assessment of the approaches pursued with the continued goal of identifying a promising approach in FY-77 for concentration of developmental effort. The most significant advancements during this reporting period for the various program areas are as follows:

NONLINEAR MIXING AND AMPLIFICATION

1. The emphasis during this reporting period has been on optimization of the tunable visible emission prior to transfer to the vacuum-UV region. The significant progress towards this end in the various components involved is in understanding the limitations on efficiencies as reported in Section II. Adaptation of the H_2 laser for integration with the frequency upconverted beam has begun.

ELECTRON-COLLISIONAL PUMPING EXPERIMENT

2. Extensive interferometric studies have resulted in the first detailed density profiles from a laser-evaporated target plasma on a 30 ps time scale. Both point and line focus configurations were studied. The results indicate a large density gradient very close to the target surface for the high densities required for absorption of a second pumping laser beam. Also, a deterioration of cylindrical symmetry at expansion distances required for densities below 10^{18} cm^{-3} is to be expected. The present conclusion is that near-critical density absorption of a normal-incidence beam is the more desirable configuration, and modeling is proceeding in this direction as summarized below.
3. Planning of tests at lower densities (consistent with confidence in present modeling) were begun, based also upon promising experience with a transverse discharge traveling-wave device at low pressure operation. Definitive measurements on this device are planned for the next reporting period in this portion of the program.

RESONANT CHARGE TRANSFER EXPERIMENT

4. A mapping of CV and CVI spectral lines in the soft x-ray region as a function of distance from the target has indicated significant reabsorption of the first resonance line in the high-density region close to the surface. However, higher series members appear to emit in reasonable intensity ratios and should be reliable for relative comparisons with helium-background spectra, particularly further from the target where the desired densities ($\leq 10^{18} \text{ cm}^{-3}$) occur for this process.

5. A very preliminary analysis of spectral features in the high-density region indicate the possibility of a critical density ($\sim 10^{21} \text{ cm}^{-3}$) layer, which would be in support of the electron collisional pumping experiment described earlier. Space-resolved visible-spectra have been obtained for He I and He II lines, from which the ratio of helium atoms to ions can be estimated as a function of distance from the surface. Present results do not indicate a high degree of preionization which would be detrimental to an efficient carbon-ion/neutral atom interaction zone.

ANALYSIS AND MODELING

6. Development of a quite general numerical model has continued with present emphasis on electron-collisional pumping in the high-density regime ($\sim 10^{21} \text{ cm}^{-3}$) appropriate for the laser/target plasma experiment. Radiative transfer effects are currently being added, which will allow convenient application to a new resonance-absorption pumping scheme of current interest because of its inherent selectivity of the upper laser level.
7. In an attempt towards an increased understanding of the selectivity of the resonance charge transfer scheme, discussions with interested theoreticians have taken place and partial assistance has been negotiated with an experienced N.R.L. theoretician for the next reporting period. It is expected that such guidance can be of significant assistance as the experimental parameters are varied in search of resonance effects.

REVIEW OF X-RAY LASER FIELD

8. An accomplishment during this reporting period has been the completion of a comprehensive review article on the x-ray laser research field, as of an October 1975 completion date. The article has been accepted for publication in Proceedings of the IEEE in 1976, and a preprint is included in the Appendix.

In brief, this reporting period has seen a definitive study of the conditions to be encountered in the laser/target plasma approach, which has precipitated a reevaluation of the associated analysis to high densities and of the experiment to a normal-incidence pump-pulse mode. Additional consideration of electron discharge pumping has resulted also from these studies. The charge transfer experiment is now yielding definitive data. The nonlinear mixing experiment is ready for conversion to the vacuum-UV in the near future with optimum efficiency. It is anticipated that a significant overall narrowing of options will continue towards our mid-FY-77 goal.

Finally, reprints of publications and presentation abstracts are included in the following Appendix, including the comprehensive review article described above. These represent work completed during this period and are included to provide further details on various portions of the program.

VI. APPENDIX

PRESENTATIONS AND PUBLICATIONS FOR THE REPORTING PERIOD

PRESENTATIONS

"Micro-Interferometric Study of Laser-Generated Plasmas Using 30 psec Probing Pulses," by J. F. Reintjes, T. N. Lee, R. C. Eckardt, R. C. Elton, and R. A. Andrews.....	54
"Formation Process of Minute Plasmas in a Vacuum Spark," by T. N. Lee.....	55
"Resonance Charge Transfer Effects Between Impurity Ions and Neutral Atoms in Plasma Boundary Regions," by R. H. Dixon, J. L. DeRosa, R. A. Andrews, and R. C. Elton.....	56
"Study of Expansion Characteristics of Laser Produced Plasmas Using a Micro-Interferometry," by J. F. Reintjes, T. N. Lee, R. C. Eckardt, R. C. Elton, and R. A. Andrews.....	57
"An Electron-Collision Pumped Quasi-CW Soft X-Ray Laser Using Helium-Like Ions," by L. J. Palumbo, and R. C. Elton.....	58
"Compensation of Self Phase Modulation by Cesium Vapor," by R. H. Lehmberg, J. Reintjes, and R. C. Eckardt.....	62

PUBLICATIONS

"Three Quasi-CW Approaches to Short Wavelength Lasers," by R. C. Elton.....	67
"Soft X-Ray Lasers Via Electron-Collisional Pumping," by R. A. Andrews.....	69
"High-Density Ionization With an Intense Linear Focus Discharge," by T. N. Lee.....	71
"Quasi-Stationary Population Inversion on $K\alpha$ Transitions," by R. C. Elton.....	73
"X-Ray Emission From Laser-Produced Magnesium Plasmas," by T. N. Lee and D. J. Nagel.....	74
"Quasi-Stationary Population Inversion on $K\alpha$ Transitions," by R. C. Elton.....	75
"Spectroscopy of Plasmas for Short Wavelength Lasers," by R. C. Elton and R. H. Dixon.....	82
"Negative Nonlinear Susceptibility of Cesium Vapor Around 1.06μ ," by R. H. Lehmberg, J. Reintjes, and R. C. Eckardt.....	91
"A Single Mode Nd:YAG Q-Switched Oscillator With Short Buildup Time," by R. C. Eckardt and J. F. Reintjes.....	125
"Review of Short Wavelength Laser Research," by R. W. Waynant and R. C. Elton.....	129

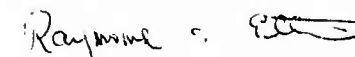
Abstract Submitted
for the 17th Division of Plasma Physics Meeting of the
American Physical Society
November 10-14, 1975

Physical Review
Analytic Subject Index
Number 35. Plasmas

Bulletin Subject Heading
in which Paper should be
placed: 32. Diagnostics

Micro-Interferometric Study of Laser-Generated Plasmas Using 30 psec Probing Pulses. J. F. REINTJES, T. N. LEE, R. C. ECKARDT, R. C. ELTON, and R. A. ANDREWS, Naval Research Laboratory--We report on a micro-interferometric study of plasmas generated by 2 ns pulses from a Nd:glass Q-switched laser containing energies of 1 J and focused to intensities of 10^{12} W/cm². The plasmas are probed with a precisely-timed 30 psec pulse from a mode-locked Nd:YAG laser, frequency doubled to 0.53 μ m. The use of mode-locked pulses allows spatial resolution to 10 μ m at typical plasma expansion velocities of 10^7 cm/sec. Measurements of plasma dimensions, electron densities and expansion velocities for both line and point foci are presented as a function of the time delay between the mode-locked and Q-switched pulses. Measurements of forward and backward streaming plasmas generated from thin targets are compared to determine effects of radiation pressure on plasma expansion.

Submitted by


Signature of APS Member

RAYMOND C. ELTON
Code 5520
Naval Research Laboratory
Washington, D. C. 20375

Abstract Submitted
for the 17th Division of Plasma Physics Meeting of the
American Physical Society

November 10-14, 1975

Physical Review
Analytic Subject Index
Number 35. Plasmas

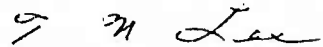
Bulletin Subject Heading
in which Paper should be
placed Plasma Focus

Session Title:
8. Plasma Focus

Formation Process of Minute Plasmas in a Vacuum Spark. T. N. LEE, Naval Research Laboratory--The vacuum spark discharge produces extremely small (10-50 μm), high power density (10^{15} W/cm²) plasmas, each of which emits a x-ray pulse of a few nanoseconds. These plasmas often form a bead-like (or clustered) structure with beads spaced as close as 50 μm in distance¹ and several nanoseconds in time. Simultaneous measurements of the distance (Δd) and the time interval (Δt) of two successive point plasma formations show a relation of $\Delta d/\Delta t \sim 10^6$ cm/sec, which corresponds to the velocity of the anode plasma front¹. This is a strong indication that the bead-like feature is not related to random break-ups of a pinched plasma column due to a sausage type ($m=0$) instability. According to the experimental results obtained, the plasma constriction takes place in two steps, i.e., a relatively uniform pinch of the plasma column to a diameter of 1 μm or less is followed by a localized micro-pinch within a time interval of a few hundred nanoseconds. Multiple micro-pinches are responsible for the observed clustered point plasma structure.

¹T. N. Lee, Annals of New York Acad. Sci. 251 112 (1975)

Submitted by



Signature of APS Member

Oral Presentation

T. N. LEE (L I E)
Code 5520
Naval Research Laboratory
Washington, D. C. 20375

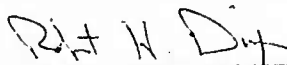
Abstract Submitted
for the 17th Division of Plasma Physics Meeting of the
American Physical Society
November 10-14, 1975

Physical Review
Analytic Subject Index
Number 35. Plasmas

Bulletin Subject Heading
in which Paper should be
placed 33. Scattering, Emission,
and Absorption of Radiation

Resonance Charge Transfer Effects Between
Impurity Ions and Neutral Atoms in Plasma Boundary
Regions. R. H. DIXON, J. L. DeROSA, R. A. ANDREWS, and
R. C. ELTON, Naval Research Laboratory--High Temperature
plasma cooling and/or lowering of plasma heating rates
caused by processes involving boundary layers impurities
are of concern for fusion devices. Resonance charge
transfer between impurity ions of charge z and neutral
atoms is of particular interest because of the large
cross-section ($\sim 10^{-16} z^2 \text{ cm}^2$) involved. An experiment is
described in which the primary objective is to demon-
strate a significant effect of the resonance charge
transfer process on the populating of certain excited
states of ions when interacting with particular neutral
atoms. Stripped ions of various typical impurity ele-
ments such as carbon and oxygen, and eventually heavier
"wall" materials, are generated by a focused laser beam
and allowed to expand into a neutral gas (such as hydro-
gen, deuterium or helium). The effect of the charge
transfer process is expected to be evidenced by enhanced
line emission in space-resolved grazing incidence
spectra. Preliminary results obtained using a laser of
500 MW peak power focused onto a carbon target surrounded
by helium at pressures ranging from 1 to 100 Torr will be
presented.

Submitted by



Signature of APS Member

ROBERT H. DIXON
Code 5520
Naval Research Laboratory
Washington, D. C. 20375

Abstract Submitted

American Physical Society Topical Conference

On Diagnostic Of High Temperature Plasmas

January 7-9, 1976

Physical Review
Analytic Subject Index
Number 35. Plasmas

Bulletin Subject Heading
in which Paper should be
placed: 32. Diagnostics

Study of Expansion Characteristics of Laser
Produced Plasmas Using a Micro-Interferometry*. J. F.
REINTJES, T. N. LEE, R. C. ECKARDT, R. C. ELTON, and R.
A. ANDREWS, Naval Research Laboratory--High quality in-
terferograms of laser produced plasmas with spatial res-
olution of 15 micrometers are obtained using a rel-
atively simple Jamin-type interferometer and a precisely-
timed 30 ps probing laser pulse from a mode-locked
Nd:YAG laser, frequency doubled to 0.53 μm . The spatial
resolution attainable with the present arrangement is
limited by the velocity of the expanding plasma and the
finite duration of the probing pulse. The plasmas are
produced by focusing a Nd:glass Q-switched laser pulse
(0.5 GW, 10^{11} - 10^{13} Watts cm^{-2}) onto slab targets of
Al, Mg, and CH_2 . Time-dependent behaviors of electron
density distribution plasma dimension, and expansion
velocity for both point and line foci are made as a
function of time delay between the mode-locked and the
Q-switched laser pulses. The results thus obtained
with different durations of the heating (Q-switched)
pulse and with the various target material are compared.

*Work supported by DARPA Order No. 2694.

Submitted by

Signature of APS Member

JOHN F. REINTJES
Code 5520
Naval Research Laboratory
Washington, D. C. 20375

A B S T R A C T

AN ELECTRON-COLLISION PUMPED QUASI-CW SOFT X-RAY LASER USING HELIUM-LIKE IONS

L. J. Palumbo and R. C. Elton

Naval Research Laboratory, Washington, D. C. 20375

A steady-state model of a quasi-cw soft x-ray laser on helium-like ions was used to calculate gain vs. temperature, density, and element. Gains greater than 10 cm^{-1} are estimated for hot, dense, moderate-Z plasmas of pellet fusion plasma characteristics.

SUMMARY

AN ELECTRON-COLLISION PUMPED QUASI-CW SOFT X-RAY LASER USING HELIUM-LIKE IONS

L. J. Palumbo and R. C. Elton

Naval Research Laboratory, Washington, D. C. 20375

A steady-state analytical plasma model has been applied to a quasi-cw electron-collisional pumping scheme for producing soft x-ray lasing on the $3s^1S \rightarrow 2p^1P$ transition in helium-like ions. The estimates of pump power requirements, gain coefficient, and optimum element indicate that lasing may be obtained in the $20 - 70 \text{ \AA}$ region with a gain of $> 10 \text{ cm}^{-1}$ in moderate-Z plasmas under conditions existing in present and forthcoming pellet fusion experiments. The $1s3s^1S$ upper laser level is pumped by electron collisional excitation from the $1s^2^1S$ ground level, lasing takes place by transitions into $1s2p^1P$, and rapid $1s2p^1P \rightarrow 1s^2^1S$ decay prevents self termination, i. e., quasi-cw operation is expected. The upper laser level is also depopulated by electron-impact excitation into the nearby $1s3p^1P$ term, which imposes an upper limit on the electron density for a given element. A population inversion is maintained, even though the electron-impact excitation rates from the ground state into both the 3s and 2p levels are comparable, because rapid $2p \rightarrow 1s$ decay prohibits accumulation in the 2p level while the 3s level is not dipole coupled directly to the ground state.

The equations for the steady-state population densities, N_3 and N_2 , of the upper and lower laser levels are,

$$N_3 = \frac{N_1 N_e X_{13}}{A_{32} + N_e (X_{32} + X_{34})} ; \quad N_2 = \frac{N_1 N_e X_{12} + N_3 (A_{32} + N_e X_{32})}{A_{21}} .$$

where the subscripts 1 through 4 refer to the $1s^2^1S$, $1s2p^1P$, $1s3s^1S$, and $1s3p^1P$ levels, respectively. The A's are spontaneous radiative decay rates, the X's are electron collisional excitation or deexcitation rate coefficients,

and the N 's are the population densities with N_e being the electron density. The deexcitation rate coefficient, X_{32} , is computed from X_{23} by detailed balancing. Required energy level spacings, etc. were taken from published data and scaled appropriately with spectrum number. The ground state density, N_1 , was obtained from N_e by assuming charge neutrality, 100 % abundance of helium-like ions, and small fractional populations of excited levels.

Figure 1 shows some results of gain at two (high) electron densities. A gain coefficient, α , of $>10 \text{ cm}^{-1}$ is desired because, even with very large pump laser systems, it may be difficult to form a plasma of the required temperature and density with a length of more than a few millimeters. These curves are typical of those computed over a wide range of electron density and temperature. The curves show an increase in gain with N_e , an optimum Z at a given density, a rapid decrease in α for Z larger than this optimum, and a Z_{min} cutoff below which the computed inversion density is negative. The gain scales analytically as $\sim(Z-1)^{-2.5}$ when collisional processes dominate the $3s \rightarrow 1s$ level depopulation (low Z or closely spaced energy levels) and as $\sim(Z-1)^{-8.5}$ when the prominent mode of depopulation is by spontaneous laser-line emission. For a given Z , the highest gain is attained when the electron temperature is approximately twice the $1s \rightarrow 3s$ excitation energy, ΔE_{13} . This is a consequence of the fact that $N_e X_{13}$, the rate for the dominant process populating the upper laser level, reaches a peak at $kT_e \approx 2 \Delta E_{13}$; for higher temperatures, this rate falls off slowly and the laser pumping rate decreases. An ion temperature less than the electron temperature, which may occur in a transient laser plasma, would increase the gain in the plotted curves by a factor of $(T_e/T_i)^{1/2}$ due to a reduced Doppler width.

The production of a plasma with the density and temperature required to

produce reasonable gains on this transition would require a pump laser with a power density $\sim 10^{17}$ W/cm² over an area of largest dimension > 1 mm on a cylindrical pellet-like target to avoid temperature decrease by thermal conductivity. Such lasers and targets are currently being developed in the laser fusion programs. Results from a micro-interferometric diagnostic experiment¹ using a Nd:YAG 30 psec probe laser synchronized with a Nd:glass 2 nsec plasma producing laser to study the evolution of a high-density critical layer at $N_e \approx 10^{21}$ cm⁻³ will be described.

¹J. F. Reintjes, T. N. Lee, R. C. Eckardt, R. C. Elton, and R. A. Andrews, Bull. Am. Phys. Soc., Vol. 20, p. 1336, Oct. 1975.

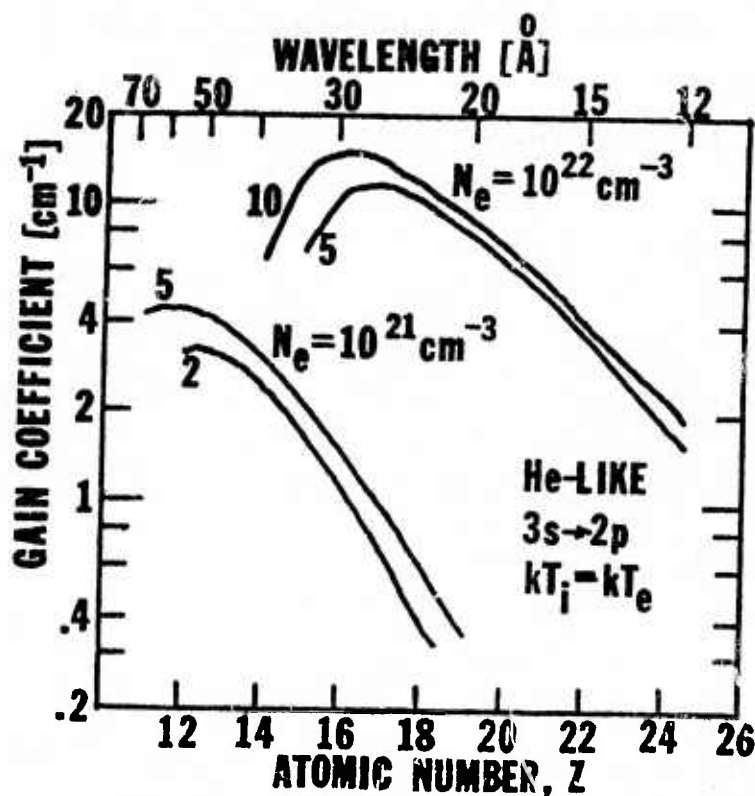


FIGURE 1. Calculated gain for $3s^1S \rightarrow 2p^1P$ lasing in helium-like ions plotted vs. atomic number for two electron densities. For each density, electron temperatures were chosen which yielded the highest gain and their values in keV are indicated by numbers next to each curve.

Accepted for 1976 International Quantum Electronics Conference, Amsterdam.

COMPENSATION OF SELF PHASE MODULATION BY CESIUM VAPOR*

R. H. Lehmberg, J. Reintjes and R. C. Eckardt
Naval Research Laboratory, Washington, D.C. 20375
(202) 757-2730

ABSTRACT

We have observed a significant reduction of Nd:YAG laser-generated self phase modulation by propagating the output pulses through a cesium vapor cell. The limitations of this technique are discussed, and a related pulse shaping experiment will be described.

*Work supported by U.S. ERDA and ARPA.

Recently, we reported the observation of self defocusing of mode locked 1.05 μ pulses in cesium vapor, and attributed it primarily to the nearby two photon resonance with the 6s-7s levels.¹ The corresponding negative value of n_2 was measured at -1.4×10^{-30} N, in reasonable agreement with the calculated value of -2.52×10^{-30} N. Since the useful output power of large Nd laser systems is ordinarily limited by self focusing and self phase modulation (SPM), the existence of this negative n_2 raises the possibility of increasing the power by using Cs vapor for compensation. Here, we report the first observation of partial compensation of the SPM generated in a Nd:YAG laser system.

The laser radiation consisted of single pulses of FWHM duration $t_p = 30$ psec, as measured by a 5 psec resolution streak camera. The bandwidths were broadened to 4-5 cm^{-1} by SPM in the YAG amplifiers, and the integrated spectra had the double-humped appearance (Fig. 1a, c) expected for a chirp of this magnitude.² The collimated beam, with a peak on-axis intensity $I \approx 1.9 \text{ GW/cm}^2$, propagated through a total path length $l = 200$ cm in Cs vapor. Its diameter was relatively large (1 cm) in order to avoid whole-beam self defocusing effects.¹ The integrated spectra of the input and output pulses were recorded by directing a portion of the center of each beam through a 1-m grating spectrograph onto an image converter camera operating in the streak mode adjusted for a 1 nsec resolution and 10 nsec/cm sweep rate. A 12.5 nsec pulse separation allowed the input and output spectra to be compared on the same film (e.g. Fig. 1). The spectral resolution is 0.2 cm^{-1} .

In Fig. 1c, the phase modulated spectrum of the incident pulse gives a maximum chirp width of $\Delta\nu_c \approx 4.3 \text{ cm}^{-1}$, which corresponds to a peak on-axis phase shift $B = 2\pi \Delta\nu_c t_p / 2.86 \approx 8.5$. In the output pulse, the double-hump

has disappeared, and $\Delta\nu_c$ has been reduced to 2.7 cm^{-1} ; hence, $B_{\text{out}} \approx 5.3$. The phase reduction $B_{\text{out}} - B \approx -3.2$ is in reasonable agreement with the value $\Delta B = 8\pi^2 n_2 I L / \lambda c \approx -4.9$ calculated from $n_2 = -1.4 \times 10^{-30} \text{ N}$ measured previously.¹

The asymmetry in these spectra arises from asymmetry in the laser pulse shape. Since the pulse changes shape within the laser, the output intensity variation - dI/dt does not correspond exactly to the instantaneous chirp frequency. Moreover, some beam degradation due to small scale self focusing was evident in the more intense pulses. It is therefore unlikely that the SPM can be completely cancelled by a single Cs cell at the output, i.e., one should compensate after each amplifier stage before self focusing and pulseshape changes become appreciable.³

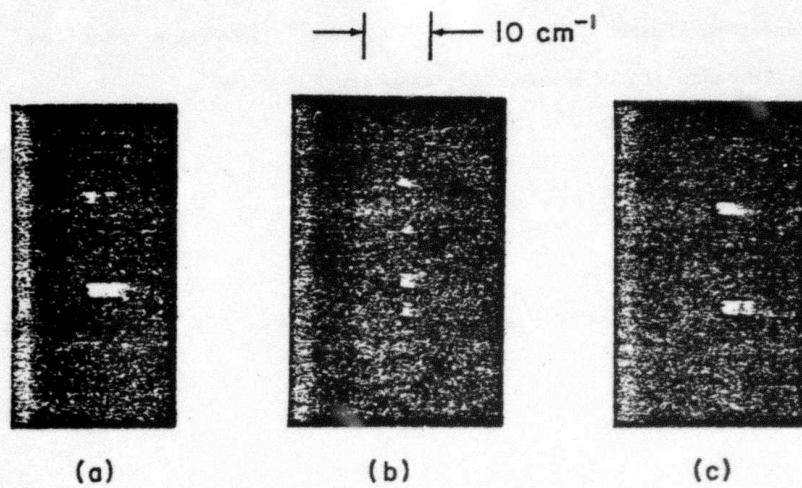
Additional experiments are in preparation to do the initial pulse chirping with CS_2 rather than in the amplifiers. This will allow better control of small scale self focusing and will ensure that the pulseshape remains the same in the chirping and compensating elements; hence, a nearly complete phase compensation should be attainable. In a second experiment, the negative SPM due to the cesium cell alone will be used to study pulse squaring effects in a grating pair.

REFERENCES

1. R. H. Lehmberg, J. Reintjes, and R. C. Eckardt, Appl. Phys. Lett. 25, 374 (1974); Phys. Rev. A (March 1976).
2. R. C. Eckardt, C. H. Lee, and J. N. Bradford, Opto-electronics 6, 67 (1974).
3. R. H. Lehmberg, J. Reintjes, and R. C. Eckardt, NRL Memo Rpt. 3130 (Sept 1975) p. 25-30.

FIGURE CAPTIONS

FIGURE 1 Integrated spectra of pulses at the Cs cell input (lower traces) and output (upper traces): (a) empty cell; (b) $N = 3.7 \times 10^{16} \text{ cm}^{-3}$ with a small double pulse ($I < .15 \text{ GW/cm}^2$) which remains essentially time-bandwidth limited; (c) $N = 3.7 \times 10^{16} \text{ cm}^{-3}$, showing a reduction of the SPM bandwidth of a pulse of intensity 1.9 GW/cm^2 .



Reprinted from: PROGRESS IN LASERS AND LASER FUSION
Edited by B. Kursunoglu, A. Perlmutter and S. M. Widmayer
Book available from: Plenum Publishing Corporation
227 West 17th Street, New York, New York 10011

THREE QUASI-CW APPROACHES TO SHORT WAVELENGTH LASERS*

R. C. Elton

Naval Research Laboratory

Washington, D. C. 20375

ABSTRACT

Three approaches towards achieving extended-period quasi-cw amplification by stimulated emission in the vacuum-UV and x-ray spectral regions are discussed, in a somewhat logical progression towards shorter wavelengths, increased complexity, and demands. Extrapolation of visible and near-UV tuned-cavity cw lasers using higher density plasma media is first discussed for the near-to-mid VUV region. Further extension to the soft x-ray region is described, using preferential resonance charge transfer pumping. This and related intense incoherent x-ray source development could ultimately lead to successful quasi-cw K α inversions, as is discussed. Experiments underway to test the first two schemes are described.

*Supported in part by the Defense Advanced Research Projects Agency, DARPA Order 2694

I. INTRODUCTION

The basic problems that hamper a rapid extension of lasers into the vacuum ultraviolet (VUV) and x-ray spectral regions can be summarized with a few simple relations. Since high reflectance cavities do not appear to be realistic for wavelengths shorter than $\sim 1000 \text{ \AA}$, significant gain must be achieved in a single pass; this immediately implies an increase by orders-of-magnitude in the inverted state density required for a given net gain at a particular wavelength. Hence, at truly short wavelengths we are usually speaking of amplified spontaneous emission (ASE) devices, which alone represent more of an amplifier than a tuned oscillator producing highly coherent radiation. In fact, the devices developed will probably prove most useful, at least for the near term, as amplifiers for coherent VUV radiation produced by frequency multiplication from the IR and visible regions.

For an amplifying medium of length L , the ASE gain is given by $I/I_0 = \exp(\alpha L)$, where α is the gain coefficient. The product αL is often written as¹

$$\alpha L = \frac{\lambda^2 A_{ul}}{4\pi^2 \Delta\nu} L \left(N_u - \frac{g_u}{g_l} N_l \right), \quad (1)$$

where g_u , g_l and N_u , N_l refer to the statistical weights and population densities of the upper and lower laser states, respectively, $\Delta\nu$ refers to the line width in frequency units, and λ refers to the wavelength of the laser transition. With the transition probability A_{ul} for spontaneous emission scaling as $f\lambda^{-2}$, and for larger inversion (i.e., $N_u \gg N_l$), Eq. (1) can be written as a proportionality:

Reprinted from: PROGRESS IN LASERS AND LASER FUSION

Edited by B. Kursunoglu, A. Perlmutter and S. M. Widmayer
Book available from: Plenum Publishing Corporation
227 West 17th Street, New York, New York 10011

SOFT X-RAY LASERS VIA ELECTRON-COLLISIONAL PUMPING*

R. A. Andrews

Naval Research Laboratory

Washington, D. C. 20375

I. INTRODUCTION

One possible technique for obtaining gain in the soft x-ray region of the spectrum is to use electron-collisional pumping of an appropriate ion species. This can be done in a manner analogous to known ion lasers which operate in the visible portion of the spectrum. The differences being: 1) more highly ionized ions are used to obtain shorter wavelength transitions, 2) the pumping electrons are at a higher temperature to populate the more energetic transitions, and 3) the lifetimes are shorter which implies higher pump intensity per unit area ($P/a \propto \nu^4$). In the case of shorter wavelength transitions one can project known laser transitions isoelectronically to higher Z ions and hence shorter wavelengths or investigate unique ionic electron configurations that are not observed in neutral or weakly ionized species. This technique works well for

*This work was partially supported by the Defense Advanced Research Projects Agency, ARPA Order 2694.

electronic configurations with relatively few electrons. With many-electron systems, level crossings and other anomalous effects with increasing Z limit the range over which a group of levels which are a viable laser scheme can be isoelectronically projected to higher Z . A further problem with short wavelength lasers is that the techniques available for generating significant amounts of energy with very short risetimes are limited. Discharges are limited to about 10^{-7} sec. Mode-locked lasers, however, can be used down to the 10^{-11} sec range with significant amounts of energy. Short wavelength requirements lead to many other problems for the attainment of an inversion and net positive gain. Several of these are discussed in this paper along with a particular approach to the short wavelength laser problem.

A particularly promising concept for an electron-collisional pumped laser is the use of a picosecond laser pulse to heat the electrons in a cold plasma which has a large fractional population of the laser ion species.^{1,2} The initial plasma can be created by a variety of techniques. However, if one is seriously considering highly ionized species then a laser produced plasma offers distinct advantages since large amounts of energy can be deposited in small volumes in short times. This initial plasma would typically be generated with a line focus laser to create a plasma/laser media with a large aspect ratio and hence maximum gain length. This plasma must be allowed to expand, cool, and develop a maximum fractional population of a particular laser ion species. Cooling is important since the laser line is Doppler broadened and Boltzmann population of low lying levels may ruin a possible inversion.

**HIGH-DENSITY IONIZATION WITH AN INTENSE
LINEAR FOCUS DISCHARGE**

Tong Nyong Lee



Reprinted from
ANNALS OF THE NEW YORK ACADEMY OF SCIENCES
Volume 251, Pages 112-125
May 8, 1975

HIGH-DENSITY IONIZATION WITH AN INTENSE LINEAR FOCUS DISCHARGE

Tong Nyong Lee

*Optical Sciences Division
Naval Research Laboratory
Washington, D.C. 20375*

INTRODUCTION

A low-pressure linear discharge (or vacuum spark) produces¹⁻⁴ one or more minute (or point) plasmas less than $50\text{ }\mu\text{m}$ in size with the electron kinetic temperature as high as $kT_e = 10\text{ keV}$. Such point plasmas emit short bursts of intense x-radiation which consists of continuum as well as line radiation arising from highly stripped high-Z atoms. In the highly constricted plasma region, the current density reaches a value of $10^{10}\text{ amps}\cdot\text{cm}^{-2}$. However, the physical processes involved in the formation of such a plasma entity are not well understood.²⁻⁴ The plasma dynamics involved in the discharge is complex and is hard to correlate with the onset of the x-ray bursts.

In the present study, some of the experimental results obtained with the device are described in order to improve the understanding of the phenomena. Measurements include plasma diagnostics made with fast photography, pinhole x-ray photography, and x-ray spectroscopy in the photon energy range of 6-350 keV.

Although there are large differences in some operating parameters (mainly in operating voltage), this low-pressure linear discharge device is believed to have some similarities with the vacuum diodes that have been studied⁵⁻⁸ intensively in recent years for the purpose of plasma heating as well as for ion acceleration. This paper therefore may also be relevant to the basic problems involved in understanding vacuum diode operation.

The experimental device⁴ used in the present study is a very simple apparatus with a total capacitive storage energy of less than 3.6 kJ. A schematic diagram of the discharge device is shown in FIGURE 1. It consists of a pair of electrodes; a cathode of 3 cm diameter and a 0.7-cm diameter bullet shaped anode, are separated by a gap of 0.6-1.0 cm. The two electrodes are isolated by a Pyrex® glass tube of 10 cm diameter, which also serves as a vacuum chamber. The positive electrode is connected directly to the high voltage terminal of a 28 μF capacitor charged to 16 kV, and the cathode is connected to the ground terminal through a pair of current-return copper straps placed outside the glass tube. The discharge chamber is evacuated to a pressure of 10^{-6} torr. The discharge is initiated by injecting a pulsed laser beam (ruby laser of 100 MW, 20 ns) focused onto the anode tip through an axial hole in the cathode (grazing the cathode hole edge). The laser beam serves as a fast-acting injection of vapor into the electrode gap by slight evaporation of both electrode materials, and has no effect on the plasma heating.

Quasi-stationary population inversion on $K\alpha$ transitions

R. C. Elton

In a search for an x-ray laser capable of operating in a quasi-cw mode, a suggested $K\alpha$ -innershell scheme is examined using recently calculated rates. This scheme involves the decay of a K -shell vacancy followed by a more rapid (for certain elements) L -vacancy decay, which maintains the inversion. The present analysis indicates that the scheme is only marginally feasible unless a depletion of resonant absorbers is accomplished through line shifts associated with multiple ionization following K -vacancy production. The pumping requirements for overcoming photoionization losses in the beam and the associated gain conditions are estimated for three elements, namely silicon, calcium, and copper, and it is concluded that photoionization pumping in a selective energy band is required, with emission approaching the blackbody level. A multiline heavy-ion plasma source is suggested.

I. Introduction and Background

For x-ray lasing, $K\alpha$ -type transitions would seem to be a first choice, both because of the inherent short wavelengths and the large transition probabilities (which imply increased gain). However, with the rapid K -vacancy decay rate is associated a short (femtosecond¹ for penetrating x rays) equilibration period τ , during which lasing is completed for a simple self-terminating transient inversion scheme.² With coherence lengths $c\tau \sim 10^{-5}$ cm, conventional cavity operation becomes impractical (even if cavities could be constructed to withstand x-ray laser intensities), and traveling-wave operation would be tedious. Sufficient pumping for significant single-pass lasing (amplified spontaneous emission) is also a formidable task during such a short lasing period.

An alternative to the short-pulse self-terminating laser approach is to somehow create a stationary (or at least quasi-stationary) population inversion by eliminating final laser states, which are potential absorbers, more rapidly than they are created. For $K\alpha$ -innershell transitions, this translates to depleting the density of atoms (or ions) with a particular L -shell vacancy more rapidly than they are created by lasing transitions from K -vacancy atoms. (It is not necessary that the L shell be filled, since isolate spectral lines are produced for each of the series of possible L -vacancy configurations as discussed below.) A particular L -vacancy state may be depleted by either adding or removing an electron to the L shell, but

again it must take place at a very rapid rate and preferably without external stimulus. Stankevich³ in 1970 first suggested that this be accomplished by electron cascading from outer shells through rapid Auger as well as radiative transitions and suggested that this combined specific rate exceeds that for K -vacancy depletion. This particular scheme depends strongly on a sufficient density of outer-shell electrons, i.e., is classified as an innershell⁴ transition scheme. Although the description of the model Stankevich used is sketchy, it is possible to reconstruct⁵ approximately his results, which were based upon K -vacancy depletion rates from experimentally obtained K -level widths,⁶ proportioned⁷ as 2:1 for $K\alpha_1$ and $K\alpha_2$ lines, and L -vacancy depletion rates estimated from the difference between the K -level widths and measured K -line widths.⁶ Some of these numerical data are included in Table I, and the ratio R_L/R_K of L - and K -vacancy depletion rates is plotted in Fig. 1 vs atomic number Z . In equilibrium, $N_2 R_K = N_3 R_L$, where N_2 and N_3 are, respectively, the upper and lower laser state densities,² populated originally by pumping from state 1. Therefore the ordinate in Fig. 1 corresponds to the population density ratio, and inversion is achieved when $N_2/N_3 > g_2/g_3$, where the statistical weight ratio g_2/g_3 is 1 for the $K\alpha_2(KL_{II})$ line and 0.5 for the $K\alpha_1(KL_{III})$ line. (Stankevich apparently assumed $g_2/g_3 = 1$ for both lines.) Thus, for the data available to Stankevich, net quasi-stationary inversion appears possible for the $Z = 20$ -45 range.

II. Present Analyses

A. Total Rate Model with Recent Data

When a similar analysis is carried out⁵ with the more recent calculations of Auger and radiative rates

The author is with the U.S. Naval Research Laboratory, Washington, D.C. 20375.

Received 11 November 1974.

X-ray emission from laser-produced magnesium plasmas

I. N. Lee and D. J. Nagel

Naval Research Laboratory, Washington, D. C. 20375
(Received 9 April 1975)

Characteristics of x-ray emission produced by focusing a 0.5-GW laser to about 10^{12} W/cm² on magnesium metal targets were measured. Approximately 0.01% of the incident laser energy of 10 J was emitted in a 11-nsec (FWHM) pulse of x rays with photon energy in the range 1.3–1.8 keV.

PAUS numbers: 52.25.P, 07.85., 42.60.Q, 84.60.R

INTRODUCTION

Reliable easy-to-maintain lasers with powers up to about 1 GW are becoming increasingly available. When focused, such lasers produce power densities in the 10^{11} – 10^{12} -W/cm² range. Plasmas produced from solid targets irradiated with such power densities typically have peak electron temperatures near 100 eV ($\sim 10^6$ K). Thus they are convenient laboratory sources of vacuum ultraviolet and soft x radiation. There are a number of plasma light sources, for example, θ -pinch machines, which are capable of producing plasmas hotter than 10^6 K. Such plasmas are large in volume but the electron density is smaller by many orders of magnitude than the density of laser-produced plasmas. In addition, the low-density plasma machines use gases for heating and, therefore, are limited to elements which occur in gases or can be made in convenient gaseous compounds. Advantages of laser plasmas over discharge sources (including vacuum and sliding sparks) are as follows: (i) spectra of all elements can be excited, (ii) the spectra are relatively free of impurity lines, (iii) the number of ionization stages contributing to a spectrum is small and somewhat controllable, and (iv) the size of the radiating plasma is small enough so that entrance slits may be eliminated for x-ray spectroscopy in some cases. Hence laser plasmas are useful to generate data for interpretation of spectra from other sources. Their radiation is also convenient for testing and calibration of spectrographs and detectors.

The physics and diagnostics of high-temperature laser plasmas are presently receiving intense study. Central problems include coupling of laser energy into the target plasma, and the division of that energy into thermal conduction losses, plasma expansion, and radiation. Plasma temperatures and densities are desired as a function of laser pulse, focusing, and target parameters. In this regard, several studies at laser powers similar to those in this work have already been made. In particular, Stumpfel *et al.*¹ used a grazing-incidence monochromator to do time-dependent studies of radiation down to 35 Å from Mg plasmas generated by a 0.5-GW laser. They found ionization stages through MgX and suggested that He-like MgXI ions should exist in plasmas produced by few-joule ~ 20 -nsec laser pulses. Recently, Peacock *et al.*² made a spectroscopic study of the satellite lines near the resonance lines of He-like Mg ions in plasmas produced using a Nd laser at about 1 GW. Donaldson *et al.*³ did a comprehensive study of lighter-atom plasmas which were generated with laser powers up to 2 GW.

In this work,⁴ we investigated several characteristics of the plasma x-ray emission produced by focusing a 0.5-GW (18-nsec FWHM) ruby laser beam (0.69 μ m) onto Mg targets, namely, the x-ray yield as a function of the lens-target distance, the time histories and correlation between laser and x-ray signals, the x-ray conversion efficiency, x-ray pinhole photographs, and the x-ray spectrum in the 7–10-Å region. Nonuniformity of the laser power distribution is evidenced by postshot microscopy of the targets. Comparisons of the present results with x-ray emission produced by 1-nsec Nd laser pulses (1.06 μ m) of similar energy are made.

EXPERIMENTAL ARRANGEMENT

The experimental arrangement is shown schematically in Fig. 1. A Korad K2 ruby laser system consisting of a Q-switched oscillator produced pulses with energies up to 10 J. The beam divergence was 8 mrad. A beam splitter and an S-1 response photodiode were used to monitor the laser pulse signal shape and the power. The laser beam (3.5 cm in diameter) was focused by a 5-cm-diam 20-cm focal length lens which was mounted on a micrometer translation stage outside of a vacuum window. Flat Mg targets, polished with abrasive paper, were placed at 45° to the incident beam in a 3×10^{-2} Torr vacuum. A silicon *p-i-n* x-ray detector located at about 60° to the beam (15° from the target normal) and 10 cm from the focus, and covered with a light-tight 25- μ m beryllium window, was used to monitor x-ray pulses. Prior to emplacement of the spectrometer shown in Fig. 1, an x-ray camera with a 25- μ m pinhole 2 cm from the focus viewed the plasma 90° to the beam and 45° to the target normal. It yielded 2 \times magnification. The simple slitless x-ray spectrometer at 90° to the

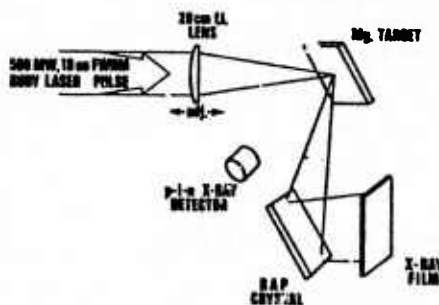


FIG. 1. Schematic diagram of experimental arrangement.

Quasi-stationary population inversion on $K\alpha$ transitions

R. C. Elton

In a search for an x-ray laser capable of operating in a quasi-cw mode, a suggested $K\alpha$ -innershell scheme is examined using recently calculated rates. This scheme involves the decay of a K -shell vacancy followed by a more rapid (for certain elements) L -vacancy decay, which maintains the inversion. The present analysis indicates that the scheme is only marginally feasible unless a depletion of resonant absorbers is accomplished through line shifts associated with multiple ionization following K -vacancy production. The pumping requirements for overcoming photoionization losses in the beam and the associated gain conditions are estimated for three elements, namely silicon, calcium, and copper, and it is concluded that photoionization pumping in a selective energy band is required, with emission approaching the blackbody level. A multiline heavy-ion plasma source is suggested.

I. Introduction and Background

For x-ray lasing, $K\alpha$ -type transitions would seem to be a first choice, both because of the inherent short wavelengths and the large transition probabilities (which imply increased gain). However, with the rapid K -vacancy decay rate is associated a short (femtosecond¹ for penetrating x rays) equilibration period τ , during which lasing is completed for a simple self-terminating transient inversion scheme.² With coherence lengths $c\tau \sim 10^{-5}$ cm, conventional cavity operation becomes impractical (even if cavities could be constructed to withstand x-ray laser intensities), and traveling-wave operation would be tedious. Sufficient pumping for significant single-pass lasing (amplified spontaneous emission) is also a formidable task during such a short lasing period.

An alternative to the short-pulse self-terminating laser approach is to somehow create a stationary (or at least quasi-stationary) population inversion by eliminating final laser states, which are potential absorbers, more rapidly than they are created. For $K\alpha$ -innershell transitions, this translates to depleting the density of atoms (or ions) with a particular L -shell vacancy more rapidly than they are created by lasing transitions from K -vacancy atoms. (It is not necessary that the L shell be filled, since isolate spectral lines are produced for each of the series of possible L -vacancy configurations as discussed below.) A particular L -vacancy state may be depleted by either adding or removing an electron to the L shell, but

again it must take place at a very rapid rate and preferably without external stimulus. Stankevich³ in 1970 first suggested that this be accomplished by electron cascading from outer shells through rapid Auger as well as radiative transitions and suggested that this combined specific rate exceeds that for K -vacancy depletion. This particular scheme depends strongly on a sufficient density of outer-shell electrons, i.e., is classified as an innershell⁴ transition scheme. Although the description of the model Stankevich used is sketchy, it is possible to reconstruct⁵ approximately his results, which were based upon K -vacancy depletion rates from experimentally obtained K -level widths,⁶ proportioned⁷ as 2:1 for $K\alpha_1$ and $K\alpha_2$ lines, and L -vacancy depletion rates estimated from the difference between the K -level widths and measured K -line widths.⁶ Some of these numerical data are included in Table I, and the ratio R_L/R_K of L - and K -vacancy depletion rates is plotted in Fig. 1 vs atomic number Z . In equilibrium, $N_2R_K = N_3R_L$, where N_2 and N_3 are, respectively, the upper and lower laser state densities,² populated originally by pumping from state 1. Therefore the ordinate in Fig. 1 corresponds to the population density ratio, and inversion is achieved when $N_2/N_3 > g_2/g_3$, where the statistical weight ratio g_2/g_3 is 1 for the $K\alpha_2(KL_{II})$ line and 0.5 for the $K\alpha_1(KL_{III})$ line. (Stankevich apparently assumed $g_2/g_3 = 1$ for both lines.) Thus, for the data available to Stankevich, net quasi-stationary inversion appears possible for the $Z = 20$ -45 range.

II. Present Analyses

A. Total Rate Model with Recent Data

When a similar analysis is carried out⁵ with the more recent calculations of Auger and radiative rates

The author is with the U.S. Naval Research Laboratory, Washington, D.C. 20375.

Received 11 November 1974.

Table I. Selected Atomic Rates Used (in 10^{-2} atu^{-1})^{a, b}

	Z = 22	30	38	47
Stankevich ³				
1. K-level width ^a (K rate) ^b	3.10	5.80	11.7	26.0
2. K-line widths ^{a, b}				
$K\alpha_1$ (K- L_{III})	5.71	10.1	18.6	35.6
$K\alpha_2$ (K- L_{II})	7.90	12.0	19.0	36.0
3. L-level widths ^a (L rate) ^{b, c}				
L_{III}	2.61	4.30	6.90	9.60
L_{II}	4.80	6.20	7.30	10.0
Present analysis				
4. K rate ^a				
X ray	0.89	3.41	10.2	24.45
Auger	2.63	3.14	4.00	4.42
Total	2.64	6.54	14.2	28.87
5. L rate ^{a, d}				
L_{III}	0.885	2.95	3.92	6.36
L_{II}	0.886	2.87	5.27	9.50
6. Total (K-line width)				
$K\alpha_1$ (K- L_{III})	3.52	9.49	18.1	35.2
$K\alpha_2$ (K- L_{II})	3.53	9.41	19.5	38.4

^a 1 $\text{atu} = 2.42 \times 10^{-17}$ sec.

^b Rate (atu^{-1}) $\approx (4.14 \times 10^{-2}) \times \text{width (eV)}$.

^c Row 2 less row 1.

^d Coster-Kronig added to L_{II} , subtracted from L_{III} ; x-ray rate included.

shown also in Table I, the prospect for quasi-stationary inversion appears considerably more marginal. K-shell rates have been calculated by McGuire,⁸ Walters and Bhalla,⁹ and Scofield^{10,11} (radiative only) in the 1970-1974 period and are in close mutual agreement for present purposes. McGuire¹² in 1971 also calculated L-shell radiative, Auger, and Coster-Kronig rates, from which are obtained total effective L subshell vacancy depletion rates by increasing the L_{II} rate and decreasing the L_{III} rate according to the tabulated Coster-Kronig rates. It is interesting to note (Table I) that the total line widths obtained from these calculated rates agree reasonably well at high Z with the widths published by Blokhin and Sachenko⁶ and used by Stankevich; however, the relative rates are different, and L depletion is not as rapid as originally supposed.³ A $K\alpha_1/K\alpha_2$ transition rate ratio of 2:1 is again assured. The result is a maximum population density inversion of about 30% in the Z = 30-35 region, as shown also in Fig. 1. Thus, even with the most recent data, quasi-stationary inversion using total decay rates remains a possibility, but with a more limited degree of inversion.

B. Final Rate Model with Line Shifting

It may only be necessary for the L-hole depletion rate to exceed the radiative x-ray rate for K-vacancy decay,^{13,14} which for low-Z elements is much less than the total rate used above. To better understand this model, a total binding-energy level¹⁵ diagram for copper is shown in Fig. 2, with various single and multiple shell vacancies designated by capital letters (e.g., K, L, M, KL, LL, etc.) and vacancy tran-

sitions by $K \rightarrow L$ etc. As indicated, the scheme evolves from creating K vacancies by pumping (P) in neutral copper, but is equally relevant beginning with a particular ion species (providing an excessive decrease in the $L \rightarrow M^2$ Auger rate does not occur with depletion of M electrons). Also the diagram is relevant to other materials with some attention to the relative importance of x-ray (X) and Auger (A) rates. The L state and some of the LM^2 states shown are potential reabsorbers of the $K \rightarrow L$ laser radiation. The newer idea here is that laser absorption by multiple-L-vacancy states (e.g., LL) and certain LM^2 states may take place at a shifted wavelength (indicated by $\lambda - \delta\lambda$ in Fig. 2) and therefore may not contribute to resonance-absorption losses in the laser beam. Indeed it has been recently shown both theoretically¹⁶ and experimentally¹⁷ that K-line shifts due to multiple-L vacancies exceed the line widths. If we then limit laser resonance absorption to L states and only consider x-ray decay of the K vacancy, a high degree of inversion is reached for both $K\alpha_1$ and $K\alpha_2$ transitions and for Z as low as 13, as shown in Fig. 3. In this figure, the low-Z cutoffs are due for α_2 to a lack of M electrons and for α_1 to a lack of 3d M-shell electrons to fill $2p_{3/2}$ (L_{III}) holes. (Data for $M_1 \rightarrow L_{III}$, l transitions, are not available.) The high degree of inversion in the Z = 20 range makes this model particularly attractive as far as pumping requirements are concerned. It should be noted that this line shift modification will not appreciably extend the high-Z, short-wavelength limit; however, it could make measurements at longer wavelengths (low-Z) considerably easier.

There are some potential problems associated with

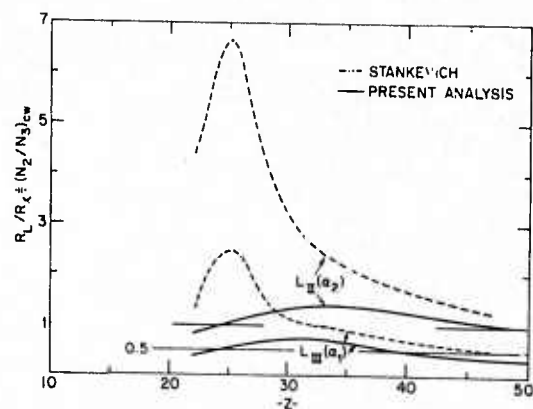


Fig. 1. Ratio of rates R_L/R_K for total transitions out of L- and K-vacancy states, respectively, vs atomic number Z. This ratio is equivalent to N_2/N_3 in Eq. (2) for equilibrium conditions reached after long times in cw operation. Values exceeding unity and one-half indicate gain for the $K\alpha_2$ and $K\alpha_1$ lines, respectively. The model here assumes all K-vacancy decay transitions produce potential absorbers for laser radiation. Present analysis is based on recent data⁸⁻¹²; an attempt to reproduce the results of Stankevich³ is shown dashed. Both $K \rightarrow L_{II}$ and $K \rightarrow L_{III}$, α_2 and α_1 respective transitions are shown.

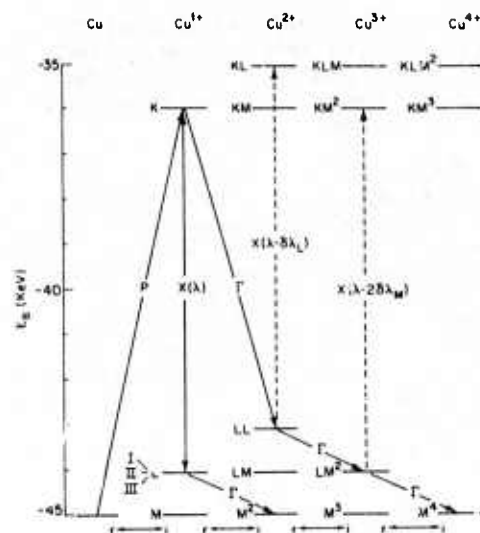


Fig. 2. Vacancy diagram according to binding energies E_b for copper. K , L , and M designate shell vacancies. P , X , and A are the rates for pumping, x-ray, [emission or absorption (dashed)] and Auger transitions, respectively.

the shifted-line model. Double L vacancies will cascade to M^4 states as indicated in Fig. 2 at a rapid rate, just as do single L vacancies, leading to decreased line shifts. The (sparse) data¹⁶ available on line shifts with multiple M vacancies indicate that an emission-absorption line overlap fortunately is not expected if only natural (x ray plus Auger) broadening is important and if M_I and M_{II} vacancies are present; an overlap for higher M -shell vacancies appears to be unavoidable. For light elements up through $Z = 20$, only M_I - and M_{II} -shell electrons exist. (Auger loss of N electrons has a low probability).¹² For Z larger than 20, further cascading may transfer M_I , M_{II} vacancies to M_{III} , M_{IV} , M_V states (by radiative and Coster-Kronig transitions), where the line shift is negligible. Rate data are available¹⁸ for including this effect, but the complexity is beyond this analysis.

A further complication in the line-shift scheme is electron-ion recombination (r in Fig. 2). As Stankovich points out,³ recombination must proceed at a sufficient rate to inhibit overdepletion of amplifying atoms. This implicitly places an upper limit on the plasma temperature. However, a recombination rate exceeding the K - and L -vacancy depletion rates will also produce $LL \rightarrow L$ recombination transitions following $K \rightarrow LL$ Auger transitions and again provide absorbers; we are then back to the less promising conditions in Fig. 1. For true cw operation, such a high recombination rate is required. However, as we show below, inversions of $\sim 1\%$ are required to achieve net gain. Thus, perhaps a lower recombination rate is possible, permitting a gradual depletion

of atom density through ionization (with an accompanying increase in pump-power requirements) in order to achieve some degree of stationary inversion for a limited time (hence quasi-stationary inversion), hopefully long enough to have multiple transverse in a resonant cavity or to permit reasonable pump-pulse risetimes. This will perhaps be a delicate balance to achieve and clearly requires a rather sophisticated numerical model for further analysis. For example, electron collisional ionization, as well as photoionization, of outer electrons should be included (i in Fig. 2). Also, the adverse effect on gain due to line shifts associated with multiple vacancy production accompanying radiative decay (radiative-Auger effect) should be included.^{11,19} The basic information for such an analysis is generally available, and the payoff, i.e., quasi-stationary population inversion, is potentially high. Further advantages of the line shift model will be indicated in the pump requirement estimations that follow, particularly for low- Z elements.

III. Pumping Requirements

A. General Requirements

Of next concern is the pumping energy required to achieve significant net gain, since photoionization of outer electrons by the laser beam will add to the normal line-absorption losses. Also, Auger decay (dominant for light elements) tends to deplete at a rapid rate the K -vacancy upper-laser states created. Both processes imply large pumping powers to maintain inversion. These are problems common to all inner-shell x-ray laser schemes (except alkalis without Auger losses for $n = 2$ vacancies) and also result in low system efficiency; on the other hand one is not overly concerned at present about efficiency if a quasi-cw mode is achievable with available pumping

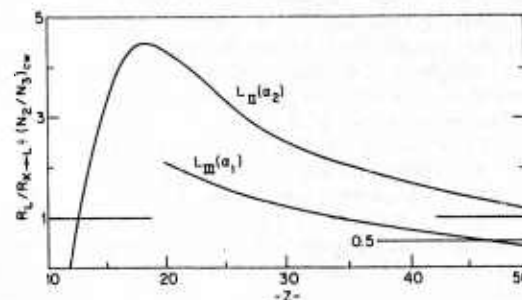


Fig. 3. Ratio of rates R_L/R_{K-L} for total transitions out of a L -vacancy state and radiative decay out of a K -vacancy state vs atomic number Z . This ratio is equivalent to N_2/N_3 in Eq. (2) for equilibrium conditions reached after long times in cw operation. Values exceeding unity and one-half indicate gain for the $K\alpha_2$ and $K\alpha_1$ lines, respectively. The model used assumes only radiative transitions produce absorbers, with Auger transitions generating shifted ion lines. Both $K \rightarrow L_{II}$ and $K \rightarrow L_{III}$, α_2 and α_1 respective transitions are shown.

powers. (It should be remembered that, were it not for the potential of quasi-stationary inversion, $K\alpha$ -innershell pumping would not be a serious candidate for x-ray lasing because of these losses.)

The restrictions set by the requirement that net stimulated emission exceed photoionization losses in the medium are derived from $\sim 2X$ the minimum threshold condition, i.e.,

$$\frac{\lambda^2 A}{4\pi^2 \Delta\nu} \left[T N_1 \left(\frac{N_2}{N_1} \right) \right] \geq \frac{2\kappa\rho}{10^{23}} N_1 \quad (1)$$

where the left side is the net gain factor due to stimulated emission² and the right side represents photoionization losses on the original states of density N_1 , with subscripts as defined above. The transition probability A is different from the x-ray rate X that is averaged over all terms. The parameter λ is the laser wavelength, $\Delta\nu$ is the line width in frequency units, κ is the solid absorption coefficient,²⁰ and ρ is the density of (solid) absorber. The factor $\kappa\rho/10^{23}$ is the $K\alpha$ photoionization cross section. The bracketed factor is the inversion density

$$\begin{aligned} \Delta N &= N_2 - (g_2/g_1)N_1 \\ &= N_1 \left(\frac{N_2}{N_1} \right) \left(1 - \frac{g_2 N_3}{g_1 N_2} \right) = T N_1 \left(\frac{N_2}{N_1} \right), \end{aligned} \quad (2)$$

where T indicates the degree of inversion and is evaluated in steady state by assuming N_3/N_2 to be given by the ratio of K - to L -vacancy depletion rates shown in Figs. 1 and 3. In a more complete time dependent model, T represents the stationary inversion achieved following the transient approach to equilibrium.²

For a first evaluation of Eq. (1), the product $\lambda^2 A$ may be approximated by 0.2 (cgs) and $2\pi\Delta\nu$ by the Auger rate, which does not vary rapidly with Z and is about 200 au^{-1} or $8 \times 10^{14} \text{ sec}^{-1}$. Thus, a first cut yields a ratio N_2/N_1 which is required to be greater than 10^{-1} to 10^{-3} depending on the absorption cross section κ and the degree of inversion (T) achieved. If the line width exceeds the natural width assumed (see below), even more inversion will be required.

Some relaxation of this requirement on inversion density could be achieved with multiple ionization, i.e., removal of some absorbing valence electrons. This could be an added advantage in the line shift model above if these valence electrons are in M_{III} shells or higher. However, ionization of electrons from lower shells will decrease the L -vacancy depletion rate and affect the degree of inversion achieved. A proper balance could come from a detailed numerical analysis.

A desired ratio $N_2/N_1 \approx 1\%$ may be considered to be achieved by electron collisions in a plasma, particle (electron) beam bombardment of a target, or by photon bombardment of a target. Only the latter appears at all feasible,⁵ since excessive plasma densities ($\geq 10^{25} \text{ cm}^{-3}$) are required for either ionization²¹ or dielectronic capture²² electron-collisional pumping schemes; and a required electron beam current of $\sim 10^{14} \text{ A/cm}^2$ is greatly in excess ($\sim 10^8 \times$) of that cur-

rently available in unfocused beams. Also, in both of these cases the rate for ionization from outershells exceeds that for the K innershell by orders of magnitude, so that efficient collisional innershell pumping seems most unpromising.

B. Photon Beams

For photon pumping, preferential innershell ionization can be achieved with a source tuned to emit predominantly in the K -absorption region, so that outershell photoionization is reduced.¹ The pumping rate P is given by $N_p \sigma_{pi}^K c$, where N_p is the x-ray photon density, and σ_{pi}^K is the K -shell photoionization cross section. In this particular case, it is possible to obtain this threshold value independent of absolute cross section, since photoionization losses are balanced against photoionization pumping. In equilibrium, $N_2/N_1 = P/(\Gamma + X)$, and Eq. (1) becomes

$$\frac{\lambda^2 A}{2\pi} T N_1 \left[\frac{N_p \sigma_{pi}^K c}{(\Gamma + X)^2} \right] \geq 2 \sigma_{pi}^L N_1, \quad (3)$$

where $2\pi\Delta\nu = \Gamma + X$ is assumed for natural line broadening (see below for validation of this assumption). With $\lambda^2 A \approx 0.2 \text{ ag}^2 \text{ in}$ and $\sigma_{pi}^K/\sigma_{pi}^L \approx 8$ near the K -absorption edge,²⁰ the required photon density is $N_p \geq 5\pi(\Gamma + X)^2/2Tc \text{ cm}^{-3}$.

Calculations are carried out for three cases, namely silicon, calcium, and copper, using published values⁸⁻¹² in Eq. (3) for the total decay rate $\Gamma + X$ (since $K\alpha_1$ and $K\alpha_2$ transitions must be pumped), values for T from Eq. (2), and the results plotted in Fig. 3, i.e., assuming the line shift mode of operation is possible. The results are listed in Table II, where for copper the results without the line shift advantage are also included in parentheses by calculating T from the data in Fig. 2. The photon densities N_p derived are converted to pump source radiances F by multiplying by $c(3hc/\lambda)$, where the latter factor represents the approximate pumping photon energy. Up to this point, the density of the laser medium has not entered.

The gain αL achievable with a chosen length L may be found from using the gain coefficient α given by the right side of Eq. (3), i.e.,

$$\alpha L = T N_1 \sigma_{pi}^K \left(\frac{L}{\sigma_{pi}^L / \sigma_{pi}^K} \right) L = T N_1 \sigma_{pi}^K L/4. \quad (4)$$

With σ_{pi}^K (see Table II) calculated from Ref. 23 at a pumping photon energy of 1.25 times the $K\alpha$ photon energy, and assuming $N_1 = 10^{23} \text{ cm}^{-3}$, the gain is calculated for a length of $300 \mu\text{m}$, which is $10 \times$ a reasonable $30\text{-}\mu\text{m}$ focal width (w). The results for the three cases are listed in Table II. For all three cases, the mean free path of a pumping x-ray photon, given by $(N_1 \sigma_{pi}^K)^{-1}$, is much less than the length, so that transverse (or oblique traveling wave) pumping is required, and the area is given by $Lw = 9 \times 10^{-5} \text{ cm}^2$. With this area and providing for a 10% efficiency of power conversion from the original pumping source to x rays of the proper energy, the pump power P required is derived and listed. Also indicated is the

Table II. $K\alpha$ Pumping Requirement.

Atom	λ (Å)	$10^{-14} \times$ ($\Gamma + A$) (sec $^{-1}$)	T	$10^{-20} N_e$ (cm $^{-3}$)	$10^{-2} F$ (TW/cm 2)	$10^{20} \frac{K}{\mu}$ (cm 2)	αL	P (TW) ^a $10^{-1} E$ (J)	kT_{BB} ^b (keV)	$(\lambda_m)_{BB}$ (Å)
^{14}Si	7.1	6.7	0.6	2	4.8	9	70	4	0.5	5
^{20}Ca	3.4	11	0.8	4	21	4	30	9	0.7	4
^{29}Cu	1.5	21	0.6	20	230	2	15	200	1.2	2
			(0.2)	(60)	(700)			(600)	(1.6)	(1.5)

() Refers to no line-shift case.

^a For 10% conversion efficiency.^b Using 1% of total blackbody spectrum.

corresponding pump energy E required for a 10-psec wide pulse, e.g., for a laser-heated-target x-ray source.

From Table II we may conclude that, with the advantage gained from line shifting, high net gain (≈ 70) is available in silicon with a reasonable pump, e.g., 40 J in a 10-psec pulse. Since it is unlikely that the vapor density can be maintained at 10^{23} cm $^{-3}$ (solid), the high gain is a safety factor, i.e., with a medium density as low as 7×10^{21} cm $^{-3}$, a gain of $\alpha L = 5$ is still possible. For shorter wavelengths the pumping energy increases (e.g., 2 kJ for copper, which is still within the realm of reality).

The assumed conversion (from pumping source to x-ray photons) efficiency of 10% is probably high, since the pump source must be converted into a somewhat narrow band of x-ray photons toward the high energy side of the K -absorption edge; at lower photon energies excessive outershell ionization will occur. If indeed the conversion could take place in the medium itself or in the immediate area and/or if a properly tuned pumping source is available, this efficiency might be realistic. An initially attractive possibility is radiation resulting from radiative recombination of electrons into $1s$ orbitals of hydrogenic and/or heliumlike ions of the lasing element in a surrounding blanket of high density plasma. As the inverse process of photoionization, the recombination spectral energy distribution complements the absorption process, i.e., there is preferential recombination emission at energies above the K -absorption edge. Taking the silicon example,⁵ the recombination emission for a 1-cm thick blanket can be calculated,²⁴ and it is found that a charged particle density of approximately 10^{23} cm $^{-3}$ is required, which is technically difficult to achieve. Broadband bremsstrahlung emission is hundreds of times lower.²¹

This difficulty with insufficient recombination radiation at reasonable plasma densities is associated with low emissivity. Blackbody radiation at a sufficiently high temperature is often considered as a limiting case (as for sodium in the VUV, for example²⁵). Included in Table I are the blackbody temperatures kT_{BB} in keV required to produce the required x-radiance with 1% utilization of the total blackbody emission. Also listed are the peak wavelengths (from Wien's law) for these temperatures. The results are

very reasonable regarding both plasma temperature and the matching of the peak of the emission with the absorption band. The problem is how to create such a blackbody source, since continuum emission is down by several orders of magnitude at reasonable densities. A possibility is a multiline source created in a heavy element, where the individual broadened lines have blended emissions approaching the continuous blackbody limit. This saturation is not unusual for intense VUV lines, and, with a careful selection of material, some tuning should be possible. For example, uranium has L and M atom and ion emission lines near 1 Å and 4 Å, respectively, and some work has already been performed on uranium discharges for intense pseudocontinuum sources in the VUV region.

IV. Line Broadening

Whenever a plasma is created in the laser medium, either intentionally to achieve a high density for pumping purposes or unavoidably due to intense ionization pumping with Auger processes contributing to the free electron production, the effect on the line width must be considered, since the gain varies inversely with line width.² Enhanced broadening (over the natural broadening assumed above) may exist due to random Doppler shifts and to charged particle interactions (Stark broadening). Both are considered here for radiation in the $K\alpha$ spectral regions for various elements. The results are not only relevant to $K\alpha$ innershell lines but to resonance lines of heliumlike and hydrogenic ions; in fact, Stark broadening rates are taken for $Ly-\alpha$ lines for convenience and availability.

An estimate of the Doppler width $\Delta\lambda_D$ is obtained from²¹:

$$\Delta\lambda_D/\lambda \approx \Delta\nu_D/\nu = 7.7 \times 10^{-5} (kT_i/\mu)^{1/2}, \quad (5)$$

where kT_i , the ion kinetic temperature, is in eV and μ is the atomic mass number of the element. Assuming as an approximation that $kT_i = h\nu/4$ (ν the $K\alpha$ -laser frequency) in an equilibrium plasma and $\lambda = \lambda$ (Lyman- α), $\Delta\lambda_D$ can be evaluated as a function of laser wavelength λ . The result is plotted in Fig. 4.

Stark widths for $K\alpha$ transitions may be estimated^{26,27} with sufficient accuracy for present purposes, from the lesser²⁶ of the widths given by formulas for

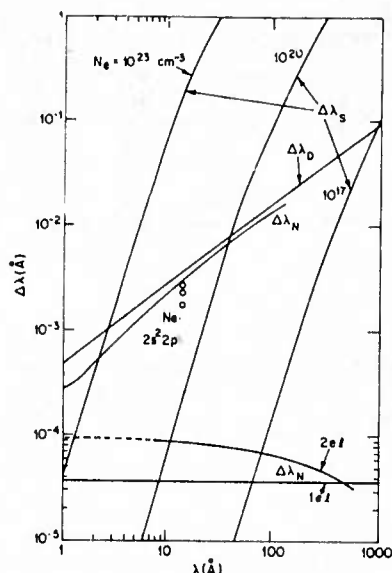


Fig. 4. Estimates of line widths for $K\alpha$ type transitions vs wavelength λ [with natural ($\Delta\lambda_N$), Doppler ($\Delta\lambda_D$), and Stark ($\Delta\lambda_S$) effects included]. The decrease in natural broadening with ionization is indicated by circles for neon; and hydrogenic and helium-like ionic species are included.

the quasi-static linear Stark effect (Holtmark theory) and for the electron impact broadening. The former is given approximately for Lyman- α transitions by

$$\Delta\lambda_H \approx \frac{2n^2\lambda^2}{\pi c} \frac{\hbar}{m} \frac{\bar{Z}_p}{Z_i} N_p^{2/3}, \quad (6)$$

where Z_i is the ion charge and \bar{Z}_p the average perturber charge of density N_p . For a single-ion plasma where $\bar{Z}_p = Z_i$ this becomes

$$\Delta\lambda_H \approx \frac{2n^2\lambda^2}{\pi c} \frac{\hbar}{m} N_e^{2/3} \quad (7)$$

for the (lesser) electron-perturber limit. The electron impact broadening²⁷ is found from

$$\Delta\lambda_e \approx \frac{3n^4\lambda^2}{c} \left(\frac{\hbar}{mZ_i} \right) \frac{N_e}{v_e}, \quad (8)$$

where the factor $n^2(n^2 - 3) \ln(\epsilon_{\max}/\epsilon_{\min})$ has been approximated numerically by n^4 for Lyman- α transitions. Also, v_e may be replaced by the mean thermal velocity for the electrons at the plasma kinetic temperature derived above, i.e., $h\nu/4$. The resulting Lyman- α ($n = 2$) Stark widths $\Delta\lambda_S$ are plotted in Fig. 4 as a function of wavelength for three electron density values. The magnitudes of these two Stark broadening processes are approximately the same for present conditions. There is, for some schemes, an advantage in increasing the electron temperature preferentially over the ion temperature for increased electron collisional pumping without additional Dop-

pler broadening. This will have the effect of decreasing the (Lorentz) width through v_e in Eq. (8).

From Fig. 4 a comparison is now possible between plasma line widths (Doppler and Stark) for $K\alpha$ transitions and natural widths $\Delta\lambda(\equiv \lambda^2\Delta\omega/2\pi c)$ determined from $\Delta\omega = \Gamma + X$, Γ being the Auger rate and X the x-ray decay rate. The Auger data used here are mostly for single K vacancies in neutral atoms; for one case, namely neon ($\lambda = 14.6 \text{ \AA}$), the reduction in natural width with multiple ionization is indicated.²⁸ Also shown for general interest are the natural widths $\Delta\lambda_N$ ($\Delta\omega = A$, the transition probability) for helium-like and hydrogenic species, where the latter is a straight line since Ly- α wavelengths were used, i.e., $A \propto \lambda^{-2}$ and $\Delta\lambda_N \propto \lambda^2 A$.

From Fig. 4 it is clear that Doppler broadening is not significantly larger than innershell natural broadening at a low degree of ionization. Also, Lyman- α type ($n = 2$) Stark broadening even at solid densities ($\sim 10^{23} \text{ cm}^{-3}$) is not dominant for wavelengths shorter than 4 \AA . Therefore, line broadening alone does not preclude a unified plasma approach to x-ray lasing on $K\alpha$ transitions. The significant reduction in line width shown and the avoidance of photoionization losses offered by hydrogenic and heliumlike ions could only be realized in a relatively tenuous, expanded, low temperature plasma with frozen-in ions of these types, where quasi-cw operation according to the present scheme is not possible.

V. Summary

Quasi-stationary population inversion appears to be possible, even with the most recent calculations of Auger rates, for elements with Z less than 40. It appears that the line shift with multiple ionization will help in maintaining inversion; however, the need for a more complete numerical rate-equation analysis is clearly indicated. Assuming quasi-cw operation is feasible, the pump power requirements necessary to overcome photoionization losses and at the same time achieve useful gain do not appear to be completely unreasonable, particularly when blackbody x-ray emission is considered as a pumping source. It is suggested that partial blackbody radiation in the selected wavelength band required for innershell photoionization pumping be acquired with intense multiline radiation from heavy atoms and ions.

References

1. M. A. Duguay and R. M. Rentzepis, Appl. Phys. Lett. 10, 350 (1967).
2. R. C. Elton, R. W. Waynant, R. A. Andrewa, and M. H. Reilly, Naval Research Laboratory Report 7412 (May 1972).
3. Yu. L. Stankevich, Sov. Phys. Dokl. 15, 356 (1970).
4. As used here, innershell implies that at least one additional electron exists in a shell of larger principal quantum number than for that shell in which the initial vacancy is produced.
5. R. C. Elton, Naval Research Laboratory Memorandum Report No. 2906, (1974); also Physica Fennica 9, Suppl. SI, 397 (1974).
6. M. A. Blokhin and V. P. Sashenko, Izv. Akad. Nauk. USSR 21, 1333 (1957).

7. M. A. Blokhin, "The Physics of X-Rays" (translated), IAEA Report AEC-tr-4502 (1961).
8. E. J. McGuire, Phys. Rev. 185, 1 (1969); Phys. Rev. A 2, 273 (1970).
9. D. L. Walters and C. P. Bhalla, Phys. Rev. A 3, 1919 (1971); At. Data 3, 301 (1971).
10. J. H. Scofield, Phys. Rev. 179, 9 (1969); also LLL Report UCRL-51231 (1 June 1972).
11. J. H. Scofield, Phys. Rev. A 9, 1041 (1974).
12. E. J. McGuire, Phys. Rev. A 3, 587 (1971).
13. P. J. Mallozzi, private communication (1973); M. A. Duguay, private communication to R. A. Andrews (1974).
14. F. T. Arecchi, G. P. Banfi, and A. M. Malvezzi, Opt. Commun. 10, 214 (1974).
15. R. L. Kelly and D. E. Harrison, Jr., At. Data 3, 177 (1971).
16. L. L. House, Astrophys. J. Suppl. 18, 21 (1969).
17. T. N. Lie and R. C. Elton, Phys. Rev. A 3, 865 (1971); earlier evidence of innershell ion transitions is reviewed here.
18. E. J. McGuire, Phys. Rev. A 5, 1052 (1973).
19. T. Åberg, Phys. Rev. A 4, 1735 (1971).
20. F. R. Gilmore, Rand Report RM 5367-AEC (10 April 1959).
21. R. C. Elton, in *Plasma Physics, Vol. 9A Methods of Experimental Physics* H. R. Griem and R. H. Lovberg, Eds. (Academic, New York, 1971).
22. S. M. R. Ansari, G. Elwert, and P. Mücklich, Z. Naturforsch. 25, 1781 (1970); A. H. Gabriel and T. M. Paget, J. Phys. B 5, 673 (1972).
23. W. D. Barfield, G. D. Koontz, and W. F. Huebner, J. Quant. Spectrosc. Radiat. Transfer 12, 1409 (1972).
24. H. R. Griem, *Plasma Spectroscopy* (McGraw-Hill, New York, 1964).
25. W. W. Jones and A. W. Ali, NRL Memorandum Report 2807; P. Bey, NRL Memorandum Report 2847 (1974).
26. H. R. Griem, private communication (1974).
27. H. R. Griem, *Broadening of Spectral Lines by Charged Particles in Plasmas* (Academic, New York, 1974).
28. C. P. Bhalla, N. O. Folland, and M. A. Hein, Phys. Rev. A 8, 649 (1973).

COPY AVAILABLE TO DDC DOES NOT PERMIT FULLY LEGIBLE PRODUCTION

SPECTROSCOPY OF PLASMAS FOR SHORT WAVELENGTH LASERS*†

R. C. Elton and R. H. Dixon

Naval Research Laboratory

Washington, D. C. 20375

ABSTRACT

The achievement of significant amplified spontaneous emission at short wavelengths requires either very high densities or very long lengths. The former approach appears more promising at present for concentrating the large pumping power required, and plasma media are anticipated under such conditions. Most often lasing times are short and extension with metastable states does not appear possible at the high density required and with competing dipole transitions. Focused high power laser beams offer the most promising source of concentrated pump energy at present. An inversion scheme of high pump probability for short wavelength lasing involving resonance charge transfer of an electron from a neutral atom to an ion has been identified, and an experiment designed to test this scheme is described. Initial space-resolved spectra are presented, as is the distribution of the measured photographic spectral line density with distance from the surface of a laser heated carbon target as obtained with a space-resolved grazing-incidence spectrograph. Early results indicate optically thick resonance lines extending to approximately 0.8 mm from the target. Charge transfer pumping is expected at distances ≥ 2 mm. No definitive data are so far available with a neutral gas background.

INTRODUCTION

It is the primary intention in this paper to present some recent spectroscopic results from helium-like and hydrogenic

*Supported in part by the Defense Advance Research Project Agency, DARPA Order 2694.

†Paper presented at the 4th International Conference on Beam Foil Spectroscopy, Gatlinburg, Tenn., September 1975 (proceedings to be published).

carbon ions obtained in a laser-produced plasma. The experiment is being conducted to investigate a potentially promising approach to achieving laser action at very short wavelengths, namely resonance charge transfer of electrons from a neutral atom into excited states of a highly-stripped ion. Although a number of articles have recently been written on the subject of short wavelength lasers and a comprehensive review article is in preparation¹, it is appropriate to include some brief introductory remarks in this paper to accent those areas of particular interest to beam foil spectroscopists and other specialists at this conference.

At present the existence of undisputed vacuum ultraviolet lasing has been achieved for wavelengths as short as 1098 Å with power levels varying from 10 kW to 500 MW, mostly with molecular transitions. Frequency multiplication of a coherent infrared laser beam has been successfully extended to wavelengths as short as 887 Å. At shorter wavelengths small degrees of population inversion have been reported for hydrogenic ion lines following recombination, but so far no undisputed claims of measured net amplification are available.

The difficulties encountered in extending lasing to wavelengths shorter than 1000 Å and into the x-ray region can easily be seen from simple scaling laws.² The problems begin with a lack of efficient resonanting cavities so that a measurable gain given by $\exp(\alpha L)$ for an amplifying length L is only achieved for a positive gain coefficient α exceeding unity. For Doppler broadened spectral lines the linear gain coefficient α_D scales as

$$\alpha_D \propto \frac{\lambda^3}{\bar{v}} \left[A_{ul} N_o \left(\frac{N_u}{N_l} \right) \right] \left\{ 1 - \frac{N_l}{N_u} \frac{g_u}{g_l} \right\}, \quad (1)$$

where \bar{v} represents the mean velocity of the lasing ion; N_o , N_u , and N_l , represent the population densities of the initial state and the upper and lower laser states, respectively; g_u and g_l are the appropriate statistical weights; A_{ul} is the transition probability for the laser transition; and λ is the wavelength of the lasing transition. Positive values of α_D are required for net gain. Written in this form, it is obvious that the achievement of population inversion is possible as indicated in the last factor (shown in braces) irregardless of the absolute value of the gain coefficient; thus the early reports of evidence of population inversion without measurable gain. A high gain coefficient at short wavelengths therefore depends primarily on the first factor (indicate in brackets) in Eq. (1). This factor may be written as

$$\left[\left(\frac{P}{aL} \right) \frac{\lambda_{ou}}{hc} \right], \quad (2)$$

where P/aL is the pump power density for a cross-sectional area a and length L of laser volume, and hc/λ_{ou} represents the pumping energy. When λ_{ou} is assumed equal to 10λ and α_D is set equal to 5, absolute values for P/aL become approximately 10^{11} W/cm² for a wavelength $\lambda = 100 \text{ \AA}$, and it is clear that this power density scales as λ^{-4} . The bracketed factor in Eq. (2) can also be written as

$$\left[N_o N_p r_{ou} \right], \quad (3)$$

where $r_{ou}(\lambda)$ is the rate coefficient for pumping from some initial state o to upper state laser u , and N_p is the density of pumping particles or photons. The rate coefficient r_{ou} depends upon the particular pumping atomic process and varies with wavelength according to the particular cross section as well as the conditions of the pumping source. Independent of the wavelength dependence of r_{ou} , the density product $N_o N_p$ varies as λ^{-3} for a fixed value of α_D . It is desirable to keep these densities low, both to avoid additional collisional effects and also to permit higher gain coefficients achievable at increased densities. Therefore, a pumping process with a rate coefficient r_{ou} bearing a strong inverse dependence on wavelength and a large absolute cross section is most desirable. From this point of view, the most promising process identified so far for pumping at short wavelengths is resonance charge transfer of an electron from a neutral atom to an ion in a collision, where the cross section³ is given approximately by $10^{-16} \pi a^2 \text{ cm}^2$ and the rate coefficient r_{ou} is given approximately by $10^{-6} \lambda^{-5/4}$, which is several orders of magnitude larger than other known pumping processes.² With this process a gain coefficient $\alpha_D = 5$ is predicted at a density of 10^{19} cm^{-3} and a wavelength as short as 8 \AA . Further details of this scaling for other processes is published elsewhere.^{2,4}

In addition to considerations of the pulse power and the lasing density requirements, the time available for lasing is also a serious consideration at short wavelengths; since for many processes it is expected to be as short as the lifetime of the upper laser state which scales as λ^{-2} and varies from 10^{-9} sec. at 1000 \AA to 10^{-15} sec. in the x-ray region. Thus, there is also a search for cw or quasi-cw laser schemes with extended lasing times. It is natural, particularly for participants at this conference, to think first of metastable states for this purpose. The above relations show that both the gain coefficient and the pump power density are proportional to the product of a density and the upper to lower state transition probability. Thus, proportionally higher densities are required for the low probability of metastable states, for a given gain coefficient, and collisional effects begin to dominate over radiative effects. (However, it is to be noted that the pump power density is independent of the lasing density or the transition probability for a fixed gain coefficient.) Also it

has so far not been possible to identify a transition from a metastable state that is not in direct competition with a dipole transition to the same lower state, which will rapidly destroy population inversion and thereby negate any advantage of the long-lived metastable state. Therefore, the only proposal published⁵ for the use of metastable states in short wavelength lasing is for the storage of electrons in the 2^1S metastable state of helium-like ions for subsequent rapid transfer (pumping) to the 2^1P state, followed by lasing on the $2^1P \rightarrow 1^1S$ resonance transition.

RESONANCE CHARGE TRANSFER EXPERIMENT

The high pumping flux required in small volumes and (most often) the short pump pulse risetime required demand the use of plasmas as a lasing medium and focused laser beams as a pumping source for the shorter wavelength regions. A typical plasma approach is the resonance charge transfer pump scheme, as originally proposed³ by Vinogradov and Sobel'man and illustrated schematically in Fig. 1 for a particular ion-atom combination, namely C^{5+} and helium, which has been shown by a simple Landau-Zener theory^{4,6} for exothermic reactions to have a large cross section for the particular plasma temperatures expected in the presence of these ions. The $n = 3$ states of the helium-like ions formed are expected

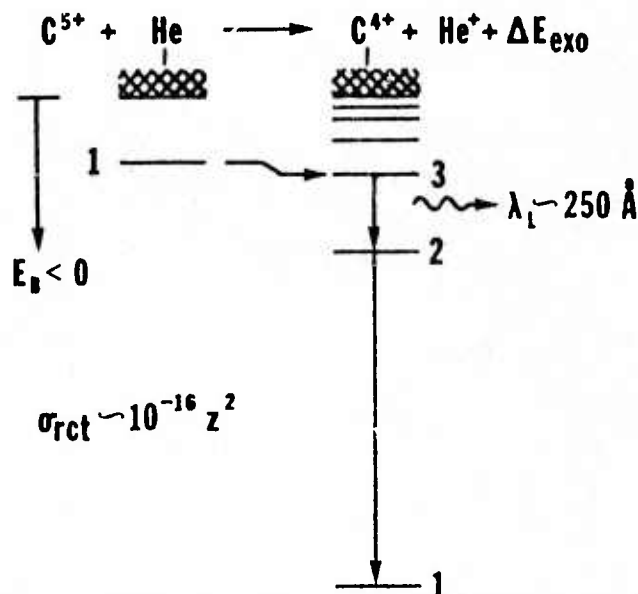


Fig. 1--
Schematic diagram of the exothermic resonance charge transfer reaction leading to population inversion between $n=3$ and $n=2$ levels in C^{4+} helium-like ions following collisions with helium atoms. E_B represents the binding energy.

to be preferentially populated at a high rate from the $1s^2 1s$ ground state of neutral helium atoms in collisions, with subsequent lasing between $n=3$ and $n=2$ states and rapid lower $n=2$ laser state depletion, with inversion obtained as long as the initial ions are maintained at a sufficient density. An experiment designed to test this scheme is shown schematically in Fig. 2, where a laser beam is focused onto a carbon slab target before the entrance slit of a grazing incidence spectrograph capable of recording the resonance series of hydrogenic and helium-like carbon lines in the soft x-ray spectral region. The slot shown between the entrance slit and the grating in Fig. 2 provides spatial resolution of the emission from the plasma plume produced, as indicated along the length of the spectral lines recorded. The neutral-atom background, namely helium in the present case, is not indicated in Fig. 2. The experiment is also shown in the photograph in Fig. 3 where the lucite chamber holding the rotatable disk carbon target is shown attached to the entrance of the grazing incidence spectrograph. A ruby laser capable of delivering 6 J, 20 ns FWHM pulses to a 500 μm focal spot is shown mounted above the spectrograph.

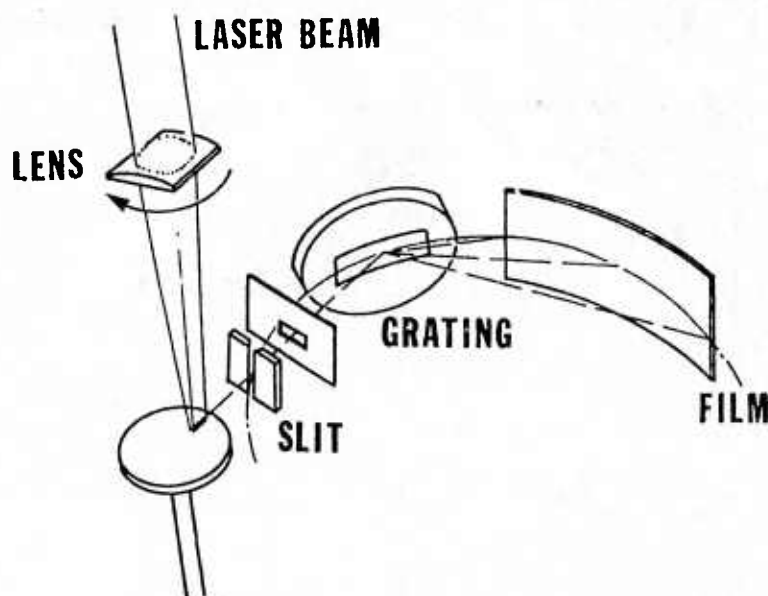


Fig. 2--
Schematic diagram of the resonance charge transfer experiment, including the grazing incidence vacuum spectrograph. The orthogonal slot shown provides spatial resolution along the direction of plasma expansion from the target surface, as traced in Fig. 5.

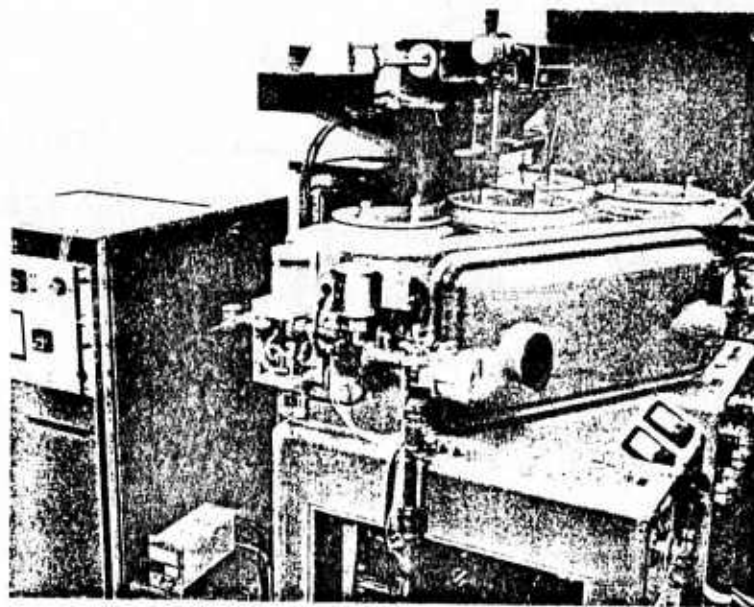


Fig. 3

Photograph of the resonance charge transfer experiment showing the lucite target chamber attached to the grazing incidence spectrograph and the laser in current use.

The initial results that can be reported at present are for expansion into vacuum, which provides a reference spectrum, as shown in Fig. 4. This is a second order spectrum of hydrogenic and helium-like resonance lines, with the true wavelength indicated in Å units and the distance from the target surface indicated in millimeters. The weaker lines indicated in this spectrum have been identified as other second order lines, known satellite lines, or in a few cases impurity lines. Significant Stark broadening of the spectral lines can be observed in the high electron density region near the target surface, and is an indicator of the electron density. At present, microdensitometer scans along the wavelength axis at various distances from the target surface are being compared with similar spectra obtained in the presence of helium background gas, in a search for evidence of enhanced population of specific levels as indicated by the resonance line emission from these levels. While the data for such comparisons is at present sparse and inconclusive, it is possible to report on the variation of the photographic densities with distance from the target surface for various spectral lines important to this experiment. The results are plotted in Fig. 5 for a vacuum expansion, where an

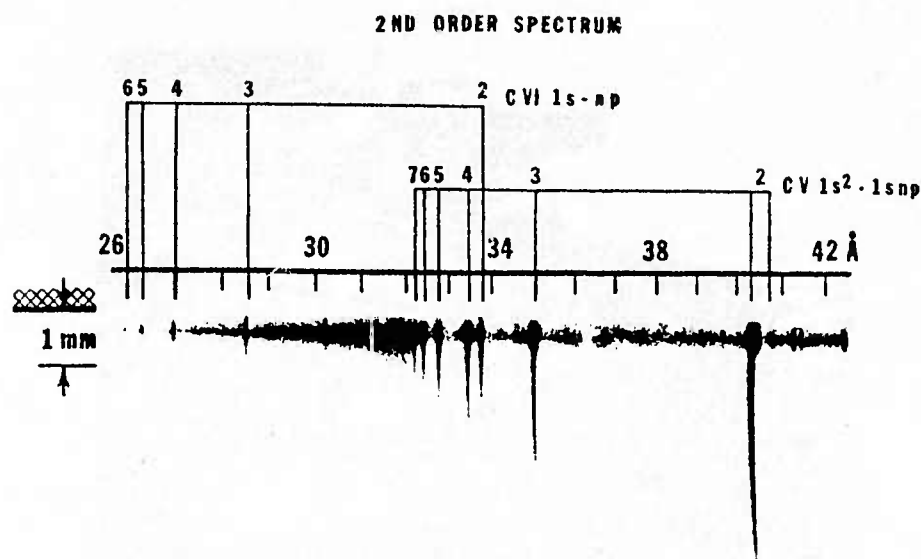


Fig. 4--
Spatially resolved CV and CVI grazing incidence spectrum using a 400 μm slot as shown in Fig. 2. No background gas was present.

instrumental resolution in distance of 1 mm is expected at the plasma.

INITIAL RESULTS

The preliminary results obtained comparing spectra with and without the neutral helium atmosphere are to date inconclusive and will not be discussed here. Under vacuum conditions, both the line (Fig. 5) and the continuum emission are observed to initially increase with distance from the target surface. This is consistent with a rising temperature and the formation during the rising laser pulse of an expanding high density critical absorption layer for the laser radiation. Association of the increasing continuum emission with density through bremsstrahlung and recombination processes is consistent with the increasing Stark broadening⁷ in the same region, as observed in the spectrum of Fig. 4.

Compared in Fig. 5 are the photographic densities (with the continuum background subtracted) of the resonance series lines⁸

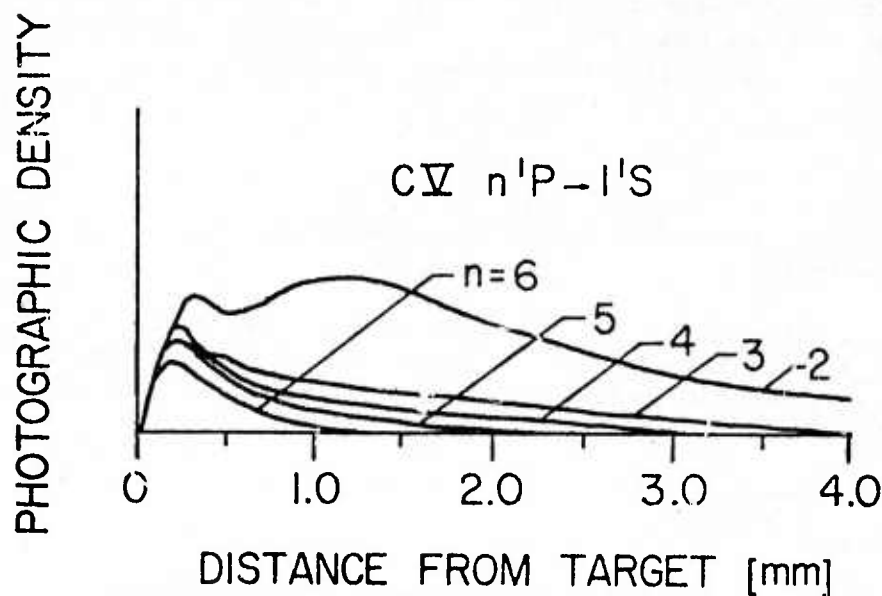


Fig. 5--

Photographic density versus distance from target from space-resolved grazing incidence spectrum for the C^{4+} (CV) resonance series.

from the helium-like C^{4+} ions in vacuum (CV reference spectrum). While these densities have so far not been converted to exposures, it is clear that at distances greater than 0.8 mm the total line intensity ratios scale approximately as expected, particularly for those lines associated with transitions originating on levels with principal quantum number $n \geq 3$. It is this "outer" region (≈ 2 mm), where the density decreases⁷ to $\leq 10^{18} \text{ cm}^{-3}$, that is of interest to the present carbon-ion/helium-atom resonance charge transfer experiment. The $2^1P \rightarrow 1^1S$ first resonance line appears to have an enhanced emission which may be associated with a considerably higher oscillator strength compared to the other lines in the series, as evidenced from data available for neutral helium⁹.

Close to the target surface, the relative line emissions are more nearly equal, for some of the series members. This can most likely be attributed to opacity effects¹⁰ in the higher density region, with perhaps the emission of lines of varying strength from separate layers. Near 0.5 mm the first series member shows a distinct dip in emission which is also evident on

the second member of the series. This also is most likely associated with increased opacity for these stronger members of the series. Indeed, the first member may be suppressed in the closest regions by reabsorption in cooler outer layers of the plasma plume. Again, it is fortunate that the resonance charge transfer effects sought will become most evident at greater distances where it appears that reabsorption is less severe a problem.

REFERENCES

1. R. W. Waynant and R. C. Elton, Proceedings IEEE (in preparation).
2. R. C. Elton and R. H. Dixon "X-Ray Laser Research; Guidelines and Progress at NRL", Proceeding Third Conference on Lasers, New York Academy of Sciences, April 1975 (to be published).
3. A. V. Vinogradov and I. I. Sobel'man, Soviet Physics JETP, 36, 1115 (1973).
4. R. C. Elton, in Progress in Lasers and Laser Fusion, A. Pearlmutter and S. M. Widmayer, eds., p. 117 (Plenum Press, New York, N.Y., 1975).
5. H. Mahr and V. Roeder, Optics Comm. 10, 227 (1974).
6. H. J. Zwally and D. W. Koopman, Physical Review A 2, 1851 (1970).
7. A. M. Malvezzi, E. Jannitti and G. Tondello (to be published).
8. R. L. Kelly and L. J. Palumbo, "Atomic and Ionic Emission Lines Below 2000 Angstroms", Naval Research Laboratory Report No. 7599 (1973).
9. W. L. Wiese, M. W. Smith, and B. M. Glennon, "Atomic Transition Probabilities", National Bureau of Standards Report No. NSRDS-NBS 4 (1966).
10. R. C. Elton, "Atomic Processes", in Methods of Experimental Physics-Plasma Physics, Vol. 9A, p. 142, H. R. Griem and R. H. Lovberg, eds. (Academic Press, New York, N. Y., 1970).

Submitted to the Physical Review, October 1975

NEGATIVE NONLINEAR SUSCEPTIBILITY
OF CESIUM VAPOR AROUND $1.06\mu^*$

R. H. Lehmberg, J. Reintjes, and R. C. Eckardt

Naval Research Laboratory
Washington, D.C. 20375

*This work was supported jointly by the Defense Advanced Research Projects Agency, ARPA Order No. ~~2694~~ and the U. S. Energy Research and Development Agency.

ABSTRACT

We outline a complete theory of the nonlinear susceptibility of cesium around 1.06μ , and present the first measurements of the negative nonlinear refractive index n_2 primarily responsible for the self defocusing that is observed. For linearly polarized light, our measured value of n_2 is $-(1.4 \pm 0.2) \times 10^{-30}$ N esu, where N is the atomic density. This is in reasonable agreement with our calculated value of -2.62×10^{-30} N. The main portion of n_2 comes from a two-photon resonance between the 6s and 7s levels, and an additional negative term arises from induced population changes between 6s and 6p. For circular polarization, n_2 arises mainly from the induced population changes, giving the measured and calculated values of $-(0.26 \pm 0.03) \times 10^{-30}$ N and -0.525×10^{-30} N, respectively. In our experiments, where the 35 psec pulses were shorter than the 6s-6p inverse linewidth, the nonlinear susceptibility depends mainly on the instantaneous intensity; however, for longer pulses, one would obtain additional contributions proportional to time integrals over the intensity. Since the useful output power from large Nd laser systems is limited by self focusing due to the laser glass, our results suggest the possibility of increasing this power by using Cs vapor for compensation.

I. INTRODUCTION

In recent years, a number of authors have observed self-focusing,¹⁻⁴ self-defocusing,⁵ and other related effects^{3,7} due to a resonant enhancement of the electronic nonlinear susceptibility in atomic vapors. These effects arise from optically induced population changes associated with single photon^{1-3,5-7} or two photon⁴ absorption.

Recently, we reported the observation of self-defocusing of mode locked 1.06 μ pulses in cesium vapor.⁸ For linearly polarized light, we attributed this primarily to a two photon resonant enhancement of the third order nonlinear susceptibility.⁹ This contribution leads to an intensity dependent refractive index $\delta n^{(3)}(t) \sim n_2 I(t) \sim I(t)/(\omega_{20} - 2\omega)$, where n_2 is the nonlinear refractive index, and ω and ω_{20} are, respectively, the optical frequency and the near resonant atomic frequency. In cesium vapor around $\lambda = 1.06 \mu$, 2ω lies slightly above the 6s-7s frequency; hence, $n_2 < 0$, and at pressures of a few Torr, its magnitude is comparable to that of laser glass.¹⁰ Since the useful output power from large Nd laser systems is ordinarily limited by self focusing in the glass amplifiers, the existence of a negative n_2 at 1.06 μ raises the possibility of increasing this power by using Cs vapor for compensation.

The nonlinear behavior of Cs is complicated somewhat by additional self defocusing contributions arising primarily from pulse induced population changes in the 6s and 6p levels. For pulsewidths t_p short in comparison to the 6s-6p dephasing time τ_{10}^{-1} , this effect remains intensity dependent,^{1,5} and for linearly polarized light, its contribution to n_2

is relatively small; however, as a result of atomic collisional relaxation, it can also contribute terms proportional to time integrated intensities,¹¹ and these "inertial" terms can easily predominate if $t_p \gg \Gamma_{10}^{-1}$. The result is then similar to thermal defocusing.¹²

In this paper, we outline a complete theory of the third order non-linear refractive index $\delta n^{(3)}(t)$, and relate this to earlier theoretical work.^{11,13-15} We then describe the first measurements of n_2 in Cs vapor at 1.064μ under conditions where the instantaneous terms are expected to predominate, and compare these results to the theory.

Assuming only that t_p is short in comparison to the atomic radiative lifetimes, and that ω and 2ω lie outside the atomic line profiles, we show that $\delta n^{(3)}(t)$ can always be expressed as the sum of instantaneous and inertial contributions. The inertial terms derived here include the effects of excited state collisional mixing (e.g., among the $6p$ sublevels) in addition to atomic phase relaxation. Specializing to a three level model applicable to Cs around 1.06μ ,³ we then derive simple approximate expressions for the two photon and induced population terms described above. We show, in particular, that the $6s$ - $7s$ two photon term disappears if the light is circularly polarized.

The measurements of n_2 were carried out by observing the self defocusing of linearly and circularly polarized mode-locked pulses in a cesium cell. We also measured the insertion loss of the cesium at different peak intensities, and found a broad minimum ($< 5\%$ absorption) centered around 5 GW/cm^2 . The measured values of n_2 are $-(1.4 \pm 0.2) \times 10^{-30} \text{ N esu}$ for linear polarization and $-(0.26 \pm 0.05) \times 10^{-30} \text{ N esu}$ for circular polarization, in reasonable agreement with the calculated values of $-2.62 \times 10^{-30} \text{ N}$ and $-0.525 \times 10^{-30} \text{ N}$, respectively.

II. THEORY

A. Basic Equations

The lowest order nonlinear refractive properties of an isotropic medium can be found from the polarization

$$\vec{P}^{(3)}(t) = N \sum_{\alpha, \beta} \vec{\mu}_{\beta\alpha} \rho_{\alpha\beta}^{(3)}(t) \quad (1)$$

induced by the optical field

$$\vec{E}(t) = \frac{1}{2} \hat{e} \mathcal{E}(\omega, t) e^{-i\omega t} + \frac{1}{2} \hat{e} \mathcal{E}(-\omega, t) e^{+i\omega t}. \quad (2)$$

Here, N is the atomic density, $\vec{\mu}_{\beta\alpha} = e\vec{r}_{\beta\alpha}$ are the atomic dipole matrix elements between states $|\alpha\rangle$ and $|\beta\rangle$, $\rho_{\alpha\beta}^{(3)}(t)$ are the corresponding third order density matrix elements, $\mathcal{E}(\omega, t) = [\mathcal{E}(-\omega, t)]^*$ is the slowly varying optical field amplitude, and \hat{e} is a unit vector defining the optical polarization state. The density matrix elements are obtained by solving the Boltzmann equations

$$\dot{\rho}^{(n)}(t) = -(i/\hbar) \left[H_0, \rho^{(n)}(t) \right] - (i/\hbar) \left[V(t), \rho^{(n-1)}(t) \right] + \left\{ \dot{\rho}^{(n)}(t) \right\}_R, \quad (3)$$

for $n = 1, 2, 3$, subject to the condition $\rho_{00}^{(0)} \approx 1$. Here,

$$H_0 = \sum_{\alpha} \hbar \omega_{\alpha} |\alpha\rangle\langle\alpha|, \quad V(t) = -\sum_{\alpha, \beta} \vec{E}(t) \cdot \vec{\mu}_{\alpha\beta} |\alpha\rangle\langle\beta|, \quad (4)$$

$|0\rangle$ is the ground state, $\hbar\omega_{\alpha}$ is the energy difference between $|\alpha\rangle$ and $|0\rangle$, and $\left\{ \dot{\rho}^{(n)}(t) \right\}_R$ describes the atomic relaxation. If we write

$\rho_{\alpha\beta}^{(3)}(t)$ in terms of its slowly varying amplitudes $\sigma_{\alpha\beta}^{(3)}(\omega, t) = [\sigma_{\beta\alpha}^{(3)}(-\omega, t)]^*$

$$\rho_{\alpha\beta}^{(3)}(t) = \frac{1}{2} \sigma_{\alpha\beta}^{(3)}(\omega, t) e^{-i\omega t} + \frac{1}{2} \sigma_{\alpha\beta}^{(3)}(-\omega, t) e^{+i\omega t} + \text{3rd harmonic terms}, \quad (5)$$

then the nonlinear contribution to the refractive index of an isotropic medium is

$$\delta n^{(3)}(t) = 2\pi N \sum_{\alpha, \beta} \hat{e}^* \cdot \vec{\mu}_{\beta\alpha} \sigma_{\alpha\beta}^{(3)}(\omega, t) / \epsilon(\omega, t) \quad (6)$$

The following two simplifications are assumed to be valid throughout the remainder of this paper: (i) One can ignore all longitudinal relaxation processes, except for collisional mixing among the excited levels, and (ii) the atomic and laser linewidths are negligible in comparison to the detuning frequencies $|\omega_{\alpha\beta} - \omega|$ and $|\omega_{\alpha\beta} - 2\omega|$ that arise in the expression for $\delta n^{(3)}(t)$. Condition (i), which is generally necessary to avoid optical pumping effects,¹⁰ requires that the laser pulsewidth t_p be short in comparison to the radiative lifetimes of the excited states. Condition (ii) is well satisfied for cesium vapor around 1.06 μ with $N \leq 10^{19} \text{ cm}^{-3}$ and laser linewidths up to several angstroms.

The resulting solution of Eqs (1)-(6), which is outlined in the appendix, yields the expression

$$\delta n^{(3)}(t) = \delta n'(t) + \delta n''(t) \quad (7a)$$

$$= n_2 \langle E^2(t) \rangle + 2\pi N \sum_{\alpha, \beta} \chi_{\alpha\beta} [q_\beta(t) - q_\alpha(t)]. \quad (7b)$$

In $\delta n'(t)$, the nonlinear refractive index is

$$n_2 \equiv \frac{2\pi N}{h} \sum_{\beta \neq 0} \left[\frac{|P_\beta^-|^2}{\omega_{\beta 0} - 2\omega} + \frac{|P_\beta^+|^2}{\omega_{\beta 0} + 2\omega} + \frac{|Q_\beta|^2}{\omega_{\beta 0}} \right] - 2\pi N \left[Q_0 \sum_{\alpha} R_{\alpha} + (|P_0^-|^2 - |P_0^+|^2)/2\hbar\omega \right], \quad (8)$$

where

$$P_\beta^- \equiv \sum_{\alpha} \frac{\hat{e} \cdot \vec{\mu}_{\beta\alpha} \hat{e} \cdot \vec{\mu}_{\alpha 0}}{\hbar(\omega_{\alpha 0} - \omega)}, \quad P_\beta^+ \equiv \sum_{\alpha} \frac{\hat{e}^* \cdot \vec{\mu}_{\beta\alpha} \hat{e}^* \cdot \vec{\mu}_{\alpha 0}}{\hbar(\omega_{\alpha 0} + \omega)}, \quad (9a)$$

$$Q_\beta \equiv \sum_{\alpha} \left[\frac{\hat{e}^* \cdot \vec{\mu}_{\beta\alpha} \hat{e} \cdot \vec{\mu}_{\alpha 0}}{\hbar(\omega_{\alpha 0} - \omega)} + \frac{\hat{e} \cdot \vec{\mu}_{\beta\alpha} \hat{e}^* \cdot \vec{\mu}_{\alpha 0}}{\hbar(\omega_{\alpha 0} + \omega)} \right] \quad (9b)$$

$$R_{\alpha} \equiv \frac{|\hat{e} \cdot \vec{\mu}_{\alpha 0}|^2}{\hbar^2(\omega_{\alpha 0} - \omega)^2} + \frac{|\hat{e}^* \cdot \vec{\mu}_{\alpha 0}|^2}{\hbar^2(\omega_{\alpha 0} + \omega)^2} \quad (9c)$$

and the bracket $\langle \rangle$ denotes an average over an optical cycle [i.e.,

$\langle E^2(t) \rangle = \frac{1}{2} |E(\omega, t)|^2$]. In $\delta n''(t)$,

$$\chi_{\alpha\beta} \equiv \frac{|\hat{e} \cdot \vec{\mu}_{\alpha\beta}|^2}{\hbar(\omega_{\alpha\beta} - \omega)} + \frac{|\hat{e}^* \cdot \vec{\mu}_{\alpha\beta}|^2}{\hbar(\omega_{\alpha\beta} + \omega)} \quad (10)$$

is a linear susceptibility, the quantities $q_{\alpha}(t)$ are solutions of the rate equations

$$\dot{q}_{\alpha}(t) = -W_{\alpha} q_{\alpha}(t) + \sum_{\beta \neq \alpha} W_{\beta\alpha} q_{\beta}(t) + S_{\alpha} \langle E^2(t) \rangle \quad (11)$$

subject to the initial conditions $q_{\alpha}(-\infty) = 0$, the driving terms are

$$S_{\alpha} \equiv (\Gamma_{\alpha 0} - \frac{1}{2}W_{\alpha})R_{\alpha} + \sum_{\beta \neq \alpha} \frac{1}{2}W_{\beta\alpha}R_{\beta}, \quad (\alpha \neq 0) \quad (12a)$$

$$S_0 \equiv - \sum_{\alpha \neq 0} \Gamma_{\alpha 0} R_{\alpha} \quad (12b)$$

$\Gamma_{\alpha 0}$ is the homogeneous relaxation rate of $\rho_{\alpha 0}(t)$, and $W_{\beta\alpha}$ is the $\beta \rightarrow \alpha$ collisional mixing rate, which satisfies the conditions

$$W_{\beta\alpha} = W_{\alpha\beta} e^{-\hbar\omega_{\alpha\beta}/kT}, \quad (13a)$$

$$W_{\alpha} \equiv \sum_{\beta} W_{\alpha\beta} \leq 2\Gamma_{\alpha 0}, \quad (13b)$$

where $W_{\alpha\beta} = 0$ if α or β are zero. From Eqs. (11), (12), (13b) and the initial condition $q_{\alpha}(-\infty) = 0$, we obtain the useful identity

$$\sum_{\alpha} q_{\alpha} = 0 \quad (14)$$

The instantaneous term $\delta n'(t)$ is equivalent to the results obtained from the usual third order perturbation theory,¹³⁻¹⁵ while $\delta n''(t)$ arises from a change in the total susceptibility as a result of incoherent population of the excited levels. According to Eq. (A8), the total population change $\sigma_{\alpha\alpha}^{(2)}(0,t)$ consists of an instantaneous (coherent) portion plus the inertial (incoherent) portion $q_{\alpha}(t)$ that arises from atomic relaxation. The coherent contributions, which can be explained in terms of Grischkowsky's adiabatic following model,^{1,5} are included in expression (8). Butylkin, et.al.¹¹ have derived results similar to ours, but their interpretation is different.

In their formalism, our $q_{\alpha}(t)$ would represent the total population change, while the coherent population terms would be included adhoc by inserting Stark shift terms in the off-diagonal density matrix equations.

For short pulses (i.e., $\Gamma_{\alpha 0} t_p \ll 1$), the inertial terms are negligible, and Eq. (7) reduces to

$$\delta n^{(0)}(t) \approx \delta n'(t) = n_2 \langle E^2 \rangle \quad (15)$$

At the opposite extreme, $\Gamma_{\alpha 0} t_p \gg 1$, and

$$\delta n^{(0)}(t) \approx \delta n''(t). \quad (16)$$

The expression for $\delta n''(t)$ can be simplified in the second case by noting that collisional mixing occurs only among the sublevels of each n_l manifold.

Since the mixing rates W_{β} are usually comparable to $\Gamma_{\alpha \beta}$,¹⁷ these sublevels are completely thermalized if $\Gamma_{\alpha 0} t_p \gg 1$.

B. Three Level Model

The theory presented so far is applicable to all atomic vapors under suitable conditions. For cesium vapor around 1.06μ , one can obtain a useful and instructive approximation to this theory by examining the lower lying energy levels, shown in Fig. 1.¹³ Around 1.06μ , $\delta n^{(3)}$ appears to be determined mainly by the $|6s\rangle \equiv |0\rangle$, $|6p\rangle \equiv |1\rangle$ and $|7s\rangle \equiv |2\rangle$ levels because of the nearby one and two photon resonances with $6p$ and $7s$, respectively (i.e., $\omega_{10} - \omega \ll \omega_{10} + \omega$, and $|\omega_{20} - 2\omega| \ll \omega_{20}$). To a first approximation, we can therefore ignore all other levels and all non-resonant contributions to $\delta n^{(3)}(t)$. We will also ignore the L-S splitting of the $6p$ level, and approximate $6p$ by the degenerate magnetic substates $|a\rangle$, $|b\rangle$, $|c\rangle$ representing $m = +1, 0, -1$, respectively. This appears to be reasonable at 1.064μ , where $(\omega_{10} - \omega)/2\pi c = 2149 \text{ cm}^{-1}$ and the L-S splitting is only 544 cm^{-1} . The error that this causes in the evaluation of n_2 is small in comparison to that caused by the neglect of higher energy states and nonresonant contributions.

For linearly polarized light, we choose $\hat{e} \equiv \hat{z}$; hence, the only non-vanishing matrix elements of interest are $\hat{z} \cdot \vec{\mu}_{bo} \equiv \mu_{10} = \mu_{10}^*$ and $\hat{z} \cdot \vec{\mu}_{2b} \equiv \mu_{21} = \mu_{21}^*$. Using the simplifications described above, one can approximate Eqs (7)-(10) by

$$\delta n^{(3)}(t) \approx n_2 \langle E^2(t) \rangle + \frac{2\pi N \mu_{10}^2}{\hbar(\omega_{10} - \omega)} [q_o(t) - q_b(t)] + \frac{2\pi N \mu_{21}^2}{\hbar(\omega_{21} - \omega)} q_b(t), \quad (17)$$

where

$$n_2 = n_{20} - n_{10} \quad (18a)$$

$$= \frac{2\pi N \mu_{10}^2}{\hbar^2 (\omega_{10} - \omega)^2 (\omega_{20} - 2\omega)} - \frac{2\pi N \mu_{10}^4}{\hbar^2 (\omega_{10} - \omega)^4} \quad (18b)$$

and $q_o(t)$ and $q_b(t)$ are solutions of Eqs (11). The term $q_2(t)$ has not been included in (17) because it is fourth order in $E(t)$, and is therefore negligible unless $\omega_{20} - 2\omega$ is comparable to the atomic linewidth. Such terms were discussed by Butylkin, et. al.,¹¹ and have recently been observed in potassium vapor.⁴

The neglect of L-S splitting allows one to obtain simple expressions for $q_o(t)$ and $q_b(t)$ with only two relaxation constants. By symmetry considerations, it follows that $\Gamma_{ao} = \Gamma_{bo} = \Gamma_{co} \equiv \Gamma_{10}$, $W_a = W_b = W_c \equiv W$, and $W_{\alpha\beta} = \frac{1}{2}W$ for $\alpha \neq \beta$ equal to a, b or c. Equations (11) then reduce to

$$\dot{q}_o = -\frac{\Gamma_{10} \mu_{10}^2}{\hbar^2 (\omega_{10} - \omega)^2} \langle E^2 \rangle \quad (19a)$$

$$\dot{q}_b = -(3/2)Wq_b - \frac{1}{2}Wq_o + (\Gamma_{10} - \frac{1}{2}W) \frac{\mu_{10}^2}{\hbar^2 (\omega_{10} - \omega)^2} \langle E^2 \rangle, \quad (19b)$$

where the identity $q_o + q_a + q_b + q_c = 0$ [Eq (14)] has been used to obtain (19b). Solving for $q_o(t)$ and $q_b(t)$, and substituting them into (17), we obtain the result.

$$\begin{aligned} \delta n^{(3)}(t) = & n_2 \langle E^2(t) \rangle + C_1 \int_{-\infty}^t \langle E^2(t') \rangle dt' \\ & + C_2 \int_{-\infty}^t e^{-(3/2)W(t-t')} \langle E^2(t') \rangle dt' \\ & + C_3 \int_{-\infty}^t e^{-(3/2)W(t-t')} dt' \int_{-\infty}^{t'} \langle E^2(t'') \rangle dt'' , \end{aligned} \quad (20)$$

$$C_1 \equiv -\Gamma_{10} n_{10} \quad , \quad (21a)$$

$$C_2 \equiv -(\Gamma_{10} - \frac{1}{2}W)(n_{10} - n_{21}) \quad , \quad (21b)$$

$$C_3 \equiv -\frac{1}{2}W\Gamma_{10}(n_{10} - n_{21}) \quad , \quad (21c)$$

and

$$n_{21} \equiv \frac{2\pi N\mu_{21}^2\mu_{10}^2}{\hbar^3(\omega_{10}-\omega)^2(\omega_{21}-\omega)} \quad . \quad (22)$$

As we indicated in the preceeding subsection, the integral terms arise from incoherent redistribution of the $6s$ and $6p$ populations, and will predominate if $\Gamma_{10}t_p \gg 1$.

For pulsewidths comparable to or less than the atomic relaxation times Γ_{10}^{-1} and W^{-1} , the most important contribution to $\delta n^{(3)}(t)$ is the two photon term n_{20} defined by Eqs (18), as we will show at the end of this section. This term is positive in most substances around 1.06μ , and is partially responsible for the self focusing observed in materials such as laser glass.¹⁹ In Cs vapor around 1.06μ , however, n_{20} is large and negative due to the strong resonant enhancement by the two photon denominator $(\omega_{20}-2\omega)/2\pi c = -261 \text{ cm}^{-1}$.

The instantaneous portion of $\delta n^{(3)}(t)$ can be interpreted physically by rewriting expression (18b) in the form⁸

$$\begin{aligned} n_2 = & \frac{\pi N\mu_{21}^2\mu_{10}^2}{\hbar^3(\omega_{20}-2\omega)(\omega_{10}-\omega)} \left(\frac{1}{\omega_{10}-\omega} - \frac{1}{\omega_{21}-\omega} \right) \\ & - \frac{\pi N\mu_{10}^2}{\hbar^3(\omega_{10}-\omega)^2} \left(\frac{2\mu_{10}^2}{\omega_{10}-\omega} - \frac{\mu_{21}^2}{\omega_{21}-\omega} \right) \end{aligned} \quad (23)$$

The first (and largest) pair of terms arise directly from the two photon

"polarization" $\sigma_{20}^{(2)}(\omega)$, which drives $\sigma_{10}^{(1)}(\omega)$ and $\sigma_{21}^{(1)}(\omega)$. The second pair arise from the coherent redistribution of the 6s and 6p populations, as described by adiabatic following theory.^{1,5} We have recently shown that the combined coherent and incoherent population terms in a two level system (i.e., in the absence of μ_{21} and W) can be described by a generalized adiabatic following approximation that takes account of the phase relaxation Γ_{10} .²⁰

For circularly polarized light, we choose $\hat{e} = \hat{r}^+ \equiv 2^{-1/2}(\hat{x} + i\hat{y})$; hence, the only nonvanishing matrix elements of interest are $\hat{r}^+ \cdot \vec{u}_{a0} = \mu_{10} = \mu_{10}^*$ and $\hat{r}^+ \cdot \vec{u}_{2c} = \mu_{21} = \mu_{21}^*$. The magnitudes of μ_{10} and μ_{21} are equal to those in the linearly polarized case. Using the same approximations and procedure as above, we again obtain Eq (20), but the constants n_2 and C_2 are now defined by

$$n_2 = -n_{10} \quad (24)$$

$$C_2 = -(\Gamma_{10} - \frac{1}{2}W)n_{10} + \frac{1}{2}Wn_{21} \quad (25)$$

The n_{20} term does not appear in this case because the corresponding virtual transition 6s \rightarrow 6p \rightarrow 7s requires zero net angular momentum transfer from the light to the atom, whereas two photons of circularly polarized light must transfer $\Delta J = \pm 2$.²¹ (Two photon contributions do arise from the n^2D levels, but they have not been included in this simple approximation.)

From Eq (24) and definitions (18a,b), we see that n_2 reduces to the expression derived by Grischkowsky,^{1,5} as one would expect in this case.

To evaluate n_{10} , n_{10} and n_{21} , we used matrix elements obtained from the total 6s²S_{1/2} - 6p²P_{1/2,3/2} and 6p²P_{1/2,3/2} - 7s²S_{1/2} line strengths calculated by Heavens,²² and took the energy of 6p to be 11547 cm⁻¹ (the weighted average of 6p²P_{1/2} and 6p²P_{3/2}). The magnitudes of the matrix elements are (in atomic

units) $|\mu_{10}| = 5.16$ and $|\mu_{21}| = 2.92$, giving the results $n_{20} = -2.36 \times 10^{-30}$ N, $n_{10} = 0.535 \times 10^{-30}$ N and $n_{21} = -0.256 \times 10^{-30}$ N esu for $\lambda = 1.064 \mu$. The resulting values of n_2 obtained from Eqs (18) and (24) for linear and circular polarization, respectively, are shown in column C of Table 1. In column D, we show the values of n_2 calculated from the exact expression [Eq (8)], taking account of the contributions from non resonant terms and higher lying states (up to 8s, 8p, and 6d), and including the effects of L-S splitting. The magnitudes of the matrix elements were again calculated from Heavens' data,²² while the signs were taken from Table 1 of Miles and Harris.²³

In the case of linear polarization, the good agreement between columns C and D justifies our simple three level model. The small discrepancy arises primarily from the contribution of the 7p levels in the exact expression. For circular polarization, the discrepancy is significantly larger, and stems primarily from the two photon 6s-5d and 6s-6d contributions that were not included in the three level model.

III. EXPERIMENT

In order to measure n_2 , we studied the self-defocusing of mode locked Nd:YAG pulses in a 100 cm long cesium vapor cell. The measurements were made at several densities between $N = 0.03 \times 10^{17} \text{ cm}^{-3}$ and $0.32 \times 10^{17} \text{ cm}^{-3}$ with linearly polarized pulses and at $0.32 \times 10^{17} \text{ cm}^{-3}$ with circular polarization. The density was controlled by adjusting the temperature of a cesium reservoir ($260-305^\circ\text{C}$), while the main cell was held at 460°C in order to minimize linear absorption from Cs dimers.²⁴ For $N = 0.32 \times 10^{17} \text{ cm}^{-3}$, the 6s-6p transverse relaxation time τ_{10}^{-1} is approximately 30 psec.

The input radiation consisted of single pulses of FWHM (intensity) duration $t_p = 35$ psec, as determined by measurements with a 5 psec resolution streak camera. Since $\tau_{10}^{-1} > 2 t_p$ at all Cs pressures, the instantaneous terms are expected to predominate in Eqs. (7) and (10); hence, expression (15) should be a good approximation, at least for the linearly polarized pulses. The input beam, which was well collimated (radius of curvature $\rho_0 \approx 20$ m), had the form of an Airy profile truncated at the first minimum, with a $1/e$ intensity radius of $a_0 = 0.58$ mm. The pulse energy entering the cell was measured with a calorimeter, and was monitored with a calibrated photodiode. For the linear polarization case, simultaneous energy measurements were made at the output to determine the transmission of the cesium, which is plotted vs input pulse energy in Fig. 2.

The energy profile at the output of the cell was recorded by imaging the exit window onto a silicon photodiode array of 25μ resolution. Figure 3a shows typical oscilloscope traces of these output profiles for the case $N = 0.32 \times 10^{17} \text{ cm}^{-3}$. At low intensities, the beam profile was identical to that obtained with linear propagation in an empty cell. At intermediate intensities, the beam size increased, but its smooth characteristic shape was retained. At the highest intensities

used, further increase in beam size was observed, accompanied by beam distortion and the appearance of ring structure near the axis. This behavior is similar to that observed in the self defocusing experiments of Grischkowsky and Armstrong.⁵ All of the data that was used in determining n_2 was taken at the intermediate intensities ($\approx 6 \text{ GW/cm}^2$) where the beam distortion and cesium insertion loss were negligible.

In analyzing the data, the output profile of the beam was calculated from a solution of the wave equation in the paraxial ray approximation. Using Eq. (15), along with a constant shape assumption,¹² and approximating the shape of the input beam with a Gaussian distribution, we obtain for the intensity profile at the end of the cell

$$I(r,t) = [P(t)/\pi a^2(t)] \exp [-r^2/a^2(t)]. \quad (26)$$

Here $P(t)$ is the input beam power and $a(t)$ is a time dependent radius given by¹²

$$a^2(t) = a_0^2 \{ (1 + z/\rho_0)^2 + [1 - P(t)/P_c] (\lambda z/2\pi a_0^2)^2 \}, \quad (27)$$

where z is the length of the Cs cell, a_0 and ρ_0 are the input radius and beam curvature, respectively, and $P_c \equiv \lambda^2 c/32\pi^2 n_2 < 0$. The energy profile was then obtained by numerically integrating expression (26) over the pulse duration. For each data point, measured values of a_0 , ρ_0 and $P(t)$ were used and the value of n_2 was chosen to give the best theoretical fit to the measured energy distribution of the half-maximum points. This procedure is justified by the good overall agreement between the calculated and experimental profiles, as illustrated by the examples shown in Fig. 3b.

IV. RESULTS AND DISCUSSION

The results of our n_2 measurements for linearly and circularly polarized light are shown as a function of density in Fig. 4, and are compared with the theory in Table 1. The first column of Table 1 gives the experimental values of n_2/N obtained using Eqs. (15), (26) and (27), as described above. Column B gives adjusted experimental values which approximately account for the contribution of the integral terms in Eq. (20), as we will discuss below. Columns C and D give the approximate and exact calculated values of n_2/N that were discussed in Sec. III, and the last column gives the value obtained from the susceptibility calculations of Miles and Harris.²³

In using Eq. (15) to analyze the data, we have, in effect, treated the small integral terms of $\delta n^{(3)}(t)$ [Eq. (20)] as instantaneous, and lumped them into an effective contribution to the measured value of n_2 . One can estimate the relative importance of these integral terms by averaging their contribution to $\delta n^{(3)}(t)$ over the incident intensity, and comparing this to a similar average of the instantaneous portion; i.e., we consider the quantity

$$\eta \equiv \int_{-\infty}^{\infty} [\delta n^{(3)}(t) - n_2 \langle E^2(t) \rangle] \langle E^2(t) \rangle dt / \int_{-\infty}^{\infty} n_2 \langle E^2(t) \rangle^2 dt, \quad (28)$$

using Eq. (20) and the exact values of n_2 from column D. The corrected values of n_2 would then be approximately $(1 + \eta)^{-1}$ times the numbers shown in column A. Assuming that $\Gamma_{10}^{-1} \approx 60$ psec,²⁵ and that $W \approx \Gamma_{10}$,¹⁷ we obtain $\eta(\text{linear}) \approx 0.08$ and $\eta(\text{circular}) \approx 0.36$ by numerical integration of Eq. (28). Integral terms thus contribute little in the case of linear polarization, but they result in a significant correction for circular polarization, where $|n_2|$ is relatively small.

The experimental and theoretical values of n_2 (columns B and D) are in reasonable agreement, considering that one is comparing ab-initio calculations with absolute measurements. Since the oscillator strengths corresponding to our matrix elements are probably too large by a factor of about 5%,²² the numbers in columns C and D could be overestimated by as much as 10%; hence, the actual discrepancy between theory and measurements is probably smaller than indicated in Table 1. The remaining discrepancy appears to arise from systematic errors in the values of the concentration N or the pulse power $P(t)$. N was obtained from vapor pressure tables²⁶ and the measured temperatures of the bulb and cell. As other authors have noted,⁵ the accuracy of this procedure is limited. In the ratio $n_2(\text{linear})/n_2(\text{circular})$ the factor N cancels, and the agreement between theory and measurements is within 8%. [i.e., the ratio is 5.4 from column B, and 5.0 from column D.]

Although the cesium insertion loss was negligible for the pulses used in the n_2 measurements, its existence at higher and lower intensities (Fig. 2) may have a bearing on the possible applications of the negative n_2 , and requires some further comment. The attenuation at low intensities appears to arise from cesium dimers, whose absorption band extends from the vicinity of the D lines to about 1.12 μ .²⁴ Using a cross section of approximately $\sigma_D \approx 4 \times 10^{-10} \text{ cm}^2$,²⁷ and concentration²⁸

$$N_D = 5.54 \times 10^{-23} N^2 e^{5200/T(^{\circ}\text{K})}, \quad (29)$$

we obtain the absorption coefficient $N_D \sigma_D = 0.017$ at $T = 460^{\circ}\text{C}$ and $N = 0.32 \times 10^{17} \text{ cm}^{-3}$. The small signal transmission for a 100 cm path length is then approximately 18%. If N is actually smaller by a factor of about two, as we suggested above, then the transmission would be approximately 65%. The increase in transmission with intensity up to about 5 GW/cm^2 is apparently due to either bleaching²⁷ or hole

burning effects in the dimers. Evidence for this is shown in Fig. 2, where one pair of points corresponds to a double pulse with a 5 nsec separation. The first pulse, whose energy density was 200 mJ/cm^2 , was virtually unattenuated. It apparently bleached out the dimers, however, because the second pulse, whose density was 40 mJ/cm^2 (indicated by the cross), had significantly higher transmission than other pulses of comparable magnitude.

One is tempted to ascribe the losses at high intensities to two photon absorption or multi photon ionization; however, the theoretical cross sections for these processes do not support such explanations. The two photon cross section $\sigma^{(2)}(1.06\mu)$, which is due primarily to the 6s-7s contribution, is approximately $3.3 \times 10^{-49} \text{ NI}^{23}$ where intensity I is measured in W/cm^2 . For $N = 0.32 \times 10^{17} \text{ cm}^{-3}$ and incident intensity $I = 3 \times 10^{10}$, the maximum absorption coefficient is $N\sigma^{(2)}(1.06\mu) \approx 10^{-8} \text{ cm}^{-1}$. The three photon absorption is also negligible. One can estimate the four photon ionization cross section from calculations carried out by Morton²⁴ for $\lambda = 1.0590 \mu$. Morton's results correspond to a cross section $\sigma^{(4)}(1.059\mu) \approx 3.7 \times 10^{-49} \text{ I}^3$; ²³ however, this number is strongly enhanced by a nearly exact resonance between 3ω and the 6f levels around 28329.7 cm^{-1} . The detuning is only $\approx 1 \text{ cm}^{-1}$, whereas for 1.064μ , it is 134 cm^{-1} ; hence, $\sigma^{(4)}(1.064\mu) \approx (1.134)^2 \sigma^{(4)}(1.059\mu) \approx 2.1 \times 10^{-53} \text{ I}^3$, giving a maximum absorption coefficient of $1.9 \times 10^{-6} \text{ cm}^{-1}$ for $N = 0.32 \times 10^{17} \text{ cm}^{-3}$. With beam spreading (and thus lowering of the intensities and cross sections), the absorption over 100 cm is negligible.

The flattening of the high power pulses, as shown in Fig. 3a, suggests that dimer absorption could also be responsible for the attenuation at these as well as at the lower powers. To see this, we assume for the moment that the constant shape approximation remains valid, even when the beam spreading is large. If this were valid [and $P(t) \gg P_c$], then Eq (27) would reduce to $a^2(t) \approx (\lambda z / 2\pi a_0)^2 P(t) / P_c$; hence, the on-axis intensity $I(0) \approx (2\pi a_0 / \lambda z)^2 P_c / \pi$ would remain independent of the total power $P(t)$. However, because the flattening does occur and

becomes more prominent as $P(t)$ increases, it is evident that the intensity $I(0,t)$ can actually decrease as $P(t)$ increases. The central portion of the beam may therefore become more susceptible to dimer absorption under these conditions.

In later publications, we will report on additional defocusing measurements using longer pulses to observe the integral terms, and on investigations of the higher power transmission under conditions where beam flattening is negligible. We will also report on both theoretical and experimental studies of the application of cesium vapor for compensation of self focusing and self phase modulation in high power laser systems.

ACKNOWLEDGMENT

We thank Hans Griem, John McMahon, and Raymond Elton for useful and informative discussions.

APPENDIX

To obtain the solution of Eqs (3), we use the harmonic expansions of $\rho_{\alpha\beta}^{(n)}(t)$, as in Eq. (5); i.e.,

$$\rho_{\alpha\beta}^{(1)}(t) = \frac{1}{2} \sigma_{\alpha\beta}^{(3)}(\omega, t) e^{-i\omega t} + \frac{1}{2} \sigma_{\alpha\beta}^{(3)}(-\omega, t) e^{i\omega t} + \text{third harmonic terms}, \quad (\text{A1a})$$

$$\rho_{\alpha\beta}^{(2)}(t) = \rho_{\alpha\beta}^{(2)}(\omega, t) + \frac{1}{2} \sigma_{\alpha\beta}^{(2)}(2\omega, t) e^{-2i\omega t} + \frac{1}{2} \sigma_{\alpha\beta}^{(2)}(-2\omega, t) e^{2i\omega t}, \quad (\text{A1b})$$

$$\rho_{\alpha\beta}^{(1)}(t) = \frac{1}{2} \sigma_{\alpha\beta}^{(1)}(\omega, t) e^{-i\omega t} + \frac{1}{2} \sigma_{\alpha\beta}^{(1)}(-\omega, t) e^{i\omega t}, \quad (\text{A1c})$$

where the amplitudes $\sigma_{\alpha\beta}^{(n)}(n'\omega, t) = [\sigma_{\beta\alpha}^{(n)}(-n'\omega, t)]^*$ vary in times on the order of the pulsewidth t_p . Substituting Eqs (A1) into (3) [and dropping the time label for brevity], one obtains

$$\begin{aligned} \dot{\sigma}_{\alpha\beta}^{(3)}(\omega) + i(\omega_{\alpha\beta} - \omega - i\Gamma_{\alpha\beta}) \sigma_{\alpha\beta}^{(3)}(\omega) \\ = i\mathcal{E}(-\omega) \hat{\epsilon}^* \cdot \vec{s}_{\alpha\beta}^{(2)}(2\omega) + 2i\mathcal{E}(\omega) \hat{\epsilon} \cdot \vec{s}_{\alpha\beta}^{(2)}(0), \end{aligned} \quad (\text{A2a})$$

$$\dot{\sigma}_{\alpha\beta}^{(2)}(2\omega) + i(\omega_{\alpha\beta} - 2\omega - i\Gamma_{\alpha\beta}) \sigma_{\alpha\beta}^{(2)}(2\omega) = i\mathcal{E}(\omega) \hat{\epsilon} \cdot \vec{s}_{\alpha\beta}^{(1)}(\omega), \quad (\text{A2b})$$

$$\begin{aligned} \dot{\sigma}_{\alpha\beta}^{(2)}(0) + i(\omega_{\alpha\beta} - i\Gamma_{\alpha\beta}) \sigma_{\alpha\beta}^{(2)}(0) \\ = \frac{1}{2} i\mathcal{E}(-\omega) \hat{\epsilon}^* \cdot \vec{s}_{\alpha\beta}^{(1)}(\omega) + \frac{1}{2} i\mathcal{E}(\omega) \hat{\epsilon} \cdot \vec{s}_{\alpha\beta}^{(1)}(-\omega), \quad \omega_{\alpha\beta} \neq 0, \end{aligned} \quad (\text{A2c})$$

$$\begin{aligned} \dot{\sigma}_{\alpha\alpha}^{(2)}(0) + W_{\alpha} \sigma_{\alpha\alpha}^{(2)}(0) - \sum_{\beta \neq \alpha} W_{\beta\alpha} \sigma_{\beta\beta}^{(2)}(0) \\ = \text{Re}[i\mathcal{E}(-\omega) \hat{\epsilon}^* \cdot \vec{s}_{\alpha\alpha}^{(1)}(\omega)] \end{aligned} \quad (\text{A2d})$$

$$\dot{\sigma}_{\alpha\beta}^{(1)}(\omega) + i(\omega_{\alpha\beta} - \omega - i\Gamma_{\alpha\beta}) \sigma_{\alpha\beta}^{(1)}(\omega) = (i/\hbar) \mathcal{E}(\omega) \hat{e} \cdot \vec{\mu}_{\alpha\beta} (\delta_{\beta 0} - \delta_{\alpha 0}), \quad (\text{A2e})$$

where

$$\vec{s}_{\alpha\beta}^{(n)}(n'\omega) \equiv (1/2\hbar) \sum_Y [\vec{\mu}_{\alpha Y} \sigma_{Y\beta}^{(n)}(n'\omega) - \sigma_{\alpha Y}^{(n)}(n'\omega) \vec{\mu}_{Y\beta}], \quad (\text{A3})$$

and $\Gamma_{\alpha\beta}$, W_{α} , $W_{\beta\alpha}$ are the phase relaxation and collisional mixing rates described in the text.

With the exception of (A2d), all of the equations (A2) have the general form

$$\dot{\sigma}(t) + (i\Omega + \Gamma) \sigma(t) = R(t), \quad |\Omega| \gg \Gamma, \quad (\text{A4})$$

with the formal solution for $\sigma(-\infty) = R(-\infty) = 0$,

$$\begin{aligned} \sigma(t) &= \int_{-\infty}^t dt' e^{-(i\Omega + \Gamma)(t-t')} R(t') \\ &= -\sum_{m=0}^{\infty} \left(\frac{-1}{i\Omega + \Gamma} \right)^{m+1} \frac{d^m R(t)}{dt^m} \end{aligned} \quad (\text{A5})$$

For example, (A2e) yields the result

$$\sigma_{\alpha\beta}^{(1)}(\omega, t) = - (i/\hbar) (\delta_{\beta 0} - \delta_{\alpha 0}) \hat{e} \cdot \vec{\mu}_{\alpha\beta} \sum_{m=0}^{\infty} \left[\frac{-1}{i(\omega_{\alpha\beta} - \omega) + \Gamma_{\alpha\beta}} \right]^{m+1} \frac{\partial^m \mathcal{E}(\omega, t)}{\partial t^m}. \quad (\text{A6})$$

Since Ω represents quantities such as $\omega_{\alpha\beta}$, 2ω , $\omega_{\alpha\beta} \pm \omega$ or $\omega_{\alpha\beta} \pm 2\omega$, but $|(1/R) dR/dt|$ is on the order of the laser linewidth, postulate (ii) leads to the condition $|(1/R) dR/dt| \ll \Omega$; hence, it is necessary to retain only the lowest order terms of (A5) and (A6).

Equation (A2d) may be rewritten by substituting (A3) and expansion (A6). Retaining only the zero and first derivative terms of (A6), and noting that $\Gamma_{\beta\alpha} = \Gamma_{\alpha\beta}$, one obtains

$$\begin{aligned} \dot{\sigma}_{\alpha\alpha}^{(2)}(0, t) + W_{\alpha\alpha}^{(2)}(0, t) - \sum_{\beta \neq \alpha} W_{\beta\alpha} \sigma_{\beta\beta}^{(2)}(0, t) \\ \approx \frac{1}{4\hbar^2} \sum_{\beta} (\delta_{\beta 0} - \delta_{\alpha 0}) \left[\frac{|\hat{e} \cdot \vec{\mu}_{\beta\alpha}|^2}{i(\omega_{\beta\alpha} - \omega - i\Gamma_{\beta\alpha})} + \frac{|\hat{e} \cdot \vec{\mu}_{\alpha\beta}|^2}{i(\omega_{\alpha\beta} - \omega - i\Gamma_{\beta\alpha})} \right] \mathcal{E}(-\omega, t) \mathcal{E}(\omega, t) \\ + \left[\frac{|\hat{e} \cdot \vec{\mu}_{\beta\alpha}|^2}{(\omega_{\beta\alpha} - \omega - i\Gamma_{\beta\alpha})^2} + \frac{|\hat{e} \cdot \vec{\mu}_{\alpha\beta}|^2}{(\omega_{\alpha\beta} - \omega - i\Gamma_{\beta\alpha})^2} \right] \mathcal{E}(-\omega, t) \frac{\partial \mathcal{E}(\omega, t)}{\partial t} \} + \text{c. c.} \end{aligned} \quad (\text{A7a})$$

$$\approx \sum_{\beta} (\delta_{\beta\alpha} - \delta_{\alpha 0}) R_{\beta} [\Gamma_{\beta 0} \langle E^2(t) \rangle + \frac{1}{2} d \langle E^2(t) \rangle / dt], \quad (\text{A7b})$$

where $\langle E^2(t) \rangle = \frac{1}{2} |\mathcal{E}(\omega, t)|^2$, R_{β} is defined by Eq. (9c), and postulate (ii) has been used to justify the neglect of $\Gamma_{\beta 0}$ in the denominator of R_{β} . Although the zero derivative term is the largest contribution to (A6), it is evident that the corresponding term $\Gamma_{\beta 0} \langle E^2(t) \rangle$ in (A7b) may be comparable to or less than the first derivative contribution $\frac{1}{2} d \langle E^2(t) \rangle / dt$. This results from the fact that the largest portions of the zero derivative terms in (A7a) cancel when they combine with their complex conjugates. If we define the variable $q_{\alpha}(t)$ by the relation

$$\sigma_{\alpha\alpha}^{(2)}(0, t) = \frac{1}{2} \sum_{\beta} (\delta_{\beta\alpha} - \delta_{\alpha 0}) R_{\beta} \langle E^2(t) \rangle + q_{\alpha}(t), \quad (\text{A8})$$

then Eq. (A7b) leads immediately to Eqs (11) and (12).

The near cancellation of the zero derivative terms occurs only in the evaluation of Eq (A2d). In the solution of Eqs (A2a-c) and (A2e), one can

therefore use postulate (ii) to omit all but the zeroth term of (A5), and to ignore all $\Gamma_{\alpha\beta}$ factors. The resulting solutions

$$\sigma_{\alpha\beta}^{(0)}(\omega, t) = \frac{\mathcal{E}(-\omega, t) \hat{\epsilon}_{\alpha\beta}^* \cdot \vec{s}_{\alpha\beta}^{(2)}(2\omega, t) + 2\mathcal{E}(\omega, t) \hat{\epsilon}_{\alpha\beta} \cdot \vec{s}_{\alpha\beta}^{(2)}(\omega, t)}{\omega_{\alpha\beta} - \omega}, \quad (A9a)$$

$$\sigma_{\alpha\beta}^{(2)}(2\omega, t) = \frac{\mathcal{E}(\omega, t) \hat{\epsilon}_{\alpha\beta} \cdot \vec{s}_{\alpha\beta}^{(1)}(\omega, t)}{\omega_{\alpha\beta} - 2\omega}, \quad (A9b)$$

$$\sigma_{\alpha\beta}^{(2)}(0, t) = \frac{\mathcal{E}(-\omega, t) \hat{\epsilon}_{\alpha\beta}^* \cdot \vec{s}_{\alpha\beta}^{(1)}(\omega, t) + \mathcal{E}(\omega, t) \hat{\epsilon}_{\alpha\beta} \cdot \vec{s}_{\alpha\beta}^{(1)}(-\omega, t)}{2\omega_{\alpha\beta}}, \quad \omega_{\alpha\beta} \neq 0, \quad (A9c)$$

$$\sigma_{\alpha\beta}^{(1)}(\omega, t) = \frac{\mathcal{E}(\omega, t) \hat{\epsilon}_{\alpha\beta} \cdot \vec{\mu}_{\alpha\beta} (\delta_{00} - \delta_{\alpha 0})}{\hbar(\omega_{\alpha\beta} - \omega)}, \quad (A9d)$$

along with the instantaneous portion of (A8), are equivalent to those obtained from ordinary perturbation theory.^{13, 15} Combining these results with expression (A3), one obtains Eqs (7) - (10) after some tedious but straightforward algebra.

REFERENCES

1. D. Grischkowsky, Phys. Rev. Lett. 24, 866 (1970).
2. S. A. Akhmanov, A. I. Kovrigin, S. A. Maksimov, and V. F. Ogluzdin, ZhETF Pis. Red. 15, 186 (1972) (JETP Lett. 12, 129 (1972)).
3. J. E. Bjorkholm and A. Ashkin, Phys. Rev. Lett. 32, 129 (1974).
4. S. A. Bakhramov, U. G. Gulyamov, K. N. Drabovich, and Ya. Z. Faizullaev, ZhETF Pis. Red. 21, 229 (1975) [JETP Lett. 21, 102 (1975)].
5. D. Grischkowsky and J. A. Armstrong, Phys. Rev. A6, 1566 (1972).
6. V. M. Artyunyan, N. N. Badalyn, V. A. Iradyan, and M. E. Movsesyan, Zh. Eksp. Teor. Fiz. 58, 37 (1970) [JETP 31, 22 (1970)].
7. D. Grischkowsky, E. Courtens, and J. A. Armstrong, Phys. Rev. Lett. 31, 422 (1973).
8. R. H. Lehmberg, J. Reintjes, and R. C. Eckardt, Appl. Phys. Lett. 25, 374 (1974).
9. P. D. Maker and R. W. Terhune, Phys. Rev. 137, A801 (1965).
10. a. R. Speck and E. Bliss, Lawrence Livermore Laboratory Semiannual Report - Jan. - June 1975;
 b. A. Owyong, Symposium on Laser Induced Damage in Optical Materials (National Bureau of Standards Special Publication 387, 1975);
 c. M. J. Moran, C. Y. She and R. L. Carman, IEEE J. Quantum Electron. QE 11, 259 (1975).
11. V. S. Butylkin, A. E. Kaplan, and Yu. G. Khronopulo, Zh. Eksp. Teor. Fiz. 59, 921 (1970) [JETP 32, 501 (1971)].

12. S. A. Akhmanov, R. V. Khokhlov and A. P. Sukhorukov, in Laser Handbook, Vol. 2, edited by F. T. Arecchi and E. O. Schulz-Dubois (North-Holland, Amsterdam, 1972).
13. J. A. Armstrong, N. Bloembergen, J. Ducuing and P. S. Pershan, Phys. Rev. 187, 1913 (1962).
14. B. J. Orr and J. F. Ward, Molec. Phys. 20, 513 (1971).
15. P. W. Langhoff, S. T. Epstein, and M. Karplus, Rev. Mod. Phys. 44, 602 (1972).
16. K. Bernheim, Optical Pumping, An Introduction (W. A. Benjamin Co., New York, NY, 1965).
17. P. R. Berman and W. E. Lamb, Jr., Phys. Rev. 187, 221 (1969); C. G. Carrington, D. N. Stacey, and J. Cooper, J. Phys. B 6, 417 (1973).
18. C. E. Moore, Atomic Energy Levels, III, (U. S. National Bureau of Standards, 1 May 1958).
19. J. T. Fournier and E. Snitzer, IEEE J. Quantum Electron. QE-10, 473 (1974).
20. R. H. Lehberg and J. Reintjes, Bull. Am. Phys. Soc. 20, 635 (1975); Phys. Rev. A, in press.
21. P. P. Bey and H. Kabin, Phys. Rev. 162, 794 (1967).
22. O. S. Heavens, J. Opt. Soc. Am. 51, 1058 (1961). This particular set of matrix elements was chosen because the corresponding oscillator strengths come closer to satisfying the Thomas-Kuhn sum rule than those tabulated elsewhere. For example the total 6s-6p oscillator strength is $f(6s, 6p) = 1.05$, whereas the value given in the tables of ref. (23) is 1.13.
23. R. B. Miles and S. E. Harris, IEEE J. Quantum Electron. QE-9, 470 (1973).
24. D. S. Bayley, E. C. Eberlin, and J. H. Simpson, J. Chem Phys. 40, 2863 (1966).
25. This was obtained by taking the weighted average of the 6p $^2P_{1/2}$ and 6p $^2P_{3/2}$ linewidths measured by C. L. Chen and A. V. Phelps, Phys. Rev. 173, 62 (1968).

26. Handbook of Tables for Applied Engineering Science, eds. R. E. Bolz and G. L. Tuve (Chemical Rubber Co., Cleveland, Ohio, 1970).
27. P. P. Sorokin and J. R. Lankard, IEEE J. Quantum Electron. QE-8, 813 (1972).
28. M. Lapp and L. P. Harris, J. Quant. Spectrosc. Radiat. Transfer 6, 169 (1966).
29. V. M. Morton, Proc. Phys. Soc. (London) 92, 301 (1967).
30. M. D. Crisp, Phys. Rev. A 8, 2128 (1973).

TABLE 1

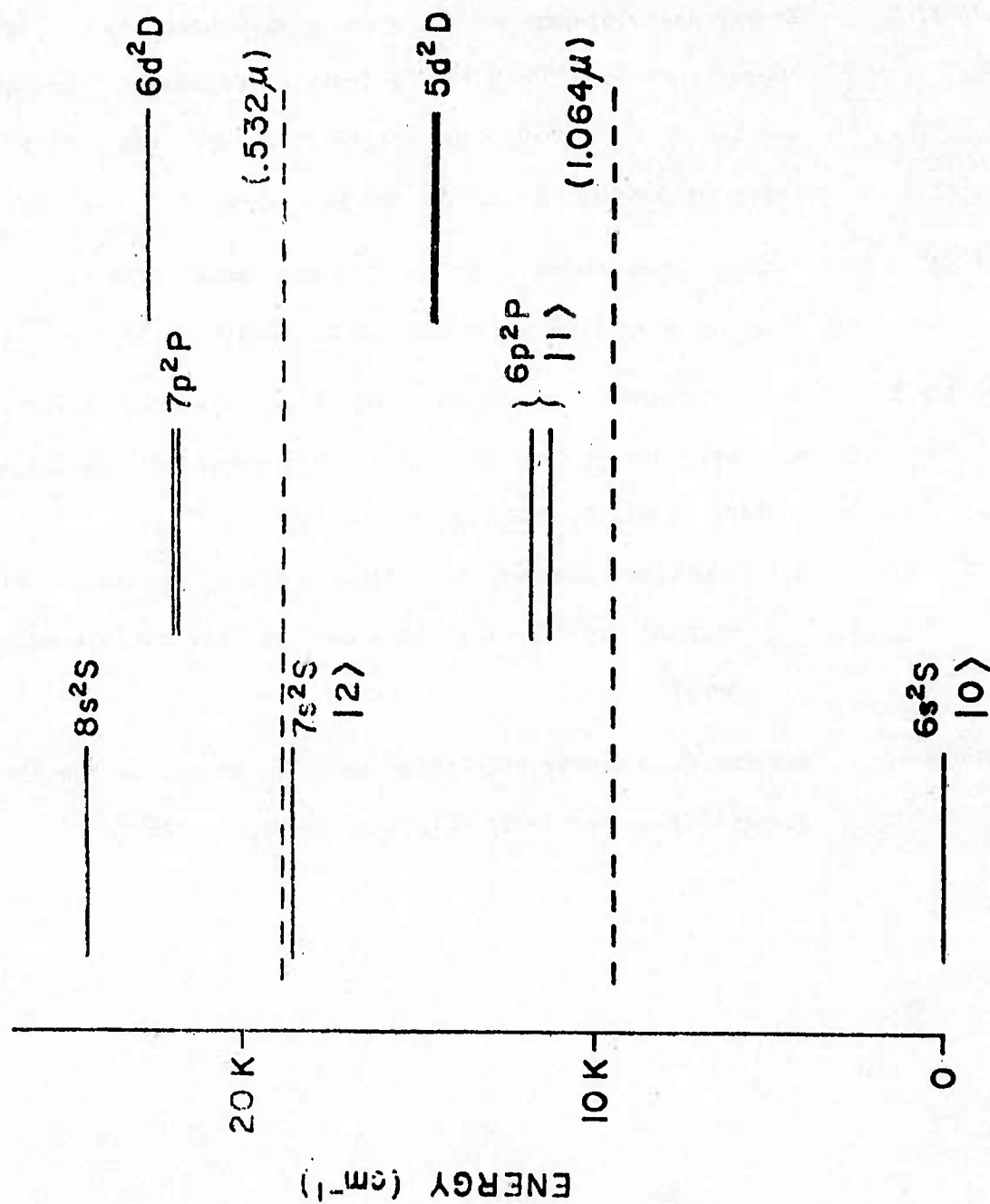
$$\frac{n_2}{N} \times 10^{30} \text{ (esu)}$$

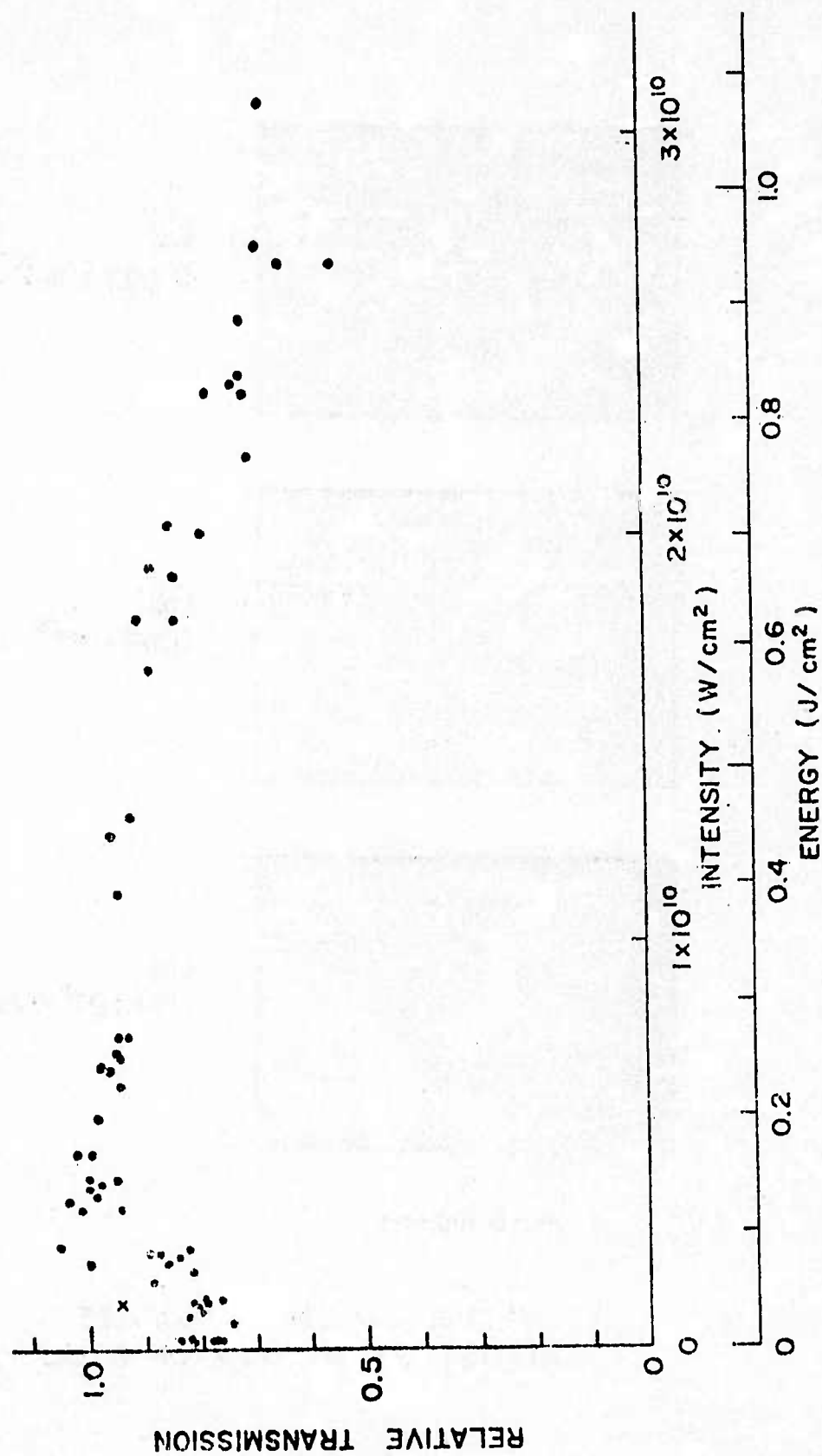
	EXPERIMENTAL		THEORETICAL MILES & HARRIS		
	(A)	(B)	(C)	(D)	(E)
↑	-1.5 ± 0.02	-1.4 ± 0.2	-2.70	-2.62	-0.66
↺	-0.35 ± 0.04	-0.26 ± 0.03	-0.335	-0.525	

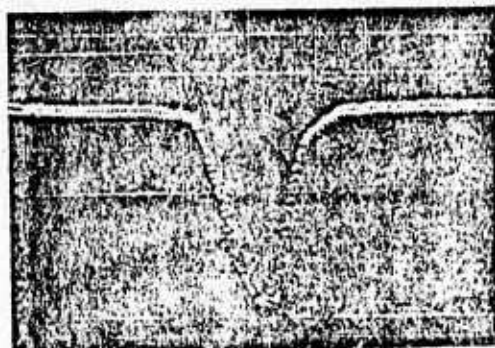
- (A) Experimental values obtained from analysis of data that ignores the integral terms of Equation (20).
- (B) Experimental values including an adjustment to approximately account for the integral terms.
- (C) Theoretical calculation using the near-resonant three level approximation [Eqs. (18) and (24)].
- (D) Theoretical calculation including antiresonant terms, higher excited states, and L-S splitting [Eq. (8)].
- (E) Theoretical calculation of Ref. 23.

FIGURE CAPTIONS

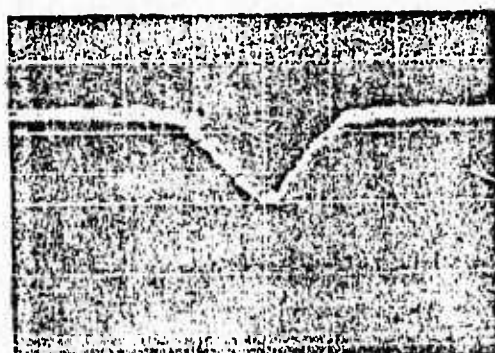
- FIGURE 1 Energy level diagram of Cs, showing the three levels $|6s\rangle \equiv |0\rangle$, $|6p\rangle \equiv |1\rangle$ and $|7s\rangle \equiv |2\rangle$ primarily responsible for self defocusing at 1.064μ . The dotted lines show the position of the laser fundamental at 1.064μ and its two-photon level at $.532\mu$.
- FIGURE 2 Cesium transmission vs pulse flux (and peak intensity) for linearly polarized light and atomic density $0.32 \times 10^{17} \text{ cm}^{-3}$.
- FIGURE 3 Spatial profiles of the pulse at the exit window of the Cs cell.
- Oscilloscope traces of photodiode array measurement at low, intermediate, and high intensity.
 - Comparison between theoretical profiles (solid lines) and measured profiles (dotted lines) at intermediate pulse energies.
- FIGURE 4 Effective nonlinear refractive index n_2 vs atomic density N for linearly and circularly polarized light at 1.064μ .







(a)
 $0.027 \times 10^{10} \text{ W/cm}^2$



(b)
 $0.64 \times 10^{10} \text{ W/cm}^2$



(c)
 $1.9 \times 10^{10} \text{ W/cm}^2$

← 5mm →

MEASURED BEAM PROFILE
 AT OUTPUT WINDOW OF CELL



$N = 0$

LINEAR POLARIZATION



$N = 0.080 \times 10^{17} \text{ cm}^{-3}$

LINEAR POLARIZATION



$N = 0.32 \times 10^{17} \text{ cm}^{-3}$

LINEAR POLARIZATION

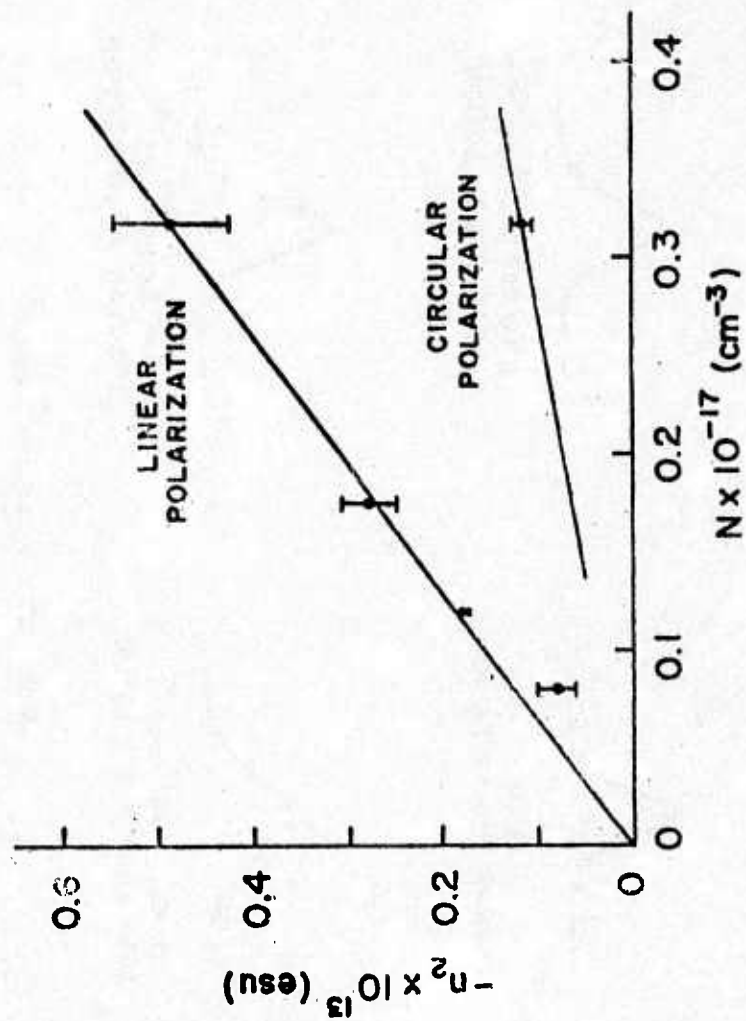


$N = 0.32 \times 10^{17} \text{ cm}^{-3}$

CIRCULAR POLARIZATION

INTENSITY $\approx 0.6 \times 10^{10} \text{ W/cm}^2$

BEAM PROFILES
AT OUTPUT WINDOW OF CELL



A SINGLE MODE Nd:YAG Q-SWITCHED OSCILLATOR WITH SHORT BUILDUP TIME*

R. C. Ecksrdt and J. F. Reintjes

Naval Research Laboratory

Washington, D. C. 20375

ABSTRACT

A single longitudinal and transverse mode Nd:YAG laser is described. The unique feature of this laser is the rapid build up time of the output pulse which appears 125 nsec after application of either an optical or electronic trigger pulse, with a jitter of ± 10 nsec. The output is further shuttered to a rectangular pulse of from 1 to 10 nsec duration. Single mode operation is obtained with a two element resonant reflector and a birefringent Lyot filter of calcite. To further aid in frequency selection, the cavity Q is not completely spoiled to allow buildup of quasi-monochromatic radiation before the cavity is switched to high Q. Problems of frequency selection and cavity stability are discussed.

Single mode operation of high power Q-switched lasers is usually obtained with long buildup times and many cavity transits which allow small differences in reflectivity of the cavity mirrors to yield a single dominant mode. Saturable absorbers are normally used for Q-switching in these lasers because they provide the required buildup time during the relatively slow bleaching process (1,2). Saturable absorbers, however, have the disadvantage of being passive devices and cannot be externally triggered. Jitter in the appearance of the output pulse in such lasers are typically of the order of ± 10 μ sec.

In many applications however a more rapid buildup time, coupled with the ability to synchronize the output pulse to other optical signals, is desirable. In such cases Pockels cell Q-switching can give the needed time reference for synchronization, but the rapid buildup time does not in general allow sufficient wavelength discrimination for single frequency operation. Here we discuss a Pockels cell Q-switched Nd:YAG laser operated under conditions which simultaneously allow rapid pulse buildup and oscillation on a single longitudinal mode. Q-switching is triggered either electrically or optically. The single mode output pulse appears 125 nsec after

application of the trigger pulse with a jitter of ± 10 nsec.

In our application, the Q-switched pulse is synchronized with the peak of a mode-locked pulse train generated in a separate laser (3). In this two laser system (Fig. 1.) the Q-switched laser is triggered on the leading edge of the mode-locked pulse train, and the 125 nsec delay places the Q-switched pulse coincident with the peak of the mode-locked pulse train. Laser triggered spark gaps are then used to drive Pockels cells that shutter out a single mode-locked pulse and a rectangular segment of the Q-switched pulse of 1 to 10 nsec duration. The two pulses are synchronized with a jitter of ± 1 nsec. Single mode operation of the Q-switched oscillator is required to allow maximum amplification while avoiding damage due to excessive instantaneous intensities and to provide a well defined pulse for laser matter interaction studies.

The single mode Q-switched oscillator is shown schematically in Fig. 2. A 3 inch long, 1/4 inch diameter, Brewster-Brewster Nd:YAG laser rod is pumped with a linear flashlamp in a single ellipse pump cavity. The flashlamp radiation has 125 μ sec full width at half maximum. Single pass gains of 16 db can be obtained in the laser rod at the full pump energy of 30 J. The resonant cavity is formed by a 4.7 m radius-of-curvature 99% reflectivity mirror and a two element resonant reflector. A circular aperture of .25 cm diameter provides transverse mode selection. A calcite polarizing prism and a KD*P Pockels cell are used for Q-switching. The same prism is also used with a calcite slab to form a Lyot filter.

Frequency selection is provided by the resonant reflector which provides discrimination against oscillation on adjacent cavity modes and the Lyot filter which discriminates against more widely spaced modes. The resonant reflector consists of a flat 45% dielectric mirror and a 5 cm thick fused silica flat with ends parallel to 3 seconds of arc. The mirror is placed 10.8 cm from the nearest surface of the flat. Fine adjustment of this spacing is provided by a translation stage driven by a differential screw micrometer with a resolution of 1/8 wavelength. The resonant reflector elements and 99% mirror are aligned interferometrically with a collimated He-Ne laser (Fig. 2.). The calcite slab is 2.1 cm

thick and is arranged to operate as a high order retardation plate with its optic axis oriented perpendicular to the direction of propagation and at an angle of 45° to the polarization vector transmitted by the polarizing prism.

For propagation perpendicular to the optic axis, the number of waves of retardation is $N = L(n_o - n_e)/\lambda$ where L is the length of the crystal, n_o the ordinary index, n_e the extraordinary index, and λ is the wavelength in free space. With the calcite crystal placed between parallel polarizers, only integer orders of retardation will be completely transmitted. In our laser oscillator, light passes through the calcite twice before it again passes through the polarizing prism; therefore we have an effective crystal length of $2L$. The filter transmission for this configuration is given by

$$T = \cos^2 \left\{ 2\pi L (n_o - n_e) / \lambda \right\}.$$

For a crystal length of 2.1 cm transmission peaks are spaced by $1.66 \times 10^{-4} \mu$ (Fig. 3.). One of the transmission maxima of the Lyot filter is tuned to the peak of the Nd:YAG fluorescence with small rotations about an axis parallel to the optic axis by finding the minimum threshold for free running laser oscillations. At the spectral position of the adjacent maxima the single pass gain in the laser rod is reduced to approximately .9 of its peak value.

The calcite birefringent filter offers advantages over a thin parallel resonant reflector element. The modulation of the Lyot filter is complete with transmission going to zero at each minimum. Also the position of the transmission peaks can be tuned by a small rotation about the optic axis or about an axis perpendicular to both the optic axis and the direction of propagation. The change in the order of retardation for a double pass through the crystal is given by

$$\Delta N = \frac{2Ld^2}{\lambda} \left(\frac{1}{2n_e} - \frac{1}{2n_o} \right)$$

where d is the angle of rotation. And the interaction of the Lyot filter is independent of spacing, but with a resonant reflector it is necessary to hold spacing constant to interferometric tolerances.

A simple two element resonant reflector is required for further frequency selection. The adjacent longitudinal cavity modes for this laser are spaced by $\Delta\lambda = 6.57 \times 10^{-7} \mu$. This spacing is much too fine to be resolved by the transmission bands of the Lyot filter. The reflectivity of the two element resonant reflector is given by

$$R = \left[1 + \frac{r_2 t_1^2 \exp(i\theta)}{1 - r_1 r_2 \exp(i\theta)} \right] \left[C.C. \right]$$

Here r_1 and t_1 are the complex amplitude reflection and transmission coefficients for a di-

electric slab (4) in this case the fused silica flat. The amplitude reflection coefficient for the mirror is r_2 , and $\theta = 4\pi d/\lambda$ where d is the spacing of the mirror end flat.

The combination of 5 cm fused silica flat and 45% mirror have peak reflectivity of 67% (Fig. 4.). Reflectivity at the adjacent longitudinal modes is reduced to .91 of this value. The next 67% reflection peak is spaced by $1.64 \times 10^{-5} \mu$. Moving this distance from the peak of the Lyot filter reduces its transmission to .91 of that peak value. In operation of the laser it is necessary to tune a reflection peak of the resonant reflector to coincide with both the maximum transmission of the Lyot filter and the peak of the rod fluorescence. This is done by translating the mirror until satisfactory laser operation is obtained.

To obtain further frequency selection the cavity Q is not completely spoiled to allow the buildup of low level quasi-monochromatic oscillations before Q-switching. A buildup time of 125 nsec in a cavity of optical length 86.2 cm only allows 22 round trip transits. Reduction in round trip gain for secondary modes to .9 times that of the dominant mode is not sufficient to provide single mode operation when these modes of oscillation buildup from the same initial intensity levels. Under that condition the intensity of the secondary modes would only be reduced to $.922^{22} = .10$ of the intensity of the dominant mode. To obtain a low level buildup the Pockels cell is operated at a voltage 500 V less than the 3500 V quarter wave voltage. Flashlamp energy is increased 2 or 3 J above the threshold for relaxation oscillations with constant unswitched Pockels cell voltage (Fig. 5.). Below this pumping energy buildup time is increased and the laser output shows spiking. Above this energy the jitter in buildup time increases. The spiking character in the output is also observed when the Pockels cell voltage is increased.

Laser output was monitored with a 5 psec resolution streak camera and a .5 nsec risetime photodiode oscilloscope combination. With proper adjustment of the resonant reflector, single mode laser operation was obtained (Fig. 6.). Single mode operation would last for typically 10 shots before readjustment of the resonant reflector was required. Single transverse mode operation was obtained routinely. Transverse intensity distribution was monitored with a 512 element silicon photodiode array (Fig. 7.). Gaussian like distributions of .19 cm FWHM were observed at a distance of 240 cm from the output mirror.

It is necessary that the resonant cavity be held stable to interferometric tolerances to maintain the frequency selection characteristics. The laser was enclosed in a box open at the ends to shield from air currents in the laboratory room. Even though the laser was assembled on a large steel beam mounted on massive concrete pedestals it was necessary to move a water cooler across the room to avoid vibration coupling. Repetition rate had to be slowed to one shot in 15 seconds to allow the laser rod to stabilize. The laser is

still susceptible to changes in temperature and air pressure. Thermal expansion coefficients for common alloys are typically $20 \times 10^{-6} (^\circ\text{C})^{-1}$. To hold the length of a 1 m bench constant to $1/4 \mu$ requires temperature stability of $.0013^\circ\text{C}$. Using formulas given in the AIP Handbook (5) it is found that $1/4 \mu$ stability in cavity optical length requires air pressure constant to 0.7 mm Hg and air temperature constant to 0.3°C . A sealed temperature controlled enclosure with constant gas density would be required to obtain longer term stability of the single mode performance.

The short buildup time and single mode character of this laser have proved useful in laser matter interaction studies. For example interferometric studies of the time evolution of laser created plasmas can be made quite easily with the dual laser system described above. In such a situation, a plasma is generated from a suitable target with a 2.5 nsec segment of the Q-switched pulse amplified to an energy of 1J. The plasma is probed from the side with a single picosecond pulse from the mode locked laser which has been frequency doubled to $.53 \mu$. A typical interferogram obtained from a 1 mil thick Al target is shown in Fig. 8, with the picosecond pulse probing the plasma 3 nsec after the start of the Q-switched pulse.

REFERENCES

1. M. Harcher, "Single-Mode Operation of a Q-Switched Ruby Laser" Appl. Phys. Lett., **7**, pp. 39-41, 1965.
2. W. R. Sooy, "The Natural Selection of Modes in a Passively Q-Switched Laser", Appl. Phys. Lett., **7**, pp. 36-37, 1965.
3. J. Reintjes, R. C. Eckardt, and J. L. DeRose, "A Multiple Pulse Laser System with Synchronized Mode-Locked and Q-Switched Outputs", Technical Digest, 1974 International Electron Devices Meeting, pp. 326-329, Dec. 9-11, 1974.
4. M. Born and E. Wolf, Principles of Optics (3rd Edition), Oxford, Pergamon Press, 1965, p. 325.
5. American Institute of Physics Handbook (2nd Edition), New York, McGraw-Hill Book Co. Inc., 1963 p. 6-96.

*This work was partially supported by the Defense Advanced Research Projects Agency (DARPA Order 2694).

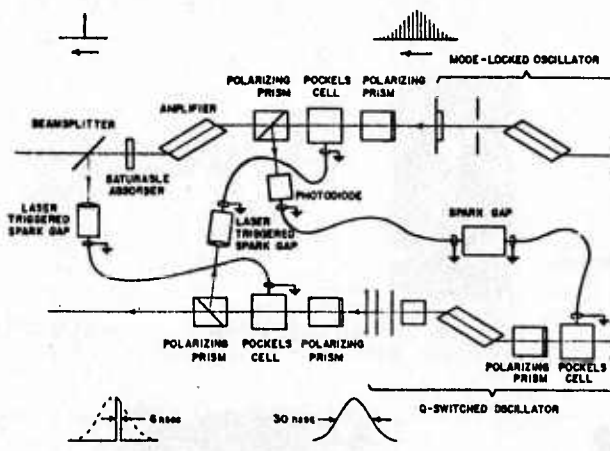


Fig. 1. Synchronized laser system

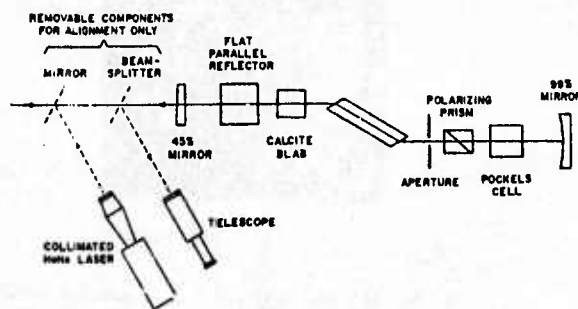


Fig. 2. Q-switched Oscillator

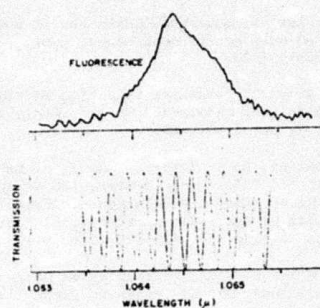


Fig. 3. Spectral fluorescence of Nd:YAG (Top) and transmission of Lyot filter (bottom).

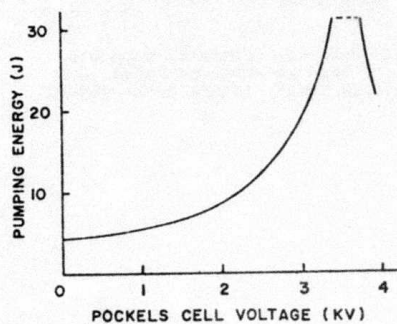


Fig. 5. Free running threshold of laser vs constant Pockels cell bias.

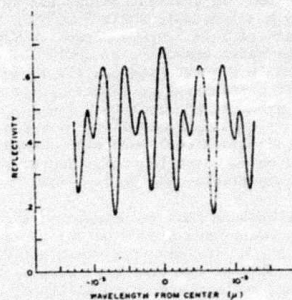
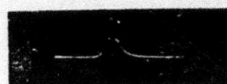
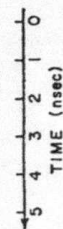
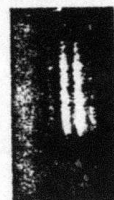


Fig. 4. Spectral reflectivity of resonant reflector



OSCILLOGRAM OF Q-SWITCHED PULSE SHOWING SHUTTERED PORTION REMOVED



STREAK RECORDING OF SHUTTERED PORTION OF PULSE

Fig. 6. Typical single mode operation of Q-switched laser.

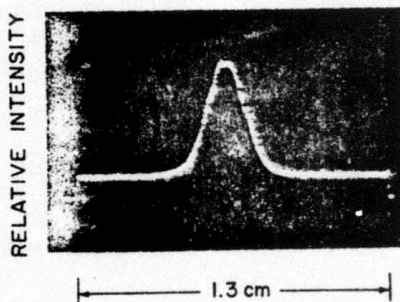


Fig. 7. Spatial profile of Q-switched pulse.



Fig. 8. Interferogram of laser produced plasma obtained with dual laser system.

(Full paper will be included
in final report.)

PREPRINT

Submitted for Publication in Proceedings IEEE

Review of Short Wavelength Laser Research

R. W. Waynant, member IEEE, and R. C. Elton

Invited Paper

Abstract-- A review of the status of research towards achieving lasing action in the vacuum ultraviolet and soft x-ray spectral regions is presented. An analysis of the general problems likely to be encountered is accompanied by numerical results for those approaches currently considered promising. Progress on each approach is detailed and various possible methods of verifying the presence of gain with their relative merits are discussed. Research areas requiring application of short wavelength lasers also are given.

Manuscript received October 1975. This work supported in part by the Defense Advanced Research Project Agency under DARPA Order No. 2694.

The authors are with the U. S. Naval Research Laboratory, Washington, D. C. 20375.

Review of Short Wavelength Laser Research

R. W. Waynant, member IEEE, and R. C. Elton

Invited Paper

Abstract-- A review of the status of research towards achieving lasing action in the vacuum ultraviolet and soft x-ray spectral regions is presented. An analysis of the general problems likely to be encountered is accompanied by numerical results for those approaches currently considered promising. Progress on each approach is detailed and various possible methods of verifying the presence of gain with their relative merits are discussed. Research areas requiring application of short wavelength lasers also are given.

Manuscript received _____. This work supported in part by the Defense Advanced Research Project Agency under DARPA Order No. 2694.

The authors are with the U. S. Naval Research Laboratory, Washington, D. C. 20375.

I. INTRODUCTION

Having been dormant for the first ten years of laser research, the development of short wavelength lasers emitting in the vacuum region¹ at wavelengths shorter than 2000 Å has advanced rapidly during the last five years. A number of new devices useful as both oscillators and amplifiers have been developed and are finding early application as diagnostic probes for materials studies. In addition, techniques have been developed for utilizing non-linear optical properties of materials to generate laser harmonic frequencies and to mix and add together several lower laser frequencies to produce tunable, coherent emission in the spectral region below 2000 Å. These advances have produced the momentum for research to develop still shorter wavelength x-ray lasers.

Perhaps the most important forerunner of the direct amplifying, self-contained lasers to be developed was the molecular nitrogen discharge laser of Heard [1]. This laser, which emits at 3371 Å from molecular electronic levels, spurred the development of the fast pumping technology required for shorter wavelength lasers, as well as pointing out the utility of molecular electronic levels for ultraviolet (uv) lasers. This laser has been developed considerably by Leonard [2], Gerry [3], Shipman, [4], and numerous others. It is now one of the most important lasers in the near uv and is used extensively as an exciter for dye lasers. French reports claim 50 MW peak power from such N₂ lasers [5]. In addition, there has

¹At wavelengths shorter than 2000 Å, oxygen and nitrogen in the atmosphere absorb radiation strongly and vacuum (or helium-purged) paths must be provided to propagate the radiation.

been success in pumping N_2 with electron beams [6], [7].

Earlier development of nitrogen lasers led directly to the realization of the first vacuum ultraviolet (vuv) laser from molecular hydrogen. The concept of a hydrogen laser was advanced by Bazhulin, Knyazev and Petrash [8] in 1965, but the actual realization of the laser awaited application by Shipman [4] of fast pulsed technology to the nitrogen laser. Using the flat plate Blumlein discharge system, both Hodgson [9] and Waynant et. al [10], [11] produced lasing on the Lyman band ($B^1\Sigma_u^+ - X^1\Sigma_g^+$) of hydrogen. Further work produced laser emission from the isotopic molecules, D_2 and HD , and also from para- H_2 [12], [13]. Hodgson also was able to produce stimulated emission on the fourth positive band of CO ($A^1\Pi - X^1\Sigma^+$) giving lines in the 1800 - 2000 Å region [14].²

Continued development of the Shipman technology enabled Waynant to generate lasing on the 1160 Å spectral region on the Werner band transitions ($C^1\Pi_u - X^1\Sigma_g^+$) from H_2 [15]. Hodgson and Dreyfus switched to a high current electron beam to generate lasing in N_2 [6], in the H_2 Lyman band [16] and also the Werner band of H_2 [17]. Considerable theoretical [18]-[22] and experimental [23], [24] work has been done on the H_2 laser. In recent reviews of the H_2 laser [25], [26], advances and limitations are detailed for both atmospheric pressure and repetitively discharged operation.

The Soviet scientists were also responsible for another theoretical prediction of a somewhat different vacuum ultraviolet laser. In 1968 Molchanov, Poluektov and Popov proposed that solid crystals of the rare

²One line reported in hydrogen experiments at 1600.44 Å [9], [13] has not been observed by other investigators and may be an impurity line.

gases could be made to lase [27]. Basov and co-workers conducted a number of experiments using the liquid form of the rare gases, principally xenon, [28]-[33] and report characteristics consistent with stimulated emission. Koehler and associates [34]-[35] used high current electron beams and high pressure gaseous xenon to form excited xenon molecules (Xe_2^*) called excimers. Lasing was observed at $\sim 1720 \text{ \AA}$ from these excimers. Extensive theoretical studies [36]-[43] and considerable experimental work [44]-[53] has been devoted to xenon, as reviewed by Rhodes [54]. Other excimers, e.g., Kr_2^* and Ar_2^* , have been made to lase in the 1260 - 1460 \AA region [34], [35], [39], [55]-[57]. These lasers appear to have a large potential for both high power and high efficiency.

A. Material Limitations

1) Optical Characteristics: Besides the difficulties of achieving high gain at short wavelengths (which will be explained in Section II), a major impediment for vacuum-uv and x-ray lasers has been a lack of suitable materials for both high transmission windows and efficient reflectors for resonators, both of traditional high priority in laser research. The field of optics in the vacuum ultraviolet has been surveyed and reviewed recently quite excellently by Hunter [58] and also previously by Tousey [59] and Samson [60]. Figure 1 from [58] shows the temperature dependence of the short wavelength transmission limit of various vacuum ultraviolet window materials. The cutoff wavelength of all materials drops with temperature, but no material has a cutoff below 1000 \AA (LiF). Below 1000 \AA the only possibility of building a Fabry-Perot mirrored cavity requires that a hole for output coupling be cut in the mirror. To do this would require sophisticated differential vacuum pumping and gas

handling.

For reflection, no material is better than aluminum for wavelengths longer than 1000 \AA . In order to use this high reflectance the oxide film which normally develops on its surface must be prevented. This is done by overcoating with magnesium fluoride or lithium fluoride films of precisely controlled thickness. Since the overcoating material cuts off at short wavelengths, the reflectance of aluminum cannot be used below 1000 \AA . Below 1000 \AA no material has very high reflectance. Platinum is usually used, but in some wavelength regions such materials as iridium, osmium, rhenium and tungsten may have higher reflectance. The reflectance of these materials is given by Hunter as a function of wavelength [58].

Already difficulties have been found in using resonators with the rare gas molecular lasers. Aluminum coatings are rapidly damaged [45], [61] when used as resonators for high power xenon lasers and presently limit the output intensity to about 1 MW/cm^2 . Intensity inside the resonator is several times higher. The primary reason for this limitation is the power absorbed in the aluminum. The same interband levels responsible for absorption in aluminum are present in other prospective reflector materials. Multilayer dielectric mirrors are a possible choice, but they are difficult to make, would likely still have considerable absorption, and would not be available below 1000 \AA .

2) Crystal Resonators:

a) Bragg Reflection: Below 1000 \AA resonant cavities with high reflectance are difficult to build for the reasons given above, but at very

short wavelengths of about 10 \AA or less it becomes possible to use Bragg reflection from the crystal planes of solids. Several papers have presented possible x-ray resonators which would be suitable - theoretically at least - for an x-ray laser. The puckered ring design of Bond, Duguay, and Rentzepis [62] is shown in Fig. 2. This design allows the resonator to be tuned to the laser transition. The losses at each crystal reflection are less than 5%, but these losses multiply as crystal elements are added and so does the difficulty of alignment. Single crystals with alignments carefully fabricated might be used as resonators. Such resonators, as proposed by Deslattes [63], are shown in Fig. 3. Cotterill [64] proposes a resonator built using pairs of parallel crystal planes as shown in Fig. 4. In this design the polarization losses are less than the puckered ring, but alignment is likely to be possible only if they are cut from a single crystal. Kolpakov, et al [65] consider the proposed resonators and add the idea of using a Borrmann crystal to insert and extract energy from the cavity. They also suggest that active substances, presumably capable of stimulated emission, might be incorporated in the Borrmann crystal.

In spite of the theoretical work done already on x-ray resonators, they remain an extremely difficult problem. To align and use them in an x-ray laser will certainly be prohibitively difficult in the early stages of laser development.

b) Distributed Feedback: Some of the problems of alignment attributed to the previously mentioned resonators may be eliminated if a distributed feedback method, already successful with dye lasers and semiconductor lasers [66]-

[71] in the infrared and visible, can be extended to the x-ray region. In these devices the feedback mechanism is distributed through the lasing medium.

Feedback is provided by Bragg scattering from a periodic variation of the refractive index of the gain medium or of the gain itself. Kogelnik and Shank [66] solve for the threshold conditions and give results for the case of large gain factors. Chinn and Kelley also analyze distributed feedback lasers [72].

Several distributed feedback lasers have been built using dyes [66]-[68] and later the principle was transferred to semiconductor lasers [70],[71]. Because of the extremely difficult problem of x-ray resonators, distributed feedback has been suggested as an alternative [73]-[75]. Fisher [73] gives numerous crystals that have the proper lattice spacing to satisfy the requirements for distributed feedback for oxygen $K\alpha$ emission. In addition, the statement is made that standing waves may arise to avoid highly absorbing atoms present in the crystal. This is an interesting possibility which further suggests that traveling-waves might experience alternating sites of attenuation and amplification, contradicting the thought that traveling-wave excitation (See Section IV.2) would be necessary in order to overcome the short gain lengths dictated by the short excited-state lifetime of x-ray transitions. The pumping requirements remain difficult to meet even if distributed feedback can be employed. In addition, the large power densities required for pumping x-ray lasers may cause expansion, distortion, or even destruction of the periodic structure. Careful integration of pumping techniques and resonant structure design will be necessary to achieve a workable short wavelength laser employing distributed feedback.

B. Amplified Spontaneous Emission

The now-traditional idea of a laser consisting of an active medium pumped in some manner to produce an inverted population between two states, and inserted between mirrors which form an optical resonant cavity, was formulated by Schawlow and Townes [76] and reinforced by early successful lasers. The discovery [77] of intense emission from systems without optical cavities (of immense importance for lasers operated in the "vacuum" region) at first led to considerable semantic confusion which developed in conjunction with the term "superradiance" coined by Dicke [78], [79] in a hypothesis concerning the addition of the spontaneous emission from quantum radiators excited in a coherent fashion. This confusion was partially side-stepped by substitution of the term "superfluorescence" which more nearly associated the enhanced emission with directed fluorescence. Fortunately, these semantic difficulties were cleared up by Allen and Peters [80] who went on to present a series of papers [81]-[85] to clarify and make respectable the high gain mirrorless systems which they appropriately termed amplified spontaneous emission (ASE) systems. Since ASE systems will be of major importance in vacuum ultraviolet and x-ray lasers, it is appropriate to treat them in some detail.

1) Threshold: By following the arguments of Peters and Allen [81], using nomenclature [86] to be used extensively in Section II and in the three-level model in Fig. 5; a threshold condition can be derived starting with basic principles. Consider a pumped ensemble of excited radiators of length, L , cross sectional area, a , and inversion density, $\Delta N \equiv [N_2 - (g_2/g_3) N_3]$, for statistical weights g_2 and g_3 . A quantity of photons n of frequency ν passing through the cross

sectional area will induce $\omega \Delta N/a$ atoms per unit volume per second to emit at that location. The resonance induced emission cross section is denoted by σ . But $\sigma n/a = B\rho(\nu)$, where

$$B = \frac{c^3}{8\pi h \nu^3} \frac{1}{\tau_2} \quad (1)$$

is the Einstein coefficient, and

$$\rho(\nu) = \frac{nh\nu}{ac\Delta\nu_D} \quad (2)$$

is the radiation density. Here $\Delta\nu_D$ is the width of the Doppler broadened transition and $\tau_2 \equiv (R_{23} + R_{2n})^{-1}$ is the natural lifetime of state 2. Solving for σ we obtain

$$\sigma = \frac{c^2}{8\pi \nu^2 \Delta\nu_D \tau_2} \quad (3)$$

The equation for the rate of change of the number of photons, δn , due to stimulated emission in the volume, La , in time, δt , is given by

$$\delta n = L\omega n \delta t \quad (4)$$

If the threshold condition for ASE is defined as the condition when a spontaneously emitted photon at one end of the column ($x=0$) just induces another photon at the other end ($x=L$), then $n\delta t = 1$ and $\delta n = 1$ in equation (4).

This yields the relation for the critical inversion density to reach threshold [equivalent to unity gain coefficient α ; see also equation (7)]

$$n_c = \frac{8\pi\Delta\nu_D\tau_2}{L\lambda^2\phi} \quad (5)$$

where ϕ is the branching ratio, i.e. $R_{23}/(R_{2n}+R_{23}) = \tau_2/\tau_{23}$. Alternatively, for a given inversion density equation (5) will give the critical length L_c required to reach threshold,

$$L_c = \frac{8\pi\Delta\nu_D\tau_2}{N\lambda^2\phi} \quad (6)$$

Allen and Peters verify their theoretical results by comparison with a series of experiments which they carry out and with the data of others. In a later paper [82] they connect their theory with the semi-classical laser theory of Stenholm and Lamb [87]. The relationship between the critical length, L_c , for ASE and the minimum length, L_T , of active discharge at which mirrored laser action takes place is $L_T/L_c = 0.71\delta_\ell$, where δ_ℓ is the fractional loss per pass in the laser resonator. To test this experimentally the 3.39 μm transition in He-Ne was used, since it would operate both as a laser and a source of ASE [82]. A 125 cm long He-Ne discharge tube was placed between 3m radius of curvature concave mirrors with mean reflectance, $R = 0.98$. The gas was uniformly excited and it was possible to vary the length by removing or adding rf electrodes. Figure 6 shows the resulting variation of output intensity with length for both modes of operation, and particularly

demonstrates the threshold for ASE.

2) Intensity and Saturation: The success of this approach served to spur further investigation by Allen and Peters [82] who solved rate equations for the populations of two levels (from a reservoir level), and the photon transport. Care was taken to include only the radiation that fell into the position-dependent solid angle. The solutions of the rate equations were used for predicting the intensity as a function of length for a constant inversion density and to fit the 3371 Å data of Leonard [2] for N_2 as a test case.

3) Beam Divergence and Spatial Coherence: The general impression of ASE beam divergence is that it is controlled by the geometry of the gain region and would be simply d/L or possibly $d/(L-L_c)$. Peters and Allen point out [84], [85] that each contribution must, however, be weighted by the amount of amplification path through which it passes. When numerical methods are used to weight each element geometrically, the theory fits the divergence data very well. The results show quite convincingly that the simple d/L ratio is not correct and that the "ASE-geometric theory" of Allen and Peters is necessary.

On the question of spatial coherence, Allen and Peters offer the experimental measurements of fringe visibility versus length. The measurements were made using the 6140 Å pulsed neon laser line and show that the coherence increases with gain length.

4) Spectral Distribution: The spectral distribution (line-width) in ASE systems has been somewhat confusing. Early predictions produced a dependency that goes as $\Delta\nu/\Delta\nu_D = 1/(\alpha L)^{1/2}$, i.e., enhanced narrowing at high gain. Allen

and Peters have developed a theory in which the linewidth is a rather complicated function of length [84]. They contrast their results with those of Yariv and Leite [88] for He-Ne and N_2 lasers as shown in Fig. 7. The theory predicts a sharp dip in $\Delta\nu$ just above L_c followed by additional broadening as length is increased. The minimum shown is due to competition between narrowing associated with increasing gain and broadening accompanying an increased range of frequencies. The existence of such a sharp minimum could be used as an indicator of stimulated emission. As yet no definitive measurements have been made to resolve the details of the theoretical predictions of Allen and Peters.

It is also important to realize that there are limits to the application of the present ASE theory to likely x-ray and vacuum ultraviolet lasers. These devices may be pulsed systems employing traveling-wave excitation. Also, the coupling of ASE amplifiers with a coherent beam produced, for example, by nonlinear mixing with harmonic frequencies may introduce new problems [89]. As yet the theory of ASE has not been extended to cover these cases. In addition, further information may be obtained from more formal and rigorous theoretical techniques such as the semi-classical laser theory of Lamb [90]. It appears that this work is in progress by Lamb [91] and by Hopf [92].

II. BASIC PHYSICS PROBLEMS

Besides the materials problems described above, the basic physical considerations pertinent to all the general schemes and the specific models tend to demand the very most that the current state-of-the-art can attain in pump power. To produce gain, high inversion densities are called-for and, for most models, very rapidly-rising pump pulses are required to achieve inversion and gain prior to equilibration. These problems will be analyzed in this section in a rather general and scalable fashion, with several examples from recently suggested schemes.

A. Wavelength Dependence of Gain

Continuing from Eqs. (3)-(6), the net gain achieved in a single pass through a medium of length, L , is given by $\exp(\alpha L)$, with the small-signal gain coefficient, α , defined by³

$$\alpha = \sigma \Delta N_{23} = \frac{\lambda^2 A_{23}}{8\pi \Delta \nu} \xi \Delta N_{23}, \quad (7)$$

where the subscripts again refer to the three state system shown in Fig. 5 with pumping from energy state 1 to 2 and lasing from 2 to 3, at rates R_{12} , R_{23} , etc., using nomenclature consistent with reference [86]. These "states" are not restricted to one atom or ion, i.e., transition 1 to 2 could be by ionization or recombination, for example, providing replenishment of state 1 is present as indicated by R_{m1} . The parameters λ , $\Delta \nu$, and A_{23} are the wavelength [93], line-width in frequency units, and transition probability, respectively. The

³ A numerical factor of $1/4\pi^2$ is sometimes used instead of $1/8\pi$; the factor-of- $\pi/2$ difference is small.

factor ξ varies from unity for a Lorentzian line profile to $(\pi \ln 2)^{\frac{1}{2}}$ for a Gaussian-shaped Doppler broadened line. The net inversion density⁴, ΔN_{23} , is again $[N_2 - (g_2/g_3)N_3]$, with g_2 and g_3 the respective statistical weights, and is approximated by N_2 when a large inversion is achieved. The product $\lambda^2 A_{23} = 0.67(g_3/g_2)f_{32}$ numerically [95], where f_{32} is the absorption oscillator strength. This relation removes the explicit wavelength dependence in equation (7), since f_{32} is nearly constant along isoelectronic sequences (and approaches unity for intense lines). However, the wavelength enters implicitly in the inversion density (Section II.B) and also in the expression chosen for the line width $\Delta\nu = (\nu/\lambda)\Delta\lambda$ or $= (c/\lambda^2)\Delta\lambda$.

Estimations of the line width, $\Delta\lambda$, as a function of wavelength are summarized in Fig. 8, reproduced from [96] where the appropriate equations and detailed references are given. A Lyman- α model is used. The Doppler width, $\Delta\lambda_D$, is dependent upon the particle thermal velocity and is associated with a kinetic temperature of $kT = hc/4\lambda$ (plasma model). The natural width, $\Delta\lambda_N$, includes both radiative and Auger decay. A reduction associated with Auger decay for outer-electron stripping is indicated for neon ions. The limits for 1- and 2-electron ions are shown, although these limits are probably not realistically reached compared to the Doppler broadening present when such ions are created at high temperatures. The importance of Stark broadening [97] due to charged particles increases rapidly with density for a specific wavelength, as indicated. In addition to producing a decline in gain at high densities, the onset of significant Stark broadening is associated with an approach of collisional (statistical) equilibrium without population inversion, as discussed in Section II.B. Fortunately, significant gain can be anticipated

⁴There is one suggestion for lasing without population inversion [94], based on Doppler recoil line shifts.

at densities below the Stark regions with the choice of efficient pumping schemes. However, it is difficult to conceive of reducing the linewidth significantly below the Doppler value, $\Delta\nu_D \approx \bar{v}/\lambda$, where \bar{v} is the mean particle velocity.

The inversion density, $\Delta N_{23} \leq N_2$, in (7) must be maintained against a depopulation rate for level 2 at least as great as A_{23} , i.e., $N_2 \leq N_1(R_{12}/A_{23})$, where R_{12} is the pumping rate, and again $A_{23} \propto \lambda^{-2}$. Thus, from these general arguments it can be seen that the gain factor depends on a number of parameters, but scales approximately as λ^3 . This will be restated from the pump requirement viewpoint in the following section, where it is seen that pump power density scales more strongly with wavelength, approximately as λ^{-4} .

B. Pumping Requirements

From the arguments of the previous section, the high-inversion gain formula for Doppler broadened lines may be approximated for non-cavity operation by

$$\alpha_D \leq \frac{\sqrt{\pi \ell n 2}}{4\pi^2} \frac{0.67 f_{32}(g_3/g_2) \lambda}{\bar{v}_1} N_1 \eta_2, \quad (8)$$

where $\Delta\nu_D$ is replaced by (\bar{v}_1/λ) with \bar{v}_1 the mean velocity for the amplifying particles and $\eta_2 \approx R_{12}/A_{23}$, the maximum ($R_{2n} = 0$) degree of pumping for level 2. Recalling that the inversion factor $(1 - g_2'N_3/g_3N_2)$ in the gain formula was assumed to be unity, it is worth noting that high inversion ratios N_2/N_3 are possible and observable [98], [99] independent of the absolute values of density, N_1 , degree of pumping η_2 , and gain. In fact, preliminary experiments

towards development of population inversion are sometimes better performed under optically thin conditions at lower densities.

On the other hand, the significant gain ultimately sought at short wavelengths must be accompanied by high densities, N_1 , and/or large fractional pumping, η . This is conveniently illustrated with equation (8) for the case of a laser-produced plasma medium, chosen since at present lasers offer the highest available concentration of pump power. Taking $\alpha L = 5$ as desirable (unity at "threshold" for ASE⁵), $L = 1$ cm, ⁶ $\bar{v}_1 = 10^7$ cm/sec and $f_{32}(g_3/g_2) \approx 0.5$ for a strong line,

$$\lambda N_1 \eta_2 \geq 10^{18} \quad (9)$$

results for λ in Å and N_1 in cm^{-3} . Thus a 1% inversion at 1 Å requires a density of $N_1 \geq 10^{20} \text{ cm}^{-3}$. This argument involves a rather arbitrary value for the degree of inversion and does not indicate specific pump requirements to achieve a high inversion density, ΔN_{23} , at a particular wavelength. By replacing $N_1 \eta_2$ by $N_1 R_{12}/A_{23}$ in the gain formula and defining $p_{12} \equiv N_1 R_{12}$ and $P_{12} \equiv p_{12}(hc/\lambda_p)$ as the volumetric pump rate and pump power, respectively, α_D may be rewritten as

$$\alpha_D \leq \frac{\sqrt{\pi \ln 2}}{4\pi^2} \frac{\lambda^3}{\bar{v}_1} p_{12} \quad (10)$$

⁵ $1-r$ with r the reflectivity, where reflecting cavities exist.

⁶ Corresponds to sustained inversion for 30 ps, or self-terminating lasing at $\lambda \geq 300$ Å. Shorter wavelengths require reduced lengths or traveling-wave synchronized pumping.

and for the pump wavelength $\lambda_p \approx \lambda/10$,

$$\alpha_D \leq \frac{\sqrt{\pi \ell n 2}}{40 \pi^2 h c} \frac{\lambda^4}{\bar{v}_1} P_{12}. \quad (11)$$

These relations demonstrate the strong λ^{-3} and λ^{-4} wavelength dependence of the volumetric pumping parameters for a fixed gain coefficient, α_D [100].

With $\alpha_D=5$ and $\bar{v}=10^7$ cm/sec again, minimum values of p_{12} and P_{12} are calculated and tabulated in Table I for several wavelengths. Note that a closely related parameter of importance is the pump irradiance, $P_{12}L$ (W/cm^2), which is fixed by the gain product, αL , and equivalent to P_{12} in Table I for a laser-produced plasma length $L=1$ cm.

TABLE I
Volumetric Pumping Requirements

$\lambda [\text{\AA}]$:	1	10	100	1000	2000
$p_{12} [\text{cm}^{-3}\text{-sec}^{-1}]$	10^{33}	10^{30}	10^{27}	10^{24}	10^{23}
$P_{12} [\text{W-cm}^{-3}]$	10^{19}	10^{15}	10^{11}	10^7	10^6

1) Wavelength Scaling: The volumetric reaction rate, p_{12} , can be expressed as $N_p \langle \sigma_p v_p \rangle$ where the subscript p denotes the pumping particle (or photon), σ_p , the reaction cross section, and $\langle \sigma_p v_p \rangle$, the rate coefficient, averaged statistically over the distribution of velocities, v_p . Estimates of the

magnitude of reaction rates for some rather general pumping schemes scaled with wavelength are listed in Table II (collisional ionization is omitted, as it favors outer electron removal).

TABLE II
Pumping Rate Coefficient Magnitudes Scaled^a

PROCESS	$\langle \sigma_p v_p \rangle$ (cm ³ sec ⁻¹)
Photoionization [96], [101]	$10^{-12} \lambda$
Electron Collisional Excitation [103]	
Plasma	$10^{-13} \lambda^{3/2}$
Beams	$10^{-13} \lambda$
Dielectronic Capture [102]	$10^{-13} \lambda^{3/2}$
Collisional Recombination ^{b,c} [103]	$10^{-13} \lambda^{5/4}$
Resonance Charge Transfer	
Plasma ^d [100]	$10^{-6} \lambda^{-5/4}$
Ion Beams ^e [104]	$10^{-5} \lambda^{-1}$

^aWavelength λ in Angstrom units

^bElectron density $N_e = N_p = 10^{21}$ cm⁻³

^cMust exceed radiative recombination [103] for which $\langle \sigma_p v_p \rangle \sim 10^{-11} \lambda^{-1/2}$; i.e., $\lambda \geq 15$ Å.

^d $\bar{v} = 10^7$ cm/sec, $\sigma_p = 10^{-16} z^2$, z the net ion charge

^e $\bar{v} = 10^8$ cm/sec, $\sigma_p = 10^{-16} z^2$, z the net ion charge

The rates shown are derived from relations in the indicated references. For photoionization, a peak cross section $\propto Z^{-2}$ was assumed (Z the nuclear charge), multiplied by c , and divided by 100 for $\sim 1\%$ absorption in the pumping band. For dielectronic capture, an autoionization (Auger) rate of 10^{14} sec^{-1} was used in the detailed balancing formalism. In addition, various approximations were necessary in relating the rate coefficients solely to wavelength, with the emphasis on short wavelengths and a plasma medium. Specifically, the laser wavelength was taken as $\lambda = 1216/z^2$ in Ångstrom units from Lyman- α scaling, where z is the ion charge. The ionization potential was assumed to be 1.3 times the excitation energy, with the latter taken to be 3 times the plasma electron temperature and also related to wavelength directly by hc/λ .

Returning to Table II, it is first noted that most rate coefficients tend to scale downward with shorter wavelength, which is detrimental for achieving high gain; only the resonance charge transfer process scales in an advantageous manner. A geometric-mean particle density, $(N_i N_p)^{1/2}$, can be derived for each of these schemes, using equation (10) and assuming $\alpha=5 \text{ cm}^{-1}$ and $\bar{v}_1=10^7 \text{ cm/sec}$ for plasmas, 10^8 cm/sec for ion beams, and c for relativistic-electron and photon beams. This parameter, plotted in Fig. 9 is particularly meaningful for plasma pumping schemes, and the reliability of the order of magnitude estimates in Table II is improved by the 0.5 power. From Fig. 9 it is seen that the density requirements are comparable between pumping schemes in the vacuum-uv ($\lambda > 100 \text{ Å}$) within an order-of-magnitude. Electron-collisional excitation is somewhat favored and the magnitude at 1000 Å agrees with the H_2 discharge laser conditions [11]; thus the interest in extending proven electron

collisionally excited ultraviolet ion laser transitions into the vacuum-uv region [105]. The resonance charge transfer process with its anticipated (Section III) large cross section appears most favorable for extrapolation to the x-ray region. It requires reasonable densities and gives a wide latitude for increasing the gain coefficient and reducing high density absorption. Collisional recombination excitation processes limit laser wavelengths to $\geq 15 \text{ \AA}$ for $N_e = 10^{21} \text{ cm}^{-3}$. This particular limit is found by requiring the collisional recombination rate coefficient ($\sim 10^{-13} \lambda^{5/4}$) to exceed the rate coefficient for radiative recombination into lower states ($\sim 10^{-11} \lambda^{-1/2}$) (See Table II). This wavelength limit also happens to correspond to the assumed density of 10^{21} cm^{-3} , which is an upper limit for present laser-produced plasmas.

Also indicated in Fig. 9 is the region in which plasma Stark-effect line broadening becomes important. Since Stark widths scale approximately as charged particle density in plasmas, the gain factor in the Stark region will tend to scale with N_1 instead of $N_1 N_p$. Approaching the region of Stark broadening importance also implies increased collisional effects on the lasing levels. Indeed, a check of several promising schemes indicates that the dominance of Stark broadening is correlated with an approach to collisional equilibrium with non-inverted statistical population distributions [106]. Thus, densities significantly exceeding the "Stark line" in Fig. 9 would not be particularly advantageous for achieving high gain, and the higher-density approaches depicted (e.g., collisional recombination) are the most limited.

2) Pump Power Limitations: The estimates plotted in Fig. 9 are continued

(except for collisional recombination) to short wavelengths and to densities exceeding those expected from present laser-produced plasmas ($\sim 10^{21} \text{ cm}^{-3}$ [107], [108]), in anticipation of eventual inertial compression as planned for laser-pellet fusion. Such compression would also aid in meeting the volumetric pump power requirements indicated above. The dashed portions of the lines in Fig. 9 indicate those regions where present technology cannot meet the density requirements. If, for example, even 10 percent of the power from a 1 TW laser could be utilized for pumping in a volume of 10^{-3} cm^3 (1 cm length, 400 μm diameter), the power density of 10^{14} W/cm^3 would place a lower limit of about $\sim 13 \text{ \AA}$ on the achievable wavelength.

Vacuum spark discharges are known to produce very hot, dense plasmas in small regions [109]. Such discharges may radiate as much as 10^{15} W/cm^3 of x-rays in a 100 μm spherical plasma [110] where a gain factor of $Q=500 \text{ cm}^{-1}$ is required due to the small dimension. Significant amplification according to Fig. 9 would only occur at wavelengths longer than 700 \AA , and with the high densities ($\sim 10^{21} \text{ cm}^{-3}$) typical for such a device, collisional domination without inversion is likely at such long wavelengths. Thus, this relatively simple and convenient source may be more useful for determining promising population inversion methods at low gain, short wavelength, and under optically thin conditions, for application to extended laser-heated plasmas of similar environment.

Electron beams of power comparable to lasers exist at present; however, the focusing volume achievable so far would be approximately 300 times larger [111] (for a cylindrical geometry) so that a short wavelength limit of $\sim 50 \text{ \AA}$ is

expected for this mode of pumping with present technology, as indicated in Fig. 9.

3) Additional Considerations:

a) Reduced Gain Factor: High density limitations can be reduced with a lower gain coefficient, α , providing the net gain determined by $\exp(\alpha L)$ for a specified degree of amplification is maintained through a correspondingly increased length, L , and eventually traveling-wave pumping for short wavelength and self-terminating transitions.⁶ (An exception to this reduced density option is the collisional recombination scheme where the high electron densities are also required to overcome competitive radiative recombination into lower levels.) Here the pump irradiance, $N_1 P_{12} L$, remains the same and must be distributed over a larger volume, which could present a technical problem for laser pumping schemes. However, other extended pumping sources have been suggested, such as traveling-wave transverse electron beams (Section IV) and swept ion beams. For example, by the scaling in Fig. 9, as well as from (10), $\alpha=0.1$ can be achieved at a wavelength of 300 Å with $(N_1 N_p)^{1/2} \sim 10^{16} \text{ cm}^{-3}$ obtained in a near-solid target of density $N_1 = 10^{22} \text{ cm}^{-3}$ and $N_p = 10^{10} \text{ cm}^{-3}$. The latter may be obtained from a swept 25 keV, 20 mA ion beam focused to a 0.2 cm radius in a resonance charge transfer reaction (see Section III.B). Equation (11) restricts the volume for a beam of this power such that a maximum depth of the order of 10 μm must be maintained. While beam currents in the hundreds of mA are suggested [112], state-of-the-art ion-beam technology appears to limit this approach to the hundreds-of-Ångstrom region.

b) Competitive Decay from State 2: So far it has been assumed that the upper laser state (designated 2 in Fig. 5) decays only through the laser transition to state 3, i.e., alternate decay rates R_{2n} are much less than A_{23} . With this assumption, the pump requirements are independent of line strength (i.e., weak lines are accompanied by an increased pump-state density) and a number of other, often weak, transitions appear to be attractive candidates for lasing at short wavelengths. With R_{2n} included, the degree of pumping, η_2 , in (7) becomes $R_{12}/(A_{23}+R_{2n})$ and the volumetric pumping parameters, p_{12} and P_{12} , as well as the mean density, $(N_1 N_p)^{1/2}$, scale up by the ratio $(A_{23}+R_{2n})/A_{23}$, where the line strength again enters through A_{23}^{-1} for R_{2n} large.

One class of schemes for which R_{2n} can be important is when alternate spontaneous decay occurs in an isolated atom or ion. An example is an inner-shell lasing transition (Section III) for which autoionization (Auger) decay is also possible, and highly probable for low-Z elements. Another example would be second-order double electron transitions, where one electron decays in a radiative transition and another changes state so that a shifted line occurs, with reduced reabsorption. In this case R_{2n} represents the "normal" decay mode with a rate much higher (typically ~ 100 times) than A_{23} .

Another class of schemes applies when R_{2n} is a collisional-depopulation rate. Again, collisional depopulation is expected to be generally important in the high density "Stark region" indicated in Fig. 9, where R_{2n} represents transitions between states 2 and 3. Collisional depopulation to other bound states, with rapid decay, or to other ionic species through ionization or recombination can also be important starting at lower densities, particularly for weak

lines and those originating on metastable upper states (see below). Obviously, each case must be treated independently, and knowledge of rates for many important collisional transitions is either very limited or non-existent.

C. Duration of the Inversion

1) Transient to CW Extremes: Using the nomenclature in Fig. 5, a population inversion can be maintained between energy states 2 and 3 as long as the rate R_{3m} of depletion of state 3 to some other state m exceeds the rate R_{23} at which it is filled, with adequate $m \rightarrow 1$ replenishment of the initial state 1. However, if $R_{3m} = 0$ (e.g., with 3 a ground state), population inversion ceases in an equilibration interval. These extremes and the intermediates have been deduced analytically [86] for this three-state model for a pump pulse with both a short risetime $t_r \ll \tau_2$ [$\tau_2 \equiv (R_{23} + R_{2n})^{-1}$, the lifetime of state 2], as well as for a linear-ramp rising pump pulse, i.e., $R_{12} = \dot{R}_{12}t$. With the inversion density in (7) written with a separate factor $T(t)$, i.e.,

$$\Delta N_{23} \approx N_1 T R_{12} / (R_{23} + R_{2n}) = N_1 R_{12} \tau_2 T, \quad (12)$$

the time dependence of the inversion density is calculated and the results are shown in Fig. 10 versus t/τ_2 for the fast rising pump pulse case. Positive T implies gain, negative values imply net loss. The parameter $G \equiv g_2 R_{23} / g_3 (R_{2n} + R_{23})$ is a modified statistical weight ratio. For R_{2n} small, and $g_2 = g_3$, $G \approx 1$ and the inversion time, $t_i \approx \tau_{23}$, i.e., inversion ceases in about the radiative lifetime of the upper laser level, as expected. A selection of $g_3 > g_2$ states could extend this time somewhat and also raise the degree of inversion. However,

decreasing G by increasing R_{2n} does not extend the inversion time appreciably, since τ_2 decreases proportionally. An equivalent parameter $T(\tau_2/t)$ for the linear-ramp pumping case yields similar results. These $R_{3m} = 0$ examples represent the self-terminating mode of pre-equilibrium population inversion.

Included in Fig. 10 is the $G=0$ limit which is also equivalent to the case when R_{3m} becomes very large, i.e., the continuous inversion cw-mode. Here the time dependent factor, $T(t)$, becomes unity and the inversion density is given by $N_1 R_{12} \tau_2$, the coronal-equilibrium value. With high inversion, ΔN_{23} approaches N_2 and $\Delta N_{23}/N_1 \approx R_{12} \tau_2 \equiv \eta$ gives the fractional pumping for the laser medium (Section II,B). This cw-mode obviously is the most desirable situation. An intermediate mode of operation is for $R_{3m} \tau_2$ to be finite with values greater or less than unity corresponding to sustained or terminated gain, respectively. The time dependent factor for the fast rising pump pulse case is plotted for $G = 1$ in Fig. 11 and illustrates the approaches to partial equilibrium inversion densities for the intermediate $R_{3m} \tau_2$ cases. Such curves can be used to determine the approximate inversion densities (see Section III,C, for example).

The detailed analytical formulas leading to these graphs can be found in reference [86]. They are necessarily approximate, but of general usefulness for preliminary analyses. Numerical modeling for specific pump modes and atomic models is essential, particularly for the quasi-cw schemes where the replenishment rates could not be included in the analytical model. Such requirements for replenishment can include both the internal pumping particle (e.g., an energetic plasma electrons or a photon) as well as the amplifying particle. As an example of the latter, the Kr quasi-cw scheme discussed in Section III.C

generates additional ionization and a sufficient recombination rate is required to sustain the inversion density.

2) Metastable States: The use of metastable states as upper laser states with extended lifetime τ_2 has been suggested as a means of reducing the pump pulse risetime requirements for rapidly terminated population inversions [113],[114]. This is particularly important for lasing at wavelengths shorter than $\sim 30 \text{ \AA}$, where sub-picosecond risetimes are required. Since both the pump power density and the gain coefficient scale as the product of density and transition probability, the pump power required remains the same for fixed gain whether the laser transition is an allowed dipole or forbidden transition. (However, the densities increase for the longer-lived upper laser states.) Unfortunately, it is difficult to find a metastable upper state that terminates in such a high energy transition on a lower state that does not also accumulate population by a dipole-allowed transition at a higher rate. For example, the well-known $n=2$ triplet levels of helium-like (and beryllium-like) ions decay to the ground state in relatively slow intercombination transitions [115] but population inversion would require filling of the triplet levels preferentially over the singlet levels. Such a selection is not known to exist, certainly not by excitation from the lower ground state [116]. Required selectivity would have to evolve from a capture process of some sort.

In the event that such preferential population should be discovered, as has been suggested [117] for a recombination radiative trapping scheme, the next most important concern is the competing depopulation (by, for example, electron collisions at the increased densities) from level 2 at a rate R_{2n}

as designated in Fig. 5. This effect is discussed in Section II. 3.b where it is pointed out that the pumping requirements increase as R_{2n}/A_{23} for $R_{2n} \gg A_{23}$. For the intercombination transition examples discussed above, collisional ionization [103] as well as spin-exchange transitions occur at a high rate [118] even at moderate densities. A rapid rise in A_{23} with Z for "forbidden" lines can be expected [115], so that R_{2n} may not dominate at very short wavelengths; however the associated short lifetime, τ_2 , would negate the advantage of the metastable state. Sparse collisional data exist for a thorough evaluation here, but again the first problem is to identify a realistic laser transition.

A somewhat different approach makes use of metastable states for the accumulation of electrons in a majority of the lasing ions (at a relatively low density) and the subsequent transfer of the electrons to a nearby dipole-coupled state by absorption of laser emission [114], [119]-[121]. Singly-ionized lithium is a popular example, with 2^1S population (followed by $2^1S \rightarrow 2^1P$ transfer) to be provided either by charge transfer collisions or by photoionization of a $1s$ electron from neutral lithium atoms. Recently the population and storage by charge transfer has been demonstrated for $(Sr^+)^*$ ions formed by a $Mg^+ + Sr$ reaction [122]. This approach obviously overlaps other areas included in this review, but the novelty lies in the use of metastable states for the accumulation of electrons in an excited state adjacent to the upper laser level.

D. Beam Propagation Losses in the Lasing

The only loss mechanism expected to be significant in the lasing medium is that due to photoionization. Compton scattering as well as inverse bremsstrahlung effects have been considered [123] and shown to be negligible.

Photoionization becomes a consideration whenever there are electrons bound with less energy than that of the laser photons. Then the density, N_0 , of atoms or ions with such bound electrons multiplied by the photoionization cross section, σ_{pi} , gives the photoionization coefficient α_{pi} , i.e., $\alpha_{pi} \sim 10^{-20} N_0$ for a rather typical value [96] of $\sigma_{pi} \sim 10^{-20} \text{ cm}^2$ and N_0 in units of cm^{-3} (σ_{pi} is strongly frequency dependent and varies approximately as ν^{-3} for laser frequencies, ν , above the absorption edges). Thus, it is for innershell transitions at high densities that propagation losses are significant and the gain must be adjusted to overcome such losses [96].

E. Summary of Laser Physics at Short Wavelengths

The achievement of significant gain at short wavelengths is limited to about 10 \AA at present by the available power density and, for self terminating schemes, by the ability to concentrate power into a short-rise-time pumping pulse. The density limits indicated in Fig. 9 are dictated by the $\alpha=5$ condition based upon a short-length laser-heated plasma model, since this is at present the highest power density source available. These "limits" can thus be scaled down with extended lengths L , keeping αL constant, with the exception of the collisional recombination scheme which depends on high density to achieve an inversion irregardless of absolute gain. Pumping requirements are not affected by the strength of the lasing line unless alternate spontaneous or collision-induced depopulation of the upper laser state occurs at a rate exceeding that for spontaneous radiative decay. This represents an additional

limitation for schemes involving weak lines, high lying states, and for most innershell transitions. Significant gain with beam pumping appears to be presently limited to the 100's of Å region by state-of-the-art technology. Metastable states appear promising mainly as slowly filled electron-storage states for rapid transfer-pumping to nearby dipole coupled upper laser states. Assuming continued advancement in pump source technology, the foreseeable wavelength limit for non-nuclear transitions occurs near 0.1 Å with the Lyman- α line for a hydrogenic $Z=100$ ion.

III. POSSIBLE DIRECT LASER APPROACHES

A number of approaches have been proposed and/or attempted for achieving sufficient population inversion for lasing in the vacuum ultraviolet and x-ray spectral regions. The more attractive and understandable approaches are treated in some detail in the following, as are some experimental observations suggesting short wavelength gain which so far defy reasonable theoretical explanation.

A. Electron Collisional Excitation

1) Electron Collisions with Molecules: Molecular lasers occupy an important place among the types of lasers which have been developed to date. They span the spectrum from the millimeter wave region to the vacuum ultraviolet. They possess characteristics which qualify them for high power cw machining in industry, for pumping dye lasers, for powerful weapons, and for attempting to create thermonuclear fusion. Since the electronic transitions in molecules have been used to generate almost all the vacuum ultraviolet lasers developed so far, they must be considered of major importance for the vacuum-uv region. Since, both the review of Rhodes [54] of ultraviolet laser physics and the review by Wood [124] of high-pressure pulsed molecular lasers cover portions of this topic very well, only the fundamental processes will be discussed here from the viewpoint of acquainting the reader unfamiliar with the topic, and for allowing discussions of future lasers to be meaningful.

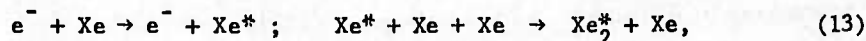
Figure 12 shows simplified potential energy diagrams for a) N_2 , b) H_2 , and c) Xe_2^* . Each of these molecules represents a somewhat different type of laser transition, but nitrogen and hydrogen have the most in common.

These two molecules have stable ground states, and at room temperature only the ground vibrational level is filled. Electron collisions fill the upper states in accordance with Franck-Condon factors and with the energy spectrum of the electrons. In nitrogen, several triplet levels are heavily populated and lasing is produced on the transition $C^3\Pi_u \rightarrow B^3\Pi_g$ in the near uv and on the transition $B^3\Pi_g \rightarrow A^3\Sigma_u^+$ in the infrared. In both cases the laser emission quickly terminates due to the long lifetime of the lower laser level. This level fills rapidly, destroying the inverted population needed for lasing. Also, these triplet levels cannot make transitions back to the ground electronic level. In hydrogen, singlet states are populated by electron impact and transitions back to the ground electronic state are possible. Lasing results on the $B^1\Sigma_u^+ \rightarrow X^1\Sigma_g^+$ and $C^1\Pi_u \rightarrow X^1\Sigma_g^+$ transitions producing vacuum ultraviolet emission from a number of vibrational-rotational lines. Several studies of possible triplet state lasing have been carried out also [123]-[128].

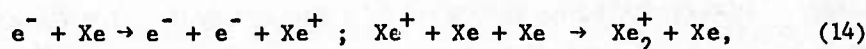
The energy level diagram for Xe_2^* is considerably different from the other molecules because the ground state is unstable. The molecule exists only in an excited state. When it gives up its excited energy and returns to the ground state, the two atoms rapidly dissociate. This is excellent for lasers because the lower laser level cannot fill and terminate the inversion. As long as the molecules exist some inversion density exists. Production of the excited rare gas molecules is a far more complicated process involving several steps. The molecules are most efficiently produced by excitation or ionization of high pressure gas volumes. At the high pressures required, the most suitable excitation source is the electron beam. Electron beams have been employed as excitation devices for almost all the rare gas lasers that have been produced (as discussed in Section I), but it seems possible that some less sophisticated

method may emerge eventually.

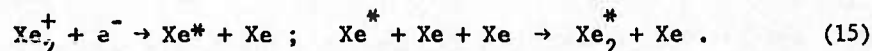
The primary high energy electrons, the secondary electrons and the return current electrons participate in the excitation process which could go as [54], [129], [130]



or as



followed by



Here the asterisk and the plus superscripts refer to excited and ionized species, respectively. Typical operating conditions are from 300 keV - 2 MeV voltages and at pressures of 100 - 500 psia. Numerous other molecules have the same characteristic of existing only in the excited state [131], [132].

Certainly additional vacuum-ultraviolet lasers can be produced using molecular transitions. The bound-free excimer transitions are especially attractive, because the dissociative lower laser level and the high pressures at which the system operates hold out the possibility of high power, high efficiency and possibly even cw operation. The possibility exists of obtaining laser emission in the 600 - 800 Å region from Ne_2^* and He_2^* . In addition, neutral molecules do exist which have sufficiently spaced electronic energy

levels to produce lasing below 1000 \AA . For example there exist in nitrogen singlet states which couple to high vibrational levels of the ground state. If these states can be excited, emission in the $900 - 980 \text{ \AA}$ region appears possible.

2) Electron Collisions with Ions: Lasing in the visible and near ultraviolet spectral regions on electron collisionally-excited transitions in singly and multiply ionized atoms is well known [54], even though the exact mechanism for population is sometimes debated in particular cases. A favorite lasing transition involves two $n = 3$ levels in light ions where excitation is most easily understood to be from the $n = 2$ ground state, with direct ionization into $n = 3$ excited states from the previous ion species considered a possibility. Electrically-excited ion lasers of the discharge variety operate in the cw mode, where excitation presumably takes place in a non-dipole transition followed by lasing on a dipole transition and rapid final state depletion in a second dipole transition.

The success of such ion lasers operated with resonant cavities, particularly the recently developed z-pinch plasma type [133], [134], has encouraged the consideration [105], [135] of extrapolation of such transitions into the vacuum ultraviolet region following isoelectronic sequences (i.e., ions with the same number of bound electrons). For example, a successful lasing transition in a six-electron carbon-like N^+ ion might also be expected to prove successful at shorter wavelengths with six-electron ions of higher-Z materials. A major obstacle in such an extrapolation arises due to the lack of efficient cavities in the vacuum ultraviolet region, so that increases in

the required gain coefficient by factors of approximately 100 or more are required. Nevertheless, a simple three-level model was formulated for carbon-like ions which supposed electron-collisional excitation of a 2p valence electron into a 3p level followed by lasing from 3p to 3s and finally rapid depletion of the lower laser level 3s to the initial 2p level, in a quasi-cw scheme [105]. (The terminology quasi-cw is used to indicate that stationary inversion is expected, but most probably is limited to the interval during which proper excitation conditions can be met in a particular plasma, as indeed was found for example in the z-pinch visible ion laser.) The basic model is illustrated in the energy level diagram shown in Fig. 13. A gain coefficient of either 1 or 5 cm^{-1} for short, noncavity, ASE operation can be expected with sufficient 2p to 3p collisional excitation at high density and/or high temperatures. A high density limit is approached, however, as the electron collisional depopulation rate from the upper 3p laser level to the 3d and 3s levels becomes comparable to the spontaneous decay rate for the laser transition, and this produces values for the upper density limit indicated for various atoms as shown in Fig. 14. A later more complete numerical analysis [136] indicated that electron densities could exceed this limit by as much as a factor-of-ten before population inversion was destroyed by collisional equilibrium; however the losses increase with increasing density above those values shown in Fig. 14. It is to be noted in Fig. 14 that electron temperatures ten times higher than the equilibrium temperatures assumed for the ions are used. This was required in order to attain sufficient gain to reduce the gain length to a length of $\sim 1 \text{ cm}$ which is considered reasonable for short wavelength lasers such as pumped in laser-produced plasmas. Such high electron temperatures only exist [137] for short times, hence the "quasi" nature of this amplification.

Numerical modeling [136], [138] on the O^{2+} ion has yielded gain coefficients consistent with operation of lasers with this species in the near ultraviolet region in cavities, and has also shown that the required temperature differential can be maintained for reasonable times at the low associated densities. However, such modeling only assumes that a certain amount of energy is deposited in the plasmas in a very short time to heat the electrons and that relaxation proceeds from that initial condition. In a practical experiment, the enhanced electron heating in a plasma will probably have to be obtained by a direct electrical process rather than by laser energy deposition [139], since the absorption length for the laser radiation in plasmas at such low density is unreasonably long. For example, proper operation of a 1 m long traveling-wave discharge which has been shown to produce C^{3+} ions [140]⁷ would seem to be a possibility at gain coefficients $\geq 0.01 \text{ cm}^{-1}$. Gain lengths $\approx 100 \text{ cm}$ are possible without enhanced electron heating as shown in Fig. 15.

As noticed from Figs. 14 and 15, $3p \rightarrow 3s$ transitions are limited as far as reaching short wavelengths. Transitions involving $n = 4$ states are even less desirable, both because of the more rapid collisional coupling between $n = 4$ levels and the associated lower density limits and longer lasing wavelengths. For shorter wavelengths it is more interesting to consider lasing on $n = 3$ to $n = 2$ transitions where, for example, again quasi-cw inversion can be expected in helium-like two-electron ions with electron collisional pumping from the 1^1S ground state to the 3^1S state, followed by lasing between 3^1S and 2^1P and rapid lower state depletion from 2^1P to 1^1S . The situation is not dissimilar to the $3p \rightarrow 3s$ scheme in that collisional coupling between $n=3$ levels enter at some density.

⁷The mechanism for 2p-2s population inversion in C^{3+} is not well understood; perhaps a dynamic mechanism as suggested by Norton and Wooding [141] for similar ions is applicable.

However, final collisional destruction of the population inversion between the $n=3$ and $n=2$ levels occurs at a much higher density, so that high gains can be expected at shorter wavelengths. An initial analysis by Palumbo [136] again indicates that electron temperatures exceeding ion temperatures are required to accomplish the necessary pumping over the large $1s \rightarrow 3s$ energy gap in helium-like ions. In this case it is reasonable to consider as a lasing layer the critical absorption layer in a plasma produced by a $\lambda = 1 \mu\text{m}$ laser at an electron density of 10^{21} cm^{-3} . Assuming a density of this magnitude, electron kinetic temperature, kT_e , varying from 1 to 5 keV, and an ion kinetic temperature of $kT_i = kT_e/2$ (prior to complete equipartition of energy), gain coefficients have been calculated for helium-like ions of various elements and are plotted versus Z in Fig. 16 [136]. The computations show a peak gain coefficient of less than 7 cm^{-1} and an optimum atomic number Z in the range 11 to 15 for these temperatures and densities. The ion temperature, T_i , affects the calculated results only through Doppler broadening of the lasing line; and a higher T_e/T_i ratio results in increased α according to $T_i^{-1/2}$. Higher electron temperatures have little effect on α , because kT_e becomes comparable to the pump energy and exponential factors are less effective. Electron temperatures $>1 \text{ keV}$ at present are mainly produced in condensed spark plasmas [109], [110] of dimensions on the order of 0.01 cm or less, resulting in low values of the product αL . Such high electron temperatures in laser-produced plasmas will probably depend upon compression in pellet experiments.

Prior to direct amplification experiments, it may be possible to measure population inversions at low net gain, as outlined in Section II.B. This is true for either the $3p \rightarrow 3s$ or the $3s \rightarrow 2p$ schemes described above. For example, in the latter case a relative intensity measurement of the $3^1S \rightarrow 2^1P$ and the $2^1P \rightarrow 1^1S$ lines would yield the relative upper and lower laser state populations using known oscillator strengths. The wavelength difference (approximately a factor-of-10) could be spanned with corresponding $3^1P \rightarrow 2^1S$ and $3^1P \rightarrow 1^1S$

lines in a branching ratio approach, since both originate on the same level. Typical population deviations from "normal" may be only a factor-of-two [136], so that available overall experimental precision must be carefully assessed.

Another experiment also involving the pumping of helium-like O^{6+} ions in a laser-produced plasmas has been proposed [142], where electron-collisional pumping from the 1^1S ground state to the 3^1P state would be followed by lasing from $3^1P \rightarrow 2^1S$. This would be a self-terminating (pre-equilibrium) scheme and also requires that electron collisional population of the lower laser 2^1S level from the ground state occur at a lower rate than the upper 3^1P level population. Indeed, at very high electron energies it is expected that the $1^1S \rightarrow 3^1P$ electron collisional excitation rate exceed the non-dipole $1^1S \rightarrow 2^1S$ rate. In this experiment it is proposed that a transient non-thermal electron energy distribution be obtained, featuring a very strong high energy component to provide the preferential 3^1P excitation at a sufficiently large $1^1S \rightarrow 3^1P$ excitation rate, in a situation somewhat similar to that above where high electron temperatures were discussed. An experiment to test this scheme using a plasma produced by a focused high power laser beam is underway.

B. Electron Attachment

1) Collisional Recombination: Population of upper laser states in ions by the capture of free electrons appears to be an efficient pumping process compared to direct excitation, although sufficient energy to produce and maintain the necessary density of free electrons in a plasma must still be attained. Free-electron capture with the release of radiant energy (radiative recombination) proceeds preferentially into tightly-bound states which is not desirable for achieving a population inversion. At high densities, however, three-body

(collisional) recombination can become significant, wherein the excess capture-energy is carried away by an additional electron. In contrast to radiative recombination, collisional recombination strongly favors capture into states with lower binding energy, i.e., potential upper laser states. Such capture is followed by cascading, for which radiative rates are highest for the low lying states; this supports population inversion.

There are a number of published suggestions for short wavelength lasers based upon this idea [133], [143]-[154], starting with the 1965 paper by Gudzenko and Shelepin [143]. Most are for hydrogen or hydrogenic ions with $3 \rightarrow 2$ lasing transitions, although some have suggested inversion with the ground state, i.e., $2 \rightarrow 1$ Lyman- α lasing. There have been both semi-quantitative, analytical and, more recently, numerical treatments of the concept, some predicting very high gain coefficients for optimum conditions.

A rather basic requirement of such collisional recombination schemes is a high pumping rate, achievable at high densities, prior to reaching a non-inverted state of equilibrium. This has led to an increasing recognition of the demand for extremely rapid cooling following the creation of the stripped ions. In fact, most of the high gains predicted numerically assume a very low temperature compared to that necessary to create the ions in an equilibrium plasma. Free expansion of, for example, a laser-produced target plasma has been proposed, but this alone may not provide a sufficient rate of cooling, and a density decrease accompanies the expansion. In one proposed experiment [145] with lasing on the Lyman- α line of neutral hydrogen at 1216 \AA , cold electrons would be produced by multiphoton ionization followed by recombination

and lasing in times shorter than the collisional heating times for the electrons. This approach seems limited to neutral hydrogen, but is still interesting for the vacuum-uv region. Most proposals involve transient phenomena, although there is one proposal [149] for a stationary inversion between $n=3 \rightarrow n=2$ in an expanding arc-heated plasma. No gain factors are given for the relatively low densities involved here and radiation trapping, which adds to the population rate for the lower state in particular, is neglected.

A fundamental difficulty in any modeling of the recombination laser is the lack of reliable collisional rate coefficient data. Collisions are of vital importance in the pumping process, in the redistribution of population between bound and free states, and in the electron cooling/heating processes. While most excitation (and de-excitation) rates are known or can be calculated, collisional ionization rates, particularly from excited states, are relatively difficult to obtain theoretically and experimental data are non-existent. Since the critical three-body collisional-recombination pumping process is the inverse of collisional ionization from excited states, it is usually deduced by detailed balancing arguments, which adds further importance to the collisional ionization rate. Therefore, at this point it seems appropriate to emphasize the obtainment of such fundamental and critical data, perhaps either through theory or by electron beam experiments on excited atoms or ions resonantly-pumped with tuned lasers, for examples. Deduction of such vital rates from high density experiments does not seem possible due to the complicated dynamics associated with most of such plasmas generated at present.

In spite of the complexities and uncertainties associated with this scheme, some direct observations [98], [99], indicate a marginal degree of

population inversion existing in expanding laser produced plasmas, at densities too low for demonstrable gain. The uncertainties are admittedly large at present but the results are encouraging, since population inversion is indeed the prerequisite for eventual useful gain devices.

It may be recalled from Section I that this approach has some basic short wavelength limitations due to the eventual dominance of radiative recombination into lower states and to densities approaching the solid level. The actual limits again, vary with formulas chosen, but this certainly appears to be most promising as a vacuum-uv and perhaps soft x-ray laser scheme.

2) Dielectronic Capture: As the name implies, dielectronic capture is an interaction involving a double transition. It occurs when a free electron interacts with an ion and is first "captured" into an excited state with the associated excitation of a bound electron. Thus, a metastable complex is formed, and the associated excitation has been suggested as an x-ray laser pumping mechanism. Since the free electron can have a kinetic energy less than the threshold value for collisional excitation of the bound electron (by the amount of its final binding energy), the process is sometimes considered as a sub-threshold resonance in the overall scattering process. The captured electron may exist in quasi-discrete levels prior to stabilization. Following capture, stabilization can occur through several possible channels, one of which is autoionization (a radiationless "Auger" transition) which is the inverse process and effectively results in an elastic scattering resonance. Relaxation of both electrons into stable bound states can also occur in an overall rearrangement collision with radiative recombination. In addition,

a radiative-Auger stabilization mode is possible causing the release of both the captured electron and a photon of variable energy due to an overall rearrangement collision with bremsstrahlung type emission [155]. It is the recombination mode that would be most attractive for achieving population inversion, and this can only be expected to dominate over autoionization for high Z ($\gtrsim 40$) elements (see, e.g., [156]).

Nevertheless, assuming that all captured electrons produce candidate ions for amplification, a pumping rate coefficient $\langle\sigma v\rangle_{\text{diel}}$ can be estimated from the capture rate. This rate, which is easily obtained from detailed balancing arguments for free electron capture into a specific state, is [102], [157]

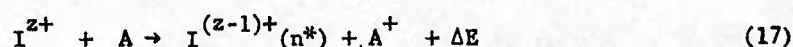
$$\langle\sigma v\rangle_{\text{diel}} = \frac{h^3 \Gamma}{2(2\pi m_e T_e)^{3/2}} \frac{g_f}{g_i} \exp [-\Delta E_{if}/kT_e]. \quad (16)$$

Here g_i and g_f are the statistical weights of the initial and final bound states, respectively, ΔE_{if} is the absolute energy difference between these states, and Γ ($\leq 10^{15} \text{ sec}^{-1}$) is the (inverse) autoionization rate. This can be summed over the few (≤ 10) bound states expected at the high densities involved in short-wavelength laser media. Numerically the rate is at best comparable to direct electron collisional excitation, which is not unexpected [158]. This conclusion is supported by the observation of somewhat weaker satellite lines to helium-like resonance lines observed in a number of laboratory plasmas and associated with dielectronic recombination [157].

It might be remarked that the large relative importance [157], [159] of this process to overall recombination rates in stellar atmospheres at low

densities, as well as the associated large population of high-lying states [160], comes about because of the multitude of very high discrete quantum states present and does not carry over to densities found in laboratory plasmas [160], [161]. Therefore dielectronic recombination appears at best to be a supplement to direct electron collisional excitation, under the conditions where the lasing ion is formed by recombination from a higher ionic species.

3) Atom-Ion Resonance Charge Transfer: As pointed out in Section II, a pumping process which has a large cross section for preferential population of specific excited states in ions is most desirable for achieving population inversion at short wavelengths. The resonance charge transfer collisional interaction



between a neutral atom, A , and an ion, I^{z+} , of net charge, z , with a cross section of approximately $10^{-16} z^2 \text{ cm}^2$, is a very promising candidate [100], since this cross section is several orders-of-magnitude higher than other excited-state population cross sections. The energy defect here is designated ΔE and the final ion excited state quantum number is shown as n^* .

Resonance charge transfer occurs spontaneously only in an exothermic reaction, where classical level crossings are expected at some distance of separation, R_x , according to the simple classical Landau-Zener theory [162]. In this theory, cross section peaks occur for a relative particle velocity V_{rel} and increase with an increasing exothermic energy defect, ΔE_{exo} , as shown

in Fig. 17. (Stimulated resonance charge transfer with an endothermic reaction has also been recently considered, where the stimulation energy would be supplied by a focused laser beam [104], [163].) Thus, this process is level-selective by its near-resonance nature. The resonance is associated with a near-coincidence between the binding energies of the initial atom's electronic state and the final ion's electronic state into which this electron is transferred. For initial ions of light elements, the coincidence may occur for low-lying (e.g., $n=3$ or 4) states (Fig. 18) resulting in direct pumping of a population inversion with a lower ($n \geq 2$) state [164]. For heavier ions, possibly leading to shorter wavelength lasing, near-coincidence occurs with higher-lying final-ion states, and population inversion through cascading is expected; this is similar to the collisional recombination schemes (Section III.B) except for the much higher cross section ($\sim 10^4$ times) with this process. This latter approach was originally proposed by Vinogradov and Sobel'man [100] for an expanding $z=10$ plasma ion source experiment.

Assuming that ions expand with thermal velocities determined from $kT = \chi^{(z-1)+}/4$ where $\chi^{(z-1)+}$ is the ionization potential of the preceding ion state, direct upper laser level population in light elements (Fig. 18) should be possible according to the theoretical curves shown in Fig. 17, including the mean velocity estimates indicated for stripped and hydrogenic initial-ionic species [164]. An inversion of these data for various charge states is plotted in Fig. 19 which yields the optimum energy defects, ΔE_{exo} . For background atoms or hydrogen, helium and neon, the principle quantum numbers, n^* , of the final excited states which are expected to be preferentially

populated are indicated.

The classical theory behind these estimates is rather inexact but illuminating. As recently emphasized by Presnykov and Ulan'tzev [165], improved theory is available giving a typical peak cross section of $\sigma_{\text{rct}} \approx \pi a_0^2 z^2 (I_H/I_A)$, where I_H and I_A are the ionization potentials of hydrogen and the atomic gas, respectively. These calculated cross sections are in agreement with measurements obtained from crossed beam experiments for low degrees of ionization. They point out that both double-electron transfer, when two equivalent outer-shell electrons exist (e.g., helium atoms) and also inner-shell electron transfer are possible, at reduced cross sections. In addition, they suggest that ion-ion resonance charge transfer might be possible when a large difference in net charge exists between the interacting particles, although no quantitative results are derived.

Experiments with laser-produced plasmas expanding into neutral atom gaseous atmospheres are underway at the U. S. Naval Research Laboratory, with space-resolved grazing incidence spectroscopy of resonance lines used in an initial search for anomalous populations in C^{5+} and C^{6+} ion excited states [106], [166]. Absorption of the laser radiation by the neutral atmosphere is minimized by the lower density possible with the large cross section, by confined regions, and by the high photon energy of the laser line relative to the neutral atom absorption edge energy.

Presnykov and Shevel'ko [167] have pointed out the advantage for Lyman- α inversion of the large proton-caesium resonance charge transfer cross section at low energies. (The general difficulty with inverting a ground state is again to be recognized [100].) Two experiments have recently been proposed

for investigating this scheme [120], [168], using a rapidly advancing plasma from a plasma gun or a duoplasmatron injected into a neutral cesium atmosphere. Cavity operation at Lyman- α at a reduced gain coefficient has been suggested [120], [167], and extension to helium (584 Å amplification) without a cavity is proposed for both experiments. Also, electron storing in 2^1S states of helium has been considered [120], [121].

A second maximum in the cross section distribution is expected to occur at high (10's of keV) particle energies [162], and one proposal is to use a high energy ion source in a traveling-wave mode to invert ionized helium. No experiments are planned unless ion beam sources of greatly increased current become available (see Section IV).

C. Photoabsorption

1) Innershell Photoionization: The terminology "innershell transitions" is meant here to designate those transitions that occur as the result of a vacancy being created in a closed shell (all n-orbitals filled) of an atom or ion for which at least one electron exists in a shell of larger principle quantum number. The vacancy can be created by, for example, collisions of electrons, ions or photons. Subsequent stabilization can occur by numerous channels including radiative, Auger, and radiative-Augur double electron transitions. Shake-off and shake-up transitions are also well known to occur during the vacancy-production phase. Activity in this area has been well summarized in the four volume proceedings of the 1972 International Conference on Inner Shell Ionization Phenomena [169], which includes some papers on x-ray lasers as future applications.

Innershell transitions for lasing are inherently more complicated than the so-called "optical" transitions of valence electrons simply because of the multitude of possible decay channels, particularly the radiationless Auger channel which cannot contribute directly to lasing but does consume pumping energy. In addition, the pumping source energy must be concentrated in a restricted energy band in order to preferentially remove the innershell electrons when outershell electrons exist. The initial attractiveness of innershell transitions is somewhat traditional for x-ray generation and does appear to offer short wavelengths in a low temperature medium, if indeed Doppler broadening were to be the dominant mechanism. However, as shown in Section I, natural broadening with Auger decay included is comparable to Doppler broadening even at the elevated temperatures where one and two-electron ions are created with optical transitions in the traditionally K region. Thus, there would not appear to be any clear advantage to innershell transitions for short wavelength self-terminating lasers, although there have been a number of published suggestions with different pumping schemes. Innershell pumping by collisions of plasma electrons has been proposed only once in a brief note [170] without apparent regard to the effect on outer electrons of the broad energy distribution of free electrons. Selective innershell pumping by collisions of ion beams with atoms (forming quasimolecules) has been suggested [112], [171]; however, the beam current required is formidable (Section II), particularly when all possible states and decay channels are considered. Greater consideration seems to have been given to photoionization pumping schemes [96], [113], [172-176] both because of the ability to concentrate the pump energy

and the likelihood of being able to tune the pump source to a spectral region of preferential innershell photoionization.

In the simplest self-terminating schemes an innershell hole is created by photon impact and lasing occurs on a radiative transition. Population inversion terminates in a time approximately equal to the lifetime of the vacancy state (see Section II). Both $K\alpha$ transitions with many outer electrons and transitions to first full-shell vacancies in alkalis (e.g., L-shell, sodium) have been studied. In the latter only one outershell electron exists and Auger effects are not present; however the wavelengths are typically 30 times longer than for $K\alpha$ transitions. A variation on the photoionized-sodium scheme which has recently been proposed by McGuire [177] involves the production of K-shell vacancies in Na^+ ions followed by K-LL vacancy Auger transitions producing Na^{3+} ions with electrons in various ($n=2$) L-subshells. Lasing is predicted in the 400 Å region on $2p \rightarrow 2s$ transitions instead of $3s \rightarrow 2p$ in the neutral sodium pumped scheme. Pumping by x-rays from laser-produced plasmas has been proposed [178]. In this proposal the laser plasmas are arranged to produce a traveling wave pumping configuration on the material to be pumped. Both sodium schemes require that photoionization losses in the medium be overcome. The principle difference is whether an $n=2$ vacancy is produced directly by L-electron photoionization or indirectly by K-electron photoionization followed by an Auger decay. The selective pumping spectrum required will fall into obviously different energy ranges. This could be a deciding factor in designing an experiment, and it is pointed out [177] that it is easier to produce a filtered hard x-ray spectrum for K-shell pumping.

It is interesting that one of the major objections to photon-pumped $K\alpha$ lasers, namely the Auger decay channels that consume pumping energy, could conceivably be utilized to alleviate a more formidable problem common to most short wavelength lasers, i.e., the extremely fast pump pulse risetime (see Section II). It was first suggested by Stankevich [173] in 1970 that L-shell vacancies created by $K\alpha$ transitions could be filled by Auger transitions at a higher rate than that at which they are created, so that a population inversion could be sustained for as long as the particular species exists. Hence, a quasi-cw laser is conceivable along with resonance cavity operation. Stankevich's analysis was based upon some very rough approximations for the relevant rates. When re-analyzed [96] in 1974 with new calculations published in the interim, the net gain coefficient on his simple model remained positive but became small. However, Stankevich also ignored the fact that the further-stripped ions created by Auger transitions possess shifted $K\alpha$ absorption lines and, therefore, decreased laser beam reabsorption. The requirement for sustained inversion then becomes one of exceeding only the K-L radiative rate, which is considerably less than the K-LL Auger rate for light elements [179]. When the analysis [96] is extended to this situation, the ratio of rates and hence the approximate ratio of population densities becomes significant for elements in the range of $Z=20$ as shown in Fig. 20. Indeed, a gain coefficient of 70 is predicted in a $30\text{ }\mu\text{m}$ by $300\text{ }\mu\text{m}$ medium of silicon atoms at a wavelength of $7.1\text{ }\text{\AA}$ and with a currently realistic photon pumping source of 4 TW power. However, actually making and maintaining a medium having the rather idealized conditions assumed is another matter. For example,

a high density of a specific atomic or ionic species must be maintained against continuing ionization with delicately balanced recombination into the proper states. This approach should be pursued further with both numerical modeling and experiments, the first experimental efforts probably being directed towards developing suitable pump sources with sufficient power concentrated in the required spectral region. Such a source may be a laser-produced plasma, an exploded wire, or even a more simple heavy-element spark discharge.

2) Photoexcitation: Absorption of discrete emission such as from a discrete spectral line leading to excitation to a specific upper laser level is an intriguing possibility for selective pumping by photons. Generally two species are required⁸ with overlapping intense lines. Considerations so far [180], [181] have centered around the intense resonance lines of hydrogenic and helium-like ions which can become "opacity broadened" for the desired frequency overlap. A typical example is absorption of the C^{5+} Lyman- α line at 33.74 Å by a C^{4+} ion in a 1^1S-4^1P transition, with the 4^1P level becoming overpopulated relative to lower 3^1S and 2^1S levels and possible lasing in the 700 Å and 200 Å regions, respectively. Considerable thought must go into a practical experiment for efficient coupling of the pumping line emission to the absorber. In this respect the practical problems are not unlike those encountered in photoionization-pumping experiments. A coaxial design utilizing an expanding cylindrical plasma from a specially tailored laser-irradiated target may prove most efficient. Obviously, many combinations of ions and elements may be considered as long as overlapping intense lines are present.

⁸Single species pumping of isotope shifted lines has been proposed [182].

D. Ion-Atom Collisions

Another method of producing inner shell inversions for lasers is based on the promotion of electrons to higher levels during the collision of atoms or ions with other atoms. These promotions of the inner shell electrons occur when violent inelastic atomic collisions take place with deep interpenetration of electron shells. During the collision the inner-shell electrons are forced into energy levels in accord with molecular orbital theory. After the collision the atoms are left in narrow, discrete states with several electrons simultaneously highly excited [183].

McCorkle [112] and McCorkle and Joyce [171] have proposed that the above method of excitation might be suitable for the production of gain by stimulated emission in the x-ray region. They propose the bombardment of thin foils with an ion beam in such a manner that the excited atoms or ions emerge from the other side of the foil where amplification can take place. They propose to use long gain-lengths, in spite of the short excited-state lifetimes, by deflection of the ion beam in the manner described by Louisell et al. [104] to produce traveling-wave excitation.

Difficulties with this approach lie in the large ion currents required and in the extremely short time before Auger decay. Recent developments in ion beam technology [184] may assist in the first problem. Auger lifetimes of $\leq 10^{-14}$ sec severely limit the cross sectional width of excited plasma and force close tolerances on traveling-wave deflection and focusing. If the planarity of the wave varies by only 10^{-3} cm, then the traveling-wave will not be of uniformly-correct velocity for amplification. In addition, diffraction losses from such regions of gain may be extremely high. Coherence brightening and laser lethargy effects for this approach have also been considered [185].

E. Nuclear Transitions

The use of nuclear transitions to produce lasing in the x-ray and γ -ray spectral region was considered as early as 1961 in laser history [186]-[189]. The conclusions at that time were that the difficulties were so great that no practical experiments could be started. The recent success in the vacuum uv and the anticipated success in the x-ray region has inspired a new look at the more penetrating gamma-ray lasers. Much of the revived interest in gamma-ray lasers has originated in the Soviet Union and emerged at the 1973 Vavilov Conference on Nonlinear Optics. Soviet scientists R. V. Khokhlov [190], V. S. Letokhov [191]-[192], and V. I. Goldanskii [193] have contributed significant new ideas or proposals on the gamma-ray laser. In England Byrne, Peters and Allen [194] have considered the gamma-ray laser and in the U.S.A., Baldwin at Rensselaer Polytechnic Institute [195], [196], Wood and Chapline [197] at the Lawrence Livermore Laboratory and a group at the Naval Research Laboratory [198] have examined the problem. No one claims that development of the gamma-ray laser will be easy, but some aspects of the problem appear no more difficult than those for hard x-ray lasers. Some of the fundamental problems of gamma-ray lasers and some of the rather elaborate schemes for producing them will be discussed below.

From Eq. (6), the threshold inversion density, ΔN , for mirrorless systems varies as

$$\Delta N \geq \frac{8\pi\Delta\nu\tau}{\lambda^2 L \phi} \quad (18)$$

For practical systems, of course, the inversion density must be much higher, as Wood and Chapline point out, but this equation illustrates the basic problem of gamma-ray lasers. An attraction of gamma-ray lasers is the availability of long-lived excited nuclear states (measured in years versus femtoseconds). These metastable lifetimes would enable the population inversion to be assembled slowly using low power level pumping sources. Such long lifetimes, however, greatly increase the inversion density required for lasing. To use these long-lived transitions, the linewidth, $\Delta\nu$, must be reduced to the point where ΔN is below the density of solid material. This implies that $\Delta\nu$ cannot exceed τ^{-1} by more than a few orders-of-magnitude. Recoilless Mössbauer transitions are a starting point for narrow linewidth. These transitions may be narrowed even further by growing more perfect crystals, by placing the crystals in a uniform temperature, uniform field environment, or by using special radio-frequency field techniques to narrow the resonance lines [199].

It should be clear that resonators would not be practical for a gamma-ray laser. No material is known to be reflective at these wavelengths and the high energy flux expected from the laser would destroy most materials placed in the beam. Therefore, gamma-ray lasers will be ASE devices of length as great as practical and with diameter $d \ll L$ to avoid radial amplification losses, but large enough to avoid diffraction losses. Absorption losses must be taken into account within the laser material. These losses may vary considerably depending upon the orientation of the crystal axes with respect to the direction of laser propagation. The gain coefficient per unit length, α , must exceed the absorption coefficient per unit length, μ , in order to have a useful laser.

In addition, the gain equation must be multiplied by the fraction, f , of excited nuclei that undergo recoilless transitions, by the branching ratio, β , for the isomeric transition, and by $(1 + \alpha)^{-1}$ where α is the internal conversion coefficient (in this process excitation energy is lost to the nucleus in a radiationless manner). The gain coefficient condition becomes

$$\alpha = \Delta N \frac{\lambda^2}{2\pi} \frac{f}{\tau \Delta \nu_T} \frac{\beta}{1 + \alpha} > \mu, \quad (19)$$

where $\Delta \nu_T$ is now the full linewidth. Khokhlov [190] estimates that the absorption coefficient, μ , is no greater than 1 cm^{-1} and that it is possible to obtain gain coefficients of

$$\alpha = (10^3 - 10^4) / \tau \Delta \nu_T \text{ cm}^{-1}. \quad (20)$$

Transitions in which the $\tau \Delta \nu_T$ product is near unity have been observed for short lifetime transitions ($10^{-7} - 10^{-9}$ sec), but when longer-lived transitions are considered there are little data available. One measurement of Ag^{107} , which has a 44 sec lifetime, showed a $\tau \Delta \nu_T$ of 10^6 .

Obviously more work is needed to investigate the linewidth of long-lived transitions. It may be that narrower bandwidth transitions exist for some long-lived isomers. If not, then techniques for reducing the linewidth must be developed if long-lived transitions are to be used for gamma-ray lasers.

The alternative to reducing the linewidth of long-lived transitions is to accept the breadth of short-lived transitions and to try to overcome

this factor by increased pumping intensity. In doing this one finds that inversion densities greater than that of solids are required and that the pumping power required to achieve the required inversion densities (10^{24} cm^{-3}) is overwhelmingly high. To reach such inversion densities, it has been proposed that laser compression techniques similar to those proposed for pellet fusion might be used. One concept consists of a cylindrical thread of beryllium as the gamma-ray laser host material. Added to the beryllium thread is a small amount of parent isotopic material [193]. The Mossbauer effect will be preserved in the impurity material. Surrounding the beryllium host with its impurity is a concentric cylinder of fissile material which will be driven to criticality by a series of laser beams aimed at the cylinder from all sides and timed to produce a wave of excitation moving at the velocity of light down the length of the cylinder. The laser beam compresses the fissile material causing a miniaturized explosion and the release of many pumping neutrons. These neutrons pass through the beryllium exciting the impurity nuclei quite rapidly and providing a gain medium for those gamma-ray photons that are emitted in the axial direction of the cylinder [195].

If pumping a gamma-ray laser is difficult when lifetimes are short, and if linewidths are too great when isomer lifetimes are long, perhaps a compromise is to use intermediate lifetimes and assemble the laser as fast as possible. One idea [192] proposes that pumped nuclear material be quickly vaporized with a laser beam and that the excited nuclei be separated isotopically, ionized and electrostatically deposited on a host substrate. The rapidly assembled laser would emit as soon as sufficient excited nuclei reached the

substrate. This approach is quite complicated, and considerable research would be required to attempt it. It would be necessary to study the isotope separation process in detail as well as the excitation-vaporization process, but it appears that this technique might work where others do not.

The question of coherent emission of Fermions (neutrons, protons, alpha particles) has come up in some discussions [200]. Byrne, Peters and Allen [194] have given further consideration to alpha particle emission. Their conclusions are that alpha particle capture and emission processes are incoherent with no phase relationship. An alpha particle with MeV energy has a wavelength of $\sim 10^{-12}$ cm. The frequency spread associated with the Doppler motion is $\sim 10^{16}$ Hz at room temperature for a heavy element ($A \sim 240$). The resulting cross section for stimulated emission is $10^{-35} \text{ to } 10^{-57} \text{ cm}^2$ for lifetimes in the range of 10^{-6} to 10^{16} sec. Absorption cross sections are many orders of magnitude larger and seem to preclude the possibility of stimulated alpha particles.

On the other hand, L. A. Rivlin, the Soviet scientist who filed an early patent disclosure on the gamma-ray laser, has proposed that antimatter might serve as an amplifying medium [201]. In discussing some aspects of the problem he chose to consider positrons. Positrons, of course, are quickly annihilated by the close presence of an electron with the resulting emission of two photons. The minimum energy for the created photon is 0.51 MeV which results in a wavelength of 0.024 \AA . Rivlin's idea is to inject a pulse of positrons into an electron-rich target and observe the emission upon annihilation of the positrons. He calculates that he needs a positron density of 10^{18} cm^{-3} .

in a time of 10^{-10} sec. While this may be feasible technologically, it appears that the question of coherence will arise, since it would not appear that any one annihilation should influence any other. In other words it appears to be an incoherent process which would not amplify in spite of the negative temperature (or inverted population) which may be produced.

F. Stimulated Compton Scattering

The idea of using stimulated Compton scattering to produce short wavelength lasers has been considered by numerous authors [202]-[205]. The attraction of such a laser is that photons injected into a relativistic electron beam can be scattered back at much higher energies. Hence it may be possible to build a laser based on stimulated Compton scattering and reach well into the x-ray region. In addition, the output wavelength would be tunable over wide frequency ranges by varying the acceleration voltage of the electron beam.

Pantell, et al. [204] have outlined the problem of stimulated Compton scattering. For a colinear geometry with the electron beam and photon beam of frequency, ν_1 , pointed toward one another, the frequency of the back-scattered wave, ν_2 , is given by

$$\nu_2 = 4\nu_1 (E/E_0)^2 \quad (21)$$

where E is the electron energy and E_0 is the electron rest mass (0.5 MeV). For 5 MeV electrons the emitted frequency is 400 times the input signal frequency. Therefore, 1000 Å input photons would emerge as 2.5 Å hard x-ray photons. Both linear and synchronous accelerators are capable of producing

electrons with more than 1 GeV of energy so that even shorter wavelengths can be reached.

Of course, there are important questions which must be answered such as the net power out of such a laser, given state-of-the-art input intensities of electron beams and lasers. Panteli has determined that the net power scattered into a single mode, for an electron velocity v , is

$$P = \frac{c^2 r_0^2 (1 + v/c)}{4 h \nu_1^2 \nu_2^2} I_1 I_2 E h \nu_2 \frac{d^2 N_e}{dE^2}, \quad (22)$$

where r_0 is the classical electron radius (2.8×10^{-13} cm), I_1 and I_2 are the intensities of incident and stimulating radiation, E is the electron energy and N_e is the electron density. The gain coefficient in cm^{-1} can be determined using the expression

$$\alpha = 0.7 r_0^2 \frac{E h \nu_2}{(\Delta E)^2} \lambda_1 \lambda_2^2 N_\nu N_e, \quad (23)$$

where λ_2 is the wavelength of the emitted signal, N_ν is the photon density in the incident beam, and ΔE is the linewidth of the energy scatter of the electrons. Calculations by Molchanov [205] for a neodymium laser beam at 1.06 μm with a photon density N_ν of $1.8 \times 10^{22} \text{ cm}^{-3}$, an electron voltage of 2 MeV, a $E/\Delta E$ of 10^5 , and N_e of $2 \times 10^{13} \text{ cm}^{-3}$ (current density of 10^5 A/cm^2) indicate a gain of 2.2 cm^{-1} at a wavelength of about 220 Å. This is a relatively large gain and it is in the soft x-ray region. Shorter wavelengths could be generated by increasing the electron energy. If similar

$E/\Delta E$ and N_e could be produced at 20 MeV, wavelengths of 2.2 \AA would be produced but the gain would drop due to the λ^2 dependence. Hence the ability to go to short wavelengths by increasing the electron energy must be accompanied by the ability to produce greater electron or photon densities to generate significant gain.

G. Unresolved Experiments

a) Gain Experiments at Univ. of Paris, Orsay: A group at the University of Paris at Orsay led by Jaeglé have recently reported [206] a measured net gain of 17 percent and a gain coefficient of 10 cm^{-1} in the dense portion of an expanding laser-produced aluminum plasma. The spectral line on which this gain was observed arises from a $2p^5 4d^3 P_1 \rightarrow 2p^6 1S_0$ intercombination transition in the Al^{3+} neon-like ion. Two identical plasmas are created by splitting a single laser beam and the transmission of the second plasma to radiation (in a region assumed to be uniform) from the first is used to ascertain absorption and the reported gain. This last paper follows approximately four years of effort with progress documented in the references listed in [206]. Other supporting evidences given are the narrowness of this particular line and a significantly shorter duration of the emission from time-resolved spectral measurements. Net gain on other lines in this particular ion or in other ions has not been reported. No explanation for how the population inversion is achieved is offered in this paper, although it was previously suggested that a series of autoionizing transitions may be responsible [207].

An attempt to reproduce this experiment has been made by Valero [208] in a similar experiment but with a somewhat more powerful ruby laser. Valero reports results in essential agreement with Jaeglé, et al., but concludes

from a comparison of relative intensities of Al^{3+} lines from various series members as well as lines from more highly stripped Al ions that the anomalies observed are due to high absorption of the "allowed" lines which have large absorption oscillator strengths, rather than net gain on the single line. Valero also disputes evidence [207] of autoionizing transitions and presents evidence of lines from different ions as an alternative explanation of some of the observed structure.

McGuire [177] has also challenged the Jaeglé, et al., results and suggests that the $4d^3P$ upper level may be overpopulated in the second plasma by Auger transitions, following innershell vacancies created by x-radiation from the first plasma (See Section IILC). Most recently, Silfvast, et al., [209] have criticized the conclusions of the Orsay group and the two plasma technique of gain measurement in general. They also explain the reported results with an opacity model.

b) Experiments at Texas Tech. University: In recent articles, Das Gupta at Texas Tech. University has presented a number of observations which could possibly imply an association with coherent x-ray emission [210], [211]. These experimental observations include a non-linear increase in intensity with excitation current, and a narrowing of x-ray lines from a micro-focus x-ray tube [210]. However, any interpretation of these results as an indication of lasing would appear to contradict the basic requirements for x-ray lasers as presently understood. More recent experiments using a Van de Graff accelerator with cylindrical bore targets yielded non-divergent discrete x-ray emission [211]. Das Gupta's model of parametric coupling between photons and electrons,

suggested as an explanation, has been scrutinized very carefully by two groups [212], [213], who conclude that Das Gupta's observations can be explained on the basis of instrumental effects. In repeated experiments [213], [214], the discrete frequencies reported by Das Gupta are not observed. It appears that there is little reason for x-ray laser enthusiasm in the results reported by Das Gupta unless a more substantial understanding and support of these results is offered.

c) CuSO₄ Experiment at University of Utah: The existence of coherent hard x-rays from a laser-heated gelatin doped with CuSO₄ was reported by Kepros, et al. at the University of Utah in 1972 [215]. The report generated a flurry of interest and activity. The main evidence on which the conclusion was drawn was the observation of clustered small ($\sim 100 \mu\text{m}$) spots on x-ray films placed at distances of 30 to 110 cm along the axis of the 10 mm by 0.1 mm portion of the gelatin that was irradiated. Ionization chamber (electrometer) results indicated a preferred axial emission of up to 10^5 photons per burst. These findings, which supported the film data, were reported in private conversations [216], [217] and added to the interest in the effect. No wavelengths were measured, but the association with x-ray emission was inferred by the apparent transmission through aluminum and paper shielding surrounding the film.

An attempt to reproduce the results at the U. S. Naval Research Laboratory, where a similar laser was available, indicated at first that indeed such spots with some degree of localization could be present in coincidence on multiple films on about 10 percent of the shots [218]. However, in continued experiments with the use of "active" x-ray detectors (capable of counting photons)

did not produce any x-rays, and thus disassociated the film anomalies with x-ray emission [219]. No other source of x-rays associated with the laser or the experiment was found. A more recent report [220] from the University of Sofia also describes the observation of 90-130 μm film spots with up to 90 percent reproducibility; however no attempt at auxiliary x-ray detection is reported. Other attempts [221] at corroborating the x-ray emission reported by the Utah group proved negative, including one so-far-unpublished study [222] by an independent team assembled by the University of Utah using the original apparatus. The original researchers have not extended their measurements and the electrometer results have never been published.

Following a visit to the University of Utah during which he exposed a number of multiple-film film packs to the "x-ray laser", Boster reported [223] the presence of a number of small features on the films and associated these with a triboelectric effect caused by improper handling of the films, i.e., independent of the laser/gelatin experiment. Boster's explanation is not entirely satisfactory, because the effects have not been duplicated at the U.S. Naval Research Laboratory or elsewhere [224] even when Boster's prescription for "mishandling" was followed exactly.

Developing a theoretical mechanism to explain population inversion in this experiment proved extremely difficult from the beginning and required complete absorption and concentration of the available laser energy (by some unknown mechanism) into a filament of about 1 μm diameter. (Indeed, the amount of absorption was found [219] to be $\sim 30\%$ and, furthermore, independent of the presence of CuSO_4 in the gelatin.) Kepros [225] recently attempted to explain his original results with a partially-

stripped model and higher peak powers. Billman and Mark [217] offered a non-lasing explanation for the presence of any collimated x-rays that may have been observed at the University of Utah. Their explanation is based upon a model of a transmitting and collimating channel created in the gelatin by the incident laser beam.

To summarize this experiment, it must be concluded that, whatever may have been the cause of the observed film effects, the absence of any further evidence of x-ray emission with the most sensitive detectors available precludes further credibility to the original claim of coherent hard x-ray emission. Credit should be given to the originality demonstrated in the approach which may someday prove interesting, particularly with more powerful lasers.

IV. PRODUCTION AND DETECTION OF GAIN

A. Pumping Sources

At present two sources are given serious consideration for pumping x-ray transitions: 1) laser beams, particularly the very short pulse-width, mode-locked picosecond beams; and 2) high energy electron beams and recently associated ion beams. All of these sources have their advantages and weaknesses. By mode-locking, Nd^{3+} laser beams can be made to have pulse widths of $\sim 10^{-12}$ sec and they can be focused to small volumes with high irradiance. However, the photon energy is too small to pump x-ray transitions directly, and they must be used either to transfer electrons from an excited metastable level, to heat electrons in a plasma with subsequent electron-collisional pumping, or to produce x-rays (again from a laser-heated plasma) which will in turn pump an x-ray laser transition. Short pulse lasers have low overall efficiency (not a primary problem for initial x-ray laser research), are power and energy limited, and are somewhat difficult to adapt to a traveling-wave pumping geometry (Section IV.A.2.b). Gain lengths tend to be restricted to about one centimeter and the ramifications of this are analyzed below. More efficient CO_2 lasers do exist having comparable energy, but the pulse widths are limited to $\sim 10^{-9}$ sec at present and the photon energy is lower by a factor-of-ten. High current electron (and ion) beams are also limited to pulse widths of about 10^{-9} sec; they have high efficiency, high energy and appear adaptable to a traveling-wave transverse pumping geometry. They produce large fluxes of high energy particles which can be converted to photons by colliding the particles with a target. A very severe additional limitation

for charged particle beams comes in focusing against space charge effects to produce a high flux in a very small volume.

1) Short Pulsed Lasers:

The process of mode-locking to produce extremely short optical pulses has been reviewed thoroughly by both DeMaria et al., [226] and Smith [227]. Pulses with a length of 10^{-12} sec can be generated at $1.06 \mu\text{m}$ using the broad bandwidth of Nd^{3+} in glass or YAG (yttrium aluminum garnet). When amplified, these narrow pulses can reach peak powers of more than 10^{12} W. Except when used for transfer pumping from an excited metastable level (Lebedev Institute, Moscow), the low photon energy of these pulses prevents direct pumping of x-ray transitions; however, several indirect methods are being actively pursued.

a) Electron Heating and Relaxation: This concept utilizes a high power laser pulse to generate a highly ionized plasma and either directly produces a population inversion by preferential excitation of an x-ray transition by a high energy electron component of the plasma (being done at the University of Rochester) or generate an inversion during the relaxation and expansion period following either electron-ion recombination (being done at Lawrence Livermore Laboratory, University of Rochester, Culham Laboratory, University of Hull) or ion-atom charge transfer (being done at U. S. Naval Research Laboratory).

b) Synchronized Double Pulse Excitation: If a highly ionized plasma can be prepared just in advance of the arrival of an intense picosecond laser pulse, then the picosecond pulse may be useful in quickly heating plasma electrons which in turn will excite the already existing ions to large population inversions prior to equilibration. Lasing would occur when sufficient ions become excited for the

ASE conditions to be met. The density must be sufficient for the laser beam to be absorbed, but not so high that collisional rates dominate.

c) Laser-Plasma X-Rays: An alternative method of pumping x-ray transitions is to use the high power laser pulse to vaporize and heat a target material to generate plasma x-rays. These x-rays fall onto a nearby material and optically pump energy levels to inverted populations. Silfvast and Wood [228] have demonstrated this technique at longer wavelengths by using the plasma generated by a CO_2 laser to pump a near-uv dye laser. There has been considerable work done to study the radiation emitted from laser plasmas in the x-ray region, and the conversion of laser radiation to x-radiation has good efficiency. With this background it may be possible to pick target materials that have sufficient emission in either the rather narrow photoionization or the discrete line photoexcitation absorption bands of the x-ray transition selected for lasing. Photoionization pumping is pursued at Battelle and Sandia Laboratories.

d) Laser Compression Techniques: Because the power densities required to produce x-ray lasers are similar to those required for laser fusion, there is a strong technology overlap between these programs. Therefore, there is activity in x-ray lasers at such laser-fusion laboratories as Lawrence Livermore Laboratory, the U. S. Naval Research Laboratory, the University of Rochester, and Battelle. For example, Chapline and Wood [123] at Lawrence Livermore Laboratories have proposed to conduct x-ray laser experiments which make use of the compressive force of numerous laser beams aimed to uniformly irradiate a cylinder and to attain inversion densities greater than the density of solids. This traveling-wave compression concept is an extremely complex one. Not only must the irradiation be radially uniform for high compression, but there is the added

difficulty that the amplified x-ray pulse velocity will be gain dependent. This added dependency will require uniform inversion density in the axial direction in order to maintain the velocity matching of the x-ray pulse and the excitational compression wave. In short, this method may encounter severe practical difficulties in addition to those common to laser fusion compression.

2) Electric Discharge Lasers:

a) Advantages: Electric discharge lasers are conceptually simple and have the advantage that electrically-stored pumping energy is transferred directly and efficiently to gases at relatively low pressures in short path lengths, due to the short mean free path Λ_{ci} for collisional ionization processes of cross section σ_{ci} , i.e., $\Lambda_{ci} = (\sigma_{ci} N_0)^{-1} \sim 10^{13}/N_0$ for N_0 in cm^{-3} . Low densities are an advantage for lasers pumped by electron collisions (Section III), but longer lengths are required for gain coefficients exceeding threshold [105]. When the required lasant length exceeds $c\tau_p$ where τ_p is the laser pump time, the pumping of the lasant must be axially synchronized with the growth of the beam; hence the need for traveling-wave pumping. Such pumping is most appropriate for transverse electrical discharge devices and has been successfully applied to molecular (see Section I) as well as ionic (C^{3+} [140]) lasants. Hence its present use at the U. S. Naval Research Laboratory for the investigation of electron-collisionally excited ionic lasers.

b) Traveling-Wave Pumping: The short lifetimes of x-ray transitions usually places a restriction on the amount of amplification that can be produced by a given population inversion density. For example in a material in which gain lasts only 10^{-15} sec a pulse can only be amplified for a distance of

3×10^{-5} cm. Also, the inversion density required to reach threshold approaches the density of a solid. Producing such densities is very difficult; they might occur only in compressed laser plasmas. These inversion density problems can be eased considerably if the region of gain can be made to travel in synchronism with the pulse to be amplified. This scheme is called traveling-wave pumping and it contains several advantages. First, the entire volume does not have to be pumped at one instant; the pumping energy delivered to the material can be spread over time and space. Secondly, a unidirectional output beam is acquired with no mirrors, so that the intensity within the laser material is not higher than the output emission. Thirdly, this method of excitation is suitable for the production of long gain paths, so that the critical length for ASE can be met, at least in principle, for low inversion densities. Traveling-wave discharge techniques have already been used successfully to produce high-power, unidirectional emission from nitrogen [4] and hydrogen [15], [10]-[12], [229] molecules. The traveling-wave was produced in a flat-plate transmission line by a series of synchronous fast-closing dielectric switches. This resulted in a fast-rising high voltage transverse traveling-wave discharge which excited the molecules. Since the closing interval of the dielectric switches can be varied, the velocity of the traveling-wave can be adjusted to match the velocity of the optical pulse.

The value of the traveling-wave approach for x-ray lasers has been appreciated, but it has somewhat wrecklessly been assumed that synchronous traveling-wave excitation could be produced with optical or electron beams by simply phasing several beams or by inclining the material at an appropriate angle to the beam. This approach must be taken with extreme caution. Casperson

and Yariv [230] have shown that the velocity of a pulse being amplified is a function of the gain and less than c . If the gain is uniform, then a simple inclination of the target can produce a traveling-wave excitation that stays in phase with the pulse being amplified. If the gain is not uniform, the problem becomes far more difficult and at least some of the gain will not be usable. Consider a pumping laser beam of circular cross section with a Gaussian radial intensity distribution, focused by a cylindrical lens to irradiate and excite a linear length of material. The focal line could have a hot spot in the center with a continuous fall off toward each end. Since the gain would vary in direct relation to the intensity distribution, the propagation velocity would vary greatly also and no one angle would produce amplification over the entire length. Even if the beam had radial uniformity of intensity, the focusing of the cylindrical lens may not produce uniform gain. The idea of phasing many laser beams on a cylinder [231] to compress a material to the necessary inversion density will be plagued by the non-uniform gain that these focused beams will produce. For gain at very short wavelengths the excitation wave and the pulse being amplified must not separate more than 3×10^{-5} cm. The focusing of many high power laser beams onto a cylinder to maintain uniformity on such small spatial dimensions is an extremely difficult practical problem.

In spite of the cautions pointed out above, it may indeed be possible to use traveling-wave pumping with laser excitation sources. To do so will require careful experimental design, where the parameters of the lasing medium must be known and uniform and where the intensity of the line focus of the laser

has also been designed to be uniform. These conditions are not trivial for lasers. It may even be easier to adapt electron beams or discharges to the traveling-wave configuration as described below.

3) Electron Beam Systems:

During the last ten years electron beam technology has made dramatic strides forward [232]. From machines which previously emitted beams of only a few amperes, progress now places current capabilities at megamperes and voltages as high as 12 MeV for pulses in the 100 ns range. The energy storage to produce these intense beams is in the megajoule region. It is difficult to ignore these new machines for the production of shorter wavelength lasers. Already electron beams with pulses as short as one nanosecond have been used to produce vacuum ultraviolet lasers in the rare gases at high pressures and also in hydrogen (See Sections I and III). Electron beams have also been used to initiate the reactions which have led to high power chemical lasers and to semiconductor lasers of small size. In addition, focused electron beams are being considered for use in the beam-pellet approach to fusion.

For short wavelength laser research, electron beams coupled into plasmas through boundaries such as thin foils offer the potential advantage of a shorter electron pump pulse risetime not limited by the collisional ionization time for discharge devices. To further implement this concept, a traveling wave electron beam adaptation of the discharge device described above was proposed [233] and a prototype of such a system is presently being tested on N_2 and H_2 at the U. S. Naval Research Laboratory. Once feasibility has been

established, it is expected to be scalable to higher energies and more rapid operation than at present.

4) High Current Ion Beams:

Recently new work in the generation of high current ion beams has been proposed and initial work carried out [184], [234]. Based on a rather simple modification to the relativistic electron beam machines already discussed above, the possibility of 10^5 A pulsed ion beams with energies of 0.5 - 10 MeV has been suggested by Sudan and Lovelace [184]. While the pulse width and focusing limitations remain, they discuss the usefulness of such beams for heating plasmas to fusion temperatures and in nuclear studies. It is also useful to speculate on the application of such beams to short wavelength lasers. Some charge exchange experiments discussed previously consider the use of ion beams to produce excited populations. The primary difficulty in these charge exchange lasers, i.e., a lack of intense ion sources, may be eliminated when these new pulsed high-current ion beams are developed. It may be possible to develop high-intensity traveling-wave ion beams for lasers by applying the same diode modifications used above to the traveling-wave electron beam mentioned above [233]. High current ion beams should find numerous uses in the development of short wavelength lasers (See Section III.B).

5) Exploding Wires:

High intensity x-ray emission can be produced when the diodes of electron beam machines are shorted by very fine short wires. The wire is vaporized early in the discharge and its atoms reach extreme stages of ionization (≤ 51 -times) over finite volumes, resulting in a copious flux of x-rays which

could be used for pumping x-ray lasers. Making the assumption that the average temperature of the exploding wire plasma is the same as a 100 eV blackbody, Jones and Ali [175], [176] calculate that it may be possible to pump Na vapor (Section III.C) using exploding wires. One remaining question in assessing the practicality of exploding wire pumping is the risetime of the x-ray radiation. If it is as short as 0.1 ns (one tenth the electron beam machine's risetime), then the Jones and Ali calculations show that the gain would be sufficient for ASE operation. If the risetime is longer, then a more complicated experiment with some form of resonant cavity may be needed. The practical problem of designing this experiment is not one to be taken lightly. It is difficult to get lasing material close to the high voltage wire, and equally as difficult to focus the x-rays at some distance. In another numerical analysis of this scheme, Bey considers what might happen if the pumping were accomplished in a traveling-wave fashion [174]. This model assumes that the risetime of the soft x-rays follows the risetime of the current and concludes that ASE would not occur unless the risetime were reduced to about 2.5 ns or that the intensity were increased by a factor-of-ten. Considering the difficulties of building an x-ray laser, these requirements for a 370 Å laser are not far beyond present capabilities.

B. Detection of Gain

1) Concepts:

The importance of this subject can be underscored by pointing to a number of experiments already claiming the existence of very short wavelength laser emission and the even more numerous alternative explanations of these experiments without the existence of gain. The confusion already demonstrated over

short wavelength lasers serves to demand that experimenters give irrefutable evidence of the existence of gain in the future. It is often necessary but not sufficient to infer lasing from small spots on film, narrowed lines, anomalously small absorption in a second medium, or non-linear intensity effects alone. A definitive test for gain must be performed. In the belief that early x-ray lasers will likely be ASE devices, a significant portion of this paper has been devoted to the theory of these systems. This can now be drawn upon to give some guidelines for determining the presence of gain.

In many experiments the detection of gain is complicated by the fact that its existence lasts for a very short period of time--as short as 10^{-15} sec! This short burst of radiation may come somewhere early in a plasma radiation process lasting nanoseconds or longer, and may not be resolvable with present techniques. In addition, many of the characteristics of lasers with resonant cavities will not exist for non-cavity ASE lasers. If gain exists however, it will amplify a signal exponentially as a function of its length unless it has saturated due to the intensity of the signal. Therefore, a good test for gain is to vary the length and observe the intensity of the line in question. If the strength of the signal is such that saturation is occurring, then the length should be reduced until an exponential dependence is observed. The gain coefficient is obtained in this manner, of course. This method for determining gain requires that the amplifying region be defined, of finite length, homogeneous, and controllable. In some experiments that have been proposed it may be difficult to determine where the amplifying region may be located, as well as the extent and uniformity, and it may be impossible to vary only the length of the gain region. If this is the case, then experimental verification

of laser action becomes very difficult.

The comparison of axial and transverse emission is a valid test for axial stimulated amplification, providing again that sufficient time resolution is available to discriminate against spontaneous emission of longer duration.

Other methods of verifying gain are difficult to use with ASE systems. Line width and beam divergence are sometimes considered good indicators of gain, but their behavior is somewhat complicated as shown in Section I.B . If length can be varied, then the intricacies of the line width can be used as support for claims of gain. For example, Jaeglé, et al. [206] claim that several soft x-ray lines are narrowed due to amplification in a two-laser-plasma experiment. While the calculations of Allen and Peters support the existence of a line width minimum just above threshold [85], additional data, both with more amplifying plasma and without a second plasma, would put this claim of line narrowing in better perspective.

D. Detectors

There are numerous techniques for detection of x-ray emission. Photographic film is available for both the vacuum ultraviolet and x-ray regions and is invaluable for recording images and large quantities of spectral data with limited (≈ 1 microsecond shuttered) time resolution. Electronic photodetectors such as photomultipliers, photodiodes, ionization chamber tubes, and semiconductor tubes are all responsive to x-radiation either directly or through the use of fluorescent scintillators, but the time response of these detectors is limited to no better than a few tenths of a nanosecond. In addition, no oscilloscopes are available with risetime much faster than a few tenths of a

nanosecond, so that conventional methods of observation are not available if very short x-ray laser pulses are produced. While some sampling techniques exist [235], a more useful device, a picosecond x-ray streak camera, has recently been developed [236]. The operation of this streak camera is sufficiently important for further discussion.

In general, the x-ray streak camera utilizes the image converter tube in which photons incident on a photocathode liberate electrons which in turn are focused onto a phosphor to reproduce the image falling on the photocathode. While the electrons are in transit, they can be deflected to move the image across the output phosphor producing a streaked image. This image can be increased in brightness by using stages of image intensifier tubes behind the streak tube until sufficient brightness for photographic recording exists. Actually these techniques have been used for some time to make picosecond cameras for infrared laser pulse measurement. The important development which allowed x-ray operation was the construction of a stable x-ray-sensitive photocathode. In one design, the cathode is made by depositing 100 Å of gold on the back of an 8 μm thick beryllium vacuum window [236]. X-ray photons in the 1 - 10 keV (12 - 1.2 Å) range are able to penetrate the beryllium foil and liberate electrons. The maximum time resolution, limited by the transit time dispersion, is presently about 50 psec. Other cameras, designed to be operated entirely in a vacuum environment, use only a gold cathode without a window and are usually attached directly to a vacuum spectrograph for vuv and soft x-ray detection purposes.

V. NON-LINEAR SHORT WAVELENGTH TECHNIQUES

While most of this paper deals with techniques for the direct production of vacuum-uv and x-ray emission, it would not be complete without the inclusion of the new and promising techniques for converting high power infrared and visible signals into the vacuum-uv and x-ray regions by using non-linear optical techniques. Some of the attractive features of pulses obtained by the non-linear techniques are that the pulses maintain the temporal and spatial characteristics of the original infrared pulses and that tunability is sometimes possible. An infrared pulse at $1.06 \mu\text{m}$ having a width of 30 psec and a good beam divergence can emerge after the non-linear stages as a 1773, 1182, or 887 \AA pulse still possessing good beam quality and still 30 psec wide. In addition to the discrete frequencies available from harmonic generation, other non-linear mixing techniques are also available which allow the mixing and summing of tunable laser frequencies to produce tunable output signals in the vacuum-uv. The possibility of extending these techniques to produce soft x-rays appears real and the fundamental concepts have already been explored.

A. Third Harmonic Generation

Under the influence of extremely intense optical fields the polarization of a material becomes a non-linear function of the electric field, i.e.,

$$P = \epsilon_0(\chi^{(1)}E + \chi^{(2)}E^2 + \chi^{(3)}E^3 + \dots) \quad (24)$$

where ϵ_0 is the permittivity of free space and $\chi^{(1)}$ is the linear and $\chi^{(2)}$,

$\chi^{(3)}$ are the non-linear components of the susceptibility. The polarization becomes a source term in the wave equation and the non-linear components give rise to harmonic frequencies. The amplitude of the harmonics depends upon the magnitude of the non-linear susceptibility terms. Second harmonic generation is possible in crystals which possess no inversion symmetry, but for the generation of short wavelengths, such crystals with useful vuv transmission are difficult to find. The transmission problem is even more severe in liquids. Gases possess the required transmission and have the added advantage of being self-repairable at damaging laser intensities, but the lack of asymmetry requires the generation of third (or higher odd) harmonic frequencies [237].

Harris and Miles [238] were the first to propose third harmonic generation in metal vapors. The third harmonic susceptibility term as given by Armstrong, et al., [239] is given as

$$\chi_{(3\omega, \omega, \omega, \omega)} = (e^4/h^3) \sum_{ijk} A_{ijk} Z_{gi} Z_{ij} Z_{jk} Z_{kg} \quad (\text{ESU}), \quad (25)$$

where the A_{ijk} are frequency-dependent coefficients with resonant denominators at $(\omega_{gp} - \omega)$, $(\omega_{gp} - 2\omega)$, and $(\omega_{gp} - 3\omega)$, where ω is the fundamental laser frequency, ω_{gp} corresponds to atomic transition frequencies to ground, and the Z terms are the dipole matrix elements. Harris and Miles recognized that by operating near the atomic resonances the susceptibility could be significantly increased. Calculations of third order susceptibility for the alkali metal vapors have been carried out by Miles and Harris [240] as a function of wavelength. A typical graph for Rb is shown in Fig. 21.

Miles and Harris also calculate the conversion efficiency, the ratio of third $P^{(3)}$ to first $P^{(1)}$ harmonic power, in terms of a factor I which accounts for focusing and dispersion, the alkali atom density, N , in atoms/cm³, the non-linear coefficient, $\chi^{(3)}$, in ESU, and the incident wavelength, λ , in cm. The conversion efficiency becomes

$$\frac{P^{(3)}}{P^{(1)}} = \frac{8.215 \times 10^{-2}}{\lambda^4} N^2 [\chi^{(3)}]^2 |I|^2 [P^{(1)}]^2. \quad (26)$$

Under the focusing conditions where the confocal beam parameter b , is much greater than the length L of the vapor cell, the I^2 term reduces to $(4L^2/b^2) \text{sinc}^2(\Delta k L/2)$ where the wave vector mismatch, $\Delta k = (6\pi/\lambda)(n_3 - n_1)$. In order to take advantage of the length of the cell, the index of refraction n_3 at 3ω must equal the index of refraction n_1 at ω . This is the condition of phase matching. Phase matching in gas vapors can be accomplished by adding an additional gas with opposite dispersion to the metal vapor. This technique is similar to the technique demonstrated by Bey, et al., [241] in liquids. The addition of xenon to the alkali atoms would enable phase matching to be achieved according to the calculations of Miles and Harris [238].

The experimental verification of the proposed third harmonic generation in Rb vapor was reported by Young, et al. [242]. This experiment was performed with 100 kW Q-switched pulses at 1.964 μm . At a Rb temperature of 262 °C and a Xe:Rb ratio of 412:1, phase matching was accomplished in the 19 cm long Rb cell, resulting in an improved power of 33-times the non-phase-matched case or an output power of 0.1 mW at 3547 Å. Having demonstrated the process of phase-matched third harmonic generation, the technique was refined and extended into the vacuum-uv [243]. Cd vapor was employed for its

negative dispersion and strong non-linear susceptibility at vuv wavelengths. The experimental apparatus is shown in Fig. 22. This experiment uses the increased power of a mode-locked laser and amplifier which produced 50 psec pulses with a total peak power of 20 MW. A KDP crystal is used to double the frequency to 5320 Å with an efficiency of up to 80%. For portions of the experiment requiring 3547 Å radiation, a second type II phase-matched KDP crystal was used to sum the 1.064 μ m with the 5320 Å radiation yielding 3547 Å radiation with an overall efficiency of about 10%. For tripling, the Cd vapor was contained in a heat-pipe to which argon was added in order to phase-match with the fundamental frequency.

Table III summarizes the three experiments which were performed. Energy conversion efficiency varies from 10^{-4} to 10^{-7} , but higher efficiencies may be expected from longer vapor cells and higher power densities, provided metal vapor absorption does not cause the process to saturate.

TABLE III
Summary of VUV Harmonic Generation Experiments Via Cd Vapor [243]

Input wavelengths (Å)	Generated wavelength (Å)	Coherence length at 10^{17} atom/cm ³ (cm)	Phase-matching ratio $N_{Cd}:N_{Ar}$	Energy conversion efficiency	$\chi^{(3)}$ (esu/atom)
5320	1773	-0.57	1 : 25	10^{-4}	2×10^{-34}
2X 3547 + 10640	1520	-0.23	1 : 15	10^{-6}	2×10^{-33}
3547	1182	...	1 : 2.5	10^{-7}	...

In more recent work, improved efficiencies were indeed accomplished by using a concentric double heat pipe to obtain higher vapor pressures, and longer cell

length and by using greater power density [244], [245]. By using a 30 psec pulse of about 300 MW focused into the 40 cm double vapor heat pipe to produce power densities of $10^9 - 10^{10} \text{ W/cm}^2$ in a Rb:Xe mixture, a conversion efficiency of 17% has been achieved in the conversion of $1.064 \mu\text{m}$ to 3547 \AA radiation. As yet there is no indication whether comparable improvements can be expected in the vacuum ultraviolet up-conversion. Some improvement in the generation of 1182 \AA radiation has been reported by Kung, et al. [246] by using the negative dispersion and decreased absorption found in Xe by operating slightly above the frequency of the strong 1192 \AA transition. By replacing the metal vapor cell of Fig. 22 with a Xe:Ar gas cell and by very tight focusing into the gas mixture to attain power densities of about $6.3 \times 10^{12} \text{ W/cm}^2$, an optimum conversion efficiency of about 2.8% is obtained for the conversion of 3547 \AA radiation to 1182 \AA radiation. Further improvement to as much as 20% efficiency is predicted at higher input power levels if the theoretical model does not break down. The shortest wavelength (887 \AA) was generated by these techniques by tripling the 2660 \AA radiation obtained from twice doubling $1.064 \mu\text{m}$ radiation. The 887 \AA radiation is obtained without phase matching in Ar gas and with an efficiency of only about 10^{-7} .

B. Tunable Coherent VUV Generation

Tunable vacuum-uv signals can be obtained by utilizing the general case of resonance enhancement of the non-linear susceptibility. Since only two photons are necessary to achieve resonance in Eq. 25, the third photon has no constraint on its frequency and can be tunable. This was exploited by Hodgson, et al. [247], who used two tunable dye lasers synchronously pumped by one N_2 laser as shown in Fig. 23. These two laser frequencies, ν_1 and ν_2 , were tuned

so that $2\nu_1$ coincided with a double-quantum allowed transition in Sr vapor. With ν_1 then fixed on the Sr resonance, ν_2 can be varied over a wide frequency range and the output of the Sr cell is the sum frequency, $2\nu_1 + \nu_2$. For the lasers used in this experiment the conversion efficiency from visible to vacuum-uv was on the order of 10^{-5} . Xenon was added to the strontium vapor to phase match. Studies of the autoionizing levels of strontium were also conducted [248].

A very similar idea was also proposed by Harris and Bloom [249] using a dye laser and a parametric oscillator. The experiment was carried out by Bloom, et al. [250] for the generation of near ultraviolet radiation and by Kung [251] for the generation of tunable picosecond vuv radiation. In the latter experiment, a 30 psec $1.064 \mu\text{m}$ pulse is doubled twice to produce the 2660 \AA fourth harmonic frequency. This radiation serves as an input to an ADP crystal with a controlled temperature which generates signal and idler frequencies. These signals are amplified further in a second ADP crystal and then tightly focused into a Xe cell. Using a combination of such third order processes as sum generation, difference generation or third harmonic generation, along with the different combinations of pump (2660 \AA), and tunable signal idler frequencies, tunable radiation over the region from 1180 \AA to 1946 \AA can be observed. Sum generation is particularly sensitive to the conditions of focusing. These conditions have been treated in detail by Bjorklund [252]. Fig. 24 shows all the ranges over which tunability has been obtained.

To summarize, there are several closely related experimental techniques which have the potential of producing tunable vuv emission from 2000 \AA to at least 1100 \AA and probably much lower. In both the experiment of Hodgson, et al. and Kung the conversion efficiency was low (10^{-7}) and the output power on

the order of 1 W. It is likely that improvement in these figures will result in the future.

C. Possible Shorter Wavelengths

Because the non-linear up-conversion process preserves the coherence of the original driving wavelength, there is an attractiveness to use the non-linear process in generating soft x-rays. Two processes have been considered: 1) using higher harmonics, and 2) amplifying and using third harmonic processes. Harris [253], [254] has proposed experimental processes using 5th, 7th and 15th harmonics to reach as low as 169 Å. Lithium ions are proposed for the non-linear generation in the soft x-ray region and tight focusing will be required. Table IV shows the proposed processes, the limiting power flux, and the theoretical efficiencies.

TABLE IV

Limiting power density and conversion efficiency
for some higher-order nonlinear processes [254]

Process	Species	$(P/A)_{\max}$ (W/cm ²)	Efficiency (%)
5320 Å ÷ 3 → 1773 Å	Xe	1.9×10^{12}	0.08
5320 Å ÷ 5 → 1064 Å	Xe	1.9×10^{12}	0.05
1182 Å ÷ 5 → 236 Å	Li ⁺	1.7×10^{15}	0.002
1182 Å ÷ 7 → 169 Å	Li ⁺	1.7×10^{15}	0.004
2660 Å ÷ 15 → 177 Å	Li ⁺	3.5×10^{15}	4×10^{-7}

The second approach proposes the use of those existing vuv lasers as amplifiers for the up-converted pulses so that other stages of non-linear generation can be used. For example, if a tunable picosecond pulse at 1161 Å could be amplified by the hydrogen laser, the tripling process could generate 387 Å radiation. The rare gas molecule lasers could also be used as amplifiers. Non-linear optical processes are likely to play a very important part in further short wavelength laser development.

D. Non-linear Techniques at X-Ray Frequencies

In anticipation of the development of x-ray lasers, Eisenberger and McCall [255], [256] worked out the theoretical details of the mixing of optical and x-ray photons and have observed x-ray parametric conversion using spontaneous x-ray photons. These techniques can be used to tune the frequency of x-ray lasers just as they are presently used for tuning in the visible. If sufficient x-ray laser intensity can be generated, efficient generation of tunable x-ray laser photons can be produced. It must be realized that the addition of optical photons and x-rays would not produce a very large change in the x-ray frequency. Other techniques which may be possible are the frequency down-conversion of two x-ray beams to produce visible radiation or the addition of two visible photons with one x-ray photon. Under ideal conditions it may even be possible to use these mixing techniques to assist in the detection of an x-ray laser pulse.

E. Non-Linear Optics with Inelastic Collision Resonances

In a recent paper [257], Harris and Lidow propose resonant energy coupling between atoms which is induced by photons and in which energy is conserved by optical photons instead of kinetic properties. In essence, resonant multiphoton absorption in one atom is followed by resonant coupling absorption for a second atom, with the associated transfer of excitation energy. Large effective cross sections are derived and examples are given.

VI. APPLICATIONS

In most of the papers referenced to this point, there is only a sentence or two devoted to potential applications of vacuum-uv or x-ray laser beams (two exceptions are [186] and [258]). This reflects the general attitude in the scientific community that probably the most important applications of an x-ray laser beam will develop after a useful device has arrived and will depend to a significant extent upon the characteristic of the particular device that proves most feasible. For examples, a sub-picosecond device could open up new areas in stop-motion radiography, while a highly coherent device will offer more promise for interferometric techniques. This attitude of invent-it-now, apply-it-later is neither unreasonable nor unprecedented in the laser field, or for that matter in other fields such as solid state physics. Indeed, it would seem most unwise at this point to attempt to narrowly channel approaches toward very specific applications while many basic physical approaches to pumping of meaningful populations inversions are still being explored on a rather fundamental scale.

Nevertheless, it is helpful and useful to periodically assess the long range applications foreseen. An excellent example is the 1973 "pre-CLEA" symposium and the summaries [178] which brought to focus the near term applications for materials analyses. Those applications requiring greater laser penetration (e.g., weapons) were placed in the more distant future with later-generation devices.

Some features associated with short wavelength radiation from a source with laser characteristics are indicated in Fig. 25 as a function of wave-

length λ and corresponding photon energy $h\nu$. The wavelength scale is also labeled with existing laser progress. It is interesting to note that progress in the last three years has mainly advanced by the optical mixing techniques (see Section V) from 1182 Å to 887 Å; this emphasizes the long road ahead if the x-ray region is to be reached systematically, as would seem most likely at present. The nuclear (γ -ray)/atomic (x-ray) interface at approximately 0.1 Å is anticipated by the short wavelength Lyman- α limit for ionized heavy atoms. It will be recalled from Section II that the 10^4 -times wavelength step indicated corresponds approximately to 10^{12} in gain and 10^{16} in pump power. Thus the quite natural turn to high power laser and electron beams under current development in other research areas (such as pellet fusion) for concentrated pump power sources. The interaction is expected to be bilateral; i.e., short wavelength lasers may be necessary for both efficient heating and for diagnostics of the extremely high density ($\sim 10^{26} \text{ cm}^{-3}$) compressed plasmas associated with pellet fusion approaches, simply because of the more penetrating character of the radiation. This is illustrated at the top in Fig. 25, where the critical electron plasma densities are indicated; only shorter wavelengths will penetrate at each of these densities. Thus it becomes doubly clear why so much activity in short wavelength laser research is done at laboratories also active in pellet-fusion programs.

A. Propagation

The long-wavelength applications indicated in Fig. 25 involve surface-photon-produced effects requiring low penetration [259]. Spectroscopy from surfaces can illuminate features without the damage of penetrating beams.

Cancer research may benefit here, for example. Penetration of thin biological membranes begins on a useful scale at about 100 \AA . A short burst of intense directional soft radiation could advance this area of research where higher photon energy radiation would neither provide contrast in thin samples nor time resolution for step-motion studies.

Between 1 and 10 \AA the atmosphere transmits at the $1/e$ level for various distances as indicated in Fig. 25. Here one can begin to consider x-ray microscopy on living tissue without a vacuum environment. At 1 \AA , absorption (mainly due to photoionization) takes place in about 10 meters of path, unless burn-through at high flux levels by non-linear effects can be invoked to enhance the transmission [260]. For the near term then, it is indeed appropriate to consider applications that either require short paths or else can function in a laboratory vacuum or extraterrestrial environment of low absorption.

At the shorter wavelengths in Fig. 25, penetration of solid materials will become possible with more selectivity and with a more specific interaction than an electron beam, thereby creating a lower background level. The fascinating "miniac" [261], miniature electron accelerator, operating in crystals on discrete impulses from metastable atomic states and on atomic-length scales would deserve more serious consideration. This has been proposed as a 1 cm version of the two mile Stanford linear accelerator (SLAC) in the rather far-off world of microminiaturization. A coherent pump source of penetrating radiation, such as afforded by the x-ray laser, is required. Also, the generation and manipulation of damaging dislocations in crystals can be considered [178].

B. Collimation

Many of these applications, given very broad-brush treatment here, require the intense, collimated characteristics of an ASE device. This will be the most likely first generation "laser" produced in the soft x-ray region. Into this category fall plasma heating and (scattering) diagnostics, photoelectron spectroscopy, microphotography of thin samples, and damage effect studies. Also, x-ray lithography [262] could become much more useful with an intense collimated beam. It can be argued that scaling of other more conventional x-ray sources to higher power may prove just as useful and perhaps sooner. Collimation may be provided by either (grazing incidence) concave mirrors, tapered cylindrical grazing-incidence lenses [263], Fresnel zone plates [264]-[266] or even waveguides [267]. The collection and collimation will never be as great as that with the laser, and huge losses are to be expected; however it could be a solution to some immediate demands. The optics developed for collimating conventional x-ray sources could become useful for future laser cavity designs, when the requirements are better formulated for the most promising laser approaches.

C. Short Pulse

An x-ray laser operating in the sub-nanosecond (to femtosecond) region could immediately surpass the time-resolving capabilities of any conventional x-ray source foreseen. This would come about by the rapid self-terminating nature of the laser. A time resolution on such scales is not even envisioned as a need at present, except in the pellet fusion area where measurements of changes in plasma parameters on picosecond time scales are desired. Flash

radiography of crystal motions under shocked conditions is another application [178]. Also relaxation and fluorescence studies could be extended.

D. Coherence

One of the most important characteristics of any laser is the coherence quality of the beam. Without resonant cavities ASE devices may indeed be limited in coherence. Thus the non-linear optical frequency multiplication techniques are important for transferring coherence to the short wavelength region and can be used in parallel with efforts to develop amplifiers to recover the power lost in the non-linear mixing devices. Coherence will be vital to the miniature accelerator idea. Furthermore it may allow stop-motion holographic microscopy and image projection with sufficient penetration for pellet fusion plasmas, biological specimens, large and complex molecules and other materials. While there is some debate at present as to the degree of resolution possible, already Fraunhofer far-field holography of $< 1.0 \mu\text{m}$ spheres (approaching virus size [178]) with a single beam of 12 ps duration has been accomplished at 1182 \AA with a frequency-upconverted beam. Also, a holographic grating with 826 \AA spacings has been produced and analyzed (Fig. 26) [254], [268]. Holograms obtained with vuv wavelengths and reconstructed with visible laser light offer the promise of enlargement according to the wavelength ratio of the two beams [268]. Phase contrast microscopy, though difficult, could improve contrast for objects with slight variations in index of refraction ($n \lesssim 1$) for radiation [178]. Such advanced investigations are most appropriate as coherent beams become available at decreasing wavelengths, even though the power available will be low at the outset.

E. Monochromaticity

Most "conventional" high emittance x-ray sources such as produced by

pulsed relativistic electron beams, vacuum sparks, exploding wires, etc., radiate as continuum and/or multi-line sources. Discrete-line sources or the utilization of dispersing elements result in greatly reduced emission levels. An x-ray laser would emit intense monochromatic emission which could be well focused for good resolution without chromatic aberrations (e.g., with a Fresnel lens). Also, such applications as crystal topography which depend on Bragg diffraction could benefit by a monochromatic beam of short duration for dislocation tracing on a temporal basis.

VII. PROGNOSIS AND SUMMARY

The recent interest and activity in short wavelength laser research is chronologically illustrated in Fig. 26, compiled from those references in the present article pertaining directly to x-ray laser schemes. A rather sudden upturn in activity beginning in 1970 can be associated with a number of factors, including the attention given to high intensity pump source development for the pellet fusion programs. This pumping requirement was already identified in the 1960's as a prerequisite for serious x-ray laser research, but could be justified only on the scale required by the potential payoff of fusion power. Added to this is the impetus given by the apparent quick success at the University of Utah [215]; the momentum generated by the controversy surrounding this experiment still can be felt. Much of the activity during the period immediately following the Utah activity could be considered a positive contribution of the bold efforts of this group. The period of peak activity around 1973-1974 may be largely attributed to an abundance of activity and advancements in specific areas (such as the recombination and molecular excimer approaches) which will probably level off as various groups pursue these approaches to further development. At this point the most promising schemes are identified, in general terms at least, and advances in the near future will be more methodical. Some areas, such as the efficient use of metastable levels for the temporary storage of populations at excited energies and the efficient coupling of strong line radiation for preferential pumping of specific levels will probably be advanced soon for more efficient

pumping with available power sources. Large cross-section reactions such as resonance charge transfer will continue to attract the attention deserved for promising high pumping efficiency. Coherence is recognized as a necessary characteristic of an x-ray laser beam, and efforts to extend frequency up-conversion of coherent beams using non-linear mixing in vapors and plasmas will undoubtedly be vigorously pursued since these processes are independent of the development of high-power pump sources. The necessary power at short wavelengths for stimulating additional non-linear processes may come either through amplification by ASE devices or through increased initial energy and pulse compression techniques. Coherence with cavities at short wavelengths may also be advanced by the development of x-ray optics for other more immediate sources.

It is important to further develop the tunable nature of vuv and x-ray lasers both for reaching atomic resonances in non-linear devices and for providing the transfer lasers required for pumping (over relatively narrow energy gaps) of metastable "storage" levels. For example, it may be necessary to couple a tunable vuv laser in the 1700 Å region with a xenon excimer amplifier to provide sufficient power to transfer-pump a helium-like ion, such as O^{6+} , from a metastable state to an allowed decay state. This could then lead to ASE amplification of another up-converted beam in the soft x-ray region. This example illustrates one way in which the interplay of the various presently-considered approaches could work together in the not-too-distant future to produce a useful coherent soft x-ray laser beam.

In summary, progress in short wavelength laser research has been most impressive in identifying reasonable approaches to follow consistent with the development of increasingly powerful pumping sources. Advancements in non-linear mixing and their initial application are impressive. Population inversions in plasmas following recombination have been reported by two groups. We can look forward in the next few years to advancements in both the generation of coherent beams at shorter wavelengths by up-conversion and the achievement of population inversion by direct methods in experiments leading to significant amplification at short vuv and soft x-ray wavelengths. The advances will result from clever and diligent pursuit of experiments using refined pump sources and further careful analysis of the fundamental ideas given here.

ACKNOWLEDGMENTS

It is a pleasure to acknowledge the initial encouragement and organizational efforts of R. A. Andrews; only the obligations associated with his leave from the Naval Research Laboratory during the period of preparation prevented his valuable contribution to this review. We are also indebted to L. J. Palumbo for permission to present his unpublished data on electron collisional pumping.

REFERENCES

- [1] H. G. Heard, "Ultraviolet gas laser at room temperature", Nature, vol. 200, p. 667, 16 November 1963.
- [2] D. A. Leonard, "Saturation of the molecular nitrogen second positive laser transition", Appl. Phys. Lett., vol. 7, pp. 4-6, 1 July 1965.
- [3] E. T. Gerry, "Pulsed-molecular-nitrogen laser theory", Appl. Phys. Lett., vol. 7, pp. 6-8, 1 July 1965.
- [4] J. D. Shipman, Jr., "Traveling wave excitation of high power gas lasers", Appl. Phys. Lett., vol. 10, pp. 3-4, Jan. 1967.
- [5] J. P. Girardeau-Montaut, M. Roumy, J. Hamelin, and L. Avan, "Realisation d'un amplificateur laser d'une puissance atteignant 50 MW a 3371 Å dans l'azote moléculaire", C.R. Acad. Sc. Paris, t. 274, pp. 607-610, 28 fevrier 1972.
- [6] R. W. Dreyfus and R. T. Hodgson, "Electron-beam excitation of the nitrogen laser", Appl. Phys. Lett., vol. 20, pp. 195-197, March 1972.
- [7] E. L. Patterson, J. B. Gerardo, and A. W. Johnson, "Intense-electron-beam excitation of the 3371 Å N₂ laser system", Appl. Phys. Lett., vol. 21, pp. 293-295, 15 September 1972.
- [8] P. A. Bazhulin, I. N. Knyazev, and G. G. Petrash, "On the possibility of stimulated emission in the far ultraviolet", Sov. Phys. JETP, vol. 23, pp. 649-650, Sept. 1965.
- [9] R. T. Hodgson, "Vacuum-ultraviolet laser action observed in the Lyman bands of molecular hydrogen", Phys. Rev. Lett., vol. 25, pp. 494-497, Aug. 1970.
- [10] R. W. Waynant, J. D. Shipman, Jr., R. C. Elton, and A. W. Ali, "Vacuum ultraviolet laser emission from molecular hydrogen", Appl. Phys. Letts., vol. 17, pp. 383-384, Nov. 1970.

- [11] R. W. Waynant, J. D. Shipman, Jr., R. C. Elton, and A. W. Ali, "Laser emission in the vacuum ultraviolet from molecular hydrogen", Proc. IEEE, vol. 59, pp. 679-684, April 1971.
- [12] R. W. Waynant, A. W. Ali, and P. S. Julianne, "Experimental observations and calculated band strengths for the D₂ Lyman band laser", J. Appl. Phys., vol. 42, pp. 3406-3408, Aug. 1971.
- [13] _____, Handbook of Lasers with Selected Data on Optical Technology, R. J. Pressley ed., Cleveland: The Chemical Rubber Co., 1971, pp. 319-322.
- [14] R. T. Hodgson, "Vacuum-ultraviolet lasing action observed in CO: 1800-2000 Å", J. Chem. Phys., vol. 55, pp. 5378-5379, Dec. 1971.
- [15] R. W. Waynant, "Observations of gain by stimulated emission in the Werner band of molecular hydrogen", Phys. Rev. Lett., vol. 28, pp. 533-535, Feb. 1972.
- [16] R. T. Hodgson and R. W. Dreyfus, "Electron-beam excitation of vacuum ultraviolet hydrogen laser", Phys. Lett., vol. 38A, pp. 213-214, Jan. 1972.
- [17] R. T. Hodgson and R. W. Dreyfus, "Vacuum UV laser action in H₂ Werner Bands: 1161-1240 Å", Phys. Rev. Lett., vol. 28, pp. 536-539, Feb. 1972.
- [18] A. W. Ali and A. C. Kolb, "Hydrogen molecular vacuum ultraviolet laser theory", Appl. Phys. Lett., vol. 13, pp. 259-261, Oct. 1968.
- [19] A. W. Ali and P. C. Kepple, "H₂ Lyman and Werner bands laser theory", Appl. Opt., vol. 11, pp. 2591-2596, Nov. 1972.
- [20] I. N. Knyazev, V. S. Letokov, and V. G. Movshev, "On the collisional four-level H₂ VUV laser", Opt. Commun., vol. 6, pp. 424-426, Dec. 1972.
- [21] M. Gailardo, C. A. Massone, and M. Garavagil, "On the inversion mechanism of the molecular hydrogen vacuum ultraviolet laser", IEEE J. Quantum Electron., vol. QE-10, pp. 525-526, June 1974.

- [22] I. N. Knyazev, "Efficiency of fast-electron-beam excitation of molecular electronic states of hydrogen in a hydrogen laser", Sov. J. Quantum Electron., vol. 4, pp. 1197-1203, April 1975.
- [23] V. S. Antonov, I. N. Knyazev, V. S. Letokhov, and V. G. Movshev, "Hydrogen laser in vacuum ultraviolet at atmospheric pressure", JETP Lett., vol. 17, pp. 393-395, 20 May 1973.
- [24] S. A. Borgstrom, "A simple low-divergence H_2 laser at 160 nm", Opt. Commun., vol. 11, pp. 105-108, June 1974.
- [25] R. W. Dreyfus and R. T. Hodgson, "Molecular-hydrogen laser: 1098-1613 Å", Phys. Rev. A., vol. 9, pp. 2635-2648, June 1974.
- [26] I. N. Knyazev, V. S. Letokhov, and V. G. Movshev, "Efficient and practical vacuum ultraviolet laser", IEEE J. Quantum Electron., vol. QE-11, pp. 805-817, Oct. 1975.
- [27] A. G. Molchanov, I. A. Poluektov, and Yu. M. Popov, "The possibility of the generation of vacuum ultraviolet radiation by electron excitation of inert-gas crystals", Sov. Phys. - Solid State, vol. 9, pp. 2655-2656, May 1968.
- [28] N. G. Basov, E. M. Balashov, O. V. Bogdankevitch, V. A. Danilychev, J. N. Kashnikov, N. P. Lantsov, and D. D. Khodkevitch, "Liminescence of condensed Xe, Kr, Ar and their mixtures in vacuum region of spectrum under excitation by fast electrons", J. Lumin., vol. 1-2, pp. 834-841, 1970.
- [29] N. G. Basov, V. A. Danilychev, and Yu. M. Popov, "Stimulated emission in the vacuum ultraviolet region", Proc. International Quantum Electronics Conf., Kyoto, 1970.

- [30] N. G. Basov, V. A. Danilychev, Yu. M. Popov and D. D. Khodkevich, "Laser operating in the vacuum region of the spectrum by excitation of liquid xenon with an electron beam", JETP Lett., vol. 12, pp. 329-331, 20 Nov. 1970.
- [31] N. G. Basov, V. A. Danilychev, and Yu. M. Popov, "Stimulated emission in the vacuum ultraviolet region", Sov. J. Quantum Electron., vol. 1, pp. 18-22, July-August 1971.
- [32] N. G. Basov, "Soviet approach to e-beam pumping", Laser Focus, vol. 8, pp. 45-47, Sept. 1972.
- [33] N. G. Basov, E. M. Belenov, V. A. Danilychev, O. M. Kerimov, I. B. Kovsh, A. S. Podsonnyi, and A. F. Suchkov, "Electric ionization lasers", Sov. Phys.-JETP, vol. 37, pp. 58-64, July 1973.
- [34] H. A. Koehler, L. J. Ferderber, D. L. Redhead, and P. J. Ebert, "Stimulated VUV emission in high-pressure xenon excited by high-current relativistic electron beams", Appl. Phys. Lett., vol. 21, pp. 198-200, Sept. 1972.
- [35] H. A. Koehler, L. J. Ferderber, D. L. Redhead, and P. J. Ebert, "Vacuum-ultraviolet emission from high-pressure xenon and argon excited by high-current relativistic electron beams", Phys. Rev. A, vol. 9, pp. 768-781, Feb. 1974.
- [36] B. L. Borovich, V. S. Zuev, and D. B. Stavrovsky, "Pressure-induced ultraviolet absorption in rare gases: absorption coefficients for mixtures of Xe and Ar at pressures up to 40 atm in the vicinity of 147 nm", J. Quant. Spectros. Radiat. Transfer, vol. 13, pp. 1241-1249, March 1973.

- [37] M. M. Mkrtchyan and V. T. Platonenko, "Feasibility of high-pressure noble-gas lasers", JETP Lett., vol. 17, pp. 19-21, 5 Jan. 1973.
- [38] V. M. Andriyakhin, V. V. Vasil'tsov, S. S. Krasil'nikov, and V. D. Pis'mennyi, "Nuclear pumping of molecular gas lasers", Sov. Phys.-JETP, vol. 36, pp. 865-869, May 1973.
- [39] A. W. Johnson and J. B. Gerardo, Model of the VUV molecular-xenon laser, Sandia Laboratories SIA-73-5872A, Oct. 1973.
- [40] E. V. George and C. K. Rhodes, "Kinetic model of ultraviolet inversions in high-pressure rare-gas plasmas", Appl. Phys. Lett., vol. 23, pp. 139-141, August 1973.
- [41] A. W. Ali, Towards shorter wavelength lasers and breaking the 1000 Angstrom barrier (II) (Bound-Continuum Emission), U. S. Naval Research Laboratory Memo Rpt. No. 2863, August 1974.
- [42] A. G. Molchanov and Yu. M. Popov, "Possibility of electric-ionization excitation of the stimulated emission of vacuum ultraviolet radiation in compressed xenon", Sov. J. Quantum Electron., vol. 4, pp. 613-615, Nov. 1974.
- [43] G. R. Fournier, "A model for electron-beam excited vuv fluorescence from xenon", Opt. Commun., vol. 13, pp. 385-389, April 1975.
- [44] S. C. Wallace, R. T. Hodgson, and R. W. Dreyfus, "Excitation of vacuum ultraviolet emission from high-pressure xenon by relativistic electron beams", Appl. Phys. Lett., vol. 23, pp. 22-24, July 1973.

- [45] E. R. Ault, M. L. Bhaumik, W. M. Hughes, R. J. Jensen, C. P. Robinson, A. C. Kolb, and J. Shannon, "Xenon molecular laser in the vacuum ultraviolet", IEEE J. Quantum Electron., vol. QE-9, pp. 1031-1032, Oct. 1973.
- [46] D. A. Emmons, "Xenon photo-absorption in the vacuum ultraviolet", Opt. Commun., vol. 11, pp. 257-260, July 1974.
- [47] D. J. Bradley, D. R. Hull, M. H. R. Hutchinson, and M. W. McGeoch, "Megawatt VUV xenon laser employing coaxial electron-beam excitation", Opt. Commun., vol. 11, pp. 335-338, August 1974.
- [48] Z. Ophir, B. Raz, and J. Jortner, "Exciton-enhanced photoemission from doped solid rare gases", Phys. Rev. Lett., vol. 33, pp. 415-418, Aug. 1974.
- [49] S. C. Wallace and R. W. Dreyfus, "Continuously tunable xenon laser at 1720 Å", Appl. Phys. Lett., vol. 25, pp. 498-500, Nov. 1974.
- [50] J. W. Keto, R. E. Gleason, Jr., and G. K. Walters, "Production mechanisms and radiative lifetimes of argon and xenon molecules emitting in the ultraviolet", Phys. Rev. Lett., vol. 33, pp. 1365-1368, Dec. 1974.
- [51] J. B. Gerardo and A. W. Johnson, "Comment on 'Dynamic model of high pressure rare-gas excimer lasers'", Appl. Phys. Lett., vol. 26, pp. 582-584, 15 May 1975.
- [52] D. J. Bradley, D. R. Hull, M. H. R. Hutchinson, and M. W. McGeoch, "Co-axially pumped, narrow band, continuously tunable, high power vuv xenon laser", Opt. Commun., vol. 14, pp. 1-3, May 1975.
- [53] E. Zamir, C. W. Werner, W. P. Lapatovich, and E. V. George, "Temporal evolution of the electron density in high-pressure electron-beam-excited xenon plasmas", Appl. Phys. Lett., vol. 27, pp. 56-58, 15 July 1975.

- [54] C. K. Rhodes, "Review of ultraviolet laser physics", IEEE J. Quantum Electron., vol. QE-10, pp. 153-174, Feb. 1974; see also G. G. Petrash, "Pulsed gas-discharge lasers", Sov. Phys.-Usp., vol. 14, pp. 747-765 May-June 1972.
- [55] P. W. Hoff, J. C. Swingle, and C. K. Rhodes, "Demonstration of temporal coherence, spatial coherence, and threshold effects in the molecular xenon laser", Opt. Commun., vol. 8, pp. 128-131, June 1973.
- [56] J. B. Gerardo and A. W. Johnson, "High pressure xenon laser at 1730 Å", IEEE J. Quantum Electron., vol. QE-9, pp. 748-755, July 1973.
- [57] P. W. Hoff, J. C. Swingle, and C. K. Rhodes, "Observations of stimulated emission from high-pressure krypton and argon/xenon mixtures", Appl. Phys. Lett., vol. 23, pp. 245-246, Sept. 1973.
- [58] W. R. Hunter, "Optics in the vacuum ultraviolet", Electro-Optical Systems Design, vol. 5, pp. 16-23, Nov. 1973.
- [59] R. Tousey, "The extreme ultraviolet-past and future", Appl. Opt., vol. 1, pp. 679-693, Nov. 1962.
- [60] J. A. R. Samson, Techniques of Vacuum Ultraviolet Spectroscopy, New York: J. Wiley and Sons, 1967.
- [61] R. W. Dreyfus, R. J. von Gutfeld, and S. C. Wallace, "Aluminum mirror degradation in a vuv laser", Opt. Commun., vol. 9, pp. 342-345, December 1973.
- [62] W. L. Bond, M. A. Duguay, and P. M. Rentzepis, "Proposed resonator for an x-ray laser", Appl. Phys. Lett., vol. 10, pp. 216-218, 15 April 1967.
- [63] R. D. Delattes, "X-ray monochromators and resonators from single crystals", Appl. Phys. Lett., vol. 12, pp. 133-135, 15 Feb. 1968.

- [64] R. M. J. Cotterill, "A universal planar x-ray resonator", Appl. Phys. Lett., vol. 12, pp. 403-404, June 1968.
- [65] A. V. Kolpakov, R. N. Kuzmin, and V. M. Ryabov, "Some characteristics of the resonators for x-ray frequencies", J. Appl. Phys., vol. 41, pp. 3549-3550, July 1970.
- [66] H. Kogelnik and C. V. Shank, "Stimulated emission in a periodic structure", Appl. Phys. Lett., vol. 18, pp. 152-154, Feb. 1971.
- [67] C. V. Shank, J. E. Bjorkholm, and H. Kogelnik, "Tunable distributed-feedback dye laser", Appl. Phys. Lett., vol. 18, pp. 395-396, May 1971.
- [68] I. P. Kaminow, H. P. Weber, and E. A. Chandross, "Poly(methyl methacrylate) dye laser with internal diffraction grating resonator", Appl. Phys. Lett., vol. 18, pp. 497-501, June 1971.
- [69] H. Kogelnik and C. V. Shank, "Coupled-wave theory of distributed feedback lasers", J. Appl. Phys., vol. 43, pp. 2327-2338, May 1972.
- [70] C. V. Shank, R. V. Schmidt, and B. I. Miller, "Double-heterostructure GaAs distributed-feedback laser", Appl. Phys. Lett., vol. 25, pp. 200-201, Aug. 1974.
- [71] D. R. Scifres, R. L. Burnham, and W. Streifer, "Distributed-feedback single heterojunction GaAs diode laser", Appl. Phys. Lett., vol. 25, pp. 203-206, Aug. 1974.
- [72] S. R. Chinn and P. L. Kelley, "Analysis of the transmission, reflection and noise properties of distributed feedback laser amplifiers", Opt. Commun., vol. 10, pp. 123-126, Feb. 1974.
- [73] R. A. Fisher, "Possibility of a distributed-feedback x-ray laser", Appl. Phys. Lett., vol. 24, pp. 598-599, June 1974.

- [74] A. Yariv, "Analytical considerations of Bragg coupling coefficients and distributed-feedback x-ray lasers in single crystals", Appl. Phys. Lett., vol. 25, pp. 105-107, July 1974.
- [75] C. Elachi, G. Evans, and F. Grunthaner, "Proposed distributed feedback crystal cavities for x-ray lasers", Appl. Opt., vol. 14, pp. 14-15, Jan. 1975.
- [76] A. L. Schawlow and C. H. Townes, "Infrared and optical masers", Phys. Rev., vol. 112, pp. 1940-1949, 15 December 1958.
- [77] A. L. Bloom, W. E. Bell, and R. E. Rempel, "Laser operation at 3.39μ in a helium-neon mixture", Appl. Opt., vol. 2, pp. 317-318, March 1963.
- [78] R. H. Dicke, "Coherence in Spontaneous Radiation Processes", Phys. Rev., vol. 93, pp. 99-111, Jan. 1954.
- [79] R. H. Dicke, "The coherence brightened laser", Quantum Electronics, Proceedings of the Third International Conference on Quantum Electronics Grivet and Bloembergen, eds, vol. I, New York: Columbia University Press, 1964, pp. 35-53.
- [80] L. Allen and G. I. Peters, "Superradiance, coherence brightening and amplified spontaneous emission", Phys. Lett., vol. 31A, pp. 95-96, Feb. 1970.
- [81] G. I. Peters and L. Allen, "Amplified spontaneous emission I. The threshold condition", J. Phys. A, vol. 4, pp. 238-243, March 1971.
- [82] L. Allen and G. I. Peters, "Amplified spontaneous emission II. The connection with laser theory", J. Phys. A, vol. 4, pp. 377-381, May 1971.
- [83] L. Allen and G. I. Peters, "Amplified spontaneous emission III. Intensity and saturation", J. Phys. A, vol. 4, pp. 564-573, July 1971.
- [84] G. I. Peters and L. Allen, "Amplified spontaneous emission IV. Beam divergence and spatial coherence", J. Phys. A, vol. 5, pp. 546-554, April 1972.

- [85] L. Allen, "Amplified spontaneous emission", in Coherence and Quantum Optics, L. Mandel and E. Wolf, eds., New York: Plenum, 1973, pp. 467-490; see also L. Allen and G. I. Peters, "Spectral distribution of amplified spontaneous emission", J. Phys. A, vol. 5, pp. 695-704, May 1972.
- [86] R. C. Elton, R. W. Waynant, R. A. Andrews and M. H. Keilly, X-Ray and Vacuum-UV Lasers (Current Status and Prognosis), U. S. Naval Research Laboratory, Rpt. No. 7412, May 1972.
- [87] S. Stenholm and W. E. Lamb, Jr., "Semiclassical theory of a high-intensity laser", Phys. Rev., vol. 181, pp. 618-635, 10 May 1969.
- [88] A. Yariv and R. C. C. Leite, "Super radiant narrowing in fluorescence radiation of inverted populations", J. Appl. Phys., vol. 34, pp. 3410-3411, Nov. 1963.
- [89] L. Allen and G. I. Peters, "Amplified spontaneous emission and external signal amplification in an inverted medium", Phys. Rev. A, vol. 8, pp. 2031-2047, Oct. 1973.
- [90] W. E. Lamb, Jr., "Theory of an optical maser", Phys. Rev., vol. 134, pp. A1429-A1450, 15 June 1964.
- [91] W. E. Lamb, Jr., "Amplification of incoherent radiation", 1974 Intern'l. Quantum Electron. Conf. Dig. Tech. Papers, IEEE, New York, 1974, p. 41.
- [92] F. A. Hopf, "Statistical changes in amplified thermal light", 1974 Intern'l Quantum Electron. Conf. Dig. Tech. Papers, IEEE, New York, 1974, p. 41.
- [93] R. L. Kelly with L. J. Palumbo, Atomic and Ionic Emission Lines Below 2000 Ångstroms, U.S. Naval Research Laboratory Report No. 7599, Washington, D. C.: U.S. Government Printing Office, 1973.

- [94] D. Marcuse, "Maser action without population inversion", Proc. IEEE, vol. 51, pp. 849-850, May 1963.
- [95] W. L. Wiese, M. W. Smith, and B. M. Glennon, Atomic Transitions Probabilities, Vol. 1, Hydrogen through Neon, National Bureau of Standards Report NSRDS-NBS-4, May 1966.
- [96] R. C. Elton, "Quasistationary population inversion on $K\alpha$ transitions", Appl. Opt., vol. 14, pp. 2243-2249, Sept. 1975.
- [97] H. R. Griem, Spectral Line Broadening by Plasmas, New York: Academic Press, 1974.
- [98] F. E. Irons, and N. J. Peacock, "Experimental evidence for population inversion in C^{5+} in an expanding laser-produced plasmas", J. Phys. B, vol. 7, pp. 1109-1112, 21 June 1974.
- [99] R. J. Dewhurst, D. Jacoby, G. J. Pert, and S. A. Ramsden, Ionization, Recombination and Population Inversion in Laser Produced Plasmas, Univ. Hull Report No. LPI-74-2, 1974.
- [100] A. V. Vinogradov, and I. I. Sobel'man, "The problem of laser radiation sources in the far ultraviolet and x-ray regions", Sov. Phys.-JETP, vol. 36, pp. 1115-1119, June 1973.
- [101] W. D. Barfield, G. D. Koontz, and W. F. Huebner, "Fits to new calculations of photoionization cross sections for low-Z elements", J. Quant. Spectrosc. Radiat. Transfer, vol. 12, pp. 1409-1433, Oct. 1972.
- [102] S. M. R. Ansari, G. Elwert, and P. Mücklich, "On dielectronic recombination", Z. Naturforsch., vol. 25e, pp. 1781-1797, Dec. 1970.

- [103] R. C. Elton, "Atomic processes", in Methods of Experimental Physics, Plasma Physics, H. R. Griem and R. H. Lovberg, eds., vol. 9A, New York: Academic Press, 1970, pp. 115-168.
- [104] W. H. Louisell, M. O. Scully, and W. B. McKnight, "Analysis of a soft x-ray laser with charge exchange excitation", Phys. Rev. A, vol. 11, pp. 989-1000, March 1975.
- [105] R. C. Elton, "Extension of 3p-3s ion lasers into the vacuum ultraviolet region", Appl. Opt., vol. 14, pp. 97-101, January 1975.
- [106] R. C. Elton and R. H. Dixon, "X-Ray laser research: guidelines and progress at NRL", Annals of the New York Academy of Sciences, vol. , pp. , 1976.
- [107] M. Galanti, N. J. Peacock, B. A. Norton, and J. Puric, "Light absorption and energy balance at the surface of a laser-irradiated solid target", in Proceedings, Fifth IAEA Conf. on Plasma Physics and Controlled Nuclear Fusion Research, Tokyo, November 1974.
- [108] A. M. Malvezzi, E. Jannitti and G. Tondello, "Observations of the Stark broadening of the resonance lines in a beryllium laser produced plasma", (to be published).
- [109] T. N. Lie (Lee) and R. C. Elton, "X-radiation from optical and inner-shell transitions in a highly ionized dense plasma", Phys. Rev., vol. 3, pp. 865-871, March 1971.
- [110] T. N. Lee, "High density ionization with an intense linear focus discharge", Annals New York Academy of Sciences, vol. 251, pp. 112-125, May 1975.

- [111] G. Cooperstein, private communication, February 1975.
- [112] R. A. McCorkle, "Practicable x-ray amplifier", Phys. Rev. Lett., vol. 29, pp. 982-985, Oct. 1972.
- [113] V. B. Rozanov, "Feasibility of producing an inverted medium by photo-ionization of the inner electrons in atoms", JETP Lett., vol. 12, pp. 340-342, 20 November 1970.
- [114] I. Freund, "Optically stimulated x-ray laser", Appl. Phys. Lett., vol. 24, pp. 13-15, January 1974. The gain estimates seem overly optimistic in this paper for reasonable line broadening.
- [115] R. C. Elton, "Intercombination line oscillator strengths in the helium isoelectronic sequence", Astrophys. J., vol. 148, pp. 573-578, May 1967.
- [116] R. C. Elton and W. W. Köppenjörför, "Measured collisional excitation rate coefficients for oxygen VII", Phys. Rev., vol. 160, pp. 194-201, August 1967.
- [117] L. I. Gudzenko, V. V. Evstigneev, and S. I. Yakovlenko, "Amplification of x-ray radiation in a decaying plasma using transitions in helium-like ions", Sov. J. Quantum Electron., vol. 4, p. 1148, March 1975; see also L. I. Gudzenko, Yu. K. Zemtsov, and S. I. Yakovlenko, "Amplification of vacuum-ultraviolet radiation in a decaying dense helium plasma", JETP Lett., vol. 12, pp. 167-169, Sept. 1970.
- [118] H. J. Kunze, A. H. Gabriel, and H. R. Griem, "Measurement of collisional rate coefficients for helium-like carbon ions in a plasma", Phys. Rev., vol. 165, pp. 267-276, January 1968.

- [119] R. H. Pantell, Reports on Contract N00014-67-A-0112-0033 (1-3),
Arlington, VA, 22217: Office of Naval Research; see also Ref. [86],
p. 18.
- [120] H. Mahr and U. Roeder, "Use of metastable ions for a soft x-ray laser",
Opt. Commun., vol. 10, pp. 227-228, March 1974.
- [121] A. A. Vekhov, V. N. Makhov, F. A. Nikolaev, and V. B. Rozanov,
"Possibility of using metastable heliumlike ions in generation of
ultrashort x-ray stimulated radiation", Sov. J. Quantum Electron., vol. 5,
pp. 718-720, June 1975.
- [122] S. E. Harris, et. al. (to be published).
- [123] L. Wood and G. Chapline, Conditions for X-Ray Laser Action, Lawrence Livermore
Laboratory Report UCRL-75184 (Rev. 2), June 1974.
- [124] O. R. Wood, II, "High-pressure pulsed molecular lasers", Proc. IEEE,
vol. 62, pp. 355-397, March 1974.
- [125] C. V. Heer, "Broadband gain with naturally inverted stable to continuum
molecular transitions", J. Appl. Phys., vol. 41, pp. 1875-1876, 15 March 1970.
- [126] A. J. Palmer, "Stimulated emission of the H_2 continuum", J. Appl. Phys.,
vol. 41, pp. 438-439, January 1970.
- [127] S. Metz, "Enhanced light emission from a pulsed discharge in hydrogen",
Phys. Lett., vol. 34A, pp. 315-316, April 1971.
- [128] A. Cohn, A. G. Rubin, and A. L. Besse, The Hydrogen Dissociation
Laser, Cambridge, Mass: AFCRL-TR-74-0110, 5 April 1974.
- [129] F. H. Mies, "Stimulated emission and population inversion in diatomic
bound-continuum transitions", Mol. Phys., vol. 26, pp. 1233-1246, November
1973.

- [130] D. C. Lorents, "A model of rare-gas excimer formation and decay and its application to VUV lasers", Radiation Research, vol. 59, pp. 438-440, 1974.
- [131] A. V. Phelps, Tunable Gas Lasers Utilizing Ground State Dissociation, Univ. Colorado, Boulder, JILA Report No. 110, 15 September 1972.
- [132] H. T. Powell, J. R. Murray, and C. K. Rhodes, "Laser oscillation on the green bands of XeO and KrO", Appl. Phys. Lett., vol. 25, pp. 730-732, 15 December 1974.
- [133] Y. Hashino, Y. Katsuyama, and K. Fukuda, "Laser oscillation of multiply ionized Ne, Ar and N ions in a z-pinch discharge", Jap. J. Appl. Phys., vol. 11, p. 907, June 1972.
- [134] Y. Hashino, Y. Katsuyama, and K. Fukuda, "Laser oscillation of OV in z-pinch discharge", Jap. J. Appl. Phys., vol. 12, p. 470, April 1973.
- [135] R. A. Andrews, "Soft x-ray lasers via electron-collisional pumping" in Progress in Lasers and Laser Fusion, A. Perlmutter and S. M. Widmayer, eds., New York: Plenum Press, 1975, pp. 235-268.
- [136] L. J. Palumbo (to be published).
- [137] K. G. Whitney and J. Davis, "The use of intense relativistic electron beams to pump VUV lasers", J. Appl. Phys., vol. 46, pp. 4103-4105, Sept. 1975.
- [138] R. C. Elton, T. N. Lee, J. Davis, J. F. Reintjes, R. H. Dixon, R. C. Eckardt, K. Whitney, J. L. DeRosa, L. J. Palumbo, and R. A. Andrews, "Towards x-ray lasers with vuv amplification on 3p-3s transitions", Physica Fennica, vol. 9, Suppl. S1, pp. 400-402, July 1974.

- [139] I. N. Knyazev and V. S. Letokhov, "Excitation of far vacuum uv lasers by fast heating of plasma electrons in ultrashort pulsed optical fields", Opt. Commun., vol. 3, pp. 332-334, July 1971.
- [140] R. W. Waynant, "Vacuum ultraviolet laser emission from C IV", Appl. Phys. Lett., vol. 22, pp. 419-420, April 1973.
- [141] B. A. Norton and E. R. Wooding, "Proposed method for obtaining population inversion for vacuum ultraviolet and x-ray transitions", Phys. Rev. A, vol. 11, pp. 1689-1691, May 1975.
- [142] T. C. Bristow, M. J. Lubin, J. M. Forsyth, E. B. Goldman, and J. M. Soures, "High-intensity x-ray spectra and stimulated emission from laser plasmas", Opt. Commun., vol. 5, pp. 315-318, August 1972.
- [143] L. I. Gudzenko and L. A. Shelepin, "Radiation enhancement in a recombining plasma", Sov. Phys.-Doklady, vol. 10, pp. 147-149, Aug. 1965.
- [144] B. F. Gordiets, L. I. Gudzenko, and L. A. Shelepin, "Relaxation processes and amplification of radiation in a dense plasma", Sov. Phys.-JETP, vol. 28, pp. 489-493, March 1969.
- [145] J. Peyraud and N. Peyraud, "Population inversion in laser plasmas", J Appl. Phys., vol. 43, pp. 2993-2996, July 1972.
- [146] B. Lax and A. H. Guenther, "Quantitative aspects of a soft x-ray laser", Appl. Phys. Lett., vol. 21, pp. 361-363, October 1972.
- [147] L. Ya. Efremenkova and B. M. Smirnov, "Ultraviolet laser using the Lyman transition", Sov. Phys.-Doklady, vol. 17, pp. 336-338, October 1972.
- [148] G. I. Gudzenko, M. V. Nezlin and S. I. Yakovlenko, "Recombination laser with a supercooled plasma generated by an electron beam", Sov. Phys.-Tech. Phys., vol. 18, pp. 1218-1221, March 1974.

- [149] Willy L. Bohn, "Possible population inversions for VUV and soft x-ray transitions in hydrogen-like ions", Appl. Phys. Lett., vol. 24, pp. 15-17, January 1974.
- [150] G. J. Pert and S. A. Ramsden, "Population inversion in plasmas produced by picosecond laser pulses", Opt. Commun., vol. 11, pp. 270-273, July 1974.
- [151] W. W. Jones and A. W. Ali, "Theory of short-wavelength lasers from recombining plasmas", Appl. Phys. Lett., vol. 26, pp. 450-451, 15 April 1975.
- [152] E. Ya. Kononov and K. N. Koshelev, "Inverse population of levels of multiply charged ions", Sov. J. Quantum Electron., vol. 4, pp. 1340-1343, May 1975.
- [153] G. Chapline and L. Wood, "X-ray and γ -ray lasers", in Progress in Lasers and Laser Fusion, A. Perlmutter and S. M. Widmayer, eds., New York: Plenum Press, 1975, pp. 269-279.
- [154] E. Kononov, "On the level population of Al XI in a laser plasma", in Proceedings of 4th International Conference on Beam Foil Spectroscopy, (to be published, 1976).
- [155] R. C. Elton and L. J. Palumbo, "Radiative-Auger transitions in soft x-ray plasma emission", Phys. Rev., vol. 9, pp. 1873-1884, May 1974.
- [156] D. L. Walters and C. P. Bhalla, "Nonrelativistic Auger rates, x-ray rates, and fluorescence yields for the K shell", Phys. Rev. A, vol. 3, pp. 1919-1927, June 1971.
- [157] A. H. Gabriel and T. M. Paget, "Measurement and interpretation of dielectronic recombination satellite line intensities", J. Phys. B., vol. 5, pp. 673-685, March 1972.

- [158] A. Burgess, "A general formula for the estimation of dielectronic recombination coefficients in low-density plasmas", Astrophys. J., vol. 141, pp. 1588-1590, May 1965.
- [159] A. Burgess, "Dielectronic recombination and the temperature of the solar corona", Astrophys. J., vol. 139, pp. 776-780, March 1964.
- [160] A. Burgess, and H. P. Summers, "The effects of electron and radiation density on dielectronic recombination", Astrophys. J., vol. 157, pp. 1007-1021, August 1969.
- [161] H. P. Summers, "The ionization equilibrium of hydrogen-like to argon-like ions of elements", Mon. Not. R. Astron. Soc., vol. 169, pp. 663-680, Dec. 1974.
- [162] H. J. Zwally and D. W. Koopman, "Single-electron capture by C^{4+} in helium, neon, and argon below 40 keV", Phys. Rev. A, vol. 2, pp. 1851-1861, Nov. 1970.
- [163] M. O. Scully, W. H. Louisell, and W. B. McKnight, "A soft x-ray laser utilizing charge exchange", Opt. Commun., vol. 9, pp. 246-248, November 1973.
- [164] R. C. Elton, "Selected analyses and experiments at NRL towards quasi-cw short wavelength lasers", in Progress in Lasers and Laser Fusion, A. Perlmutter and S. M. Widmayer, eds., New York: Plenum Press, 1975, pp. 117-145.
- [165] I. P. Presnyakov and A. D. Ulantsev, "Charge exchange between multiply charged ions and atoms", Sov. J. Quantum Electron., vol. 4, pp. 1320-1324, May 1975.

- [166] R. C. Elton and R. H. Dixon, "Spectroscopy of plasmas for short wavelength lasers", in Proceedings 4th International Conf. on Beam Foil Spectroscopy (to be published, 1976).
- [167] L. P. Presnyakov and V. P. Shevel'ko, "Possibility of producing inverted population in atomic beams by charge exchange of protons with atoms", JETP Lett., vol. 13, pp. 203-204, 20 March 1971.
- [168] C. D. Cantrell and M. C. Scully, "Review of soft x-ray lasers using charge exchange", in Progress in Lasers and Laser Fusion, A. Perlmutter and S. M. Widmayer, eds., New York: Plenum Press, 1975, pp. 147-234.
- [169] _____, Proc. of the International Conf. on Inner Shell Ionization Phenomena and Future Applications, USAEC Report CONF-720404, vols. 1-4, R. W. Fink, S. T. Manson, J. M. Palms, and P. V. Rao, eds., 1973.
- [170] V. V. Kokorin and V. F. Los, "The pumping of an x-ray laser by means of an optical laser", Phys. Lett., vol. 45A, pp. 487-488, 5 November 1973.
- [171] R. A. McCorkle and J. M. Joyce, "Threshold conditions for amplified spontaneous emission of x-radiation", Phys. Rev. A, vol. 10, pp. 903-912, Sept. 1974.
- [172] M. A. Duguay and P. M. Rentzepis, "Some approaches to vacuum UV and x-ray lasers", Appl. Phys. Lett., vol. 10, pp. 350-352, June 1967.
- [173] Yu. L. Stankevich, "The possibility of induced intensification of characteristic x-radiation", Sov. Phys.-Doklady, vol. 15, pp. 356-357, October 1970.
- [174] P. P. Bey, Analysis of VUV and X-Ray Lasers Pumped by a Traveling-Wave Source, U.S. Naval Research Laboratory Memo Rpt. No. 2847, July 1974.

- [175] W. W. Jones, and A. W. Ali, Calculations for a VUV Laser From Sodium Vapor Pumped by Radiation From an Exploding Wire, U. S. Naval Research Laboratory Memo Rpt. No. 2807, June 1974.
- [176] W. W. Jones and A. W. Ali, "Sodium vapor laser (372 Å) calculations using exploding wire radiation", Phys. Lett., vol. 50A, pp. 101-102, Nov. 1974.
- [177] E. J. McGuire, "Soft x-ray amplified spontaneous emission via the Auger effect", Phys. Rev. Lett., vol. 35, pp. 844-848, 29 Sept. 1975.
- [178] R. A. Andrews, X-Ray Lasers—Current Thinking, U. S. Naval Research Laboratory, Memo Rpt. No. 2677, October 1973; also summarized in Laser Focus, vol. 9, pp. 41-46, Nov. 1973.
- [179] F. T. Arecchi, G. P. Banfi, and A. M. Malvezzi, "Threshold evaluations for an x-ray laser", Opt. Commun., vol. 10, pp. 214-218, March 1974.
- [180] A. V. Vinogradov, I. I. Sobel'man, and E. A. Yukov, "Possibility of construction of a far-ultraviolet laser utilizing transitions in multiply charged ions in an inhomogeneous plasma", Sov. J. Quant. Electron., vol. 5, pp. 59-63, July 1975.
- [181] B. A. Norton and N. J. Peacock, "Population inversion in laser-produced plasmas by pumping with opacity-broadened lines", J. Phys. B, vol. 8, pp. 989-996, April 1975.
- [182] G. Moruzzi and F. Strumia, "A technique for optical pumping in vacuum ultraviolet", Opt. Commun., vol. 2, pp. 279-281, November 1970.
- [183] W. Lichten, "Molecular wave functions and inelastic atomic collisions", Phys. Rev., vol. 164, pp. 131-142, 5 December 1967.

- [184] R. N. Sudan and R. V. Lovelace, "Generation of intense ion beams in pulsed diodes", Phys. Rev. Lett., vol. 31, pp. 1174-1177, Nov. 1973.
- [185] F. A. Hopf, P. Meystre, M. O. Scully and J. F. Seely, "Coherence brightening and laser lethargy in x-ray laser amplifiers", Phys. Rev. Lett., vol. 35, pp. 511-513, 25 August 1975.
- [186] L. A. Rivlin, Soviet Invention Disclosures No. 709414 of January 1961 and 710508 of 1 April 1961.
- [187] V. Vali and W. Vali, "Induced γ -ray emission", Proc. IEEE, vol. 51, pp. 182-184, Jan. 1963.
- [188] G. C. Baldwin, J. P. Neissel, and L. Tonks, "Induced gamma-ray emission", Proc. IEEE, vol. 51, pp. 1247-1248, Sept. 1963.
- [189] B. V. Chirikov, "The kinetics of induced Mossbauer radiation", Sov. Phys.-JETP, vol. 17, pp. 1355-1359, Dec. 1963.
- [190] R. V. Khokhlov, "Concerning the feasibility of a γ laser based on radioactive crystals", JETP Lett., vol. 15, pp. 414-416, 5 May 1972.
- [191] V. S. Letokhov, "Narrow-frequency tunable γ -ray nuclear resonances induced by laser radiation", Phys. Rev. Lett., vol. 30, pp. 729-732, April 1973.
- [192] V. S. Letokhov, "Pumping of nuclear levels by x-ray radiation of a laser plasma", Sov. J. Quantum. Electron., vol. 3, pp. 360-361, Jan.-Feb. 1974; see also V. S. Letokhov, "On the problem of the nuclear-transition γ -laser", Sov. Phys.-JETP, vol. 37, pp. 787-793, Nov. 1973.
- [193] V. I. Gol'danskii and Yu. Kagan, "The possibility of creating a nuclear γ laser", Sov. Phys. - JETP, vol. 37, pp. 49-52, July 1973.

- [194] J. Byrne, G. I. Peters, and L. Allen, "Stimulated emission from nuclei", Appl. Opt., vol. 13, pp. 2499-2504, November 1974.
- [195] G. C. Baldwin and R. V. Khokhlov, "Prospects for a gamma-ray laser", Phys. Today, vol. 28, pp. 33-39, February 1975.
- [196] G. C. Baldwin, Problems of the Gamma Ray Laser, Aberdeen, Md.: BRL-CR-179, Contract DA-ARO-D-31-124-73-G162, August 1974.
- [197] L. Wood and G. Chapline, "Towards gamma-ray lasers", Nature (Lond.), vol. 252, pp. 447-450, 6 December 1974.
- [198] L. Cohen (chairman), J. B. Aviles, Jr., C. Bond, L. Cox, I. Manning, K. W. Marlow, and D. J. Nagel, Gamma-Ray Lasers (Grasers) A Status Report, U. S. Naval Research Laboratory Memo Rpt. No. 2947, Dec. 1974.
- [199] Y. A. Il'inskii and R. V. Khokhlov, "Narrowing of γ -resonance lines in crystals by radio-frequency fields", Sov. Phys.-JETP, vol. 38, pp. 809-812, April 1974.
- [200] _____, Fund. and Appl. Laser Phys. (Proceedings of the Esfahan Symposium 29 August to 5 September 1971), M. S. Feld, A. Javan, and N. A. Kurnit, eds., New York: John Wiley, 1973, p. 17.
- [201] L. A. Rivlin, "Antimatter as a source of negative-temperature states", Sov. J. Quantum Electron., vol. 4, p. 1151, March 1975.
- [202] R. H. Milburn, "Electron scattering by an intense polarized photon field", Phys. Rev. Lett., vol. 10, pp. 75-77, 1 February 1963.
- [203] F. R. Arutyunian and V. A. Tumanian, "The Compton effect on relativistic electrons and the possibility of obtaining high energy beams", Phys. Lett., vol. 4, pp. 176-178, 1 April 1963.
- [204] R. H. Pantell, G. Soncini, and H. E. Putoff, "Stimulated photo-electron scattering", IEEE J. Quantum Electron., vol. QE-4, pp. 905-907, November 1968.

- [205] A. G. Molchanov, "Lasers in the vacuum ultraviolet and in the x-ray regions of the spectrum", Sov. Phys.-Usp., vol. 15, pp. 124-129, July-Aug. 1972.
- [206] P. Jaeglé, G. Jamelot, A. Carillon, A. Sureau, and P. Dhez, "Super-radiant line in the soft-x-ray range", Phys. Rev. Lett., vol. 33, pp. 1070-1073, Oct. 1974.
- [207] A. Carillon, G. Jamelot, A. Sureau, and P. Jaeglé, "Autoionizing series in the Al^{3+} ion spectrum of a laser-produced plasma", Phys. Lett., vol. 38A, pp. 91-92, 17 January 1972.
- [208] F. P. J. Valero, "Intensity anomalies in the extreme VUV spectrum of Al^{3+} obtained in a laser-produced plasma", Appl. Phys. Lett., vol. 25, pp. 64-66, 1 July 1974; see also, K. N. Koshelev and S. S. Churilov, "A possible interpretation of the observed superradiance in the spectra of Al IV ions in the plasma of laser jet", Sov. J. Quantum Electron., vol. 5, pp. 400-402, April 1975.
- [209] W. T. Silfvast, J. M. Green and O. R. Wood, II, "Population inversions and the measurement of gain in laser-produced plasmas", Phys. Rev. Lett., vol. 35, pp. 435-438, August 1975.
- [210] K. Das Gupta, "Non-linear increase in Bragg peak and narrowing of x-ray lines", Phys. Lett., vol. 46A, pp. 179-180, Dec. 1973.
- [211] K. Das Gupta, "Nondivergent radiation of discrete frequencies in continuous x-ray spectrum", Phys. Rev. Lett., vol. 33, pp. 1415-1418, Dec. 1974.
- [212] P. J. Ebert, "Comments on 'Nondivergent radiation of discrete frequencies in continuous x-ray spectrum'", Bull. Am. Phys. Soc., vol. 20, p. 549, April 1975.

- [213] H. Aiginger, E. Unfried, and P. Wobrauschek, "Interpretation of 'Non-divergent radiation of discrete frequencies in continuous x-ray spectrum'", Phys. Rev. Lett., vol. 35, pp. 815-816, 22 September 1975.
- [214] P. J. Ebert and C. E. Dick, "Comments on the observation of non-divergent radiation of discrete frequencies", Phys. Rev. Lett., vol. 34, pp. 1537-1539, 16 June 1975.
- [215] J. G. Kepros, E. M. Eyring, and F. W. Cagle, Jr., "Experimental evidence of an x-ray laser", Proc. Natl. Acad. Sci., USA, vol. 69, pp. 62-63, July 1972.
- [216] J. G. Kepros, private communication, 1972.
- [217] K. W. Billman and H. Mark, "Cautionary note concerning the CuSO_4 x-ray laser", Appl. Opt., vol. 12, pp. 2529-2531, Nov. 1973.
- [218] R. C. Elton, L. J. Palumbo, R. A. Andrews, R. C. Eckardt, and J. N. Bradford, "Further evidence of collimated x-ray emission from CuSO_4 doped gelatin", Appl. Opt., vol. 12, p. 155, Jan. 1973.
- [219] J. N. Bradford, R. C. Elton, T. N. Lee, R. A. Andrews, L. J. Palumbo, and R. C. Eckardt, "Further comments on collimated x-ray emission from laser-heated CuSO_4 -doped gelatin", Appl. Opt., vol. 12, pp. 1095-1096, June 1973.
- [220] S. G. Dinev and I. V. Tomov, "Further results concerning x-ray collimated emission from CuSO_4 doped targets", Opto-Electronics, vol. 6, pp. 197-198, March 1974.
- [221] P. D. Rowley and K. W. Billman, "Experimental attempts to confirm x-ray lasing from CuSO_4 ", Appl. Opt., vol. 13, pp. 453-455, March 1974.

- [222] J. Rasmussen, Technical University of Denmark, private communication, 1973; see also [225].
- [223] T. A. Boster, "Some questions on the evidence of laser x-ray emission from CuSO_4 doped gelatin", Appl. Opt., vol. 12, pp. 433-434, Feb. 1973.
- [224] K. E. Siegenthaler, H. Weichel, A. C. Saxman, R. D. Wick, and A. H. Guenther, Appl. Opt., vol. 12, pp. 2005-2006, Sept. 1973.
- [225] J. G. Kepros, "Theoretical model explaining some aspects of the Utah x-ray laser experiments", Appl. Opt., vol. 13, pp. 695-696, April 1974.
- [226] A. J. DeMaria, W. H. Glenn, Jr., M. J. Brienza, and M. E. Mack, "Pico-second laser pulses", Proc. IEEE, vol. 57, pp. 2-25, Jan. 1969.
- [227] P. W. Smith, "Mode-locking of lasers", Proc. IEEE, vol. 58, pp. 1342-1357, Sept. 1970.
- [228] W. T. Silfvast and O. R. Wood II, "A 3400 Å p-terphenyl dye laser pumped by a CO_2 -laser-produced plasma", Appl. Phys. Lett., vol. 26, pp. 447-449, 15 April 1975.
- [229] R. W. Waynant, "A traveling wave vacuum ultraviolet laser", Proc. Electro-Optical Systems Design Conference, Anaheim, CA, 1971, pp. 1-5.
- [230] L. Casperson and A. Yariv, "Pulse propagation in a high-gain medium", Phys. Rev. Lett., vol. 26, pp. 293-295, 8 February 1971.
- [231] G. Chapline and L. Wood, "X-ray lasers", Phys. Today, vol. 28, pp. 40-48, June 1975.
- [232] H. H. Fleischmann, "High-current electron beams", Phys. Today, vol. 28, pp. 34-43, May 1975.
- [233] R. W. Waynant, "A transverse traveling-wave electron beam pump for short wavelength lasers", Conf. Laser Engr. Applic. Digest, Washington, D.C., 1973, p. 28.

- [234] S. Humphries, J. J. Lee, and R. N. Sudan, "Generation of intense pulsed ion beams", Appl. Phys. Lett., vol. 25, pp. 20-22, 1 July 1974.
- [235] M. A. Duguay and A. Savage, "Picosecond optical sampling oscilloscope", Opt. Commun., vol. 9, pp. 212-215, October 1973.
- [236] C. F. McConaghy and L. W. Coleman, "Picosecond x-ray streak camera", Appl. Phys. Lett., vol. 25, pp. 268-270, 1 September 1974.
- [237] J. F. Ward and G. H. C. New, "Optical third harmonic generation in gases by a focused laser beam", Phys. Rev., vol. 185, pp. 57-72, 5 September 1969.
- [238] S. E. Harris and R. B. Miles, "Proposed third-harmonic generation in phase-matched metal vapors", Appl. Phys. Lett., vol. 19, pp. 385-387, Nov. 1971.
- [239] J. A. Armstrong, N. Bloembergen, J. Ducuing and P. S. Pershan, "Interactions between light waves in a nonlinear dielectric", Phys. Rev., vol. 127, pp. 1918-1939, 15 Sept. 1962.
- [240] R. B. Miles and S. E. Harris, "Optical third-harmonic generation in alkali metal vapors", IEEE J. Quantum Electron., vol. QE-9, pp. 470-484, April 1973.
- [241] P. P. Bey, J. F. Giuliani, and H. Rabin, "Generation of a phase-matched optical third harmonic by introduction of anomalous dispersion into a liquid medium", Phys. Rev. Lett., vol. 19, pp. 819-821, 9 October 1967.
- [242] J. F. Young, G. C. Bjorklund, A. H. Kung, R. B. Miles, and S. E. Harris, "Third-harmonic generation in phase-matched Rb vapor", Phys. Rev. Lett., vol. 27, pp. 1551-1553, Dec. 1971.

- [243] A. H. Kung, J. F. Young, G. C. Bjorklund, and S. E. Harris, "Generation of vacuum ultraviolet radiation in phase-matched Cd vapor", Phys. Rev. Lett., vol. 29, pp. 985-988, 9 October 1972.
- [244] D. M. Bloom, G. W. Bekkers, J. F. Young, and S. E. Harris, "Third harmonic generation in phase-matched alkali metal vapors", Appl. Phys. Lett., vol. 26, pp. 687-689, 15 June 1975.
- [245] D. M. Bloom, J. F. Young, and S. E. Harris, "Mixed metal vapor phase matching for third-harmonic generation", Appl. Phys. Lett., vol. 27, pp. 390-392, 1 October 1975.
- [246] A. H. Kung, J. F. Young, and S. E. Harris, "Generation of 1182 Å radiation in phase-matched mixtures of inert gases", Appl. Phys. Lett., vol. 22, pp. 301-302, 15 March 1973.
- [247] R. T. Hodgson, P. P. Sorokin, and J. J. Wynne, "Tunable coherent vacuum-ultraviolet generation in atomic vapors", Phys. Rev. Lett., vol. 32, pp. 343-346, Feb. 1974.
- [248] J. A. Armstrong and J. J. Wynne, "Autoionizing states of Sr studied by the generation of tunable vacuum uv radiation", Phys. Rev. Lett., vol. 33, pp. 1183-1185, 11 November 1974.
- [249] S. E. Harris and D. M. Bloom, "Resonantly two-photon pumped frequency converter", Appl. Phys. Lett., vol. 24, pp. 229-230, 1 March 1974.
- [250] D. M. Bloom, J. T. Yardley, J. F. Young, and S. E. Harris, "Infrared up-conversion with resonantly two-photon pumped metal vapors", Appl. Phys. Lett., vol. 24, pp. 427-428, 1 May 1974.
- [251] A. H. Kung, "Generation of tunable picosecond VUV radiation", Appl. Phys. Lett., vol. 25, pp. 653-654, 1 Dec. 1974.

- [252] G. C. Bjorklund, "Effects of focusing on third-order nonlinear processes in isotropic media", IEEE J. Quantum Electron., vol. QE-11, pp. 287-296, June 1975.
- [253] S. E. Harris, "Generation of vacuum-ultraviolet and soft-x-ray radiation using high-order nonlinear optical polarizabilities", Phys. Rev. Lett., vol. 31, pp. 341-344, 6 August 1973.
- [254] S. E. Harris, J. F. Young, A. H. Kung, D. M. Bloom and G. C. Bjorklund, "Generation of ultraviolet and vacuum ultraviolet radiation", in Laser Applications to Optics and Spectroscopy, S. F. Jacobs, M. Sargent III, J. F. Scott, and M. O. Scully, eds., Reading, Mass: Addison Wesley, 1975, vol. 2, pp. 181-197.
- [255] P. Eiserberger and S. L. McCall, "X-ray parametric conversion", Phys. Rev. Lett., vol. 26, pp. 684-688, 22 March 1971.
- [256] P. M. Eisenberger and S. L. McCall, "Mixing of x-ray and optical photons", Phys. Rev. A, vol. 3, pp. 1145-1151, March 1971.
- [257] S. E. Harris and D. B. Lidow, "Nonlinear optical processes by Van der Waals interaction during collision", Phys. Rev. Lett., vol. 33, pp. 674-676, 16 September 1974.
- [258] { A. Ferguson, "How to make an x-ray laser", New Scientist, vol. 67, pp. 207-209, 23 October 1975.
- [255] D. E. Eastman and M. I. Nathan, "Photoelectron spectroscopy", Phys. Today, vol. 28, pp. 44-51, April 1975.
- [260] H. D. Jones, D. Eccleshell, and J. K. Temperley, Propagation Characteristics of Narrow X-Ray Pulses, U. S. Army Ballistic Research Laboratory Report No. 1781, May 1975.

- [261] R. Hofstadter, The Atomic Accelerator, Stanford University High Energy Physics Laboratory Report No. 560, 23 April 1968.
- [262] P. V. Lenzo and E. G. Spencer, "High-speed low-power x-ray lithography", Appl. Phys. Lett., vol. 24, pp. 289-291, 15 March 1974.
- [263] T. Zehnpfennig, R. Giacconi, R. Haggerty, W. Reidy and G. Vaiana, A Laboratory Program to Develop Improved Grazing Incidence X-Ray Optics, National Aeronautics and Space Administration Report No. NASA-CR-717, February 1967.
- [264] A. V. Baez, "Fresnel zone plate for optical image formation using extreme ultraviolet and soft x-radiation", J. Opt. Soc. Am., vol. 51, pp. 405-412, April 1961.
- [265] C. D. Pfeifer, L. D. Ferris and W. M. Yen, "Optical image formation with a Fresnel zone plate using vacuum-ultraviolet radiation", J. Opt. Soc. Am., vol. 63, pp. 91-95, January 1973.
- [266] B. Niemann, D. Rudolph and G. Schmahl, "Soft x-ray imaging zone plates with large zone numbers for microscopic and spectroscopic applications", Opt. Commun., vol. 12, pp. 160-163, October 1974.
- [267] E. Spiller and A. Segmüller, "Propagation of x-rays in waveguides", Appl. Phys. Lett., vol. 24, pp. 60-61, 15 January 1974.
- [268] G. C. Bjorklund, S. E. Harris, and J. F. Young, "Vacuum ultraviolet holography", Appl. Phys. Lett., vol. 25, pp. 451-452, 15 October 1974.

FIGURE CAPTIONS

Fig. 1. Short wavelength transmission cutoff versus temperature for various optical materials [58].

Fig. 2. Simplified drawing of the puckered ring resonator [62].

Fig. 3. X-ray resonator cut from a single crystal [63]. The arrows show x-rays entering and exiting the resonator.

Fig. 4. X-ray resonator and possible amplifier using several Bragg reflections [64].

Fig. 5. Schematic defining nomenclature of the simple three-energy-state system referred to in the text and originally defined in [86]. Pumping occurs from state 1 to 2; lasing from 2 to 3; and losses from 2 to n and lower state depopulation from 3 to m . Replenishment of state 1 can occur for $n = 1$, $m = 1$ or through m to 1 transitions.

Fig. 6. Output intensity versus length for three different inversion densities when the system is operated with a resonator (laser) and without a resonator (ASE) [85].

Fig. 7. Spectral distribution versus length as calculated by Allen and Peters for an ASE system. Deviations from the earlier theory of Yariv and Leite are shown for several values of K_3 , a term in the numerical calculation. The case of $K_3 = 0$ is that of no saturation whereas $K_3 \neq 0$ is that of some saturation of the amplifier [85].

Fig. 8. Estimates of line widths for $K\alpha$ type transitions versus wavelength λ , with natural ($\Delta\lambda_N$), Doppler ($\Delta\lambda_D$) and Stark ($\Delta\lambda_S$) effects included. The decrease in natural broadening with ionization is indicated by circles for neon; and hydrogenic and helium-like ionic species are included [96].

Fig. 9. Mean particle densities (solid and dashed lines) versus wavelength for selected pumping mechanisms and for a gain factor of $\alpha=5$ ($\alpha=0.1$ for ion beams). Stark broadening becomes important for large charged particle densities (same scale) in the region above the dotted line, also a region of approaching collisional equilibrium. Collisional recombination is plotted for fixed $N_e=10^{21} \text{ cm}^{-3}$ and terminates at $\sim 15 \text{ \AA}$ due to dominance of radiative recombination to lower levels [106].

Fig. 10. Time dependence $T(t)$ of inversion density ΔN_{23} for the fast rise pumping case. Positive values indicate net gain; negative values loss. For R_{2n} small, $\tau_2 \approx R_{23}^{-1}$, the laser transition upper-state lifetime. The $G = 0$ case is also the case for self-depleting final laser states where $R_{3m} \gg R_{23} + R_{2n}$ [86].

Fig. 11. Time dependence $T(t)$ of the inversion density, ΔN_{23} , for the fast-rise pumping case and for $G=1$ only. Positive values indicate net gain; negative values loss. For R_{2n} small, $\tau_2 \approx R_{23}^{-1}$, the laser transition upper state lifetime. The effect of a lower laser state depletion rate R_{3m} exceeding τ_2^{-1} on the steady state inversion density is indicated for long times.

Fig. 12. Simplified potential energy versus internuclear distance of several molecules. Both nitrogen (a) and hydrogen (b) are stable molecules; xenon (c), however, has no stable ground state and exists as a molecule only in the excited state.

Fig. 13. Schematic energy level diagram for carbon-like ion species. Collisional excitations are designated by C, radiative decays by A, ionization by I, and collisional depopulation by D. Competing collisional depopulation to the 3d level is indicated.

Fig. 14. Minimum length L_{\min} for amplification in carbon-like ions with a gain of $\exp(\alpha L)$ versus atomic number Z , wavelength λ , and ion kinetic temperature kT_i . The electron temperature T_e is assumed equal to $10 T_i$ and is plotted. The electron density $(N_e)_{\max}$ at which collisional mixing becomes important is also plotted [105].

Fig. 15. Minimum length, L_{\min} , for amplification in carbon-like ions with a gain of $\exp(\alpha L)$ versus atomic number Z , wavelength λ , and ion kinetic temperature kT_i . The electron temperature T_e is assumed equal to T_i . The electron density $(N_e)_{\max}$ at which collisional mixing becomes important is also plotted [105].

Fig. 16. Gain coefficient in cm^{-1} calculated from a steady state model for the $3^1S \rightarrow 2^1P$ transition in helium-like ions. The electron density, N_e , was chosen to be 10^{21} cm^{-3} for efficient plasma heating by $1.06 \mu\text{m}$ lasing radiation. Curves are shown for the highest temperature range expected for state-of-the-art laser-produced plasmas. At values of $Z < 11$, the calculational results show a negative inversion density ΔN due to collisional mixing of the upper and lower laser levels; the decrease in gain at higher Z is caused by a small ΔN resulting from a larger energy gap for pumping from the ground state [136].

Fig. 17. Resonance charge transfer cross section from s-Landau-Zener theory versus scaled relative velocity V_{rel} for the atom-ion combination (data adapted from [162]). ΔE represents the energy defect in eV for the exothermic reaction, z the effective charge of the ion. Velocities for the ions designated are assumed thermal and the kinetic temperature was chosen as one-fourth of the ionization potential for creating the ion [106].

Fig. 18. Schematic diagram of exothermic s-s resonance charge transfer reaction leading to a quasi-stationary population inversion between $n = 3$ and $n = 2$ levels in certain helium-like or hydrogenic ions [106]. Refer to Fig. 19 for other possible ion/atom combinations. E_B is the binding energy.

Fig. 19. Resonance charge transfer cross section obtained by inversion of Fig. 17 data [106]. Final quantum states n of high capture probability for each ion, I^{m+} , and atom, A, combination are indicated by numerals, with parentheses to indicate less probable transitions. ΔE is the exothermic energy defect and z is the effective ion charge.

Fig. 20. Ratio of rates $R_L/R_{K \rightarrow L}$ for total transitions out of an L vacancy state and radiative decay out of a K vacancy state versus atomic number, Z . This ratio is equivalent to N_2/N_3 for equilibrium conditions reached after long times in cw operation. Values exceeding unity and one-half indicate gain for the $K\alpha_2$ and $K\alpha_1$ transitions, respectively. The model used assumes that only radiative transitions produce absorbers and that Auger transitions generate shifted ion lines. Both the $K \rightarrow L_{II}$ (α_2) and $K \rightarrow L_{III}$ (α_1) transitions are shown [96].

Fig. 21. Nonlinear susceptibility of rubidium as a function of wavelength [240].

Fig. 22. The experimental apparatus used by Kung, et al. to generate vacuum ultraviolet wavelengths by up-conversion [243].

Fig. 23. Schematic of the apparatus used by Hodgson, et al. to produce tunable vacuum-uv emission using Sr vapor [247].

Fig. 24. The ranges of wavelength covered by the tuning methods described by Kung [243] using parametrically generated frequencies and by Hodgson, et al. [247] using tunable dye laser frequencies.

Fig. 25. Useful characteristics of a collimated and coherent laser beam at short wavelengths.

Fig. 26. Fringes produced in polymethyl methacrylate (PMMA) at 836 Å spacing and analyzed with a scanning electron microscope. The round object is a 0.5 μm latex sphere placed after development for magnification calibration [268].

Fig. 27. Record of activity in short wavelength laser research as compiled from the references on this topic in the present review. The data for 1975 are as of October and still incomplete, particularly for those articles not yet translated.

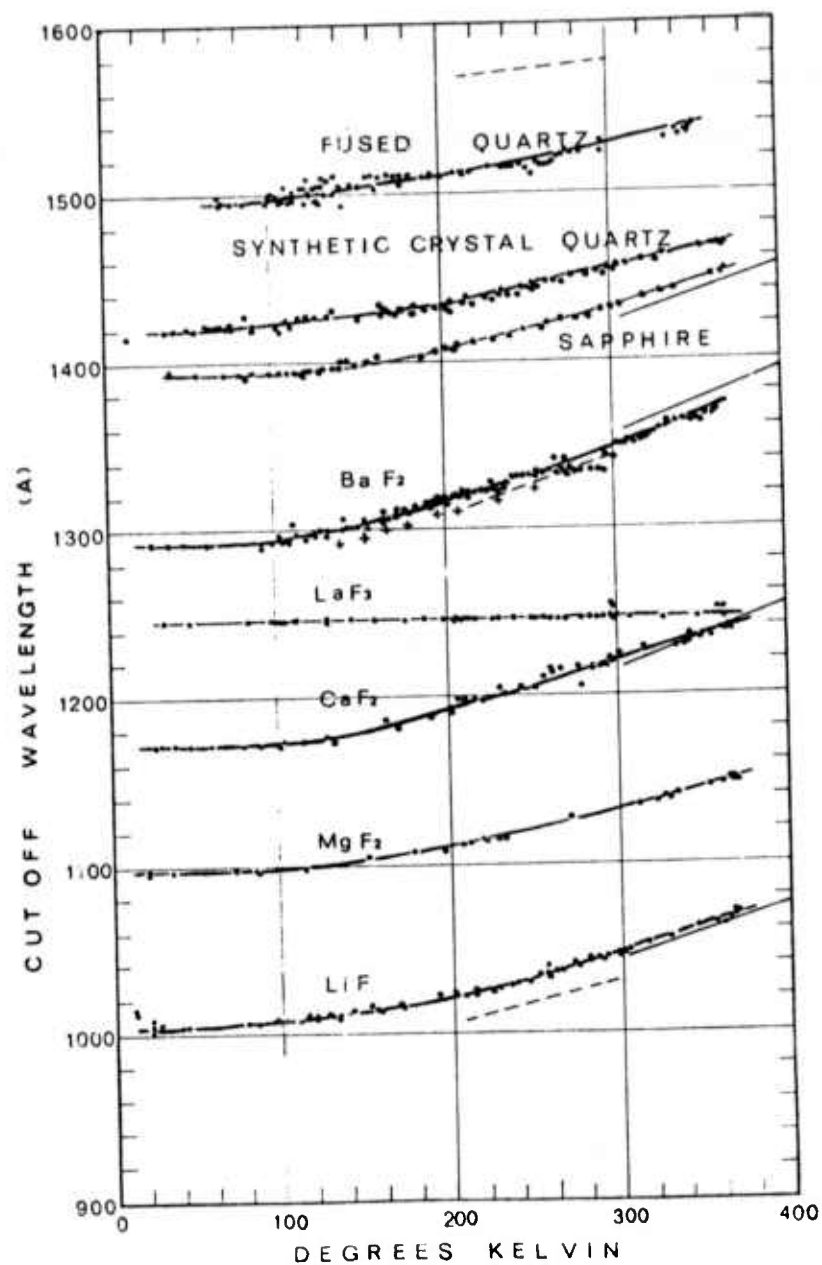


Fig. 1. Short wavelength transmission cutoff versus temperature for various optical materials [58].

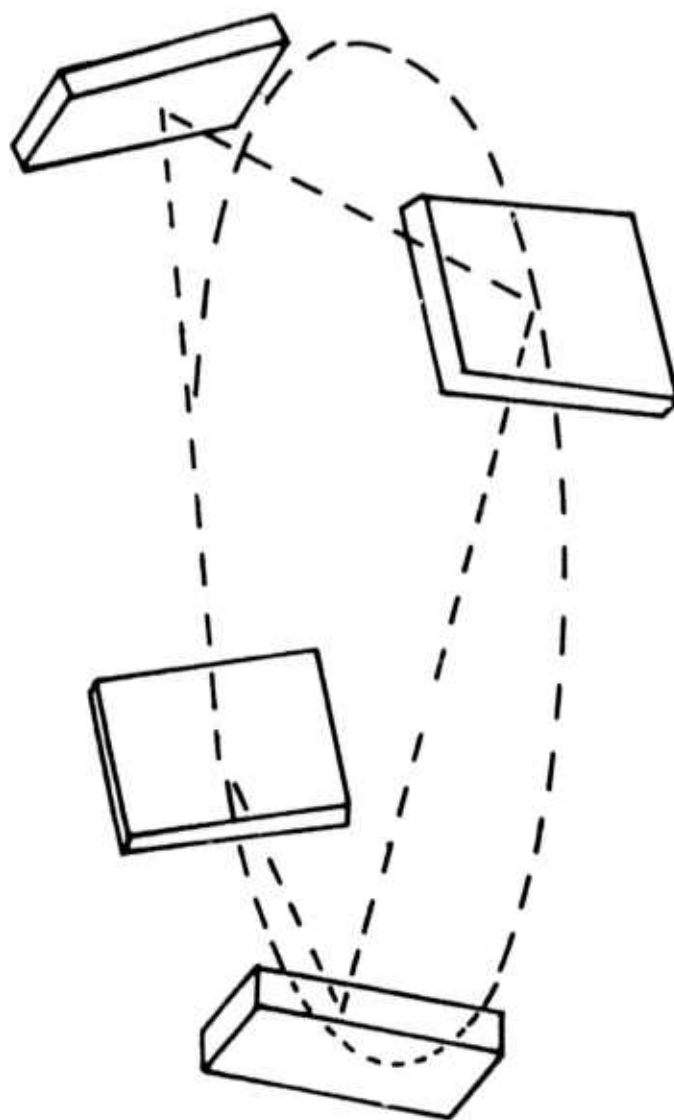


Fig. 2. Simplified drawing of the puckered ring resonator [62].

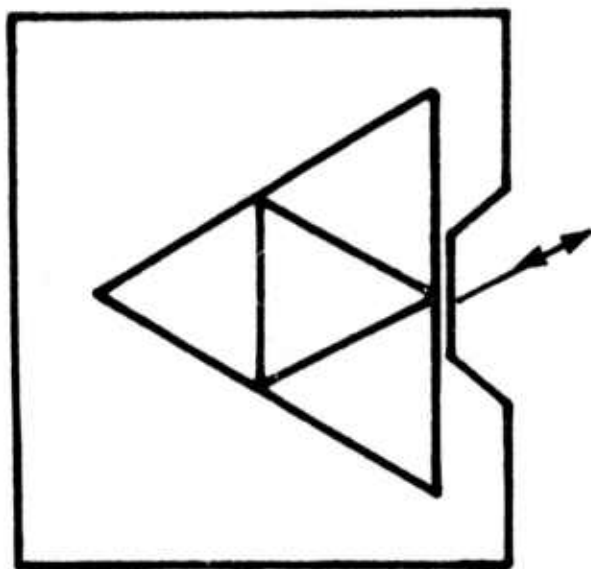


Fig. 3. X-ray resonator cut from a single crystal [63].

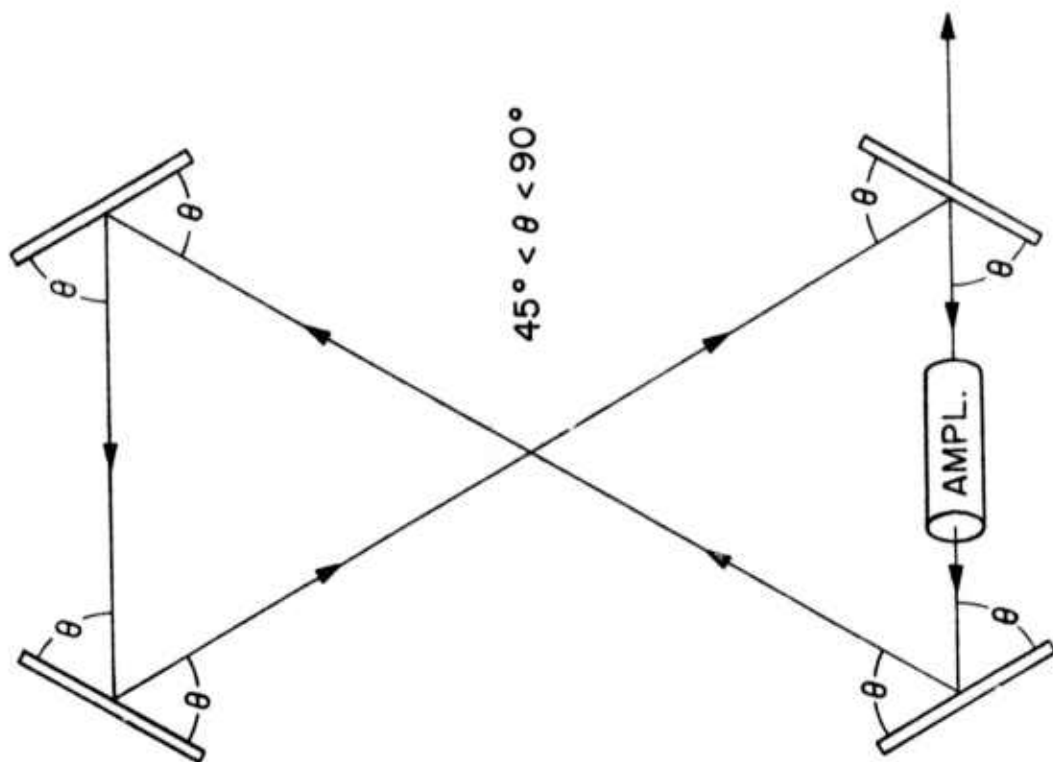


Fig. 4. X-ray resonator and possible amplifier using several Bragg reflections [64].

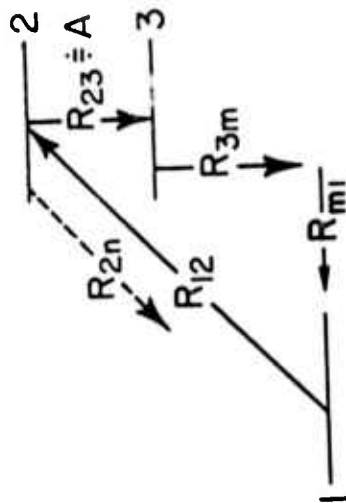


Fig. 5. Schematic defining nomenclature of the simple three-energy-state system referred-to in the text and originally defined in [86]. Pumping occurs from state 1 to 2; lasing from 2 to 3; with losses from 2 to n and lower state depopulation from 3 to 1. Replenishment of state 1 can occur for $n = 1$, $m = 1$ or through m to 1 transitions.

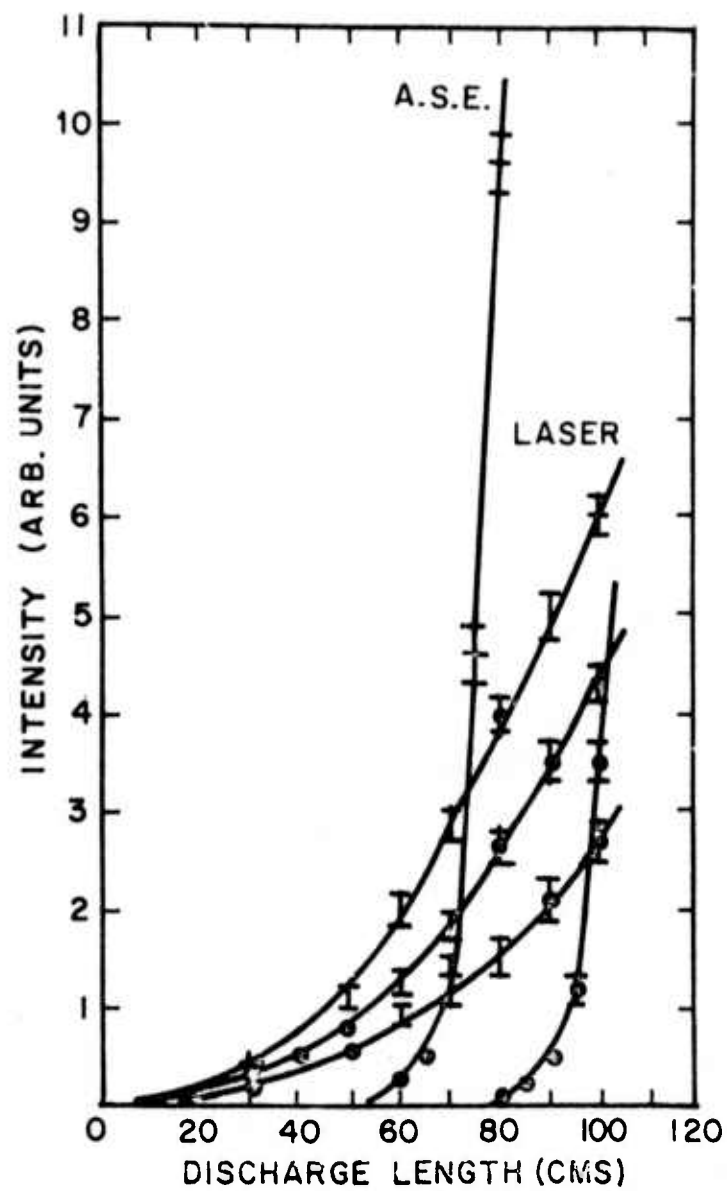


Fig. 6. Output intensity versus length for three different inversion densities when the system is operated with a resonator (laser) and without a resonator (ASE) [85].

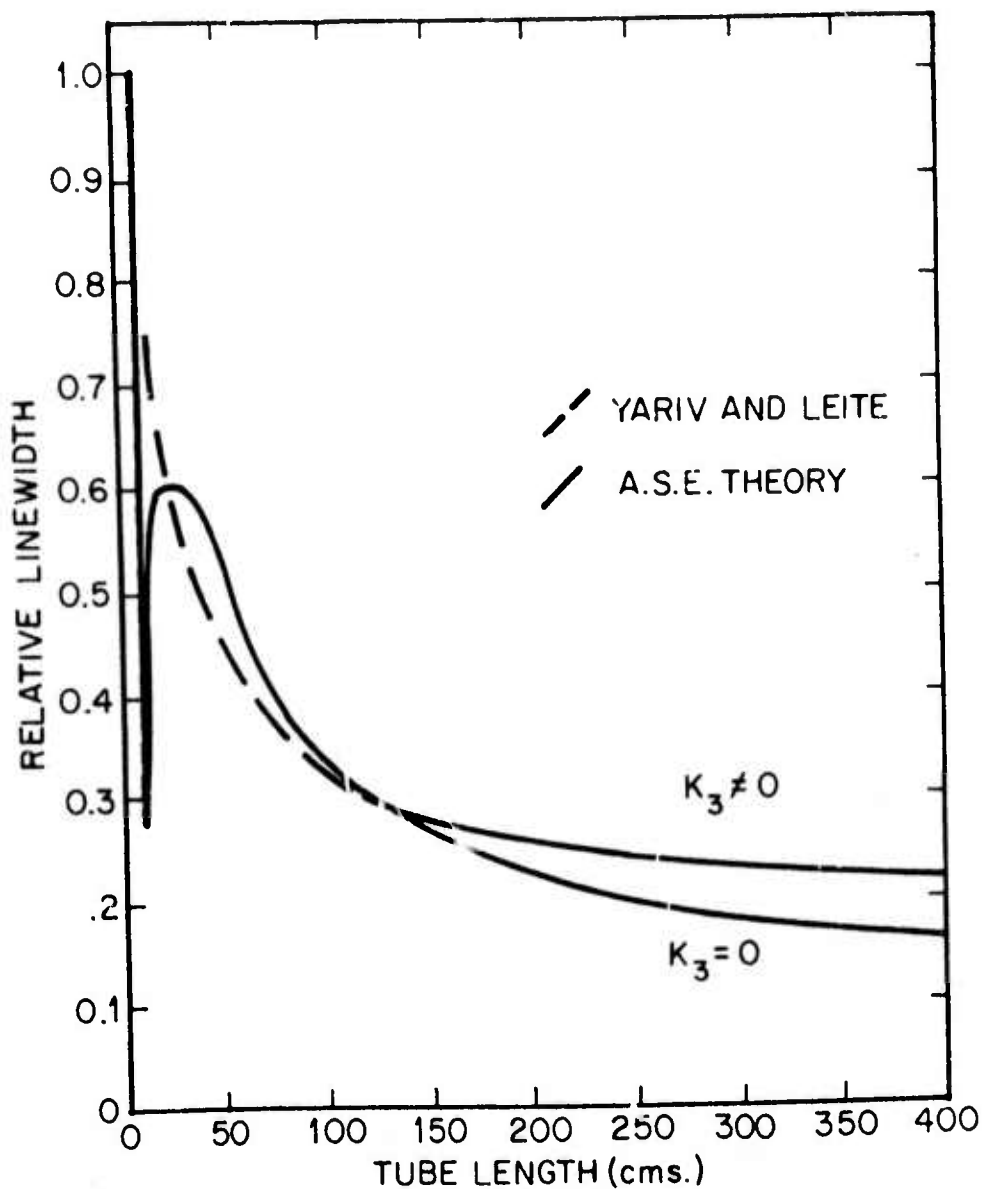


Fig. 7. Spectral distribution versus length as calculated by Allen and Peters for an ASE system. Deviations from the earlier theory of Yariv and Leite are shown for several values of K_3 , a term in the numerical calculation. The case of $K_3 = 0$ is that of no saturation whereas $K_3 \neq 0$ is that of some saturation of the amplifier [85].

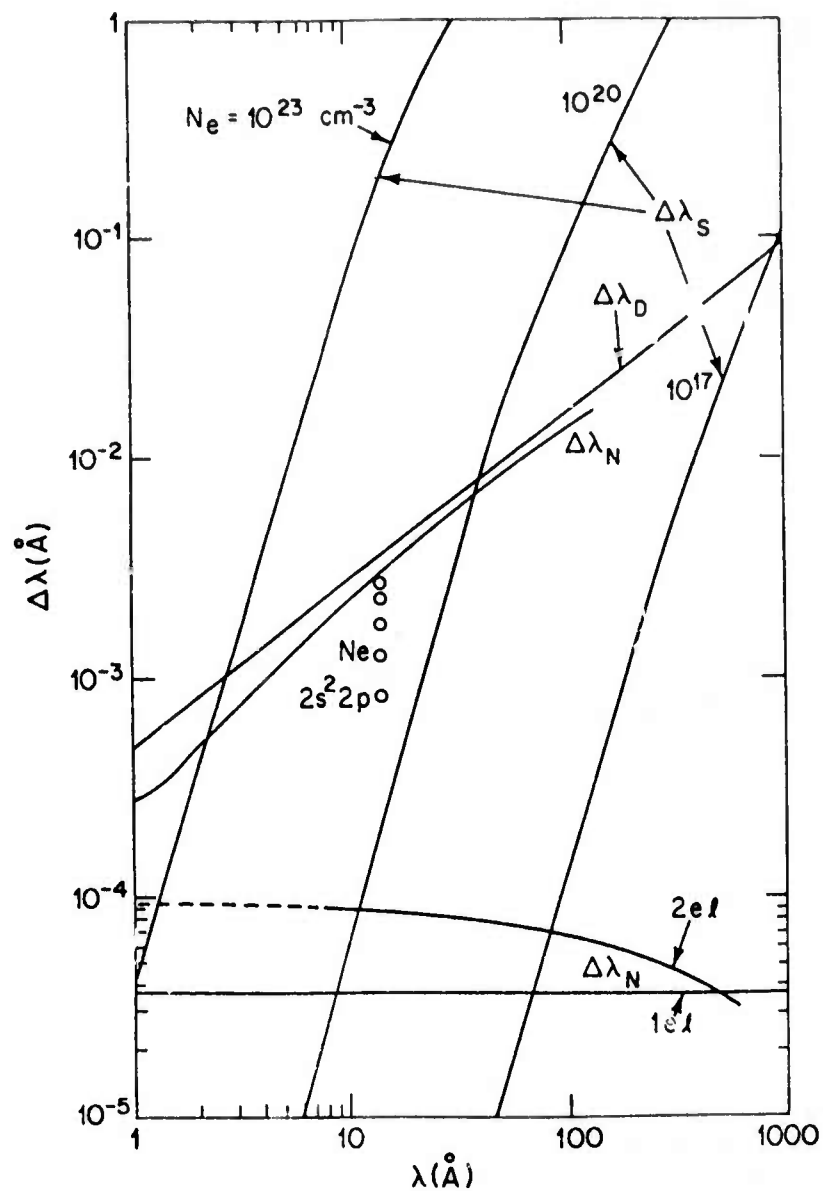


Fig. 8. Estimates of line widths for $K\alpha$ type transitions versus wavelength λ , with natural ($\Delta\lambda_N$), Doppler ($\Delta\lambda_D$) and Stark ($\Delta\lambda_S$) effects included. The decrease in natural broadening with ionization is indicated by circles for neon; and hydrogenic and helium-like ionic species are included [96].

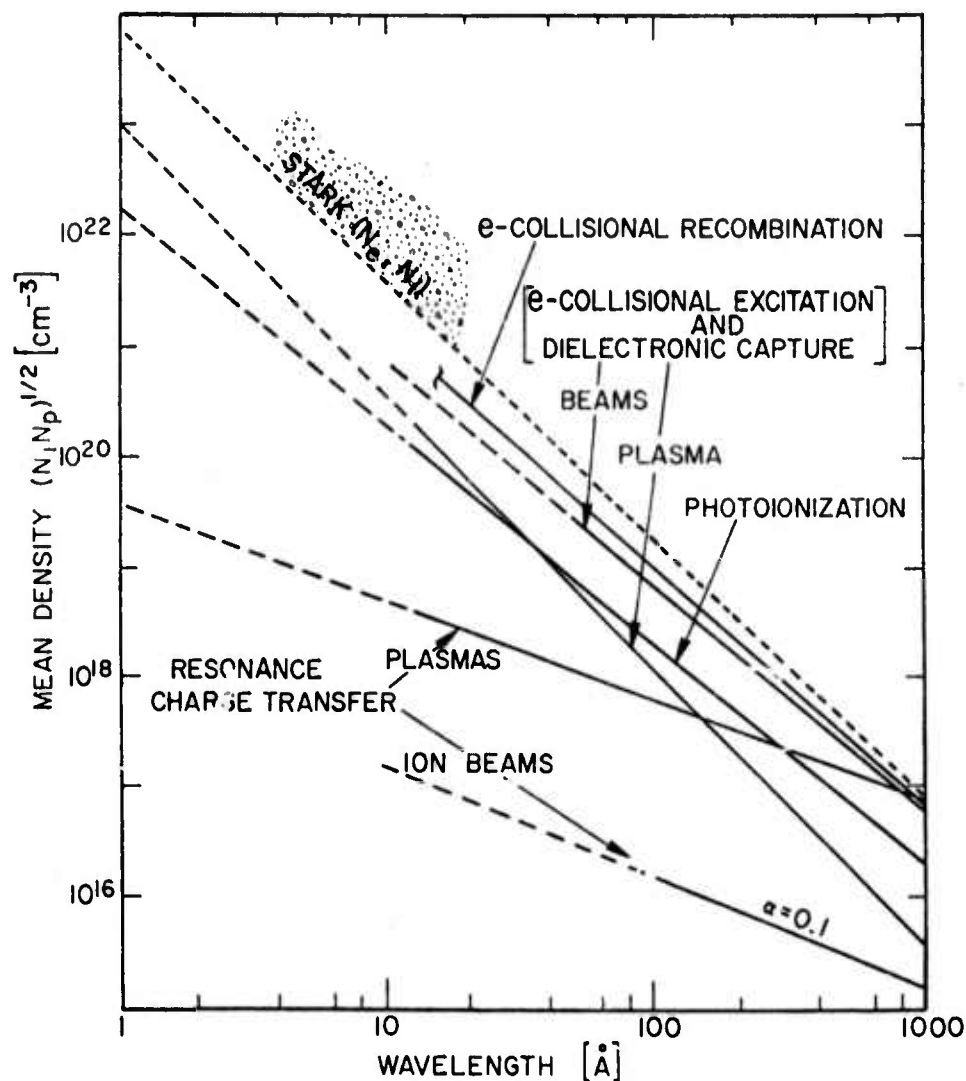


Fig. 9 — Mean particle densities (solid and dashed lines) versus wavelength for selected pumping mechanisms and for a gain factor of $\alpha=5$ ($\alpha=0.1$ for ion beams). Stark broadening becomes important for large charged particle densities (same scale) in the region above the dotted line, also a region of approaching collisional equilibrium. Collisional recombination is plotted for fixed $N_e=10^{21} \text{ cm}^{-3}$ and terminates at $\sim 15 \text{\AA}$ due to dominance of radiative recombination to lower levels [106].

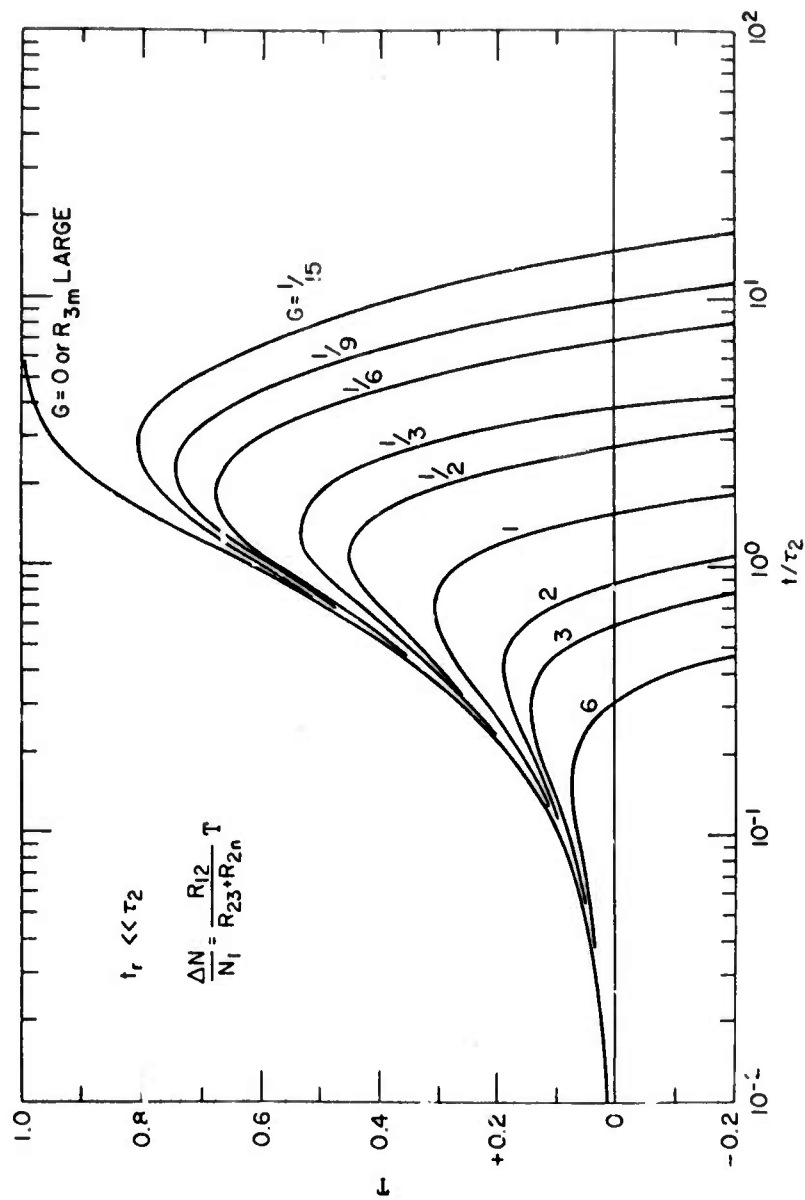


Fig. 10. Time dependence $T(t)$ of inversion density ΔN_{23} for the fast rise pumping case. Positive values indicate net gain; negative values loss. For $R_{2n} \text{ small, } \tau_2 \approx R_{23}$, the laser transition upper-state lifetime. The $G = 0$ case is also the case for self-depleting final laser states where $R_{3m} \gg R_{23} + R_{2n}$ [86].

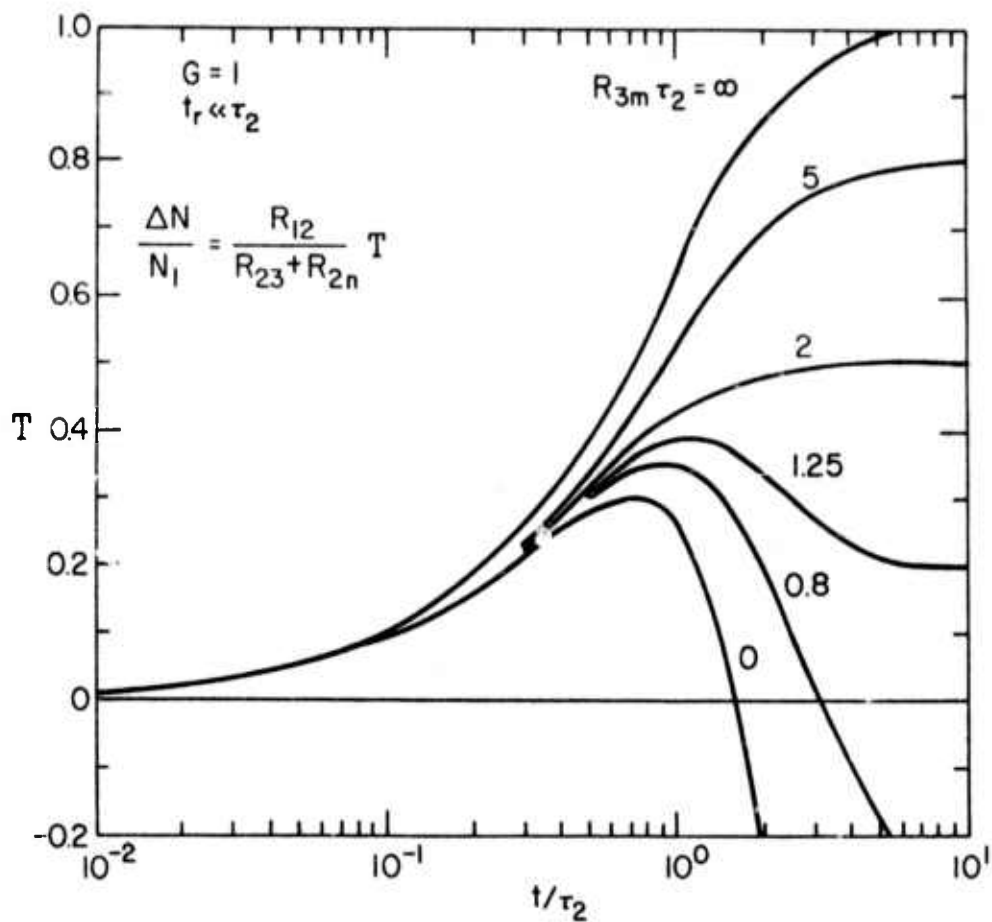


Fig. 11 — Time dependence $T(t)$ of the inversion density, ΔN_{23} , for the fast-rise pumping case and for $G=1$ only. Positive values indicate net gain; negative values loss. For R_{2n} small, $\tau_2 \approx R_{23}^{-1}$, the laser transition upper state lifetime. The effect of a lower state depletion rate R_{3m} exceeding τ_2^{-1} on the steady state inversion density is indicated for long times.

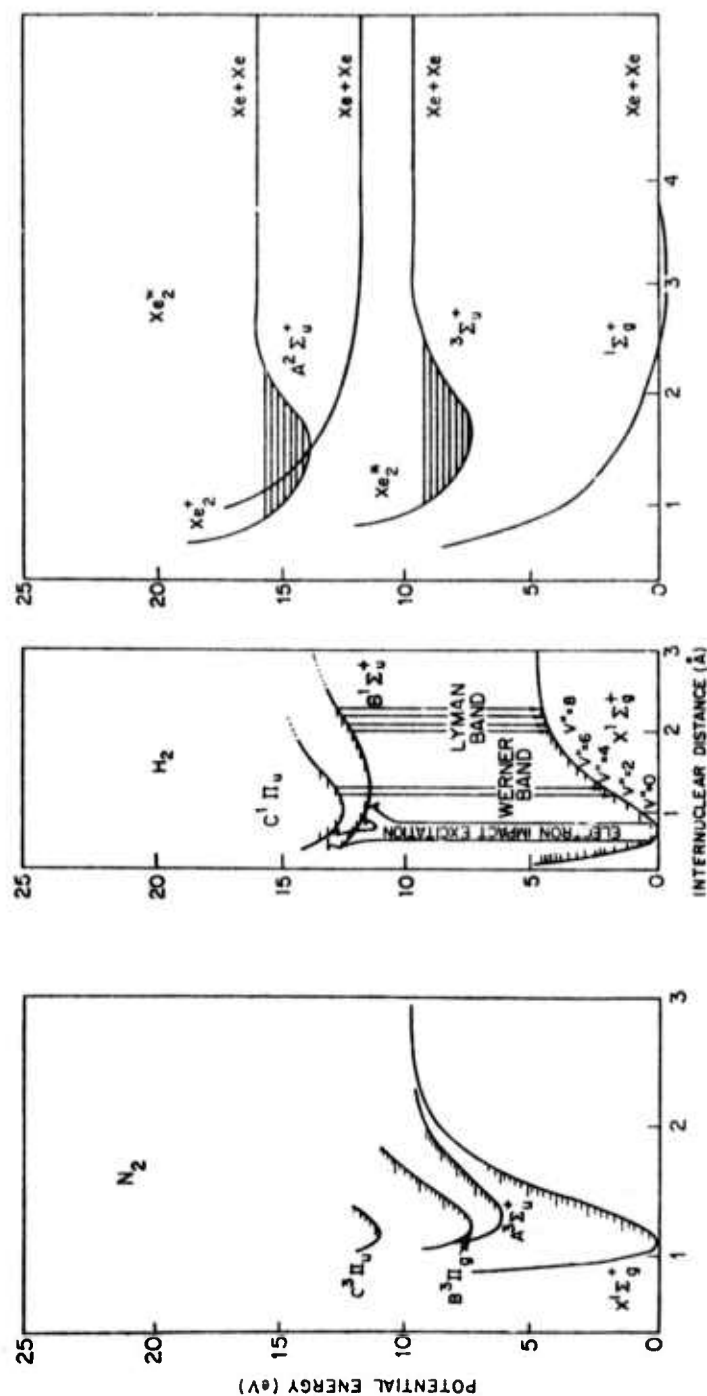


Fig. 12. Simplified potential energy versus internuclear distance of several molecules. Both nitrogen (a) and hydrogen (b) are stable molecules; xenon (c), however, has no stable ground state and exists as a molecule only in the excited state.

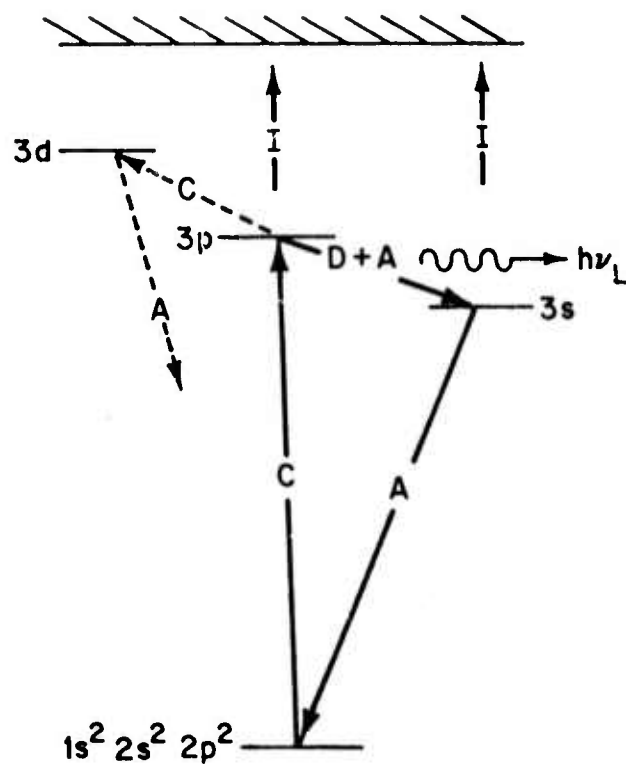


Fig. 13. Schematic energy level diagram for carbon-like ion species. Collisional excitations are designated by C, radiative decays by A, ionization by I, and collisional depopulation by D. Competing collisional depopulation to the 3d level is indicated.

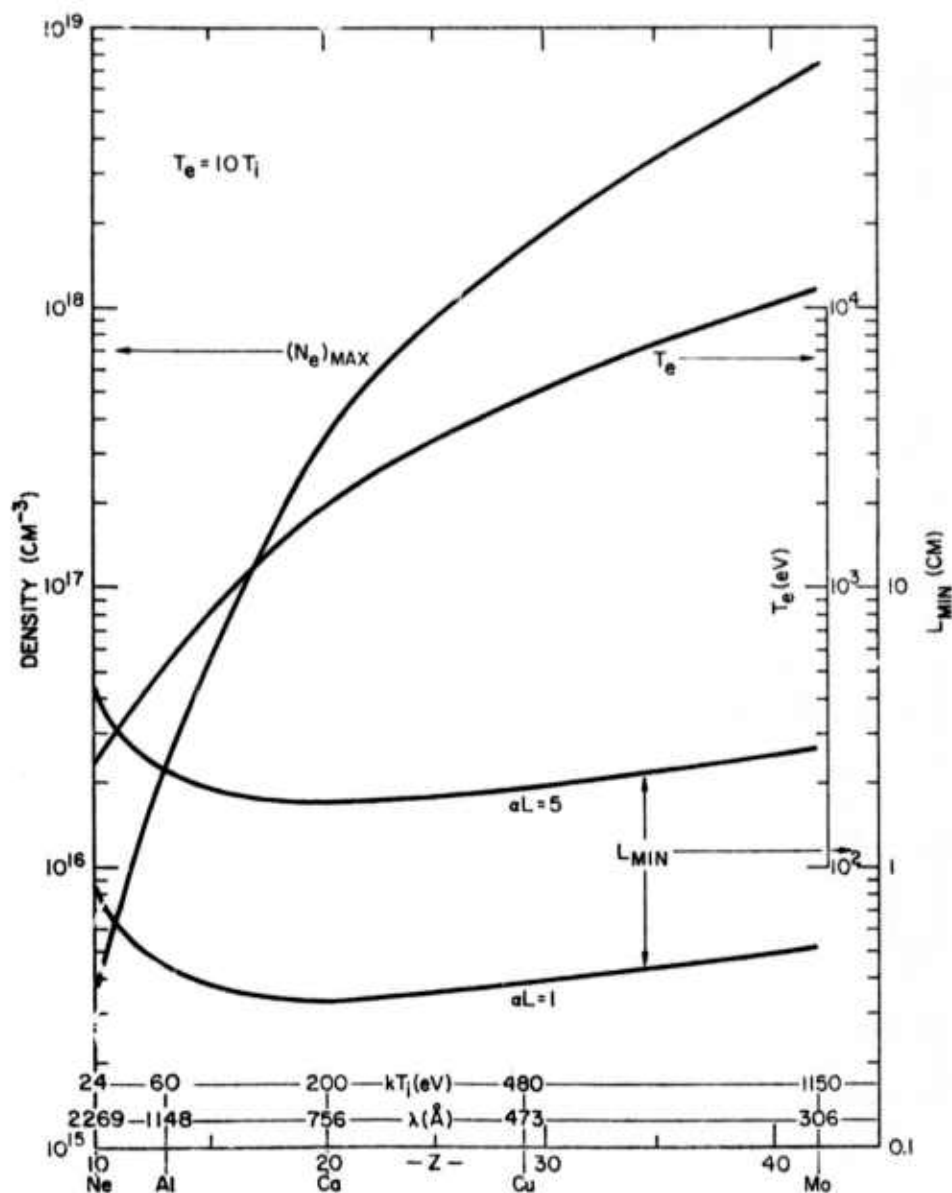


Fig. 14. Minimum length L_{\min} for amplification in carbon-like ions with a gain of $\exp(\alpha L)$ versus atomic number Z , wavelength λ , and ion kinetic temperature kT_i . The electron temperature T_e is assumed equal to $10 T_i$ and is plotted. The electron density $(N_e)_{\text{MAX}}$ at which collisional mixing becomes important is also plotted [105].

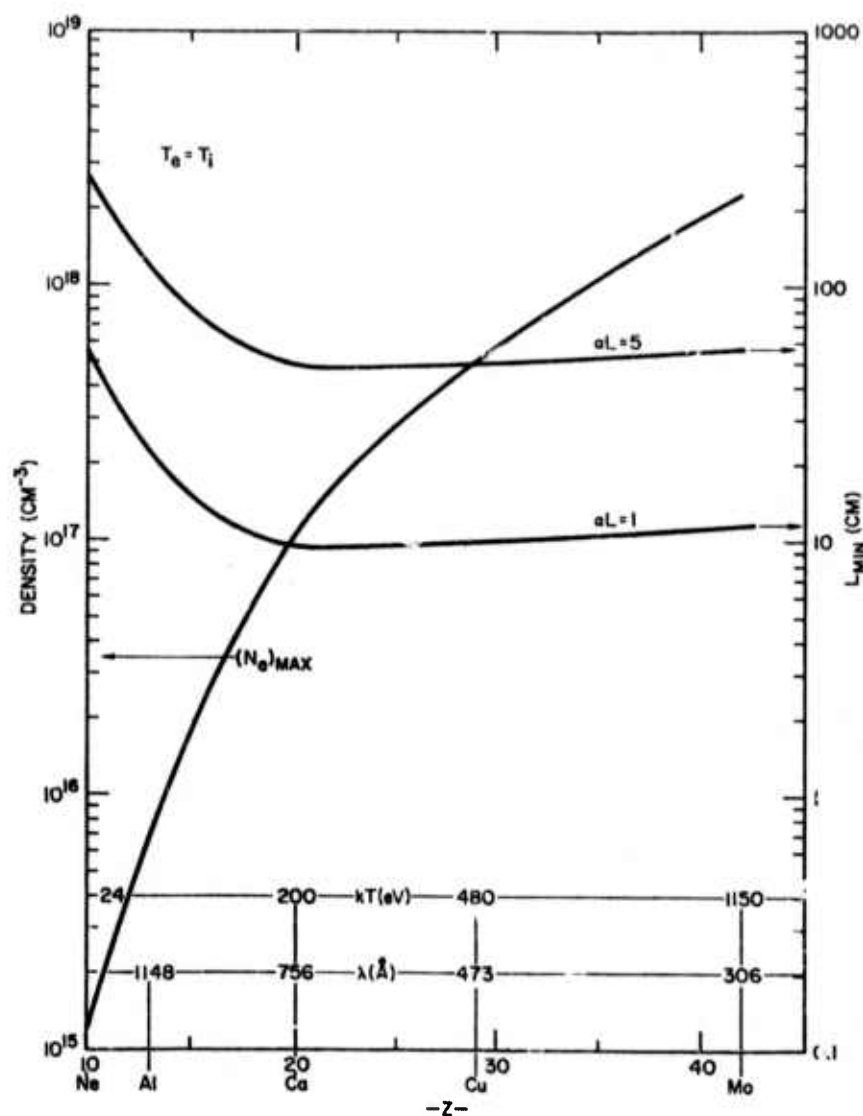


Fig. 15. Minimum length, L_{\min} , for amplification in carbon-like ions with a gain of $e^{\gamma p} (\alpha L)$ versus atomic number Z , wavelength λ , and ion kinetic temperature kT_i . The electron temperature T_e is assumed equal to T_i . The electron density $(N_e)_{\max}$ at which collisional mixing becomes important is also plotted [105].

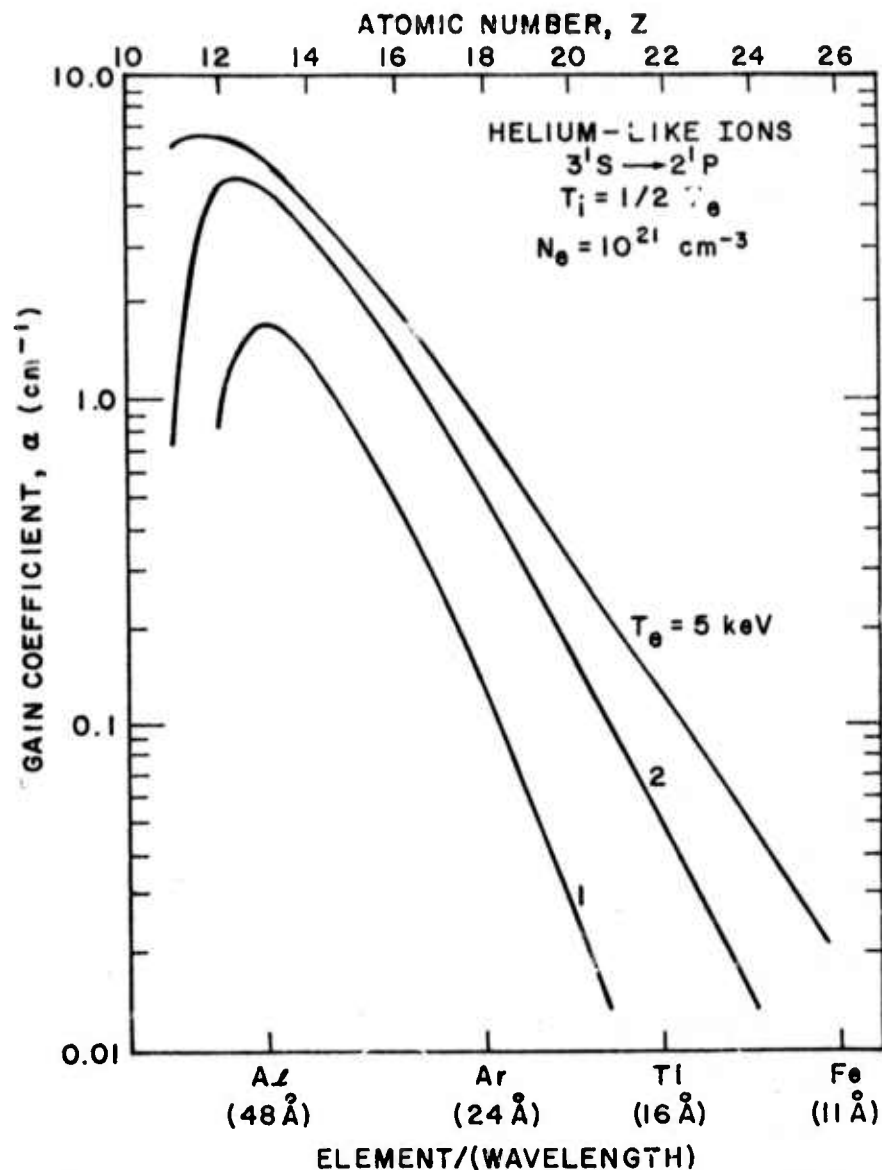


Fig. 16. Gain coefficient in cm^{-1} calculated from a steady state model for the $3^1S \rightarrow 2^1P$ transition in helium-like ions. The electron density, N_e , was chosen to be 10^{21} cm^{-3} for efficient plasma heating by $1.06 \mu\text{m}$ lasing radiation. Curves are shown for the highest temperature range expected for state-of-the-art laser produced plasmas. At values of $Z < 11$, the calculational results show a negative inversion density ΔN due to collisional mixing of the upper and lower laser levels; the decrease in gain at higher Z is caused by a small ΔN resulting from a larger energy gap for pumping from the ground state [136].

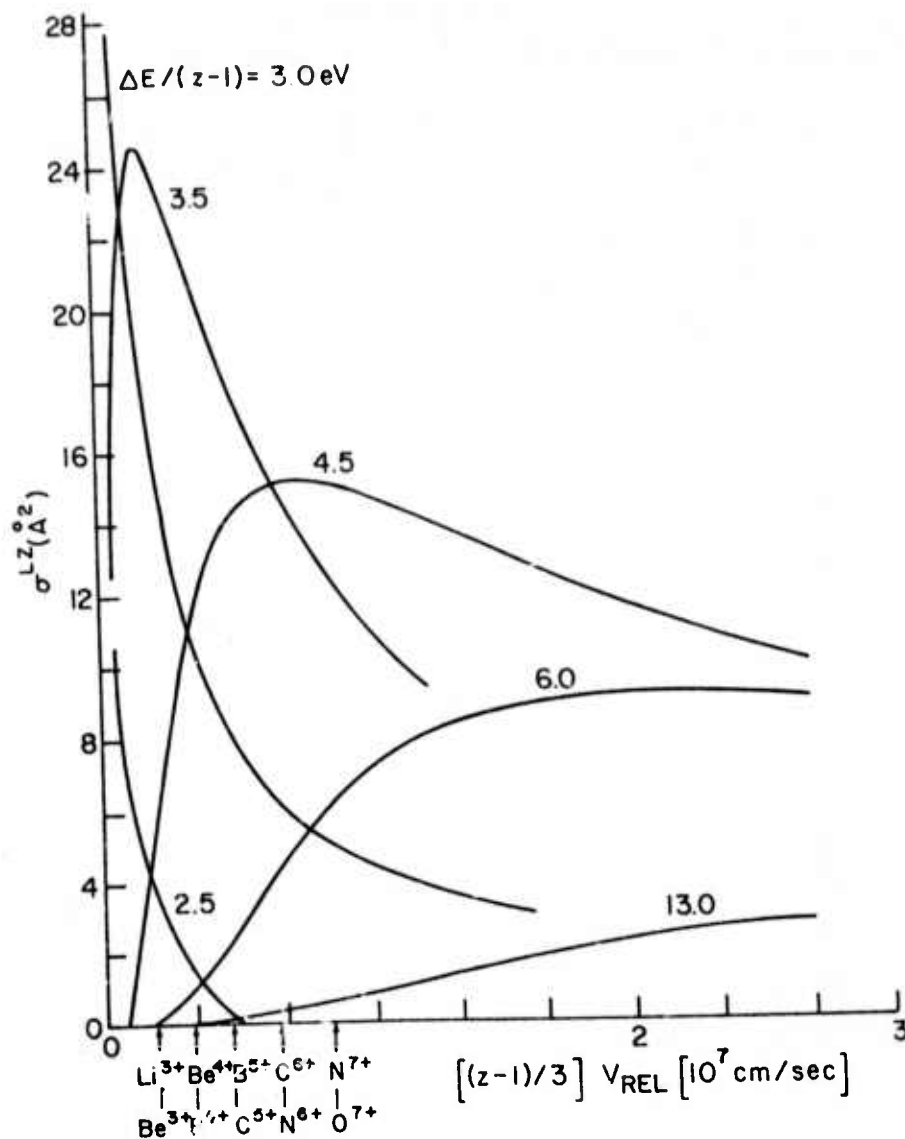


Fig. 17. Resonance charge transfer cross section from s-s Landau-Zener theory versus scaled relative velocity V_{rel} for the atom-ion combination (data adapted from [162]). ΔE represents the energy defect in eV for the exothermic reaction, z the effective charge of the ion. Velocities for the ions designated are assumed thermal and the kinetic temperature was chosen as one-fourth of the ionization potential for creating the ion [106].

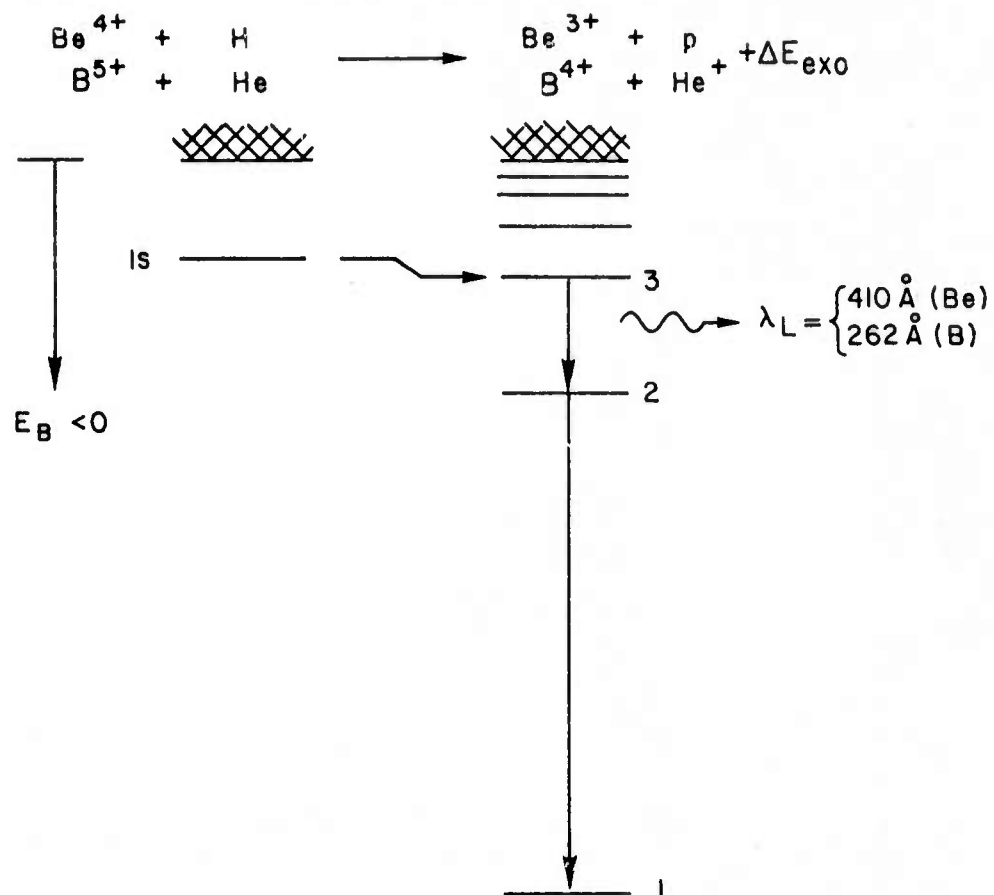


Fig. 18. Schematic diagram of exothermic s-s resonance charge transfer reaction leading to a quasi-stationary population inversion between $n = 3$ and $n = 2$ levels in certain helium-like or hydrogenic ions [106]. Refer to Fig. 19 for other possible ion/atom combinations. E_B is the binding energy.

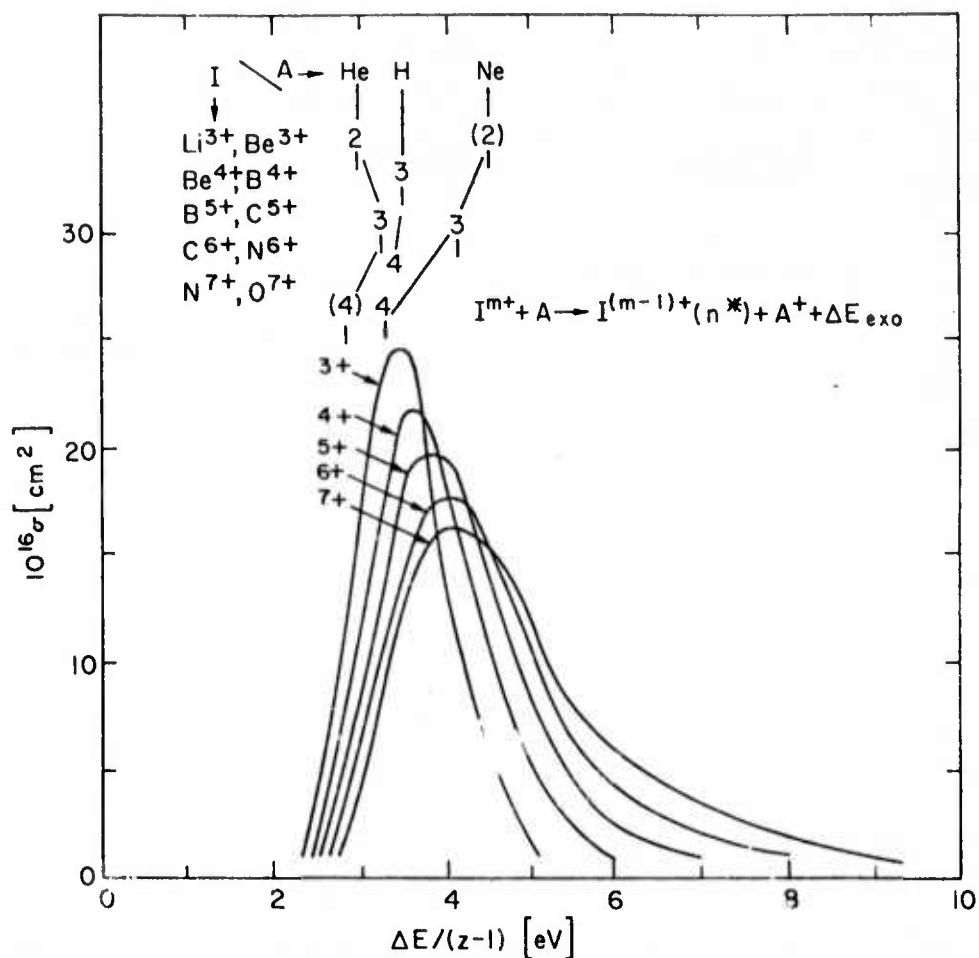


Fig. 19. Resonance charge transfer cross section obtained by inversion of Fig. 17 data [106]. Final quantum states n of high capture probability for each ion, I^{m+} , and atom, A , combination are indicated by numerals, with parentheses to indicate less probably transitions. ΔE is the exothermic energy defect and z is the effective ion charge.

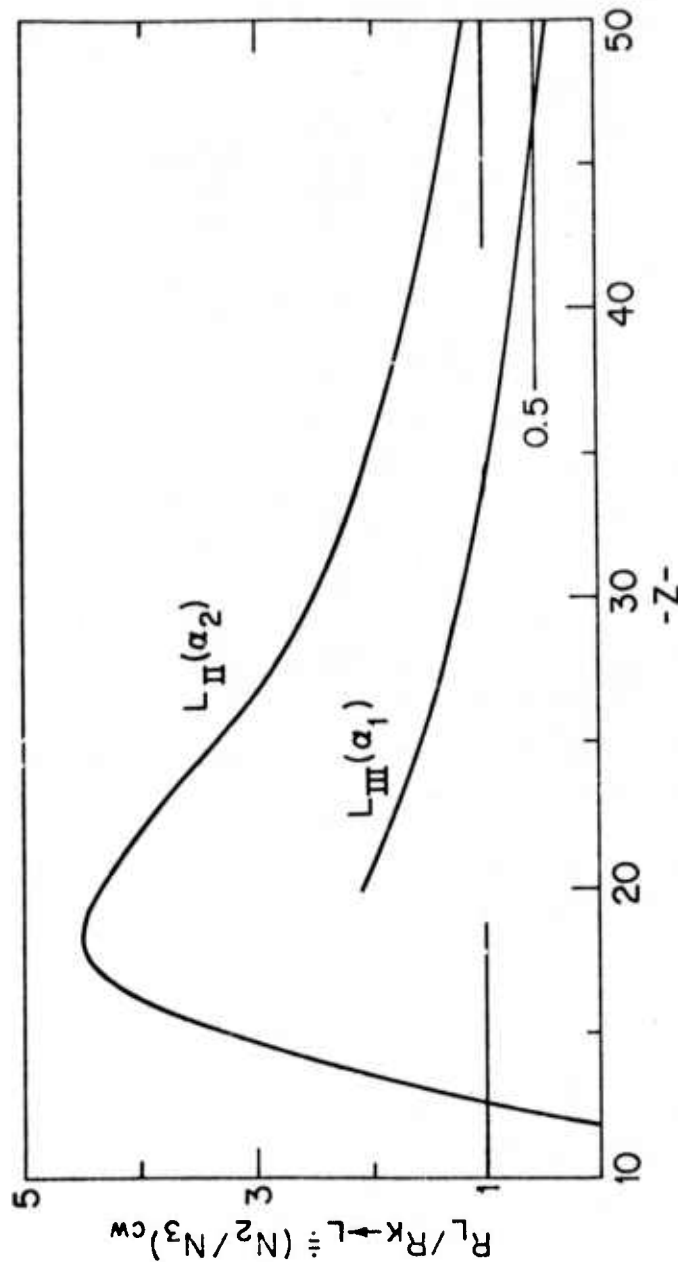


Fig. 20. Ratio of rates R_L/R_K for total transitions out of an L vacancy state and radiative decay out of a K vacancy state versus atomic number, Z . This ratio is equivalent to N_2/N_3 for equilibrium conditions reached after long times in cw operation. Values exceeding unity and one-half indicate gain for the $K\alpha_2$ and $K\alpha_1$ transitions, respectively. The model used assumes that only radiative transitions produce absorbers and that Auger transitions generate shifted ion lines. Both the $K\alpha_{II}$ (α_2) and $K\alpha_{III}$ (α_1) transitions are shown [96].

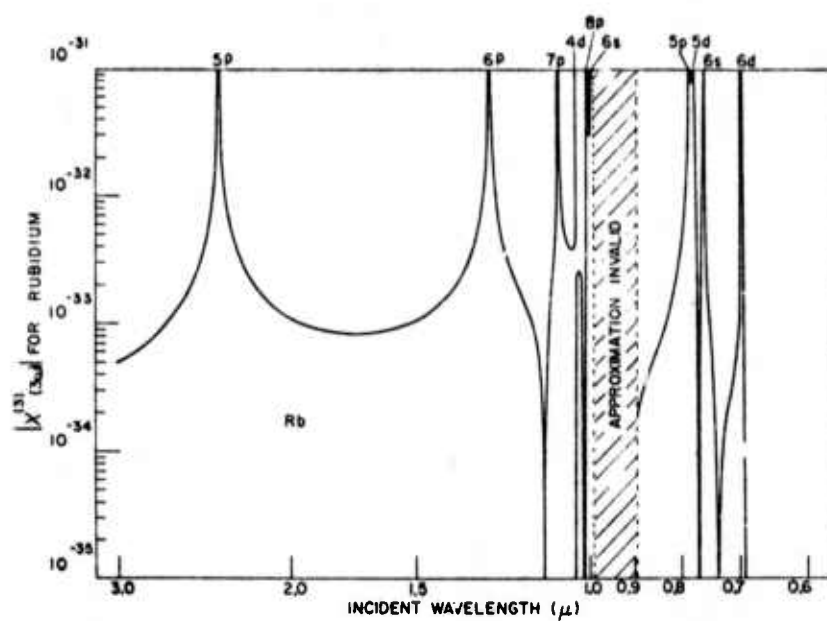


Fig. 21. Nonlinear susceptibility of rubidium as a function of wavelength [240].

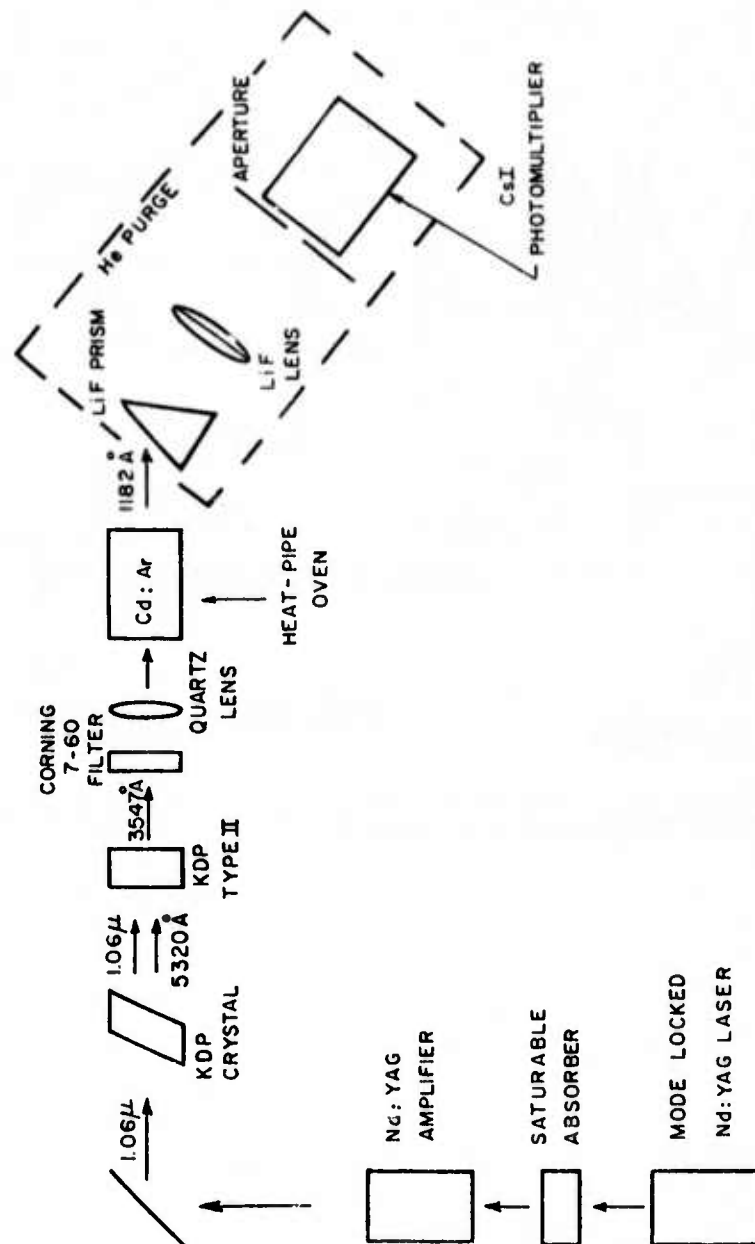


Fig. 22 — The experimental apparatus used by Kung, et al. to generate vacuum ultraviolet wavelengths by up-conversion [243]

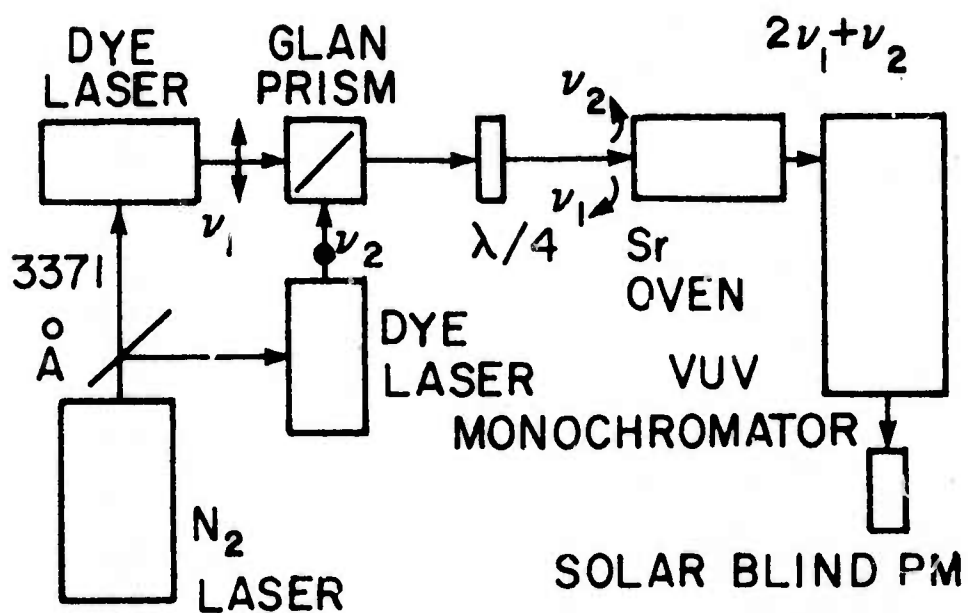


Fig. 23. Schematic of the apparatus used by Hodgson, et al. to produce tunable vacuum-uv emission using Sr vapor [247].

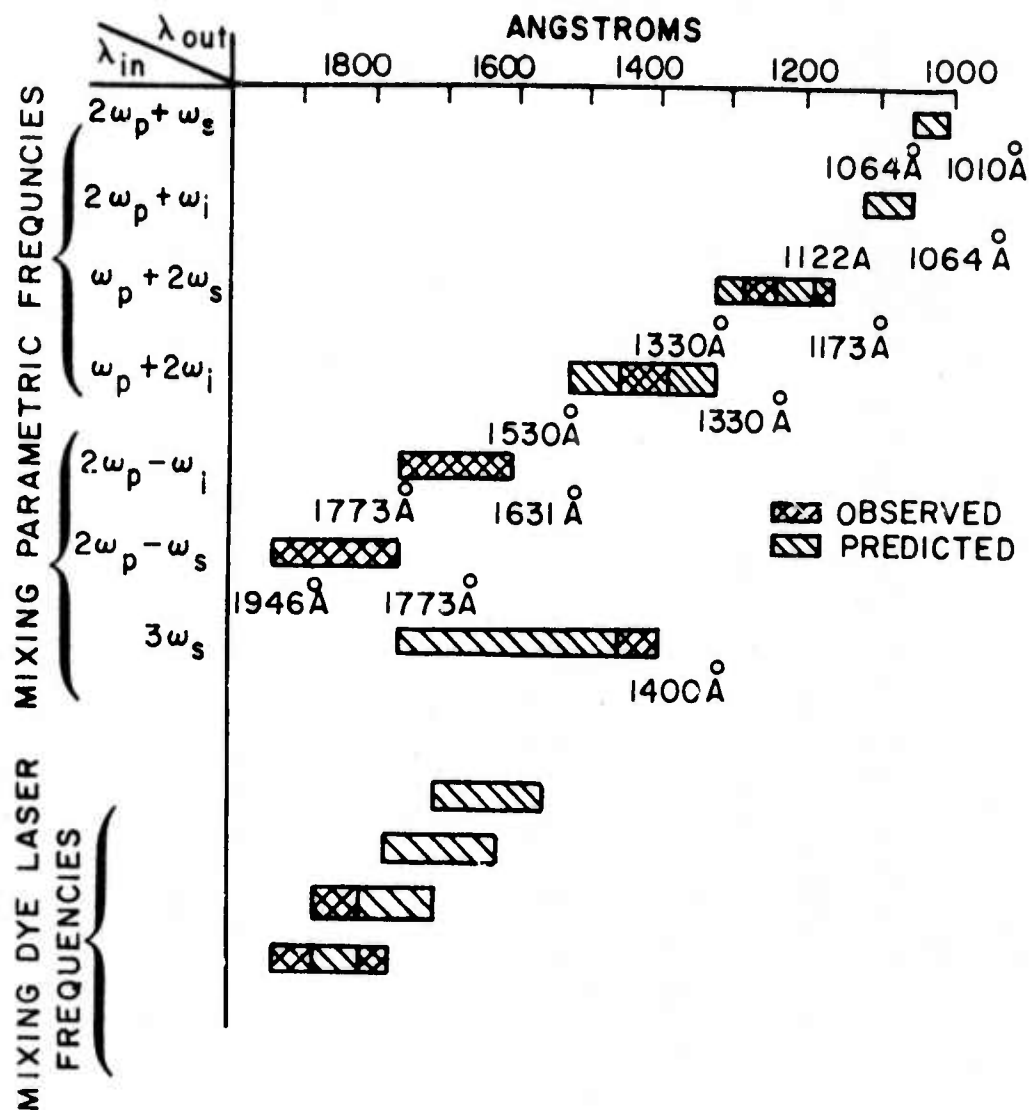


Fig. 24. The ranges of wavelength covered by the tuning methods described by Kung [243] using parametrically generated frequencies and by Hodgson, et al. [247] using tunable dye laser frequencies.

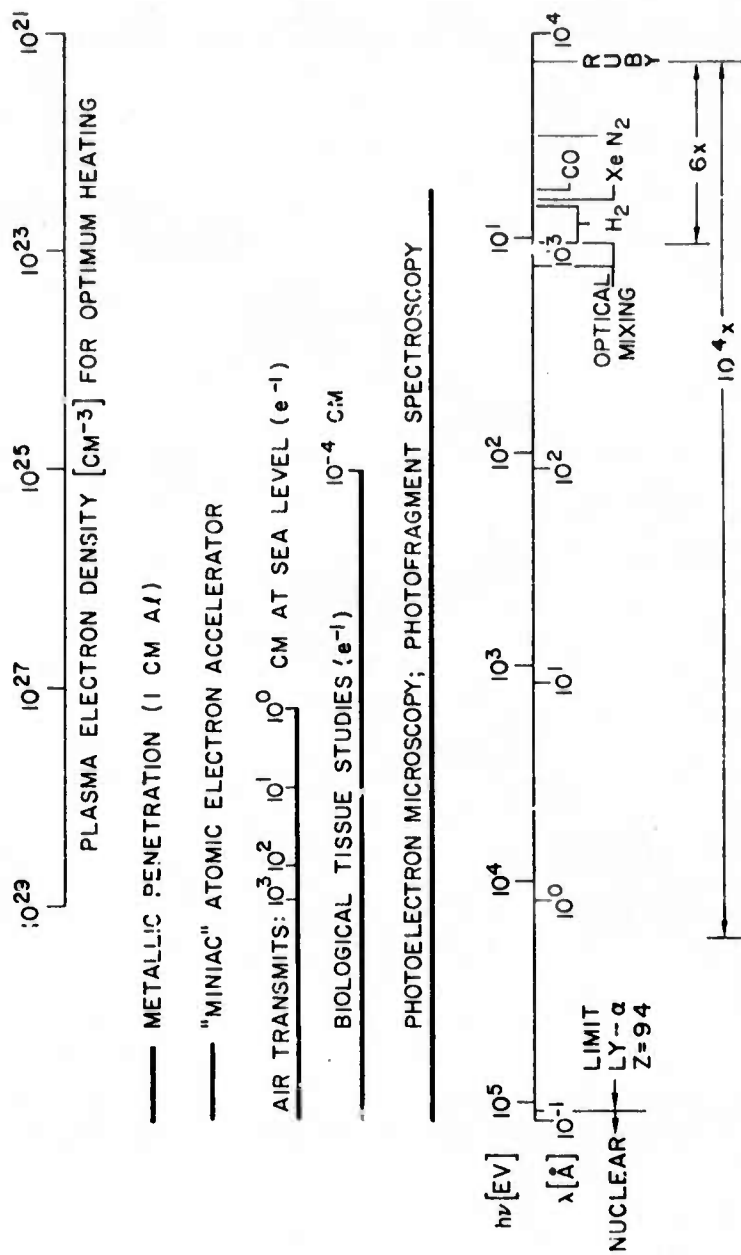


Fig. 25. Useful characteristics of a collimated and coherent laser beam at short wavelengths.



— 1 μ —

836 Å FRINGES
PRODUCED IN PMMA
BY 1182 Å RADIATION

Fig. 26. Fringes produced in polymethyl methacrylate (PMMA) at 836 Å spacing and analyzed with a scanning electron microscope. The round object is a 0.5 μ m latex sphere placed after development for magnification calibration [268].

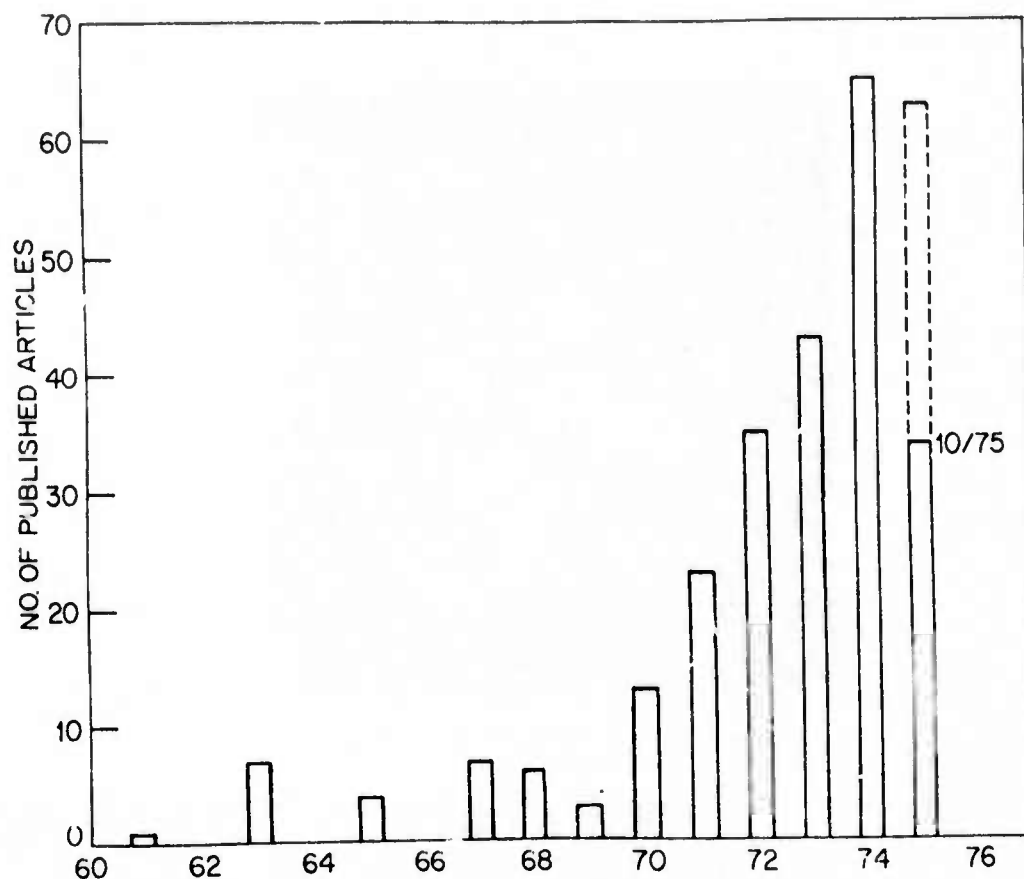


Fig. 27. Record of activity in short wavelength laser research as compiled from the references on this topic in the present review. The data for 1975 are as of October and still incomplete, particularly for those articles not yet translated.

END